The Ionic Hydrogen Bond

Michael Meot-Ner (Mautner)*

Department of Chemistry, Virginia Commonwealth University, Richmond, Virginia 23284, and Department of Chemistry, University of Canterbury, Christchurch 8001, New Zealand

Received January 27, 2004 (Revised Manuscript Received October 29, 2004)

Contents

* E-mail: m.mautner@solis1.com.

1. Introduction and Overview

1.1. Historical Background

Hydrogen bonds[1,2] are one of the principal intermolecular forces. A special class are ionic hydrogen bonds (IHBs) that form between ions and molecules with bonds strengths of 5−35 kcal/mol, up to a third of the strength of covalent bonds. These strong interactions are critical, for example, in ionic clusters and nucleation, in electrolytes, ion solvation, and acid−base chemistry, in the structures of ionic crystals, surfaces, silicates, and clays, in surface adsorption, and in self-assembly in supramolecular chemistry and molecular crystals.[3] IHBs are also important in bioenergetics including protein folding, enzyme active centers, formation of membranes and proton transport, and biomolecular recognition. With such wide-ranging roles, the fundamental properties of IHB interactions need to be understood.

The energetics of IHB interactions cannot be isolated and quantified in the condensed phase. However, these interactions can be isolated and studied quantitatively in gas phase. These studies lead to a fundamental understanding of relations between IHB bond strengths and molecular structure, the solvation of ions, especially in the critical inner shells, and acid-based phenomena and bioenergetics.

This review will present the basic insights that have been obtained in the past four decades. It will present a comprehensive review of the thermochemistry and its structural implications obtained from ab initio calculations. Relevant recent results from spectroscopy will be also illustrated.

The advent of variable temperature high-pressure mass spectrometry (HPMS) introduced by Field and co-workers in the 1960s[4] and pulsed high-pressure mass spectrometry (PHPMS) introduced by Kebarle in the late 1960s[5] have been particularly significant. These workers realized that at pressures of several torrs and gas densities of $10^{16}-10^{17}$ cm^{-3} in ion sources, ions can undergo 10^3-10^6 collisions with neutral molecules during typical residence times of 0.1−10 ms and establish thermal ion populations and

10.1021/cr9411785 CCC: $53.50
Published on Web 01/12/2005

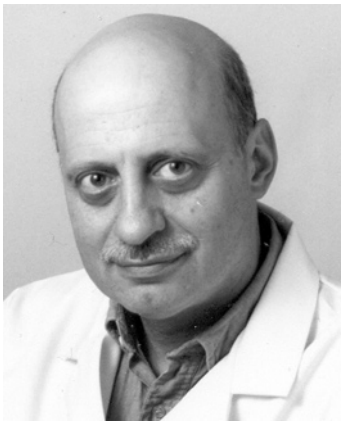

Michael Mautner was born in 1942 in Budapest, Hungary, and was saved from the Holocaust by a courageous woman, Irene Gigor-Horvath. He obtained a B.Sc. from the Hebrew University (Meot-Ner, meaning "Hundreds of Lights", is a transliteration of Mautner), a M.Sc. from Georgetown University, and a Ph.D. from Rockefeller University, New York, using the historic mass spectrometer on which Prof. F. H. Field invented chemical ionization. Current research interests are fundamental ion kinetics and thermochemistry, gas-phase acidities and basicities, cluster ions, charge-transfer complexes, and ionic processes in astrochemistry and bioenergetics. The author served on the faculty of Rockefeller University and as Research Chemist at NIST, is currently Research Professor at Virginia Commonwealth University, and is also affiliated with The University of Canterbury and Lincoln University in New Zealand. Other current research interests concern space colonization, the biological fertilities asteroid and meteorite materials as future space resources, and the science and ethics of seeding other solar systems with life (www.astroecology.com).

equilibria. This method can measure equilibrium constants for ion−neutral association reactions usually involving one to eight, sometimes up to 20, ligand molecules.

Many of these studies addressed hydrogen-bonded adducts formed in reaction 1 where the hydrogen

$$BH^+ + B' \rightarrow BH^+ \cdot B' \quad (1)$$

donor ion, BH^+, is usually a protonated base and the hydrogen receptor, B′, is a base with an electron donor heteroatom ("unconventional" carbon-based IHBs will be also reviewed). The anionic counterpart is reaction 2, where A^- is usually a deprotonated

$$A^- + A'H \rightarrow A^- \cdot HA' \quad (2)$$

Bronstead acid, and AH is a hydrogen donor, usually a Bronstead base.

In pulsed, time-resolved experiments, equilibrium can be verified when the product/reactant ion ratio, $[BH^+ \cdot B']/[BH^+]$, reaches a constant value as a function of reaction time. The equilibrium constant K is then calculated from eq 3, where $P(B')$ is the partial

$$K = \frac{[BH^+ \cdot B']}{P(B')[BH^+]} \quad (3)$$

pressure of B′ in the ion source. Temperature studies yield the IHB bond dissociation enthalpies, ΔH°_D, and entropies, ΔS°_D. The uncertainty of ΔH°_D values measured by pulsed high pressure mass spectrometry is usually ±1 kcal/mol, and that of ΔS°_D is ±1.5 cal/(mol K).

Information on IHB bond strengths can also be obtained from ligand exchange equilibria, which were used in low-pressure ion-cyclotron resonance (ICR)[6−10] and selected injection ion flow (SIFT) measurements.[11] More recently, equilibria are being measured by variable temperature drift cell ion mobility apparatus.[12,13] Thermochemical data are also being obtained by threshold dissociation measurements on cluster ions,[14] and recently, by zero-pressure blackbody infrared thermal dissociation (BIRD) measurements.[15−18] The latter can be applied to systems not amenable to equilibrium measurements, for example, clusters with involatile ligands and clusters generated by electrospray, allowing studies on bio-ions and multiply charged ions.

Cluster data correlate with proton affinities (PAs) and gas-phase acidities and basicities. Extensive PA scales were constructed by Yamdagni and Kebrale,[19] Taft,[20] Meot-Ner and Sieck,[21] Szuleko and McMahon,[22] and Radom and co-workers[23,24] and tabulated by Hunter and Lias.[25] Our recent review found that these scales can be reconciled within ±0.8 kcal/mol for 38 key reference compounds spanning a PA range of 120 kcal/mol.[26] PA values in the NIST database[27] that are used here are accurate to this level.

Experimental thermochemical data on cluster ions, including hydrogen-bonded clusters, were compiled by Keesee and Castleman.[28] A recent updated computer-based compilation contains over 2000 items of thermochemical data,[29] and anion cluster data also appear in a tabulation of anion thermochemistry.[30] Theoretical work on IHB interactions was reviewed recently.[31,32]

The present review will progress through systems of increasing complexity. It will progress from hydrogen-bonded dimers to higher clusters that give insights into shell filling and relationships between stepwise and bulk solvation and solvation factors; IHBs in complex molecules; intramolecular and polydentate bonds; and cluster models of bioenergetics. Supplementary subjects, such as the spectroscopy and structure of IHB systems in the gas phase and solution, and some special kinetic effects of IHB formation will be also reviewed briefly.

1.2. An Overview of IHB Structures and Energetics

The main structure−energy relations in IHB systems are illustrated by the examples in Table 1 and then summarized in a general overview. The following are the major trends observed in ionic hydrogen bond systems.

1.2.1. Dimers

1. Ionic hydrogen bonds (IHBs) are strong intermolecular forces with bond strengths usually of 5−35 kcal/mol. IHBs form both in cationic and in anionic systems.

2. The formation of the $B-H^+ \cdot B'$ bond involves partial proton transfer from the donor to the acceptor. The bond strengths correlate with the efficiency of proton transfer. The bonding proton becomes more positive, the acceptor and donor heteroatoms become

Table 1. Representative Thermochemistry of Homodimers $BH^+ \cdot B$ and Hydrated Complexes $BH^+ \cdot H_2O$ and $BH^+ \cdot 4H_2O$[a]

BH^+	PA(B)[b]	$\Delta H^\circ_{internal}$ (ΔH°_{strain})[c]	ΔH°_D (BH^+-B)[d]	ΔH°_D ($BH^+ \cdot H_2O$)[d]	ΔH°_D ($BH^+ \cdot 4H_2O$)[d]	$-\Delta H^\circ_{g\to aq}$ (BH^+)[e]	$-\Delta H^\circ_{g\to aq}$ (IHB)[e]	$-\Delta H^\circ_{g\to aq}$ (hydrophobic)[e]	$-\Delta H^\circ_{g\to aq}$ ($BH^+ \cdot 4H_2O$)[e]	ΔS°_D ($BH^+ \cdot B$)[d]
H_3O^+	165.0		32.1	32.1	81.9	117.0	44.5		75.3	26.4
$MeOH_2^+$	180.3		32.5	26.4	72.8	101.3	38.0	13.2	70.5	28.8
$(Me)_2OH^+$	189.0		31.4	23.4	62.3	92.6	26.8	24.9	72.8	30.8
$(MeOCH_2CH_2OMe)H^+$	205.1	10 (21)	27.4	16.4	54.2					30.9
$(Me(OCH_2CH_2)_2OMe)H^+$	219.6	25	21.3	17.6	51.1					38.0
NH_4^+	204.0		25.2	20.2	59.0	88.6	28.5	(0)	68.1	26.3
$MeNH_3^+$	214.9		23.6	17.8	55.1	81.0	25.6	8.1	69.0	25.5
$Me_2NH_2^+$	222.2		22.5	15.0	50.3	74.6	20.2	15.3	67.2	26.9
Me_3NH^+	226.8		22.2	14.5	45.2	66.8	12.6	21.2	64.5	28.8
Et_3NH^+	234.7		23.8	13.2		63.9	9.8	34.0	68.6	41.0
pyridineH^+	222.2		25.0	15.6	41.1	66.3	10.3	25.3	67.2	29.5
$H_2NCH_2CH_2CH_2NH_3^+$	235.9	16 (8)		11.4						
H_3S^+	168.0		15.1	21.2						20.3

[a] Internal hydrogen bond strengths, cluster bonding energies, solvation enthalpies, and solvation factors were derived using cluster thermochemistry. All ΔH° values are in kcal/mol and ΔS° in cal/(mol K). [b] Proton affinities from ref 27. [c] Bond strength and strain (in parentheses) of internal IHBs.[33] [d] Average or recommended values from ref 34. [e] Calculated as in ref 35 but using updated thermochemistry (see Tables 11 and 12). Ionic hydrogen bonding and hydrophobic solvation factors in ion solvation are based on solvation factor analysis.[35]

more negative, the $B-H^+$ bond of the donor lengthens upon the formation of the complex, and part of the charge is transferred to the acceptor. In anions, similar changes occur in forming $A-H \cdot A'^-$ bonds.

3. In homodimers $BH^+ \cdot B$, for example, $(H_2O)_2H^+$, $(MeOH)_2H^+$, and $(Me_2O)_2H^+$, and in anionic homodimers, $A-H \cdot A'^-$, both components have equal proton affinities (PAs) or acidities and share the proton efficiently. The bond strengths in the homodimers $R_2OH^+ \cdot OR_2$ and $R_3NH^+ \cdot NR_3$ are affected little by the absolute proton affinities of the monomers (see Table 1, column 4).

4. In heterodimers $BH^+ \cdot B'$, the bond strengths decrease with increasing PA difference (ΔPA) between the components, as a donor with a higher PA transfers proton less efficiently to an acceptor with a lower PA (for example, see the $BH^+ \cdot H_2O$ complexes in Table 1, column 5). Quantitatively, inverse linear correlations are observed between the bond dissociation energies, (ΔH°_D), and ΔPA over wide ranges of ΔPA (up to 60 kcal/mol). In anions, similar correlations are observed between $AH \cdot A'^-$ bond strengths and the relative acid dissociation energies.

5. The formation of dimers involves significant negative entropy changes, that is, the dimers have large positive entropies of dissociation, (ΔS°_D), usually 20−30 cal/(mol K). These entropy changes are smaller than those associated with covalent bond formation, due to internal rotation and low-frequency vibrations that are retained about the hydrogen bond in the dimers. However, steric hindrance (e.g., $(Et_3N)_2H^+$ in Table 1) or polydentate bonding can lead to ΔS°_D values up to 60 cal/(mol K).

6. Unconventional carbon-based IHBs form where the donors are hydrocarbon CH groups and/or the acceptors are carbon lone pairs, olefin double bonds, or aromatic π systems.

1.2.2. Higher Clusters

7. Several ligand molecules can add stepwise to ions to form clusters $BH^+ \cdot nL$. In many clustering sequences, the consecutive binding energies, $\Delta H^\circ_{n-1,n}$, decrease by a factor of 0.7 ± 0.1 with each consecutive step.

8. The bonding energies of consecutive solvent molecules to ions approach the condensation enthalpy of the bulk solvent within ± 1 kcal/mol, usually after as few as four to six solvent molecules.

9. Large clusters often have many isomeric structures with similar energies, which may coexist in equilibrium under thermal conditions.

10. Clusters of nonblocked components can form indefinite hydrogen-bond networks. Filled solvent shells and cyclic solution-like IHB networks may start to develop already after two to four solvent molecules bind. In mixed nonblocked clusters of a given size, the stability of the IHB network increases with increasing mole fraction of the stronger base.

11. The filling of solvent shells can cause drops of 1−4 kcal/mol in the consecutive binding energies. Larger drops are observed when blocked components (e.g., Me_2O, Me_3N) fill a shell and prevent the formation of further strong IHBs.

12. In mixed clusters of unblocked and blocked components, the protons can be transferred to the former, often water, to form a $(H_2O)_nH^+$ core where the proton is stabilized by a network of strong hydrogen bonds. The proton can remain in a water core even when it is surrounded by alkyl-blocked molecules that have higher proton affinities. This has significant biological consequences, as in membrane transport.

13. Solvation compresses, and sometimes reverses, the intrinsic gas-phase acidities and basicities of molecules. The solvent effects on acidities and basicities can be as significant as the effects of the intrinsic molecular parameters themselves. Energies of ionic aggregation to form B_nH^+ aggregates are also compressed by stepwise solvation.

14. Cluster studies show the stepwise development of solvation effects. A large fraction of these effects, often 80% or more, results from the first four to six solvent molecules.

15. All the above observations are paralleled in anionic clusters, where the role of proton affinity (PA(B)) is replaced by PA(A^-) (i.e., the acid dissociation enthalpy, ΔH°_{acid}(AH)).

1.2.3. Polyfunctional Molecules, Biomolecules, and Cluster Models of Bioenergetics

16. Polyfunctional molecules show increased proton affinities and significant negative entropies of protonation compared with monofunctional analogues. These effects indicate the formation of internal hydrogen bonds (iIHBs) of 4−30 kcal/mol (see polyethers and diamine in Table 1).

17. Internal IHBs can create strained cyclic structures. The strain decreases and the bond becomes stronger with increasing ring size.

18. External solvation decreases the strength of internal hydrogen bonds. Conversely, internal bonds weaken bonding to external solvent molecules.

19. The bonding of ions to polydentate ligands shows increased bond strengths and negative entropies of complexation compared with monodentate ligands, due to multiple IHBs and electrostatic stabilization of the charge by several polar groups.

20. In solvated polyfunctional ions, hydrogen-bonded solvent bridges can form between functional groups.

21. Ligands bond strongly to multiply protonated ions. The bonding becomes stronger with decreasing separation and increasing Coulomb repulsion between the charges.

22. Internal and polydentate IHBs are common in protonated polyfunctional biomolecules. Interactions between internal IHB and external solvation can affect the conformation of biomolecules.

23. Cluster models suggest that IHBs to protein backbone amide NH or CO groups can stabilize ionic intermediates by 35 kcal/mol. In proton transport, cluster models suggest that the proton can remain in a water chain surrounded by strongly basic protein groups.

1.2.4. Relationship between Gas-Phase and Bulk Solvation

24. The *relative* solvation energies by four H_2O molecules reproduce the *relative* bulk hydration enthalpies of diverse ions. This applies although continuum solvent terms and hydrophobic hydration are present only in solution but not in the clusters.

25. This relation shows that the energies of solvent cavity formation, dielectric charging, and hydrophobic solvation vary in an almost exactly canceling manner in the hydration of ions of diverse sizes and structures, although these terms are physically independent.

26. Quantitatively, the cluster solvation enthalpies, $\Delta H^\circ_{g\rightarrow aq}(BH^+\cdot 4H_2O)$, are 70 ± 3 kcal/mol for diverse ions (Table 1, column 10). This result quantifies the cumulative excess cluster ion binding energies from $n = 4$ to ∞ of diverse ions as a constant 70 ± 3 kcal/mol.

27. Alternatively, result 26 yields cluster-based, purely single-ion solvation energies smaller by 70 ± 3 kcal/mol than the conventional solvation energies that are derived from solutions with ion pairs.

28. The binding energies of solvent molecules approach within ±1 kcal/mol the macroscopic condensation enthalpy of water, −10.5 kcal/mol, already after four to six solvent molecules. If this value remains constant in higher clusters, the cluster-based ion solvation energies in point 27 apply. The correct interpretations of cluster data, point 26 or 27, may be identified by accurate data on large clusters.

29. A cluster-based analysis decomposes ion solvation into a few simple factors. It shows that each protic hydrogen contributes a constant term and each CH hydrogen contributes a smaller constant term to the enthalpies of hydration.

30. In extension of the gas-phase bond energy/ΔPA correlations, the bulk hydration energies of diverse onium ions, $\Delta H^\circ_{g\rightarrow aq}(BH^+)$, can be predicted from the gas-phase proton affinities of the bases B.

2. Hydrogen-Bonded Dimers

2.1. Thermochemistry and Structures of Hydrogen-Bonded Dimers

2.1.1. Structural Effects of Ionic Hydrogen-Bond Formation

The formation of IHBs causes a redistribution of atomic charges and changes in bond lengths and angles. The changes affect primarily the bonding proton, the donor and acceptor heteroatoms, and the B−H^+···B′ or A−H···A'^- bond lengths. The IHB bond strengths are correlated with these changes.

Examples of the strengths of IHBs in dimers are given in Table 1, and the bond strengths are illustrated in the 0,1 equilibria in Tables 4−6. The thermochemistry and structures were subject to extensive theoretical studies that were reviewed recently.[31,32]

Some of the basic effects of IHB formation are illustrated in Figure 1 by the prototype homodimer $NH_4^+\cdot NH_3$ and heterodimer $NH_4^+\cdot H_2O$.[36] The changes in charge densities upon complex formation are illustrated in Figure 2. The bonding hydrogen always loses electron density and becomes more positive (dotted lines), while the acceptor and donor heteroatoms always gain electron density and become more negative (solid lines). The same areas experience gain or lose charge in the ionic and in the analogous neutral complexes, but the changes are larger in the more strongly bonded dimer ions. Also, the changes are larger in the more strongly bonded $NH_4^+\cdot NH_3$ homodimer than in the $NH_4^+\cdot H_2O$ heterodimer. In the heterodimer, an area of electron density gain develops between the proton and the acceptor O atom. This gain becomes more pronounced with acceptor atoms of greater electronegativity, such as in complexes of NH_4^+ with HF, PH_3, H_2S, and HCl. Charge loss about the proton decreases in the same order. A strong correlation exists between the bond strength and the electron gain in the donor bond. This shows the significance of the proton donor in determining the properties of the hydrogen bond.[37]

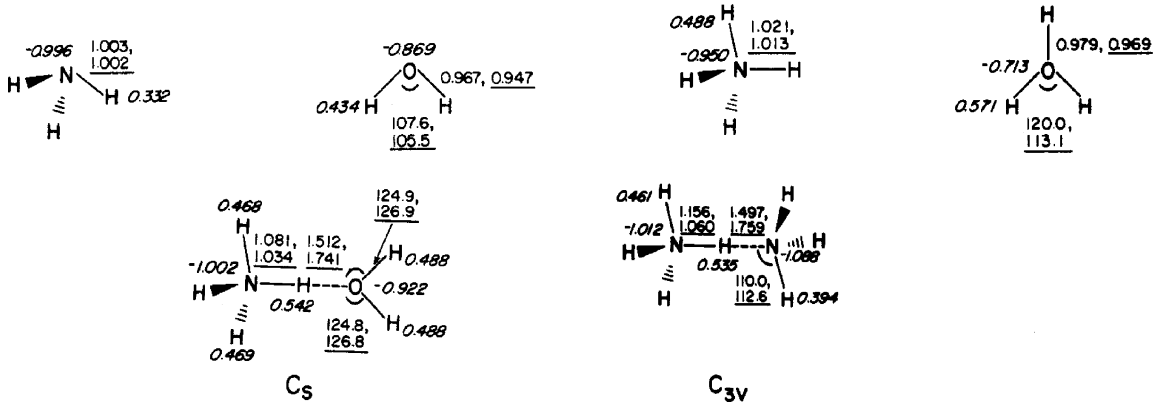

Figure 1. Geometries and atomic charge densities of H_2O, NH_3, NH_4^+, $NH_4^+ \cdot H_2O$, and $NH_4^+ \cdot NH_3$. Structures were calculated from 3-21G and 6-31G* (underlined) optimizations. Only the values of the bond lengths (in Å) and bond angles (in deg) that were varied in the computations are shown. Atomic charges from population analysis (6-31G* basis set) are given in italics. Reproduced from ref 36 with permission. Copyright 1986 American Chemical Society.

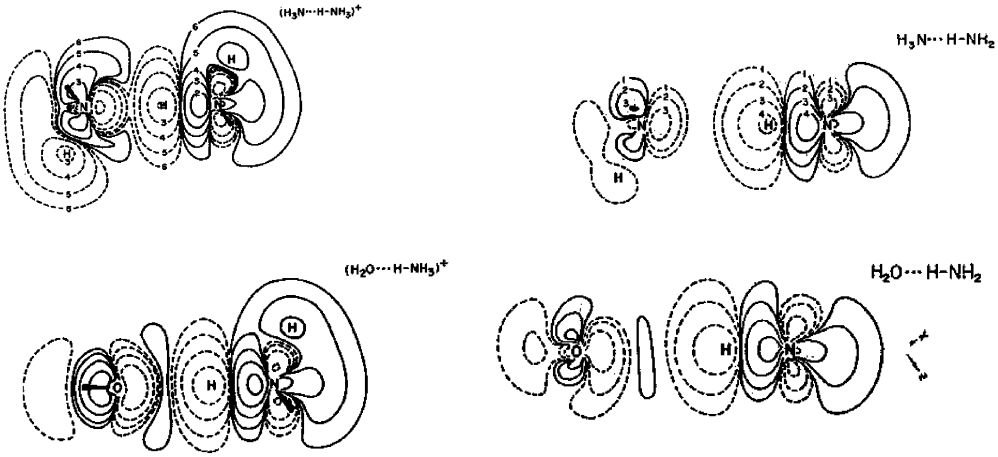

Figure 2. Charge density changes upon the formation of hydrogen-bonded ionic and analogous neutral complexes. Solid lines correspond to electron density gain and dotted lines to loss, as obtained from 4-31G calculations. The scale (in e/Å^3) is as follows: 1 = 0.676; 2 = 0.214; 3 = 0.0676; 4 = 0.0214; 5 = 0.00676; 6 = 0.00214. Reproduced from ref 37 with permission. Copyright 1980 American Physical Society.

The examples in Figures 1 and 2 show that, compared with the uncomplexed species, the formation of the hydrogen bond increases the positive charge on the bonding proton, increases the negative charges on the hydrogen donor and acceptor atoms, delocalizes some of the net positive charge from the donor molecule onto the acceptor molecule, and increases the $B-H^+$ bond length of the hydrogen donor.

These changes are largest when the two components are identical and the proton is shared efficiently. In heterodimers, the effects of forming the bond, along with the bond strengths, decrease with increasing proton affinity difference (ΔPA) between the components.[38,39] All of the above features are observed in the model dimers $NH_4^+ \cdot NH_3$ and $NH_4^+ \cdot H_2O$ in Figure 1, which compares the homodimer $NH_4^+ \cdot NH_3$ where $\Delta PA = 0$ and $\Delta H_D^\circ = 25.7$ kcal/mol with the more weakly bonded heterodimer $NH_4^+ \cdot H_2O$ where $\Delta PA = 39.5$ kcal/mol and $\Delta H_D^\circ = 20.2$ kcal/mol. Comparing $NH_4^+ \cdot NH_3$ with $NH_4^+ \cdot H_2O$, the amount of charge transferred from the ion to the neutral decreases from 0.094 to 0.054 unit charge and the $N-H^+$ bond becomes less stretched, from 1.060 to 1.034 Å, in the more weakly bonded heterodimer. Also, the length of the hydrogen bond increases with decreasing bond strength. Similar trends were found by Desmeules and Allen in an ab initio 4-31G study of complexes of NH_3, H_2O, FH, PH_3, SH_2, and HCl.[37] These workers, as well as Kebarle and co-workers, analyzed IHB bond strengths as a function of proton transfer in the bond. The curves in Figure 3 show that the bond strengths correlate with the degree of proton transfer in the bonds, as measured by the $B-H^+$ bond length.[40]

As suggested in Figure 3, Desmeules and Allen showed that in hydride dimers the stretching of the $B-H^+$ bond is related inversely to the ΔPA (Figure 4). In turn, the lengths of the $B-H^+$ bonds correlate linearly with the bond strength (Figure 5). Together, these theoretical results imply a direct relation between the bond strength and ΔPA.[37] These results are consistent with experimental observations.

In a set of dimers, the IHB bond strengths also correlate with charges on the acceptor and donor atoms before and after bond formation. In a set of dimers between various hydrogen donor ions and a given ligand, the main parameter that affects the bond strength is the charge on the bonding hydrogen atom (q_h). Examples were found by the Kebarle group for (pyridinium)$H^+ \cdot H_2O$ complexes[40] (Figure 6) and for bonds of ROH with halide anions.[41]

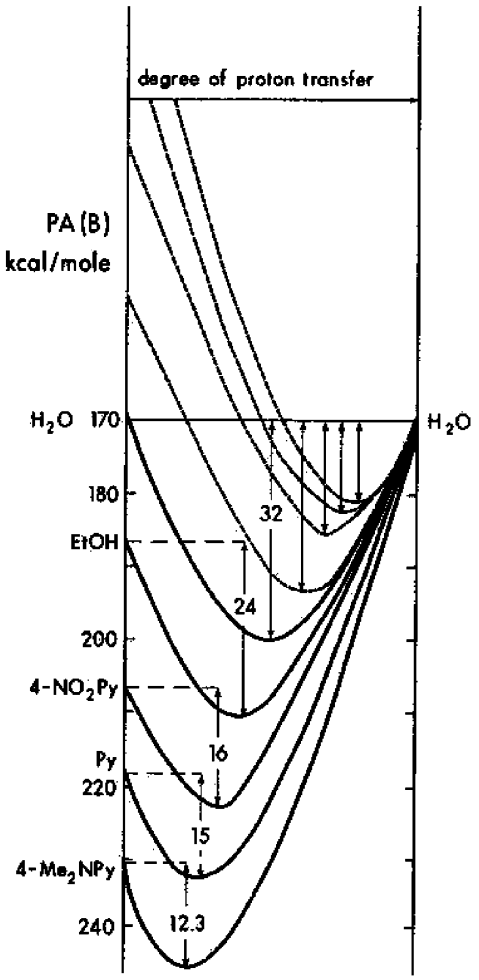

Figure 3. Plot of stabilization energies, E_s, due to hydrogen bonding in $BH^+ \cdot H_2O$ complexes, corresponding to dissociation to $BH^+ + H_2O$ (solid curves) or to $H_3O^+ + B$ (dashed curves), where B are substituted pyridines with proton affinities shown on the y coordinates. The minima show the hydrogen bond energies from experimental data. The degree of proton transfer from BH^+ to H_2O (horizontal coordinate) is arbitrarily chosen. The diagram illustrates how the energy minima may be reached at further distances from the donor on the left and may be deeper as PA(B) decreases and approaches PA(H_2O) and the proton can be transferred more efficiently to H_2O, proceeding up from lower to higher curves. The hypothetical dashed curves suggest that the binding energy would decrease further and the proton would be bound to H_2O with proton donors when the PAs of the proton are lower than those of water. Reproduced from ref 40 with permission. Copyright 1979 American Chemical Society.

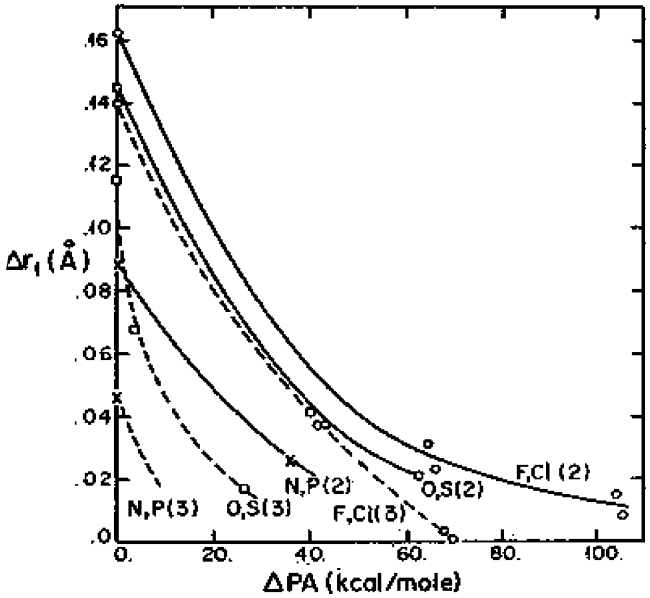

Figure 4. Correlation of the calculated proton movement, that is, increase of $B-H^+$ bond length upon bond formation, with ΔPA for the hydrides of the electron donors as indicated with second row proton donors (solid lines) and third row proton donors (dashed lines). The inverse correlation shows that with increasing ΔPA the proton is shared less efficiently, which in turn decreases the bond strength (see Figure 5). Reproduced from ref 37 with permission. Copyright 1980 American Physical Society.

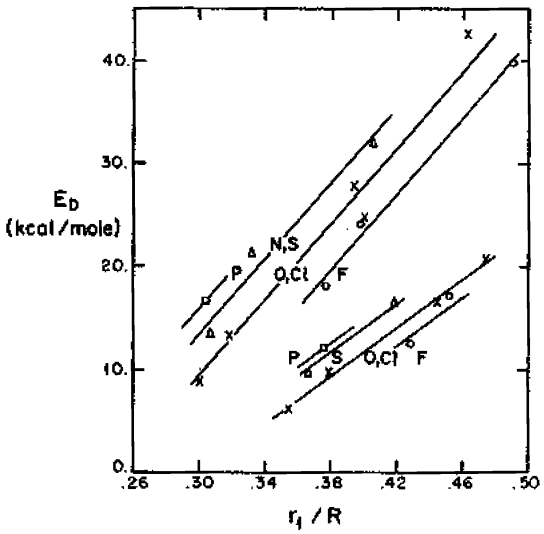

Figure 5. Correlation of calculated bond dissociation energies, E_D, with the $B-H^+$ bond length expressed as r_1/R ($r_1 = B-H^+$ bond length, R = B to B′ bond length in $B-H^+ \cdot B'$) for various hydrides as electron donors. Upper set of four lines are for complexes with second row proton donors and the lower set of four for those with third row proton donors. Increasing r_1/R corresponds to shifting the proton from the donor to the acceptor, that is, better proton sharing. The plot shows that this correlates with increasing bond strength. Reproduced from ref 37 with permission. Copyright 1980 American Physical Society.

The relation between charge densities on the donor (q_H), the electron density on the receptor, the amount of charge transfer in the complex (Δq_{CT}), and bonding energies apply both in conventional and in unconventional, carbon-based IHBs. For example, both in $RNH_3^+ \cdot RCN$ (with nitrogen acceptors) and in $BH^+ \cdot$ RNC complexes (with C lone-pair acceptors), ΔE_D correlates with the parameter $q_H q_B/r_2$ (q_B is the charge on the hydrogen receptor atom prior to hydrogen bond formation and r_2 is the distance between the hydrogen-bonded proton and the receptor atom), and also with the amount of charge transferred, Δq_{CT}.[42] Interestingly, the bonding energies of complexes of cyanide and isocyanide ligands are comparable, but the charge transfer, Δq_{CT}, and the stretching of the donor bond are larger with the isocyanide acceptors, consistent with the greater σ-donating ability and lower ionization potential of the isocyano bases. These data suggest that the relative importance of the electrostatic and delocal-

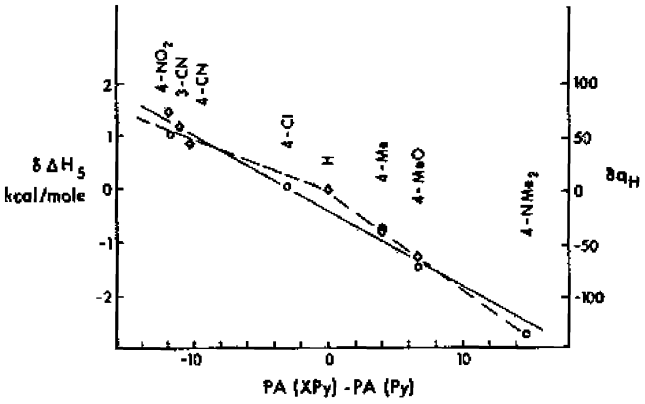

Figure 6. Correlation between the proton affinity differences and the relative positive charge on the bonding hydrogen atom (q_H) and bond strength in (pyridinium ion)-$H^+ \cdot H_2O$ complexes. Reproduced from ref 40 with permission. Copyright 1979 American Chemical Society.

ization components differ in the cyano and isocyano complexes.[42] The effect of q_H on the bond strength depends on the donor−ligand geometry and distance. For example, the interaction energy of NH_4^+ with a model dipole depends strongly on the charge distribution in NH_4^+, on its orientation, and especially on the ion−dipole distance. At short distances, the charge on the bonding hydrogen would be significant, but at realistic bond distances, the ion acts as if it were a point charge concentrated at its center (see Figure 17).[43]

2.2. Hydrogen Bond Strengths and Correlations with Proton Affinities

2.2.1. Cationic Dimers and Correlations with Proton Affinities

In the preceding sections, we noted relationships between hydrogen bond strengths and relative proton affinities of the components. Such relations apply from dimers of small molecules to those of complex organics.

In small molecules, such relations were observed spectroscopically; in the infrared, vibrational predissociation spectra of $OCH^+ \cdot H_2$ and $N_2H^+ \cdot H_2$ indicated T-shaped complexes.[44,45] The proton assumes a position between B and H_2 in these complexes that depends on the relative PAs. With increasing PA(B), the system is transformed from an $H_3^+ \cdot B$ to a $BH^+ \cdot H_2$ structure. When the bond $BH^+ \cdot H_2$ is formed, electron density shifts from the H_2 ligand σ bond to the protonated ion to establish the intermolecular bond. The H−H stretching motion becomes coupled to the intermolecular motion, weakening the H_2 bond and resulting in a red shift of the H−H vibration. These effects are inversely related to the PA difference. For example, the $BH^+ - H_2$ shift is largest, 251 cm^{-1} in $H_3^+ \cdot H_2$, 199 cm^{-1} in $N_2H^+ \cdot H_2$, 100 cm^{-1} in $OCH^+ \cdot H_2$, and 115 cm^{-1} in $OH_3^+ \cdot H_2$. Similar trends were observed in the complexes of HeH^+, NeH^+, ArH^+, KrH^+, N_2H^+, and HCO^+ with H_2.[46] In a complex where the PAs are reasonably close, such as in $N_2H^+ \cdot H_2$ where $\Delta PA = 18$ kcal/mol, a significant shift of -170 cm^{-1} also occurs in the H_2 stretch and more than 700 cm^{-1} in the $N-H^+$ stretch, and rapid vibrational predissociation was observed in the H−H and $N-H^+$ stretches. The magnitudes of all of these changes correlate with the PA differences.[44,45]

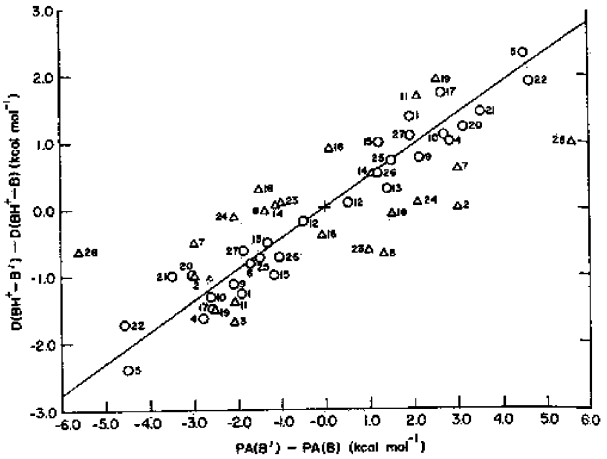

Figure 7. Correlations of $\Delta\Delta H_D^\circ$ and $\Delta PA = PA(B') - PA(B)$ for homodimers and heterodimers of protonated oxygen compounds. Here $\Delta\Delta H_D^\circ = \Delta H_D^\circ(BH^+ \cdots B') - \Delta H_D^\circ(BH^+ \cdots B)$ is the difference between the bond strength of a heterodimer and an optimized homodimer. Reproduced from ref 50 with permission. Copyright 1982 American Chemical Society.

In all the above dimer ions, the components are free to assume geometries where the hydrogen bond can optimize. In a constrained system, the bond may be stretched or bent, causing significant weakening.[47]

In more complex molecules, the bonding energies of several hundred IHB dimers have been measured. Some of the major studies concern $NH^+ \cdot N$ amine dimers,[39] $BH^+ \cdot H_2O$ complexes,[40,48,49] $OH^+ \cdot O$ dimers,[50] complexes $CH_3NH_3^+ \cdot B$ and $NH^+ \cdot O$ dimers,[48] and $BH^+ \cdot CH_3CN$ complexes.[51] The large amount of data yields some general structure−energy relations.

Correlations between the bond dissociation energies, ΔH_D°, and the proton affinity difference between the components, ΔPA, were first observed by the Kebarle group.[38,39,52] For anions, similar relations apply between ΔH_D° and the acid dissociation energy difference, $\Delta\Delta H_{acid}^\circ$, between the components. Note that this is equivalent to proton affinity differences as $\Delta H_{acid}^\circ(A^- - H^+) = PA(A^-)$. Kebarle and co-workers interpreted these relations in terms of the efficiency of partial proton transfer in $R_3NH^+ \cdot NR_3$ and $Cl^- \cdot HR$ complexes and showed an extended correlation between ΔPA (from 0 to 64 kcal/mol) and ΔH_D° (from 32 to 12 kcal/mol) for the association of H_2O with OH^+ and NH^+ groups in protonated O and N bases, especially in substituted pyridines.[40]

For a set of $OH^+ \cdot O$ dimers, Larson and McMahon[50] found linear relations involving the ΔH_D° and ΔPA in homodimers $BH^+ \cdot B$ and heterodimers $BH^+ \cdot B'$ for dissociations to BH^+ or $B'H^+$ (Figure 7), leading to eqs 4 and 5.

$$\Delta H_D^\circ(BH^+ \cdots B') - \Delta H_D^\circ(BH^+ \cdots B) = 0.46(PA(B') - PA(B)) \quad (4)$$

$$\Delta H_D^\circ(B'H^+ \cdots B) - \Delta H_D^\circ(BH^+ \cdots B) = -0.54(PA(B') - PA(B)) \quad (5)$$

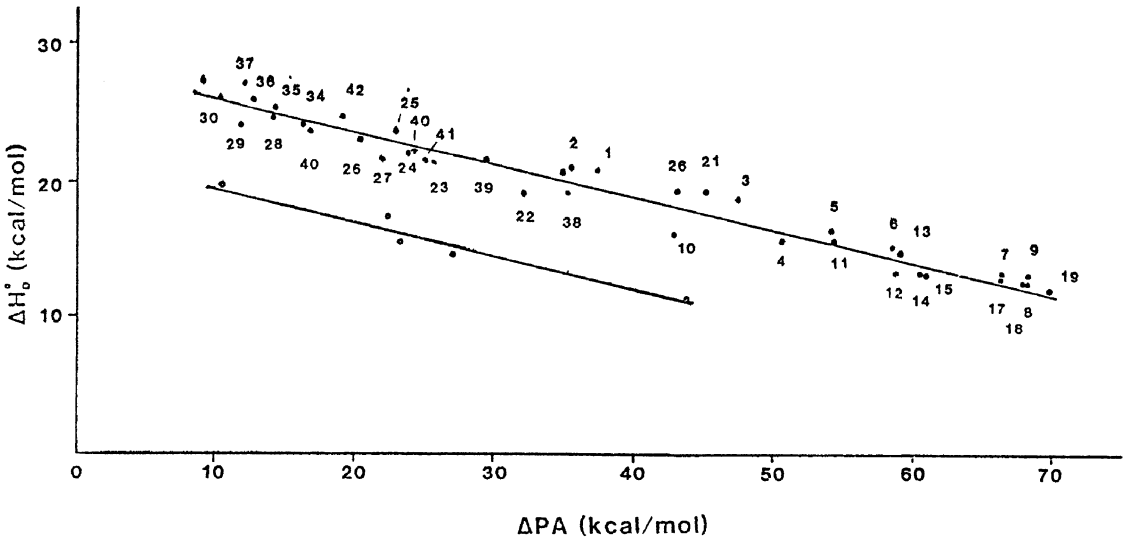

Figure 8. Correlation between the bond strength, ΔH°_D, and the difference between the proton affinities of the components ΔPA for $NH^+\cdots O$ bonds (top line) and $NH^+\cdots S$ bonds (bottom line). Reproduced from ref 48 with permission. Copyright 1984 American Chemical Society.

Table 2. Parameters for Linear Correlations $\Delta H^\circ_D = a - b\Delta PA$ and $\Delta H^\circ_D = a - b\Delta\Delta H^\circ_{acid}$ between Bond Dissociation Energies and Proton Affinity Differences or Acid Dissociation Energy Differences between the Components (kcal/mol) for Reactions $BH^+\cdot B' \rightarrow BH^+ + B'$, Where PA(B) ≥ PA(B′), and Analogous Relations for Anions[a]

bond type	*a*	*b*	*n*	coeff	refs
$OH^+\cdots O$	30.4	0.40		0.999	53
$OH^+\cdots OH_2$	30.4(0.4)	0.30(0.01)	20	0.979	48
$OH^+\cdots NCR$	30.9	0.43			33
$NH^+\cdots O$	28.3(0.3)	0.23(0.01)	48	0.979	48
$NH^+\cdots OH_2$	30.0(1.5)	0.26(0.03)	19	0.923	48
$NH^+\cdots N$	23.2(0.7)	0.25(0.05)	8	0.897	48
$NH^+\cdots NCR$	35.3(0.5)	0.34(0.01)	4	0.984	42
$NH^+\cdots CNR$	25.7((1.0)	0.22(0.01)	5	0.914	42
$NH^+\cdots S$	22.3(0.9)	0.26(0.03)	5	0.970	48
$RCNH^+\cdots N$	33.2	0.31		0.812	53
$RCNH^+\cdots NCR$	28.1	0.37			33
$RCNH^+\cdots O$	28.3(0.7)	0.31(0.01)	5	0.977	42
$RCNH^+\cdots O$	31.9	0.38		0.991	53
$RNCH^+\cdots O$	23.9(0.2)	0.25(0.01)	3	0.998	42
$SH^+\cdots OH_2$	22.7(0.3)	0.26(0.01)	4	0.998	48
$SH^+\cdots OH_2$	18.6(0.3)	0.16(0.01)	8		54
$OH\cdots O^-$	28.1(0.4)	0.29(0.01)	13	0.981	55
$ROH\cdots S{-}R$	19.9(03)	0.15(0.01)	5	0.989	56
$ROH\cdots S{-}C_6H_5$	22.1(0.2)	0.20(0.01)	6	0.997	56
$ROH\cdots F^-$	34.2	0.59	11		57
$ROH\cdots Cl^-$	27.2	0.22	7		7
$c\text{-}C_5H_5^-\cdots HOR$	24.4	0.41	5		58

[a] Here *n* is the number of data points and coeff is the correlation coefficient in each experimental correlation.

In the same period, many dimers $BH^+\cdot B'$ with various *n*-donor heteroatom combinations were investigated by Meot-Ner and co-workers.[33,42,48] Linear correlations were found between ΔPAs and bond dissociation energies, ΔH°_D, over ΔPA (for anions, $\Delta\Delta H^\circ_{acid}$) ranges up to 60 kcal/mol in $NH^+\cdots O$ and $NH^+\cdots S$ bonds (Figure 8). Table 2 shows correlation parameters for various bond types.

$$\Delta H^\circ_D(BH^+\cdot B') = a - b\Delta PA \quad (6)$$

$$\Delta H^\circ_D\,(AH\cdot A'^-) = a - b\Delta\Delta H^\circ_{acid} \quad (7)$$

The intercepts (*a*) in Table 2 give the bond strengths for ΔPA = 0, that is, the maximum bond strengths for a given type of reactant pair when the proton sharing is optimal. This can be seen as the intrinsic bond strength for a given type of hydrogen bond. For $OH^+\cdot O$, $OH^+\cdot N$, $NH^+\cdot O$, and $O^-\cdot HO$ bonds, the intrinsic strengths are about 30 kcal/mol, while $NH^+\cdot N$ and $SH^+\cdot S$ bonds are intrinsically weaker. Cyanide ligands give stronger bonds than other nitrogen bases, possibly due to the larger dipole moment, the highly directional sp hybridization of the nitrogen lone pair, or both. In relation to hybridization effects, the correlations do not apply to dimers of small molecules with hybridization of the acceptor lone pair other than sp^3 such as in $O_2H^+\cdot O_2$ (ΔH°_D = 20.6 kcal/mol), $CO_2H^+\cdot CO_2$ (16.2 kcal/mol), $N_2H^+\cdot N_2$ (16.0 kcal/mol), and $CS_2H^+\cdot CS_2$ (11.1 kcal/mol).[59] These homodimers have much smaller bond energies than organic or hydride $OH^+\cdot O$, $NH^+\cdot N$, or $SH^+\cdot S$ homodimers.[60,61]

A relationship is noted between the intercepts of the correlation lines and their slopes. The energies of intrinsically stronger bonds tend to decrease faster with increasing proton affinity difference. This can be explained in simple electrostatic terms because both the bond energy, ΔH°_D, and its partial derivative with respect to PA, that is, $\partial\Delta H^\circ_D/\partial PA$, depend on the polarizability and dipole moment of the ligand.[54]

The correlations suggest that the bond strengths should be constant for homodimers of a given type because ΔPA = 0 for all homodimers. On the other hand, it could be expected that in a series of homodimers $BH^+\cdot B$ where the proton affinity of B increases, the charge in BH^+ becomes more delocalized in the donor ion away from the bonding hydrogen, decreasing the electrostatic interactions with the ligand and weakening the bond. Such trends are observed but the effect is small, because when BH^+ becomes a less efficient hydrogen donor, the neutral B becomes a more efficient hydrogen acceptor. For example, in a series of $OH^+\cdot O$ homodimers, the bond strength of 32 kcal/mol in $H_3O^+\cdot H_2O$ decreases by

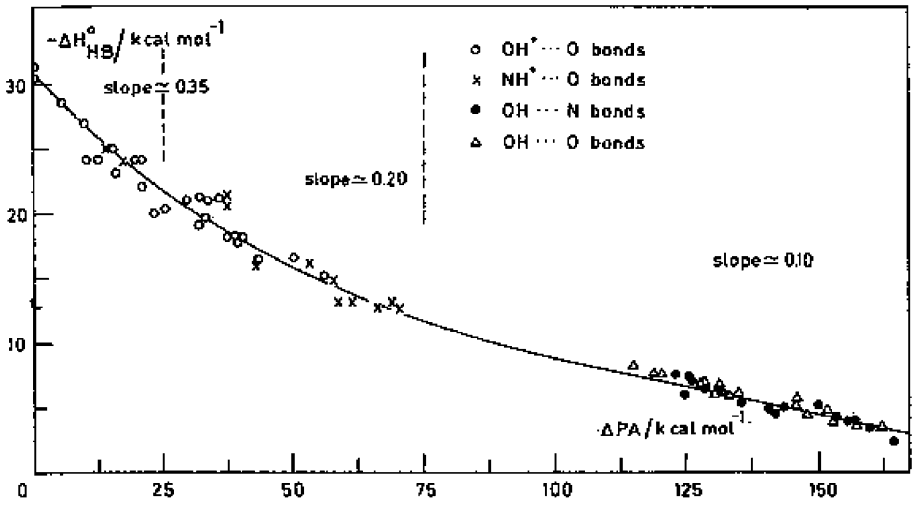

Figure 9. Correlations between hydrogen bond energies and proton affinity differences for ionic and neutral O and N bases. The neutral bonds are considered $RO^--H^+\cdots N$ or $RO^--H^+\cdots O$ bonds, and ΔPA represents the difference between the PAs of RO^- and of the proton acceptor N or O base. Reproduced from ref 68 with permission. Copyright 1986 Elsevier.

only 2 kcal/mol in going to $(C_2H_5)_2OH^+\cdot(C_2H_5)_2O$, while PAs of the monomer components increased by 35 kcal/mol, and similarly small changes in bond strengths are observed in $NH^+\cdot N$ dimers of alkylamines and pyridines.[62] The IHB bond energies of proton-bound dimers of primary amides are constant at 27 ± 2 kcal/mol despite a variation of the gas-phase basicities (GBs) by 16 kcal/mol, but the IHBs were weaker in *N*,*N*-dimethylamides the GBs of which are still higher. In this set, the protonated dimer of formamide with the lowest GB had the highest bond energy, and that of *N*,*N*-dimethylpivalamide with the highest GB had the weakest IHB.[63] Similarly, homodimers of the amino acids alanine, glycine, and lysine all have bonding energies of 26.5 ± 1.5 kcal/mol, similar to amine dimers, despite their various PAs and structures.[18]

However, $SH^+\cdot S$ bonds behave differently. Bond energies of 12.8 or 15.4 kcal/mol were reported for $H_2SH^+\cdot H_2S$,[61,64] but much larger values of 26.4 kcal/mol for $(CH_3)_2SH^+\cdot(CH_3)_2S$ and 26.4 kcal/mol for $(CH_3)(C_2H_5)SH^+\cdot(CH_3)(C_2H_5)S$ were measured.[54]

Other than S, there are only a few studies on IHB interactions with acceptors or donors of third or higher row elements. An early study found a relatively weak binding energy of $PH_4^+\cdot PH_3$ of 11.5 kcal/mol, decreasing to 9.2, 7.3, 6.2, and 5.5 kcal/mol for the bonding of further PH_3 molecules. The bonding energies of $P_2H_5^+$ and $P_3H_6^+$ to PH_3 were 9 and 10.8 kcal/mol, respectively. The small bonding energy in $PH_4^+\cdot PH_3$ was attributed to the small dipole moment and the large radius and large ion−neutral separation.[65]

The bonding energy of protonated ferrocene Cp_2FeH^+ to CH_3CN was found to be <8 kcal/mol. H/D exchange reactions indicated that Cp_2FeH^+ is protonated on Fe, and this suggested that $-FeH^+$ is a poor IHB donor.[66] However, the poor bonding of Cp_2FeH^+ may be a special case resulting from a shielded or agostically bonded proton, because subsequently $(CO)_5FeH^+$ was found to bond to CH_3CN by 17 kcal/mol, and proton affinity correlation considerations suggested that the donor efficiency of the $-FeH^+$ is similar to $-SH^+$ donors.[67]

Although the above linear correlations reproduce measured hydrogen bond energies for practical purposes, there is no basic reason that these correlations should be linear. Zeegers-Huyskens pointed this out and proposed an exponential form of the correlation, where $\Delta H^{\circ}_D = x \exp(-x')\ |\Delta PA|$. This was found to agree better with experiment than the Marcus equation. The derivative of the exponential equation was found to be related to the potential curve and barrier for proton motion between the components. Interestingly, Zeegers-Huyskens and co-workers also showed that the correlations between proton affinity or acidity differences and hydrogen bond energies include even neutral OH···O and NH···N hydrogen bonds from dimers of simple molecules to complexes of nucleic bases with water.[68−73] Such dimers may be considered as $A^--H^+\cdots B$ dimers and the hydrogen bond energy is correlated with the proton affinity difference between A^- and B. The relationship in Figure 9 shows a continuous nonlinear relation over hydrogen bonds from 3 to 30 kcal/mol and over a very wide ΔPA range from 0 to 170 kcal/mol. It can be seen to be composed of three linear ranges, and the slopes are correlated with the absolute strengths of the bonds in each range. The neutral hydrogen bonds involve substituted phenol donors and various organic O and N bases as acceptors. The value of ΔPA was found to be an important determinant of hydrogen bond energy, but since not all homodimers (ΔPA = 0) have equal bond energies, it was concluded that other factors are also significant.[68]

2.2.2. Dimer Anions: Bond Strengths and Correlations with Acidities

Correlations similar to the cationic IHBs also apply in anionic $A^-\cdots HA'$ hydrogen bonds. The first linear correlation between ΔH°_D and the difference between the gas-phase acid dissociation energies of the components, $\Delta\Delta H^{\circ}_{acid}$, was observed by the Kebarle group in 1971 in the hydration of the halide and NO_2^-, NO_3^-, and OH^- anions.[38,74] Larson and McMahon presented several major data sets for anionic IHBs in $OH\cdot F^-$, $SH\cdot F^-$, and $CH\cdot F^-$ type bonds and discussed the factors that contribute to bonding.[57]

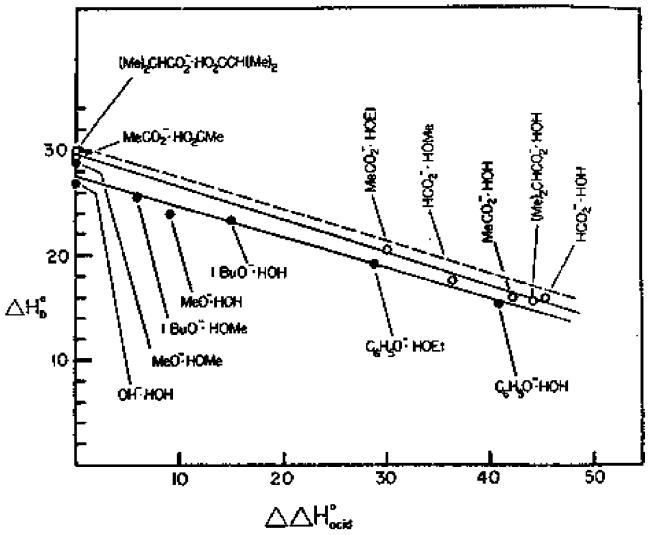

Figure 10. Correlation between ΔH°_D and $\Delta\Delta H^\circ_{acid}$ for $RCOO^-\cdot HO$ bonds (○) and $RO^-\cdot HO$ bonds (●) and for protonated cationic $OH^+\cdot O$ bonds (dashed line). Reproduced from ref 55 with permission. Copyright 1986 American Chemical Society.

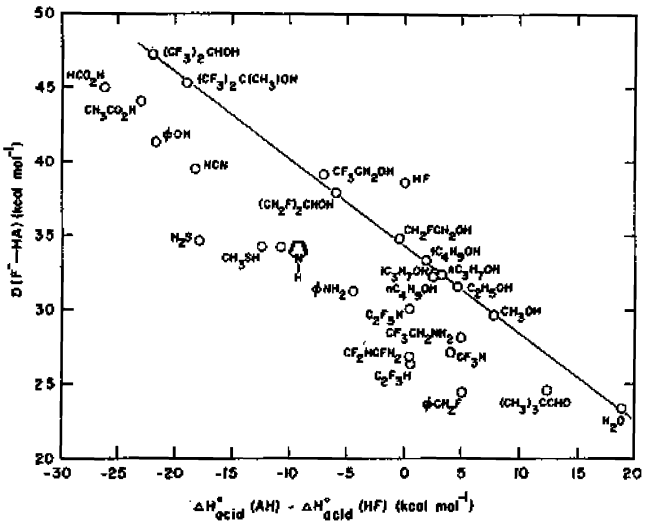

Figure 11. Correlation of fluoride bonding energies with the difference between the acid dissociation enthalpies of the hydrogen donor Bronsted acids and that of HF. Reproduced from ref 57 with permission. Copyright 1983 American Chemical Society.

Other bond types investigated include $OH\cdot Cl^-$ and $CH\cdot Cl^-$,[7,41] bihalide ion XHX^- and XHY^- complexes,[75] halide ion complexes with ROH and RCOOH[76] and with NH_3,[77] complexes of CN^- with OH, SH, and CH donors,[8,78] the bonding of CH_3COO^-, HS^-, CN^-, and Cl^- with ROH, RCOOH. and CH hydrogen donors,[79] further studies of $OH\cdot O^-$ bonds,[33] and bonds of carbanions with OH and CH donors.[58] Table 2 lists empirical linear correlation parameters between ΔH°_D and $\Delta\Delta H_{acid}$ from some of these studies.

a. Oxygen Acids. Anionic IHBs of the $OH\cdot O^-$ type involving neutral and ionic H_2O, RCOOH, and ROH groups are of general interest because they occur in solution as well as in biology. As in the formation of cation dimers, in these bonds the positive charge also increases on the bonding hydrogen, the bonding O atoms become more negatively charged, and the $H-O^-$ bond stretches upon the formation of the hydrogen bond.

Correlations between ΔH°_D and $\Delta\Delta H^\circ_{acid}$ for $OH\cdot O^-$ bonds were expressed by a two-parameter linear equation for $ROH\cdot O^-R'$ complexes.[6]

$$\Delta H^\circ_D = -0.31\Delta H^\circ_{acid}(ROH) + 0.40\Delta H^\circ_{acid}(R'OH) - 15.0 \text{ kcal/mol} \quad (8)$$

Subsequently, it was found that a single-parameter correlation covers $RO^-\cdots HO$ and $RCOO^-\cdots HO$ bonds adequately, as shown in Figure 10, leading to the parameters in Table 2.

The parameters in Table 2 show the similarity between the $OH^+\cdot O$ and $OH\cdot O^-$ bond strength for an equal ΔPA or $\Delta\Delta H^\circ_{acid}$ difference (as noted above, the ΔPA or $\Delta\Delta H^\circ_{acid}$ parameters are equivalent as $\Delta H^\circ_{acid}(A^- - H^+) = PA(A^-)$). In terms of the absolute PAs of the components, we note that $OH^+\cdot O$ and $OH\cdot O^-$ complexes for components with a given ΔPA or $\Delta\Delta H^\circ_{acid}$ have similar bond energies although the absolute proton affinities of the components of cationic dimers (PA(B)) are usually 160−240 kcal/mol while those for the anionic dimers ($PA(A^-)$) are much higher, usually 360−420 kcal/mol.

Linear correlations were also found to apply to further dimers of CH_3COO^-, CN^-, Cl^-, and SH^- with ROH, RCOOH, and C_4H_4NH (pyrrole), while the carbon acids CH_3CHO, $(CH_3)_2CO$, and CH_3CN gave bonds weaker by about 4 kcal/mol.[56,58,79]

A special case of $OH\cdot O^-$ and $OH\cdot N^-$ bonds involves the carbanions CH_2CN^-, CH_2CO^-, $CH_3COCH_2^-$, and $CF_3COCH_2^-$, which bond to H_2O by 13−15 kcal/mol. The thermochemistry and theoretical calculations suggested that the oxygen atoms are the favored acceptor sites to bind the hydrogen of the donor H_2O molecules.[80]

The pyrrolide anion, $c\text{-}C_4H_4N^-$, also bonds fairly strongly to H_2O (15.7 kcal/mol) and to CH_3OH (18.6 kcal/mol), more strongly than the bonding of the delocalized $c\text{-}C_5H_5^-$ anion to these ligands. This suggests localized $OH\cdot N^-$ interactions in the complexes of the pyrrolidine anion.[58]

b. Complexes of Halide Ions. Early studies showed correlations between ΔH°_D and the acid dissociation energy, $\Delta\Delta H^\circ_{acid}$, of the hydrogen donor ligands in complexes of Cl^- with substituted phenols[81] and with substituted acids.[41] A two-parameter correlation for various $AH\cdot A'^-$ bonds was given by Yamdagni and Kebarle.[39]

$$\Delta H^\circ_D = -0.134\Delta H^\circ_{acid}(AH) + 0.20\Delta H^\circ_{acid}(R'OH) \quad (9)$$

Similar relations were observed in complexes of F^- with alcohols, and parallel correlation lines were established for complexes of F^- with various carboxylic and CH, SH, and NH acids over a ΔH°_D range of 22−48 kcal/mol and a $\Delta\Delta H^\circ_{acid}$ range of 40 kcal/mol (Figure 11). The weaker bonding energies for the complexes of ROOH and C_6H_5OH vs ROH donors suggests that IHB formation decreases the resonance stabilization of the neutral donors.[57,82]

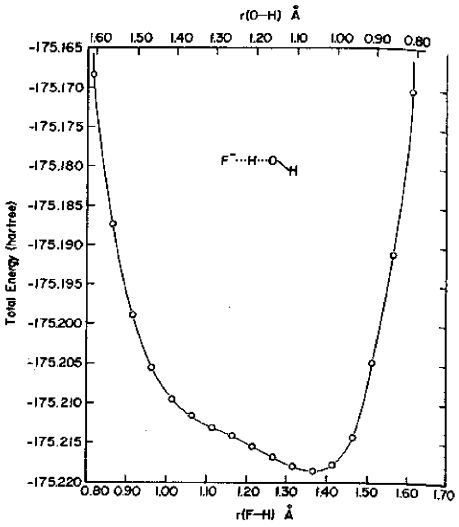

Figure 12. Proton potential for the hydrogen-bonded adduct of F^- and H_2O obtained at a total separation of 2.52 Å, using 4-31G basis set calculation. Reproduced from ref 57 with permission. Copyright 1983 American Chemical Society.

The fact that the relation is continuous for donors with ΔH°_{acid} both below and above HF suggested that the nature of the bonding does not change whether the proton is near F or O in the FH···O^- bonds, indicating a single-well or a low-barrier double-well bonding surface. Figure 12 shows that this was confirmed theoretically.

Inverse correlations along continuous nonlinear lines between ΔH°_D and $\Delta\Delta H^\circ_{acid}$ were also found in the association of alcohols and acids with Cl^-, NO_2^-, and $C_6H_5NO_2^-$, the first two ions giving bonding energies higher by about 2.1 kcal/mol than the latter ion.[83]

Larson and McMahon suggested an empirical correlation based on the gas-phase acidities and electronegativities, χ, of the components.[8]

$$\Delta H^\circ_D(X^-\cdots HY) = (443 - \Delta H^\circ_{acid}(Y^- - H))[(\chi(X) + \chi(Y))/12 + (\Delta H^\circ_{acid}(X^- - H^+))/300 - 1.4] \quad (10)$$

The authors applied the equation successfully with a standard deviation of 2.0 kcal/mol to 56 dimers of a wide range of complexes involving halide, alkoxide, acetate, and $C_6H_5C_2^-$ anion acceptors and alcohols, acids, hydrogen halides, H_2S, and several carbon acids, such as C_6H_6, CH_3COCH_3, CF_3H, and C_6H_5-CH_2F, as donors.[8]

Interestingly, the bond strengths of CH_3COO^-, CN^-, Cl^-, and HS^- with a given neutral ligand are usually similar.[79] This occurs although different factors affect the bond strengths in these complexes. Bonding to the first two ions is weakened by delocalization, while that to the last two is weakened by polarization and ionic radius effects.[80] The complex forces seem to balance to give a fortuitously simple uniform behavior.

Hydrogen bonding of the Cl^- ion was investigated extensively. The Kebarle group determined the binding free energies of Cl^- with 40 OH and CH donors. The OH donors included H_2O, CH_3OH, t-C_4H_9OH, HCOOH, CH_3COOH, and C_6H_5OH and the CH donors included various ketones and toluenes. For the OH donors continuous inverse correlations were found between $\Delta\Delta H_{acid}$ and ΔH°_D over an acidity range of 60 kcal/mol. Similar relations applied for the CH acids, but for a given $\Delta\Delta H^\circ_{acid}$, the bonding energies were lower by about 8−10 kcal/mol. Cyclopentadiene, although a strong carbon acid, gave much weaker bonding as a hydrogen donor than expected from these correlations. Apparently, its strong acidity reflects resonance stabilization of the $C_5H_4^-$ anion, rather than a large positive charge on the protons of this donor molecule.[41]

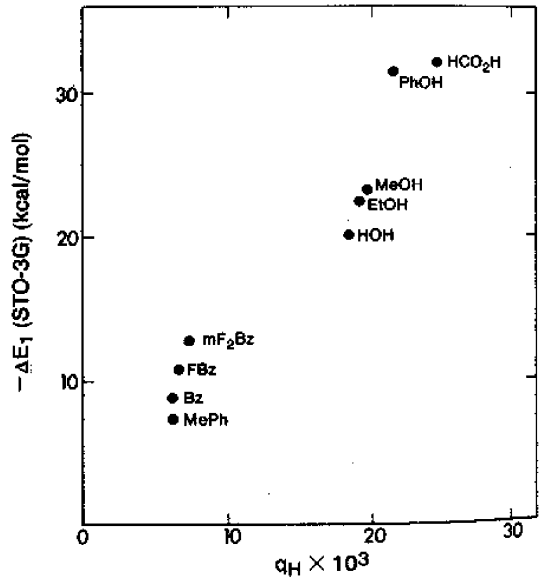

Figure 13. Correlation between the bonding energy, ΔH°_D, of Cl^- complexes and the charge on the bonding hydrogen atoms of the donor molecule, q_H, before bond formation. The plot illustrates the significance of the electrostatic interactions between the bonding hydrogen and the chloride anion. Reproduced from ref 41 with permission. Copyright 1982 NRC Research Press.

Molecular orbital STO-3G calculations showed good correlations between the bond dissociation energies and the charge on the donor protons (Figure 13) and also a correlation with the charge transferred from Cl^- to the proton donors (Figure 14).[41]

A further study of the bonding of ROH and RCOOH (R = H, Me, Et, i-Pr, or t-Bu) to F^-, Cl^-, and I^- showed bonding energies from 23 to 34 kcal/mol for ROH·F^- and as large as 41.7 and 45.3 kcal/mol in MeCOOH·F^- and HCOOH·F^-, respectively. Bonding energies to Cl^- and I^- were smaller, as may be expected on the basis of the ionic radii. An interesting feature illustrated in Figure 15 is the bifurcated structure in H_2O·I^- and both an OH and a CH bond to the ion in RCOOH·I^- complexes.[76]

Complexes of halide ions with NH_3 were found by Castleman and co-workers to have relatively small bonding energies of 8.2 kcal/mol (NH_3·Cl^-), 7.7 kcal/mol (NH_3·Br^-), and 7.4 kcal/mol (NH_3·I^-), corresponding to the low acidity of NH_3.[77] These workers analyzed the electrostatic factors that contribute to the bonding and found various orientations of the NH_3 molecule with respect to the various halide ions with significant effects of the quadrupole moments.

Most of the thermochemistry of dimers was obtained by equilibrium measurements, but some were

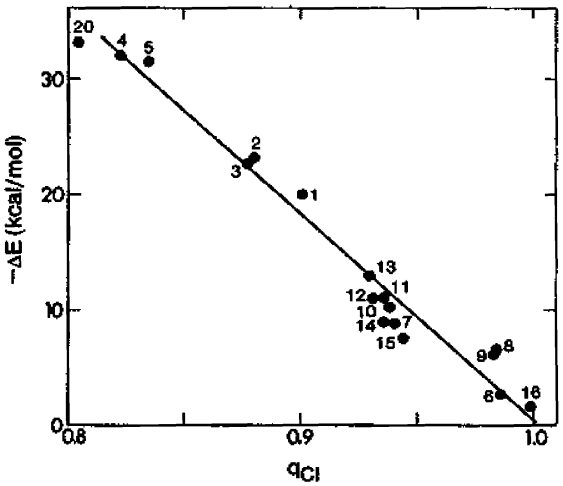

Figure 14. Correlation between ΔH°_D of Cl^- complexes and the negative charge on Cl^- in $RH\cdot Cl^-$ complexes after bond formation. The plot shows good correlation between the bonding in the complex and the negative charge transferred from Cl^- to RH on formation of the complex. Reproduced from ref 41 with permission. Copyright 1982 NRC Research Press.

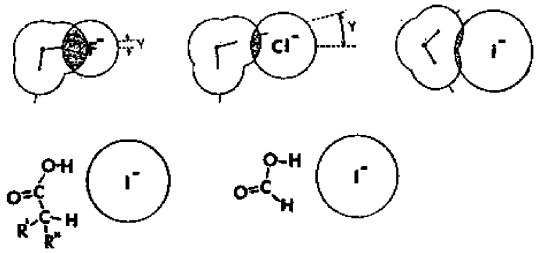

Figure 15. Geometries of complexes of halide anions. The geometries of the $HOH\cdot F^-$ and $HOH\cdot Cl^-$ complexes were obtained from ab inito calculations. The geometries of $HOH\cdots I^-$ and the proposed polydentate structures for complexes of carboxylic acids with I^- were obtained from electrostatic calculations. These geometries maximize the interactions of OH, CO, and CH dipoles with the ions. Reproduced from ref 76 with permission. Copyright 1984 American Chemical Society.

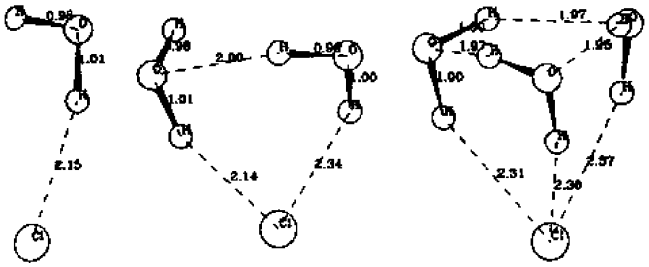

Figure 16. Hydrogen-bond networks in $Cl^-(H_2O)_n$ complexes calculated using density functional theory (DFT) with a DZVP basis set. Reproduced from ref 15 with permission. Copyright 1995 American Chemical Society.

verified by different techniques. One such verification concerned $Cl^-(H_2O)_n$ bonding energies, which were measured by thermal radiation-induced dissociation as 11.6 and 9.5 kcal/mol for $n = 2$ and 3, respectively, in good agreement with equilibrium studies.[15] The calculated DFT minimum-energy structures in Figure 16 show that even in these small clusters, a network of water−water IHBs was formed. Also, the bonding energies of water clusters $(H_2O)_nH^+$ were verified by collisional dissociation measurements.[14]

c. Theory and Spectroscopy of Anionic Complexes. Theoretical calculations support the experimental bonding energies of dimer ions. For example, Pudzianowski studied 10−15 key anionic $O^-\cdot HO$ and cationic $OH^+\cdot O$, $NH^+\cdot N$, and $NH^+\cdot O$ type dimers both at high-level ab initio and density function theory methods. In most dimers, the calculations agreed with experiment within the experimental uncertainty of ±2 kcal/mol of the binding energies.[84,85] Numerous other theoretical studies agreed with experiment for various dimers and larger clusters.

The development of IHB networks about halide ions was investigated by IR spectroscopy. A recent review summarized the applications of vibrational dissociation spectroscopy to the morphology of small water networks attached to anions. Charge transfer to the solvent affects the structures of IHB networks about the ions. The negatively charged water clusters $(H_2O)_n^-$ provide information on how diffuse excess electrons interact with the water networks.[86] Important factors contributing to the ion-bound OH stretch frequencies were found to be the radius and excess charge associated with the halide, which determine the electric field at the surface of the ion.[87]

As to the location of the ion, the solvation of F^- by up to five H_2O molecules indicated the ion to be inside the solvent shell. In contrast, Cl^-, Br^-, and I^- remain on the surface of solvating water clusters. Similarly, Cl^- and I^- remain on the surface of solvating methanol clusters, in which methanol−methanol hydrogen bonds appear after four or more methanol molecules.[88]

d. Bihalide Complexes. A strong IHB of 38.6 kcal/mol was observed in $F^-\cdot HF$ by Larson and McMahon, who also investigated many complexes of F^-, Cl^-, and CN^- with OH hydrogen donors (alcohols and acids), as well as CH hydrogen donors. These studies showed a stronger dependence of the F^- binding energies on the gas-phase acidity of the donors, with a correlation slope of 0.5, than in the Cl^- bonding energies, with a correlation slope of 0.2. The F^- bonding also shows more preference to OH vs CH donors than Cl^- bonding. Both trends are consistent with a stronger covalent component in the F^- complexes, while the Cl^- complexes are mostly electrostatic.[7]

Bond strengths in bihalide ions were measured by Caldwell and Kebarle, as well as the bonding energies to SO_2. In the homodimers $XH\cdot X^-$, the ΔH°_D values decrease from 38.6 to 23.5, 20.9, and 17.0 kcal/mol for X = F, Cl, Br, and I, as may be expected based on the ionic radii. In mixed dimers $YH\cdot X^-$, the ΔH°_D values increase with increasing acidity of YH, similar to other correlations of ΔH°_D and $\Delta\Delta H^\circ_{acid}$.[75]

2.3. Structural Effects: Isotropy, Resonance, and Steric Hindrance

2.3.1. Does Isotropy Affect the Bond Strengths?

The bond strengths of complexes of CH_3COO^-, CN^-, and HS^- with a variety of ligands are comparable to the complexes of Cl^-, although the former are anisotropic while the latter is a spherical monatomic ion. Similarly, bond strengths in complexes

of CN^- vs Cl^- with HCN and of NH_4^+ vs K^+ with various neutrals were comparable, as is also the thermochemistry of CN^- vs Cl^-, of H_3O^+ vs Na^+, and of NH_4^+ vs K^+ in the condensed phase.[43,89,90] Whether the ion appears isotropic or anistotropic to a ligand depends on the distance. For example, the interaction energy of NH_4^+ with a model dipole depends strongly on the charge distribution and orientation of the ion when the distance from the central N atom to the center of the dipole is <2.5 Å since at such short hypothetical distances the effects of the atoms closest to the ligand would dominate. However, these factors have little effect at realistic separations of >3 Å, as illustrated in Figure 17. At these distances the contributions of the various atoms of the ion balance so that NH_4^+ appears to the ligand as an isotropic spherical ion with unit charge at the central N atom.[89] However, larger ions where some partially charged groups are much more distant from the ligand may not act as point charges, and the charge density at the bonding proton may be dominant.

2.3.2. Resonance

The hydrogen bond strength can be affected by special structural factors. For example, when an ion is stabilized by charge resonance such as $(CH_3COOH)H^+ = CH_3C(OH)_2^+$, then formation of the IHB can perturb the resonance, and the loss of this stabilization energy makes the overall bond formation less exothermic. This occurs when protonated acids such as $CH_3C(OH)_2^+$ bond to a neutral CH_3COOH molecule to form the dimer ion in $(CH_3COOH)H^+ \cdot CH_3COOH$. In this case, ΔH°_D is lower by about 2 kcal/mol than in protonated dimers of alcohols and ketones.[50]

In anions, weaker bonding energies were observed in the complexes of ROOH and C_6H_5OH versus ROH donors in their complexes with a common anionic hydrogen acceptor, even when the relative acidities of the components were similar. The decreased bond energies with the ROOH and C_6H_5OH donors suggests that IHB formation increases the negative charge on the bonding oxygens of the ligands, which decreases their resonance stabilization.[57,82] Resonance effects can also affect the IHB strength of heterocyclic aromatics.[73]

2.3.3. Steric Hindrance

The components of gas-phase dimers can usually assume optimized geometries and free rotation about the IHBs, but bulky substituents may impose constraints.

The effects of steric hindrance were examined in bulky alkylamines and alkylpyridines,[91] and ΔG°_D was found to decrease systematically with increasing steric hindrance. However, this was found to be an entropy rather than enthalpy effect, and even in dimers of bulky 2,6-dialkylpyridines, ΔH°_D remained constant at about 23 kcal/mol, similar to other $NH^+ \cdot$ N bonds. The optimal bonding energy suggested that the $NH^+ \cdot N$ bonds could reach their optimal lengths. Space-filling models confirmed this but showed that substituents on the two component molecules interfere with each other within the volumes of rotation

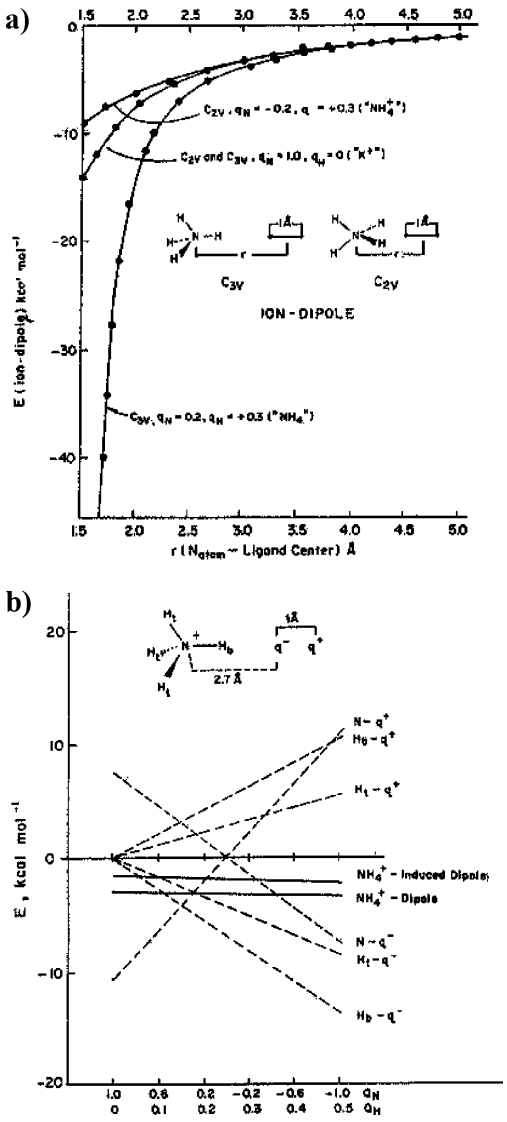

Figure 17. Calculated electrostatic bonding energies between NH_4^+ and its atoms and a model polar molecule with polarizability of 1 Å^3 and dipole moment of 1 D. Panel a illustrates effects of orientation. The panel shows the variation of the ion−dipole energy with the N atom to ligand center distance r for complexes in which the NH_4^+ ion has two different orientations and two different charge distributions. In the C_{2v} geometry NH_4^+ is shown with charge distribution $q_N = 1.0$ and $q_H = 0$ unit charge, equivalent to the spherical K^+ cation, and with $q_N = -0.2$ and $q_H = +0.3$, which represents the NH_4^+ cation. The C_{2v} and C_{3v} curves for the K^+ like spherical charge distribution are identical. The graph shows that the overall binding energy of the complex in either geometry or ionic charge distribution become nearly equal when $r(N_{atom}-\text{ligand center}) > 3$ Å, at realistic ion−ligand distances. The ion-induced dipole forces were found to behave similarly. Panel b illustrates effects of charge distribution. Interaction energies of individual atomic charges on NH_4^+ in a C_{3v} complex with the polar molecule at a N to negative dipole end distance of 2.7 Å are shown as the charge distributions on NH_4^+ vary from $q_N = 1.0$ and $q_H = 0$, simulating a spherical K^+ ion, to an extreme anisotropic charge distribution of $q_N = -1$ and $q_H = 0.5$. The distribution of the ionic charge affects the interaction energies of each atom of NH_4^+ with the dipole of the ligand. However, the total ion−dipole and ion-induced dipole interaction energies are nearly constant due to canceling effects of the individual interaction energies. Reproduced from ref 89 with permission. Copyright 1991 American Chemical Society.

of the alkyl groups. Correspondingly, the entropy of dimer formation changes from −28.2 cal/(mol K) in $(pyridine)_2H^+$ to −33.2, −37.4, and −48.4 cal/(mol K) in the dimers of the protonated 2,6-di-Me, 2,6-di-Et, and 2,6-di-*i*-pyridine compounds.

In the amine dimers $(R_3N)_2H^+$, the bonding energy first decreases from 25.2 kcal/mol in $(NH_3)_2H^+$ to 22.2 kcal/mol in $(Me_3N)_2H^+$, but the trend reverses, and the bonding energy increases again to 23.8 kcal/mol in $((Et)_3N)_2H^+$ and 24.4 kcal/mol in $((n\text{-}Bu)_3N)_3H^+$, possibly due to attractive dispersion forces between the interacting alkyl substituents of the two components. While the bonding energies change little, interference between the rotational volumes of the alkyl groups of the two components results in very large negative entropies of dimer formation, from −32.0 cal/(mol K) in $(Me_3N)_2H^+$ to −41.0 cal/(mol K) in $(Et_3N)_2H^+$ and −56.5 cal/(mol K) in $((n\text{-}Bu_3)N))$-H^+.

Even bonding to the small H_2O molecule can interfere with large alkyl rotors. From $(pyridine)H^+\cdot H_2O$ to $(2,6\text{-}(di\text{-}t\text{-}Bu)pyridine)H^+\cdot H_2O$, the entropy of dimer formation changes from −27 to −41 cal/(mol K), and from $Me_3NH^+\cdot H_2O$ to $(n\text{-}But)_3NH^+\cdot H_2O$, the entropy of association changes from −24.1 to −36.4 cal/(mol K). The small H_2O ligand molecule seems to interpose between the large alkyl groups and inhibit their rotations (Figure 18). The low basicity of 2,6-(di-*t*-Bu)pyridine in solution may be due therefore to the unfavorable entropy of hydration of the protonated ion. Similarly, steric interference with methyl groups and NH_3 leads to nonlinear IHBs in complexes with methylated pyrazoles and imidazoles.

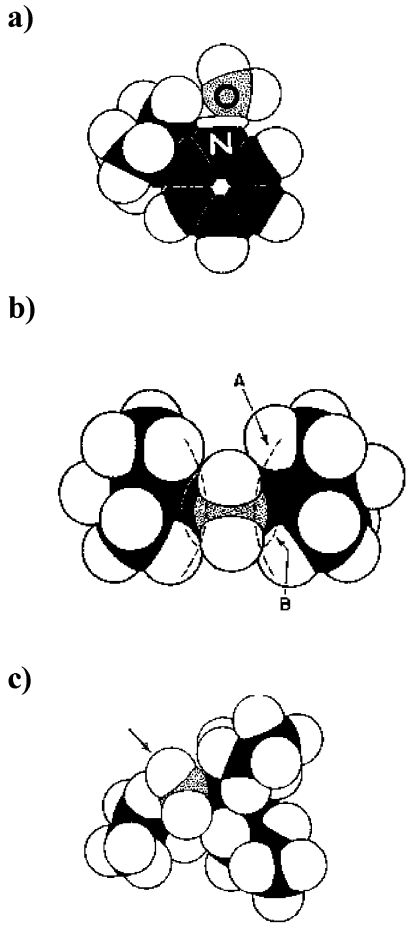

Figure 18. Steric interference between the rotations of the alkyl groups in complexes (a) $(2\text{-}tert\text{-}butylpyridine)H^+\cdot H_2O$, (b) $2,6\text{-}(di\text{-}tert\text{-}butylpyridine)H^+\cdot H_2O$, and (c) $(n\text{-}But)_3NH^+\cdot H_2O$. The water molecule (gray oxygen) interferes with the volumes of rotation of the alkyl groups leading to large negative entropies of association. Reproduced from ref 91 with permission. Copyright 1983 American Chemical Society.

2.4. Carbon-Based Bonds

A special class of IHBs involves bonds where the acceptor or donor groups are carbon-based. The first carbon-based hydrogen bond was identified in 1937 by Glasstone in $(CH_3)_2CO\cdot HCCl_3$.[92] In ionic systems, the donors may be alkyl hydrogens in $CH^{\delta+}\cdots$O, N, or S bonds and in $CH\cdots O^-$, N^-, S^-, or $halide^-$ bonds. The acceptors may be π electrons of olefins or aromatics in $BH^+\cdot\pi$ complexes or the π systems of aromatic anions in $BH\cdot\pi^-$ bonds, or carbon lone pairs in $BH^+\cdot$C (isonitrile) bonds. In some complexes both the acceptor and donor may be carbon-based, as in $CH^{\delta+}\cdot\pi$ bonds. Several of these bond types appear in biological systems.

In the first thermochemical studies on ionic CH·X systems, Larson and McMahon studied a large number of complexes of F^- and Cl^- with hydrocarbon CH donors.[7,57] In cations, Meot-Ner and Deakyne studied unconventional carbon-based IHBs in complexes of quaternary ammonium ions and in π complexes.[93,94] Recently, Blades and Kebarle studied bonds where doubly charged quaternary ions served as donors.[95] Table 3 shows the available thermochemical data. Some unconventional IHBs have biological roles, for example, in the interactions of acetylcholine neurotransmitters with receptors.

2.4.1. Cationic Complexes with CH Donors

A theoretical study by Uggerud found that CH_3^+ can serve as a hydrogen donor for IHB interactions with NH_3 and H_2O molecules.[96] Experimentally, $CH^{\delta+}\cdot$B bonds were investigated in complexes of quaternary ammonium ions with O acceptors.[93] The bond strengths range between 9 and 20 kcal/mol. The bond strength of 9 kcal/mol seems to be typical for $CH^{\delta+}\cdot H_2O$ bonds as this value is observed for diverse ions such as $C_3H_3^+$, $C_6H_6^{\bullet+}$, and $N(CH_3)_4^+$ (Table 3). Ab initio calculations showed that in the complex $(CH_4)_4N^+\cdot OH_2$, where ΔH°_D is 9.4 kcal/mol, the most stable conformation involves a cavity formed by three H atoms of two methyl groups that accommodate the ligand molecule (Figure 19). The second water molecule seems to bond preferentially to the first water molecule in an outer position forming a conventional $OH^{\delta+}\cdot$O hydrogen bond. This may account for the anomaly that the second bond is slightly stronger than the first bond. An isomeric structure where the two H_2O molecules bond directly to two cavities formed by the methyl groups of the ion is less stable, although only by 1.2 kcal/mol, and the two isomers may be present in the observed equilibrium populations. However, in complexes of $(CH_3)_4N^+$ with blocked ligands such as Me_2CO, both the first and second ligand molecules can form only CH·X bonds, and here the second molecule is indeed bonded more weakly

Table 3. Thermochemistry of Unconventional Carbon-Based Ionic Hydrogen Bonds

ion	ligand	ΔH°_D[a]	ΔS°_D[a]	refs
		$CH^+\cdots B$ bonds		
Me_3C^+	H_2O[b]	11.2	22	64
		[11][c]	[35][d]	
	MeOH[b]	15.1[e]	21.1[e]	123
		$[24.9]_{cond}$[c]		
		$[29.1]_{cond}$[f]	[54.0][f]	
	EtOH[b]	20.4[e]	27.6[e]	123
		$[35.6]_{cond}$[c]		
		$[38.6]_{cond}$[f]	$[72.9]_{cond}$[f]	
	Me_2O[b]	23.2[e]	36.0[e]	123
		$[33.2]_{cond}$[f]	$[62.1]_{cond}$[f]	
	Et_2O[b]	33.7[e]	52.4[e]	123
		$[46.3]_{cond}$[f]	$[86.4]_{cond}$[f]	
	Me_2CO[b]	19.2[d]	24.2[d]	123
		$[33.5]_{cond}$[e]	$[54.4]_{cond}$[e]	
	MeCN[b]	20.4[e]	20.5[e]	123
		$[35.0]_{cond}$[f]	$[45.4]_{cond}$[f]	
	HCN	16.3	25.0	102
		$[24.4]_{cond}$[g]		
		$[30.9]_{cond}$[h]		
$MeCHOMe^+$	H_2O[b]	11.2	19	100
		$[7]_{cond}$[c]	$[31]_{cond}$[d]	
	MeOH[b]	13.1	21	100
		$[14]_{cond}$[c]	$[40]_{cond}$[d]	
Me_2COMe^+	H_2O[b]	10.8	23	100
		$[4]_{cond}$[c]	$[31]_{cond}$[d]	
Me_4N^+	H_2O	9.0	21.5	93
	H_2O (2)[i]	9.4		93
	MeOH	9.8	23.2	93
	MeOH (2)[i]	9.2	24.0	93
	Me_2CO	14.6	24.7	93
	Me_2CO (2)[i]	13.0	29.2	93
	Me_2CO (3)[i]	11.7		93
	$MeO(CH_2CH_2O)_2Me$	20.6	28.7	93
	$MeO(CH_2CH_2O)_3Me$	24.2	33.8	93
	$MeCONMe_2$	18.0	21.6	93
	$MeNH_2$	8.7	17.0	93
	Me_3N	9.9	20.6	93
	MeCO-gly-OMe	20.1	29.4	93
Et_4N^+	H_2O	7.0		93
	Me_2CO	12.4	26.7	93
Me_3O^+	Me_2O	13.0	28.4	93
$MeCNMe^+$	H_2O	10.0	22.0	42
$Me_3N(CH_2)_2NMe_3^{+2}$	H_2O	12.7	19.3	95
	H_2O (2)[i]	12.2	19.8	95
$Me_3N(CH_2)_3NMe_3^{+2}$	H_2O	11.0	16.5	95
	H_2O (2)[i]	10.7	19.0	95
$MeOCH_2CH_2NMe_3^+$ (acetylcholine)	H_2O	8.0	22.0	124
	Me_2CO	13.2	21.7	124
$(c\text{-}C_4H_4O)H^+$	H_2O	10.2	19.7	101
$MeNCH^+$	H_2O	14.8	19.7	42
	MeOH	19.0	23.2	42
	Me_2O	21.2	21.9	42
	MeCN	19.1	18.7	42
$c\text{-}C_3H_3^+$	H_2O	10.6	16.7	117
	H_2O(2)	9.2	16.6	117
$C_6H_6^{\bullet+}$	H_2O	9.0	19.5	117
	H_2O (2)[i]	8.0	18.9	117
	H_2O (3)[i]	8		117
	H_2O (4)[i]	10.3	22.4	117
	H_2O (5)[i]	8.6	18.1	117
	H_2O (6)[i]	7.8	15.1	117
		$BH^+\cdots C$ and $CH^+\cdots C$ Bonds (Isocyanide Ligands)		
NH_4^+	MeNC	24.0	20.2	42
$MeNH_3^+$		23.8	22.7	42
$Me_2NH_2^+$		20.6	21.5	42
Me_3NH^+		19.5	20.7	42
$MeNH_3^+$	EtNC	23.8	24.3	42
$MeNCH^+$	MeNC	25.2	24.7	42
$EtNCH^+$	EtNC	25.2	23.8	42

Table 3. (Continued)

ion	ligand	ΔH°_D[a]	ΔS°_D[a]	refs
	$BH^+\cdot\pi$ Bonds			
NH_4^+	C_2H_4[b]	10		94
		$[26]_{cond}$[c]		
	C_6H_6	19.3	23.3	94
	C_6H_5F	14.4	18.0	94
	1,3,5-$C_6H_3Me_3$	21.8	21.2	94
$MeNH_3^+$	C_6H_6	18.8	25.1	94
	c$-C_6H_{10}$	11.6	16.9	94
	c$-C_4H_4N$	18.6	21.0	94
Me_3NH^+	C_6H_6	15.9	27.7	94
$EtOH_2^+$	C_6H_6	21		94
	$CH^+\cdots\pi$ Bonds			
Me_4N^+	C_6H_6	8.6	18.4	124
	$C_6H_5CH_3$	9.5	20.3	93
$MeOCH_2CH_2NMe_3^+$ (acetylcholine)	$C_6H_5CH_3$	8.1	15.5	124
	$X^-\cdots HC$ Bonds			
$CH_3C(CH_2)O^-$	CH_3CN	15.3	18.9	58
CH_2CN^-		12.8	13.4	58
$CH_2NO_2^-$	CH_3NO_2	15.9	25	114
$CH_3NO_2^-$		15.2		114
$CH_3NO_4^-$		13.0	22	114
F^-	HCN	39.5		57
	CH_2CO	35.3		57
	C_2F_5H	30.4		57
	CF_3H	27.1		57
	Me_3CCHO	24.6		57
	$C_6H_5CH_2F$	24.4		57
	t-C_4H_9F	22.3		57
	H_2CCH_2	8.8	14	113
	CH_3CHCH_2	9.8	16	113
Cl^-	HCN	21.0		7
	CH_3F	11.5		7
	CH_3CN	15.8		7
	CH_3Cl	12.2		7
	CH_2Cl_2	15.8		7
	CHF_3	16.7		7
	C_6H_6	9.9		7
	MeCHO	14.4		7
	Me_3CCHO	15.0		7
	Me_2CO	14.8		7
	(Me)(Et)CO	14.8		7
	Et_2CO	14.1		7
	CH_3NO_2	15.6	21.4	114
	H_2CCH_2	5.4	18	113
	CH_3CHCH_2	5.9	16	113
Br^-	H_2CCH_2	4.7	15	113
	CH_3CHCH_2	5.5	15	113
I^-	H_2CCH_2	3.7	14	113
	CH_3CHCH_2	4.6	15	113
NO_2^-	CH_3NO_2	14.5	22.5	114
	$C^-\cdots HO$ and $\pi^-\cdots HO$ Bonds			
HCC^-	H_2O	16.2	18.6	58
	MeOH	21.6	33.6	125
	CF_3	19.3	28.9	126
c-$C_5H_5^-$	H_2O	15.7	17.5	58
	H_2O (2)[i]	10.0	17.4	58
	MeOH	13.2	21.1	58
	t-BuOH	17.0	32.1	58
c-$C_4H_4N^-$	H_2O	15.7	23.1	58
	MeOH	18.6	27.5	58
	$\pi^-\cdot HC$ Bonds			
c-$C_5H_5^-$	Me_2CO	13.5	21.8	58
	MeCN	15.5	22.8	58
c-$C_4H_4N^-$	Me_2CO	13.1	20.5	58
	MeCN	15.8	23.4	58

[a] ΔH°_D values are in kcal/mol and ΔS°_D in cal/(mol K). [b] In these systems, covalent bonds with larger ΔH°_D and ΔS°_D are also possible. [c] Enthalpies of condensation reactions calculated from thermochemical data of refs 127 and 128. [d] Entropies of condensation reactions as estimated in the references for the cited reactions. [e] Thermochemistry of association reactions to form cluster ions at high temperatures usually above 400−450 K. [f] Thermochemistry of association reactions to form covalent adducts, usually below 400−450 K.[123] [g] Bond dissociation energy (ΔH°_D) corresponding to the condensation reaction to form t-$C_4H_9NCH^+$ as estimated from data for isocyanides.[127,128] [h] Bond dissociation energy (ΔH°_D) corresponding to the condensation reaction to form t-$C_4H_9CNH^+$ from the thermochemistry in refs 127 and 128. [i] Shorthand for second or higher ligand molecule.

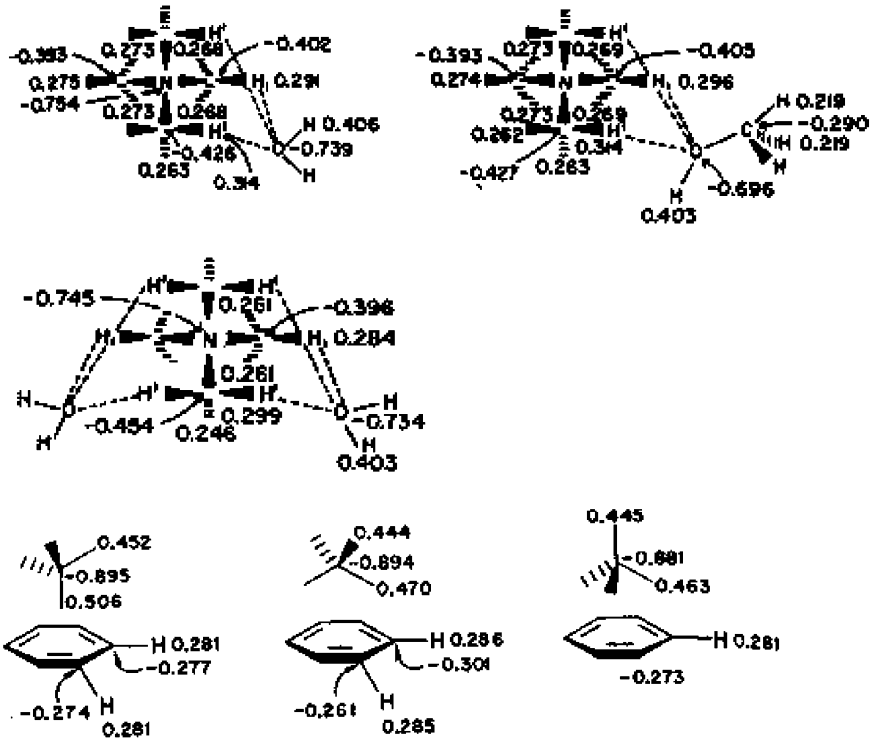

Figure 19. The top panel (from ref 94) shows the structures of $(CH_3)_4N^+ \cdot H_2O$ and $(CH_3)_4N^+ \cdot CH_3OH$ where the oxygen functions fit in a cavity formed by three hydrogens on two methyl groups. The center panel (from ref 93) shows the structure of $(CH_3)_4N^+ \cdot 2H_2O$ where both H_2O molecules are bonded to cavities formed by the methyl groups. This isomer is less stable by 1.2 kcal/mol than a structure where the second water molecule is bonded to the first by an $OH^{\delta+} \cdot O$ bond. The bottom panel (from ref 93) shows the structure of the $NH_4^+ \cdot C_6H_6$ complex in three orientations of NH_4^+ showing $NH_4^+ \cdot \pi$ interactions. Reproduced from refs 93 and 94 with permission. Copyright 1985 American Chemical Society.

than the first, the first two bonds being 14.6 and 13.0 kcal/mol, respectively.[93]

Complexes of doubly charged diquaternary ions were measured recently.[97] Bond strengths in the complexes $(CH_3)_3N(CH_2)_pN(CH_3)_3^{2+} \cdot H_2O$, $p = 2$ and 3, are 11−13 kcal/mol. These bonds are somewhat stronger than the bond of H_2O to the singly charged $(CH_3)_4N^+$ ion, which is 9.0 kcal/mol, because Coulomb interactions between the two charge groups increase the positive charge on the bonding methyl hydrogen of each group in the doubly charged ion. These electrostatic interactions between the ionic groups decrease with increasing separation between the charged groups, and as the charges on the bonding end methyl group hydrogens decrease from $p = 2$ to 3, the bonding energies to the H_2O molecules decrease from 12.7 to 11.0 kcal/mol. The bonding energies of the first and second water molecules to these ions are similar, which indicates that consecutive H_2O molecules add alternatingly to the two functional groups. However, the $\Delta S°$ values observed for $p = 3$ suggest that here the second H_2O molecule may bond to the first H_2O molecule rather than to the second quaternary amine group.[95]

Recently, Hiraoka and co-workers studied the clusters $CH_3(N_2)_n^+$. The thermochemistry and ab initio calculations showed covalent bonding to the first N_2 molecule, a threefold shell structure in $H_3CN_2^+(N_2)_3$ with $n = 4$, and the fourfold shell structure $(N_2)H_3CN_2^+(N_2)_4$ with $n = 6$.[98]

In complexes of $C_2H_5^+$ with CO_2 and N_2O, the nonclassical proton-bridged structure of the ion rearranged to the classical structure in the complexes. The s-$C_3H_7^+$ and t-$C_4H_9^+$ ions bonded to these ligands only by 4−5 kcal/mol due to hyperconjugation.[99]

Complexes with $CH^{\delta+} \cdot B$ bonds in (furan)$H^+ \cdot H_2O$, (pyrrole)$H^+ \cdot H_2O$, and (thiophene)$H^+ \cdot H_2O$ were also investigated.[100,101] The furan and thiophene complexes have small bonding energies, 10.2 kcal/mol. The H_2O molecules bond to the acidic proton on the unprotonated α carbon. In comparison, (pyrrole)H^+ is also ring-protonated, but the N−H hydrogen is strongly acidic, and it is the most strongly hydrogen bonding site. Weak $CH^{\delta+} \cdot OH_2$ bonds may also form in the complexes of the radical ions of these heterocyclic aromatics, such as in (furan)$^{\bullet+} \cdot H_2O$ ($\Delta H_D° =$ 9.8 kcal/mol) and (thiophene)$^{\bullet+} \cdot H_2O$ ($\Delta H_D° = 9.5$ kcal/mol), where the charge is delocalized and the charge densities on the bonding CH sites are smaller than those in the protonated analogues.[101] The complexes of the (benzene)$^{\bullet+}$ ion discussed below also belong to this group.

Bonds with CH donors may also occur in the blocked clusters $(CH_3CNH^+ \cdot NHCH_3) \cdot CH_3CN$,[102] and $((CH_3)_2OH^+ \cdot O(CH_3)_2) \cdot (CH_3)_2O$,[103] where the third molecule is bonded relatively weakly (9.3 and 10.1 kcal/mol, respectively), suggesting that the third ligand is bonded by weak CH·N− or CH·O− hydrogen bonds. Alternatively, these complexes may have T-shaped geometries with a long second H^+−N or H^+−O bond.

Bonds of CH·N type occur in the linear protonated clusters of HCN, that is, in ···HCN·$HCNH^+$·NCH···. The cyanide CH groups are efficient hydrogen donors because of the carbon acidity of the sp carbon hydrogen.[102] In these complexes, the core $HCNH^+$ ion

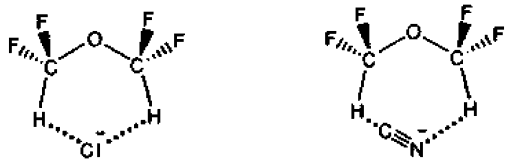

Figure 20. Bidentate cyclic structures with CH donors in the complexes of $(CHF_2)_2O$ with Cl^- and CN^- anions. Reproduced from ref 8 with permission. Copyright 1987 American Chemical Society.

is both an −NH and a −CH donor. Similar CH·N bonds occur in complexes of protonated isocyanides with amines, $RNCH^+ \cdot NR_3$. The intrinsic strengths of these $CH^{\delta+} \cdot N$ bonds are shown in the correlation parameters in Table 2.

Complexes of CH donors were investigated also spectroscopically[104−106] and as reaction intermediates.[94,107−111]

2.4.2. Anionic Complexes with Carbon-Based Bonds

Carbon CH donors can also bond to neutral or anionic halide acceptors. In ionic systems, the Kebarle group reported CH···Cl^- complexes with an inverse correlation between $\Delta H°_{acid}$ of the carbon acid and the $\Delta H°_D$ value.[41] As another example, $CN^-(H_2O)$ involves a C^-···HO bond, and cyclic structures involving CH···Cl^-···HC and CH···CN^-···HC bonds were indicated by the thermochemistry in $Cl^-((CHF_2)_2O)$[8] (Figure 20). In a series of complexes of CH_3CN, $(CH_3)_2CO$, CH_3NO_2, and C_6H_5Cl with Cl^-, Sieck found an inverse correlation between $\Delta H°_D$ and the $\Delta\Delta H°_{acid}$ of these carbon acids.[83]

Hydrogen bonds between alkyl CH donors and anion receptors can also form as intramolecular bonds. Evidence for CH···O^- internal bonds were observed in carboxylate anions with long-chain hydrocarbon substituents such as in n-$CH_3(CH_2)_8COO^-$ anions.[112]

The thermochemistry of further anionic systems with CH donors was investigated recently by Hiraoka and co-workers. In clusters of halide anions with C_2H_4 and CH_3CHCH_2, the bonding energies were <10 kcal/mol. Shell-filling effects were observed in complexes of the smaller halide ions $F^-(C_2H_4)_4$ and $Cl^-(CH_3CHCH_2)_3$ but not in the complexes of the larger halide anions.[113] In other anionic systems, Wincel studied the binding energies of CH_3NO_2 to Cl^-, NO_2^-, $CH_2NO_2^-$, $CH_3NO_2^-$, and $CH_3NO_4^-$ by CH···X^- bonds.[114]

2.4.3. Complexes of Carbon Lone-Pair Acceptors

Carbon lone pairs of isocyanides and of some anions can serve as hydrogen acceptors in ionic hydrogen bonds. Such complexes form, for example, between protonated amines and neutral isocyanides. These complexes have bonding energies comparable with the analogous complexes of cyanides, where the cyanide nitrogen lone pairs are the hydrogen acceptors. The correlation parameters in Table 2 show that the intrinsic strengths of NH^+···CNR bonds are significantly smaller (25.7 kcal/mol) than those of NH^+···NCR bonds (35.3 kcal/mol). Although the isocyanide complexes are weaker, the charge transfer and the stretching of the donor bonds are greater in these complexes. The electrostatic and delocalization components are different in the cyano and isocyano complexes, and the covalent contributions are larger when the acceptors are the carbon lone pairs of the isocyanides.[42] In a special case, CH^+···C bonds form in the complexes of protonated and neutral isocyanides. In such a complex, $CH_3NCH^+ \cdot CNCH_3$, the bonding is weaker, but only by 4 kcal/mol, than in the analogous $CH_3CNH^+ \cdot NCCH_3$ cyanide complex.

In anions, bonds with carbon lone-pair acceptors occur in $HCC^- \cdot H_2O$ ($\Delta H°_D$ = 14.6 kcal/mol)[58] and possibly in $CN^- \cdot 2H_2O$, where the second H_2O molecule may attach to the carbon lone pair. Anionic complexes of the $CH \cdot C^-$ type with carbon-based acceptors and donors also occur, but these bonds are expected to be weak according to electronegativity considerations.[8] For example, the $CH_3CN \cdot CH_2CN^-$ dimer with $\Delta H°_D$ of 12.8 kcal/mol is relatively weakly bonded.

2.4.4. Complexes of π Acceptors

Examples of unconventional bonds between cations and π acceptors were investigated in gas-phase complexes[94] and, more extensively, in solution.[115] In complexes of protonated amines with benzene derivatives, the bonding energies range from 15.9 kcal/mol for the bonding of the large, charge-delocalized ion Me_3NH^+ to C_6H_6 to 21.8 kcal/mol for the bonding of the small NH_4^+ ion to the efficient acceptor 1,3,5-$C_6H_3Me_3$. In the most stable conformation of NH_4^+···C_6H_6, two hydrogen atoms point toward the benzene; 0.033 of a unit charge is transferred to the aromatic ligand, compared with 0.055 in $NH_4^+ \cdot H_2O$ and 0.094 in $NH_4^+ \cdot NH_3$, in the same order as the bonding energies of these complexes, 19.3, 20.6, and 24.4 kcal/mol. In $Me_2NH_2^+ \cdot C_6H_6$ two and in $MeNH_3^+ \cdot C_6H_6$ three hydrogens point toward benzene, and in $Me_3NH^+ \cdot C_6H_6$, the one hydrogen points toward the center of the benzene ring. The distances from the nitrogen to the benzene centroid are 2.91−3.01 Å, and the distances from the bonding hydrogens to the aromatic plane are 2.0−2.3 Å.[116] The proton gains positive charge, but the changes in the charge density and geometry of the hydrogen donor are small.

The bonding energies of NH_4^+ to up to four C_6H_6 molecules were found to be similar to the respective K^+ bonding energies, which shows that NH_4^+ behaves essentially as a spherical ion in these complexes.[89]

Complexes of the type CH^+···π such as $N(CH_3)_4^+ \cdot C_6H_6$ ($\Delta H°_D$ = 9.0 kcal/mol), where both the acceptor and donor are carbon-based, are weakly bonded. In the most stable conformer of this complex, one hydrogen from each of three methyl groups bonds to three different C−C bonds of the benzene molecule. The distance from the methyl carbons to the aromatic center is 4.22 Å, and that from the bonding hydrogens to the benzene plane is 2.6 Å.[116] Electrostatic NH···π and CH···π interactions and exchange repulsion $\pi-\sigma^*$ interactions are both important in these NH^+···π and CH^+···π complexes.[94,116]

A stronger CH^+···π bond forms in the T-shaped isomer of the $(C_6H_6)_2^{\bullet+}$ radical dimer cation. A CH group on one component is bonded to the partially negative aromatic ring of the other component with a calculated bond energy of 15.8 kcal/mol. However,

an isomer where the benzene rings are parallel is bonded by 17.8 kcal/mol, due to charge-transfer interactions between the components.[117]

The π bond system of aromatics can also serve as a hydrogen acceptor. Such OH·π bonds occur in complexes of $C_5H_5^-$ with H_2O and alcohols. The bond strengths of $ROH{\cdot}C_5H_5^-$ show a linear correlation with $\Delta\Delta H^\circ_{acid}$ (Table 2) with an intercept of 24.4 kcal/mol, which shows intrinsically strong interactions. Nevertheless, the bonds are weaker by 4 kcal/mol than a localized OH···C^- bond in $HCC^-\cdots H_2O$, which has a similar $\Delta\Delta H^\circ_{acid}$, demonstrating the difference between the delocalized π acceptor and the localized C^- acceptors.[58]

Bonds between carbon π acceptors and CH donors occur in complexes of $C_5H_5^-$ with CH_3CN and CH_3COCH_3. Despite the expected weak CH···π interactions, these complexes have fairly strong bonds of 15.5 and 13.1 kcal/mol, respectively, which may imply multiple hydrogen bonds between the methyl groups and the π ring.[58]

Spectroscopic studies of unconventional IHBs of aromatic molecules were summarized recently.[118] Bonds of OH···π type were found in radical ion complexes of phenol with acetylene, ethylene, and benzene. In $(benzene/water)^{\bullet+}$ and $(benzene/methanol)^{\bullet+}$ clusters, the spectra showed evidence of CH···OH_2 bonds, where one ligand molecule bonds to one or two benzene hydrogen atoms, while further ligand molecules form ligand−ligand bonds.[118−120] Spectroscopic evidence for OH···π interactions was found also in complexes of benzene with acetic acid.[121] A novel IHB was found in 1,2-$CH_3C_6H_4OH^{\bullet+}$ and 1,2-$C_2H_5C_6H_4OH^{\bullet+}$ ions where the alkyl groups serve as hydrogen acceptors.[122]

2.4.5. Hydrogen-Bonded Isomers of Covalent Ions

Some noncovalent hydrogen-bonded adducts can form even when covalently bonded isomers are also possible. The noncovalent adducts have in some cases comparable bond strengths, more favorable entropies, or both, or they persist because rearrangement to the covalent adduct involves an energy barrier. Hydrogen-bonded noncovalent complexes can also form as reaction intermediates in the rearrangement or dissociation of covalent ions.

The first example was observed by Hiraoka and Kebarle in the complex of $C_2H_5^+$ with H_2. The van't Hoff plot had two sections, corresponding to a noncovalent adduct at low temperatures and the $C_2H_7^+$ protonated ethane at high temperatures where the complex can overcome an activation barrier to form covalent bonds.[129] Similarly, the bonding energy of $H_3O^+{\cdot}CO$ of 11.5 kcal/mol indicates the formation of the cluster rather than the 18.6 kcal/mol exothermicity to form $(HCOOH)H^+$.[117]

Other examples of IHB isomers include protonated ethyl compounds $CH_3CH_2BH^+$ (B = H_2O, Cl, Br, I) where the proton of the nonclassical proton-bridged $(H_2C{=}CH_2)H^+$ ion may be hydrogen-bonded to BH.[109,110,130,131] We also found in earlier work that protonated amines such as $CH_3NH_3^+$ bond weakly to CO_2 to form hydrogen-bonded isomers of covalently bonded protonated amino acids, in this case of $(H_2NCH_2COOH)H^+$ (glycineH^+).

Carbonium ions can add to nitrogen and oxygen bases to form either noncovalent $CH^+\cdots N$ or $CH^+\cdots O$ adducts or covalent protonated alcohols or ethers. For example, the methyl cation can form strong hydrogen bonds with NH_3 and H_2O molecules, which form noncovalent isomers of $CH_3NH_3^+$ or $CH_3OH_2^+$, respectively.[96]

Protonated ions can bond to $H_2C{=}CH_2$ to form a $BH^+\cdots\pi$ complex, such as in $NH_4^+\cdots C_2H_2$,[94] which is bonded by 10 kcal/mol although the formation of $C_2H_5NH_3^+$ would be exothermic by 26 kcal/mol (see Table 3). In this case, the noncovalent adduct persists because of an activation barrier to forming the covalent ion. Another example of a hydrogen-bonded adduct of ethylene is the complex with $HCNH^+$, which is an intermediate in the rearrangement between $CH_3CH_2CNH^+$ and $CH_3CH_2NCH^+$.[111]

In the hydrogen-bonded complexes, the reactants retain free rotation and low-frequency vibrations about the hydrogen bond, while in covalent adducts, this internal freedom is absent. Correspondingly, the value of ΔS°_D is usually about 20−25 cal/(mol K) for the loose noncovalent complexes but over 35 cal/(mol K) for covalent adducts. Because of the $T\Delta S^\circ$ contributions, ΔG° can favor the loose noncovalent adduct at high temperatures, even if the covalent bond is somewhat stronger.

Noncovalent adducts are especially competitive with covalent adducts when the reactants are highly stabilized carbonium ions such as t-$C_4H_9^+$ or oxocarbonium ions. The stabilities of the ions weaken the covalent bonds to oxygen or nitrogen bases, and their strengths become comparable to $CH^{\delta+}\cdots B$ bonds, while entropy favors the hydrogen-bonded isomers. In such cases, the hydrogen-bonded complex may be favored at high temperatures and the covalent adduct at low temperatures.

In early examples, covalent condensation was indicated in s-$C_3H_7^+ + HCN \rightarrow s$-$C_3H_7NCH^+$ with $\Delta H^\circ_D = 30.8$ kcal/mol and $\Delta S^\circ_D = 32$ cal/(mol K). On the other hand, noncovalent adducts were indicated in t-$C_4H_9^+ + HCN$, where the values of $\Delta H^\circ_D = 16.3$ kcal/mol and $\Delta S^\circ_D = 25$ cal/(mol K) are too small for covalent addition. The thermochemistry suggests a loose complex where the ligand is hydrogen-bonded to methyl hydrogens of the t-$C_4H_9^+$ ion rather than forming the covalent t-$C_4H_9CNH^+$ or t-$C_4H_9NCH^+$ adducts, the ΔS°_D of which can be estimated as 35 cal/(mol K) (see Table 3).[102]

A system with oxygen acceptors is t-$C_4H_9^+{\cdot}H_2O$ for which Hiraoka and Kebarle measured a binding energy of 11.2 kcal/mol.[132] This small binding energy may correspond to a covalent or noncovalent adduct. The formation of a $CH^{\delta+}\cdots OH_2$ type noncovalent adduct rather than the t-$C_4H_9OH_2^+$ covalent adduct was suggested by Meot-Ner and co-workers on the basis of the small $\Delta S^\circ_D = 22$ cal/(mol K), and this was confirmed by the collisional dissociation mass spectrum of the adduct, which was different than that of t-$C_4H_9OH_2^+$.[100] The adducts of the oxocarbonium ions $CH_3CHOCH_3^+$ and $(CH_3)_2COCH_3^+$ with H_2O and CH_3OH in Table 3 also appear to be noncovalent complexes rather than unstable protonated hemiacetals or acetals.[100]

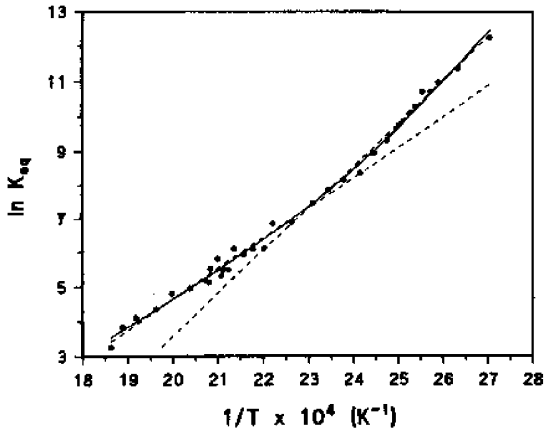

Figure 21. Van't Hoff plot for the association of t-$C_4H_9^+$ with CH_3OH. The plot shows two areas, below 440 K corresponding to the formation of t-$C_4H_9OCH_3H^+$ and above 440 K corresponding to the formation of t-$C_4H_9^+\cdots CH_3OH$. The solid line represents an exponential fit over the temperature range according to calculated equilibrium between the two dimers, and the dashed line represents equilibrium independently for the two types of complexes. Reproduced from ref 123 with permission. Copyright 1996 American Chemical Society.

Subsequently, the analogous adducts of t-$C_4H_9^+$ with CH_3OH, C_2H_5OH, $(CH_3)_2O$, $(C_2H_5)_2O$, $(CH_3)_2CO$, and CH_3CN were investigated by Norrman and McMahon.[123] The van't Hoff plots were curved between 360 and 670 K (Figure 21), and the thermochemistry suggested the covalent adducts at low temperatures and hydrogen-bonded $CH^+\cdots O$ complexes at higher temperatures (Table 3).

The reaction of t-$C_4H_9^+$ with CH_3OH gave ΔH°_D = 29.1 kcal/mol and ΔS°_D = 54.0 cal/(mol K) at 370−435 K, suggesting the covalent adduct (t-$C_4H_9OCH_3$)-H^+, while at higher temperatures of 435−540 K, the van't Hoff plots gave ΔH°_D = 15.1 kcal/mol and ΔS°_D = 21.1 cal/(mol K), suggesting a noncovalent complex. In the other complexes, ΔH°_D ranged from 15 to 34 kcal/mol for the noncovalent complexes and 29 to 46 kcal/mol for the covalent adducts, and ΔS°_D ranged from 21 to 52 cal/(mol K) for the noncovalent complexes and from 45 to 86 cal/(mol K) for the covalent adducts. The thermochemistry of the noncovalent complexes suggested structures in which the oxygen bases are protonated and they form hydrogen bonds with the double bond of i-C_4H_8.[123]

In summary, due to a combination of enthalpy and entropy effects, loose hydrogen-bonded complexes can sometimes be favored over covalent isomers.

2.5. Radical Ions and Distonic Dimers

2.5.1. Reaction Intermediates and Distonic Dimers

Ionic hydrogen bonds occur also in open-shell radical ions. Such systems can be generated in the ionization of clusters, for example, to generate $(H_2O)_n^{\bullet+}$ or $(NH_3)_n^{\bullet+}$ or other clusters with $OH^{\bullet+}\cdots O$ or $NH^{\bullet+}\cdots N$ bonds.

The thermochemistry of these clusters can be obtained from the ionization energies of the neutral clusters, which were measured for clusters of N, O, and S bases, and also for neutral clusters containing $CH\cdots O$, $CH\cdots N$, $NH\cdots\pi$, or $CH\cdots\pi$ bonds. For example, the bonding energy of the presumably hydrogen-bonded complex $(C_6H_6\cdot HCl)^{\bullet+}$ was measured as 7.3 ± 1.2 kcal/mol.[133] Note however that adiabatic ionization energies and the bonding energies of the neutral clusters are needed to calculate the hydrogen bond energies of the cluster ions, but these data are often hard to obtain.

Hydrogen-bonded complexes can also occur as reaction intermediates, as discussed below.[134−140]

Complexes formed from a radical ion and a neutral molecule can undergo internal proton transfer to form a distonic hydrogen-bonded complex where the radical and charged sites are different. For example, we observed a strongly bonded complex $C_6H_6^{\bullet+}\cdot C_5H_5N$ in the benzene/pyridine system.[117] The complex does not undergo exchange with an additional C_5H_5N molecule to form the protonated pyridine dimer $(C_5H_5N)_2H^+ + C_6H_5$, although the overall process $C_6H_6^{\bullet+} + 2C_5H_5N \rightarrow (C_5H_5N)_2H^+ + C_6H_5$ would be exothermic by 32 kcal/mol. Theory and ion mobility suggested that the adduct $C_6H_6^{\bullet+}\cdot C_5H_5N$ is covalently bonded. However, it also has a stable C_5H_5-$NH^+\cdot C_6H_5^\bullet$ distonic isomer.

The thermochemistry of the rearrangement of radical dimer ions to form the distonic hydrogen-bonded dimers, reaction 11a, can be calculated from thermochemical relations as eq 11b.

$$B^{\bullet+}\cdots RH \rightarrow BH^+\cdots R^\bullet \qquad (11a)$$

$$\Delta H^\circ_{11a} = \Delta H^\circ_D(B^{\bullet+}\cdot RH) - \Delta H^\circ_D(BH^+\cdot R^\bullet) + BDE(R-H) + IE(H) - IE(B) - PA(B) \qquad (11b)$$

The second term on the right-hand side (RHS), the hydrogen bond energy of a proton donor to a carbon lone pair of a radical, ($\Delta H^\circ_D(BH^+\cdot R^\bullet)$), is expected to be substantial. In comparison, the bond energies, $\Delta H^\circ_D(B^{\bullet+}\cdot RH)$, with $CH\cdots O$ or $CH\cdots N$ bonds are expected to be weaker, and the sum of the first two terms on the RHS side of eq 11b should be negative. The sum of the other terms is negative for most oxygen and nitrogen bases if the bond dissociation energy, BDE(R−H), is less than 110 kcal/mol, which applies for most hydrocarbons. Therefore proton transfer from hydrocarbons to most ionized O and N bases is usually exothermic. Such proton transfer in the complexes forms even-electron hydrogen-bonded dimers with protonated $-OH^+$ or NH^+ donors and carbon lone-pair radical acceptors. These distonic dimers are generally more stable than the electrostatically bonded radical dimer ion isomers with $CH\cdots O$ or N bonds.

2.5.2. Complexes of Ionized Aromatics: Solvation of the Benzene and Pyridine Cations

Carbon-based $CH^{\delta+}\cdots O$ bonds appear in the solvation of ionized aromatics, such as the solvated benzene ion $C_6H_6^{\bullet+}(H_2O)_n$. The binding energies of H_2O molecules to $C_6H_6^{\bullet+}$ were measured by equilibrium studies in a mobility cell.[117] The results in Table 3 show that $\Delta H^\circ_{n-1,n}$ for the first six H_2O molecules are nearly constant, possibly because the water molecules bond to individual benzene hydrogens, causing little charge delocalization from the remaining benzene hydrogens. However, the binding energies are also close to the limiting values in other

hydrated clusters that contain water−water bonds, and the results may suggest that a water network builds up attached to the benzene ion.

IR spectroscopy and ab initio calculations showed that the first solvent molecule forms IHBs with two adjacent protons of $C_6H_6^{\bullet+}$. The spectra with two to four H_2O or two CH_3OH molecules showed isomers where each water molecule is bonded directly to the benzene ion ("inner solvation") and isomers where the benzene ion is attached to a cluster of solvent molecules ("external solvation").[118,120,141] Both types of isomers were present in equilibrium, consistent with ab initio calculations that showed them to have similar energies.[117]

With the addition of three to four H_2O molecules, proton transfer becomes energetically possible from $C_6H_6^{\bullet+}$ to form a $(H_2O)_nH^+$ cluster ion. This can result in intracluster rearrangement to form a $C_6H_5^{\bullet}$-$(H_2O)_nH^+$ cluster with an OH···π bond to the phenyl radical (Figure 22). Alternatively, the proton transfer may be dissociative and produce protonated water clusters.[117] In relation to these structures, the IR dissociation spectra of $C_6H_5^{\bullet}(H_2O)_nH^+$ clusters after $n = 4$ showed very similar spectra of $(H_2O)_nH^+$ clusters, indicating that internal proton transfer formed a protonated water cluster attached to the phenyl radical.[141] On the other hand, isotope exchange experiments under thermal ion mobility conditions showed that $C_6H_6^{\bullet+}(D_2O)_n$ ($n = 2-8$) did not react with D_2O to yield a $C_6H_5^{\bullet}(D_2O)_nD^+$ ion, although this would be expected for $C_6H_5^{\bullet}(D_2O)_nH^+$ structure formed by internal proton transfer. It is possible that the intracluster proton transfer has an energy barrier that cannot be overcome in thermal systems below 280 K in the ion mobility experiments.[117] We also observed recently the more strongly bonded pyridine$^{\bullet+}(H_2O)$ cluster ion, bonded by 15.6 kcal/mol, similar to pyridine$H^+(H_2O)$. This suggests an $NH^+{\cdot}OH_2$ bond in a $^{\bullet}C_5H_4NH^+(H_2O)$ complex involving distonic pyridine radical cation. Cluster binding energies can therefore identify distonic ions.[117]

3. Larger Clusters and Hydrogen-Bond Networks

3.1. Neat Aggregates and Solvation Sequences

Beyond dimers, further ligand molecules can be added stepwise to ionic clusters. In principle, the process can be carried up to forming condensed-phase aggregates. In practice, equilibrium measurements cover in most cases 4−8 and in some instances 10−18 ligand molecules,[142−146] and collisional dissociation measurements were applied up to 26 solvent molecules.[147,148]

The thermochemistry of the clusters gives valuable information about the inner solvent shells where ionic forces are most significant. Data on the inner-shell interactions allows quantification of the physical factors in ion solvation.[35]

The thermochemistry also gives structural indications. Do distinct solvent shells form? How closely do the ligand binding energies and IHB networks resemble the condensed phase? Is the ion inside or on the surface of the incipient solvent? Where is the proton in clusters? This information is indicated by the thermochemistry and can be tested further by computation, reactivity, ion chromatography, collisional dissociation, and photodissociation spectroscopy.

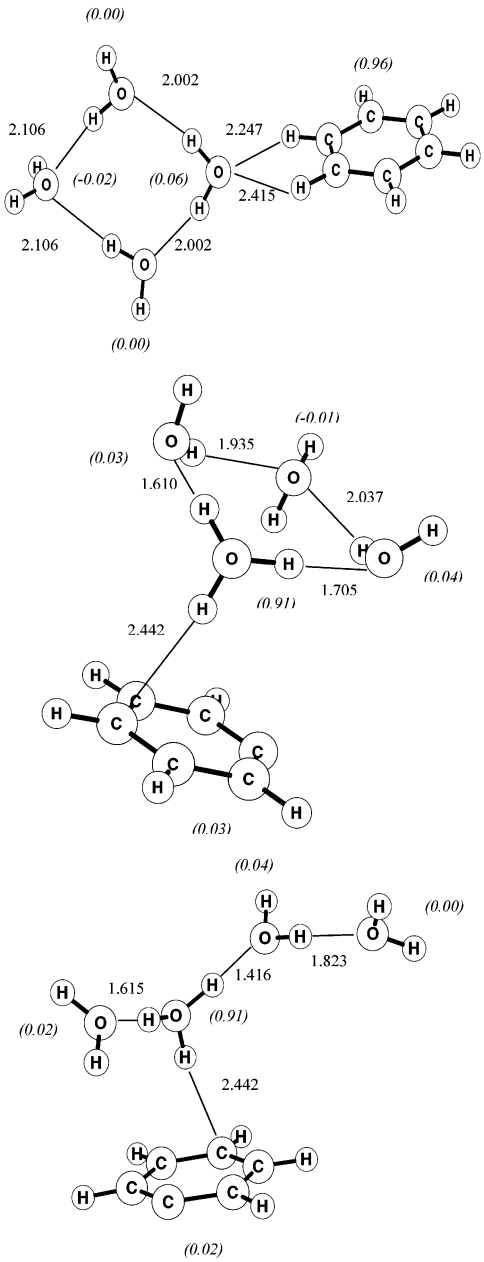

Figure 22. Stable structures of the $C_6H_6^{\bullet+}(H_2O)_4$ cluster. The top panel shows a ring structure with bifurcated $CH^{\delta+}$···O bond; the center and bottom panels show ring and linear isomers of $C_6H_5^{\bullet}(H_2O)_4H^+$ after proton transfer to water with OH^+···π bonds to the phenyl radical. In the latter two, the proton is located on the water bonded to the phenyl radical. The lengths of hydrogen bonds and Mullikan group charges (in parentheses) are shown. Note that in $C_6H_6^{\bullet+}(H_2O)_4$, 0.96 of the charge remains on benzene, while in $C_6H_5^{\bullet}(H_2O)_4H^+$, 0.91 of the charge is on the H_3O^+ center. Total bonding energies vs $C_6H_6^{\bullet+} + 4H_2O$ monomers, from ROHF/6-31+G* calculations were, for the isomers from top to bottom, −43.6, −41.0, and −41.3 kcal/mol. The calculations suggest that intracluster proton transfer is slightly endothermic in this cluster but becomes exothermic in larger clusters.[117]

3.1.1. Thermochemical Studies of Stepwise Solvation

Thermochemical studies have been applied to many solvation sequences. Hydration studies by four

or more water molecules were applied to NH_4^+,[149−151] a set of oxonium and ammonium ions,[5,150,152] protonated amides[48] and alcohols,[153] and polyfunctional ions such as protonated polyethers[154] and diamines.[95,155] In the solvation of anions, hydration sequences were measured for OH^-,[52,156,157] the halide ions,[158−160] HCO_3^-,[161] CN^-,[162] NO_2^-,[158,163] O_2^-,[52,158] Cl^- and other halide ions,[159,160,164−166] and polyfunctional anions such as $O_3S_nO_3^{2-}$,[167] PO_3^-,[168] diacids,[167] diphosphate,[169] and adenosine 5′-diphosphate,[169] and other biomolecules discussed below.

Hydrogen bonding occurs also in the outer hydration shells of both hydrogen-bonding and non-hydrogen-bonding ions including the metal ions Li^+,[170] Na^+,[171,172] K^+,[173] Rb^+,[171] Ag^+,[174] Bi^+,[175] Ca^+,[176] Cu^+,[174] Pb^+,[172] and Sr^+.[177]

Solvation series were studied also with nonaqueous solvents. Studies covering at least four solvent molecules were extended to solvation by CH_3OH of $CH_3OH_2^+$,[103,178] $(CH_3)_2OH^+$,[152] $(CH_3OCH_2CH_2OCH_3)H^+$,[154] Na^+,[179] K^+,[77] CH_3O^-,[180] and the halide ions,[164] solvation series by the higher alcohols EtOH, *n*-PrOH, and *n*-PeOH including the solvation of ROH_2^+,[178,181] and the halide ions,[164] and solvation series by carboxylic acids in $HCOO^-{\cdot}n$HCOOH, $Cl^-{\cdot}n$HCOOH,[182] $(CH_3COOH)H^+{\cdot}nCH_3COOH$, and $CH_3COO^-{\cdot}nCH_3COOH$[178,183] and by sulfuric and nitric acids in $HSO_4^-(H_2SO_4)_m(HNO_3)_n$ clusters.[184,185]

Solvation by nitrogen base ligands were studied with ammonia, mostly by the Castleman group;[77,174] neutral amines about protonated amines,[178] clustering of HCN molecules about NH_4^+,[186] $HCNH^+$,[102] CN^-,[43,162,187] CH_3COO^-,[43] and halide ions,[43,188] and CH_3CN molecules about NH_4^+,[89] which were also investigated theoretically as to ΔPA/bond strength correlations[189] and also association of CH_3CN with alkali cations[190] and halide anions were also studied.[160,191,192] A few studies addressed hydrogen-bonded clusters involving the hydrides of heavier elements such as the solvation of H_3S^+ by H_2O and H_2S[61,64] and of PH_4^+ by PH_3.[65]

3.1.2. Effects of Stepwise Solvation on Charge Distributions and Hydrogen Bond Lengths

The changes in structures and charge distributions with increasing cluster size can be illustrated by protonated neat water clusters and water/ammonia mixed clusters that were studied both experimentally and theoretically.[36,186]

Figure 23 shows the structures and atomic charges in $H_3O^+(H_2O)_n$ clusters. In forming the dimer, the bonding proton becomes more positive because the electronegative oxygen of the ligand attracts electron density away from the proton. However, on addition of further solvent molecules, the positive charge dissipates and the bonding proton or protons of the H_3O^+ core ion become less positive. When one to three water molecules are added in the inner shell, the ligands attach directly to the core ion as in Figure 23. The charge on the bonding protons changes from 0.571 to 0.591, 0.554, and 0.528, while the overall charge on the central H_3O^+ ion changes from 1.000 to 0.796, 0.724, and 0.659 unit charge. Even when the inner solvent shell is filled by three H_2O molecules, 66% of the charge remains on the core ion.

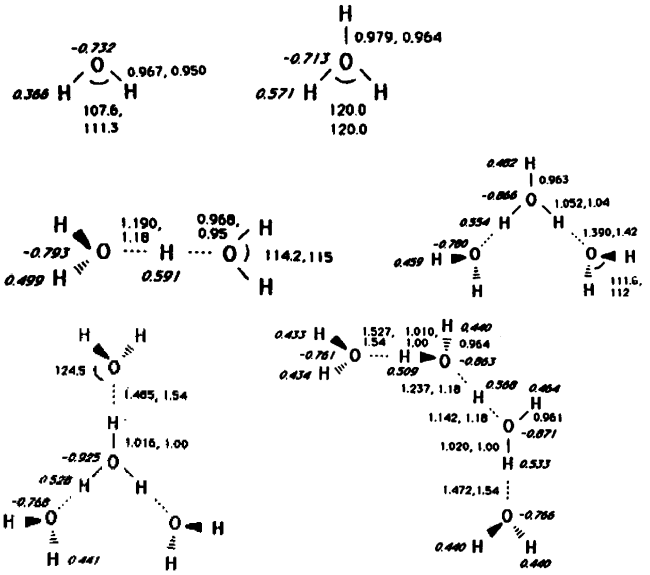

Figure 23. Structures and atomic charges in $H_3O^+(H_2O)_n$ clusters. Reproduced from ref 36 with permission. Copyright 1986 American Chemical Society.

Similar trends were observed in $NH_4^+(NH_3)_n$ clusters. With inner-shell solvation as *n* changes from 0 to 3, the charge on the bonding proton changes from 0.488 to 0.535, 0.521, and 0.507 while the charge on the NH_4^+ core ion changes from 1.000 to 0.906, 0.858, and 0.832 unit charge. Again, a large fraction of the charge, 83%, remains on the core ion. Anionic clusters behave similarly. Calculations on $OH^-(H_2O)_n$ showed that 75% of the charge remains on the hydroxyl anion.[193,194]

In these clusters, the protonated core species and ligands were identical. More commonly, a core ion is solvated by a different solvent, especially water. This is illustrated in Figure 24 by $NH_4^+(H_2O)_n$ clusters in the ammonia/water system. The charge on the bonding proton increases again at the first solvation step and decreases in the further steps as *n* changes from 1 to 4, changing from 0.488 to 0.542, 0.527, 0.513, and 0.499, while the charge on the core NH_4^+ ion changes from 1.000 to 0.945, 0.908, 0.881, and 0.861 as *n* increases. In all clusters, most of the charge remains on the protonated core ion even after the inner solvent shell becomes filled.

These examples concerned clusters where the solvent molecules are bonded directly to the core ion. Figures 23 and 24 also show isomers in which ligand molecules bond to inner ligand molecules in the outer shell before the inner shell is filled. In either case, charge delocalization to the solvent increases with added solvent molecules, but less additional charge becomes delocalized in each solvation step. Adding further ligand molecules in the outer shells should have even smaller effects, which suggests that most of the charge remains on the protonated core ion even in bulk solution.

The above trends are physically sensible although the charge densities were derived from Mullikan population analysis based on relatively low-level 6-31G* calculations. Higher level calculations are needed, especially on the larger clusters.

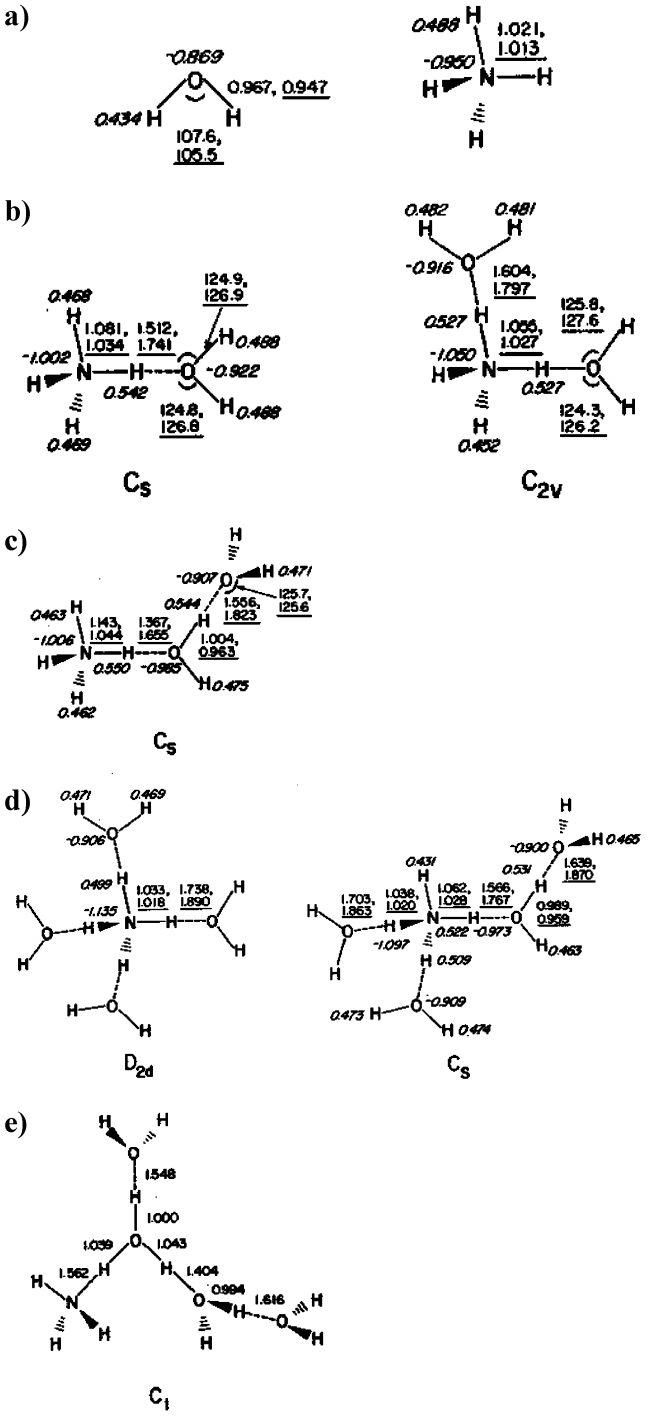

Figure 24. Geometries of $NH_4^+ \cdot nH_2O$ clusters from 3-21G and 6-31G* (underlined) optimizations. Atomic charges from population analysis using 6-31G* basis set are given in italics. Reproduced from ref 36 with permission. Copyright 1986 American Chemical Society.

Generally, when consecutive ligand molecules are attached directly to a protonated core ion, the following changes occur in charge distributions: As more solvent molecules are attached to the core ion, the positive charge q_H on each of its bonding protons decreases, although it is always larger than that in the unsolvated ion. The charge becomes dispersed and the charge remaining on the core ion decreases. The total charge transferred to the solvent increases, but the charge on each solvent molecule decreases.

In parallel, structural changes occur: The $B-H^+$ bond lengths of the donor become less extended. With increasing cluster size, individual hydrogen bonds in the assembly weaken and become more extended.

In addition, especially in larger clusters, the following are possible: Shell filling may occur. Isomeric clusters of similar energies may be possible and may coexist in equilibrium. Cyclic and clathrate hydrogen-bonded systems may form.

Anionic clusters show similar trends, because they form IHB bonds that are shorter than those in neutral clusters and similar to cationic IHBs. For example, the calculated ab initio bond lengths in the anionic $OH^-(H_2O)_3$ clusters were similar to those in the $H_3O^+(H_2O)_3$ cationic clusters.[194]

The individual IHBs usually weaken with increasing cluster size when the ion is surrounded by solvent molecules. However, the IHB may strengthen when the ion is solvated externally, as in comparing the $NH_4^+(H_2O)$ and $NH_4^+(H_2O)_2$ (C_s) clusters in Figure 24, where upon the attachment of outer-shell solvent molecules, q_H on the bonding hydrogen increases, $r(N-H)$ increases, $r(H\cdots O)$ shortens, and the inner-shell hydrogen bond strengthens. However, this effect is balanced by the weak bonding of the outer-shell molecule, making the inner-shell solvated C_{2v} ion more stable than the mixed inner-and-outer shell C_s ion by 1−4 kcal/mol depending on the level of calculation.

In summary, the charge on the bonding protons decreases with increasing solvation. Some of the charge dissipates from the protonated core ion, but it retains most of the charge even in large clusters, suggesting that this applies even in solution. In parallel, ionic hydrogen bonds become longer and weaker with increasing cluster size.

Thermochemical studies can be extended recently to the solvation of doubly charged ions, such as diprotonated diamines,[95] and to biological ions, as discussed below.

3.1.3. Consecutive Bonding Energies and Some Predictive Relations

With increasing cluster size, the consecutive bonding energies, $\Delta H^\circ_{n-1,n}$, should decrease due to repul-

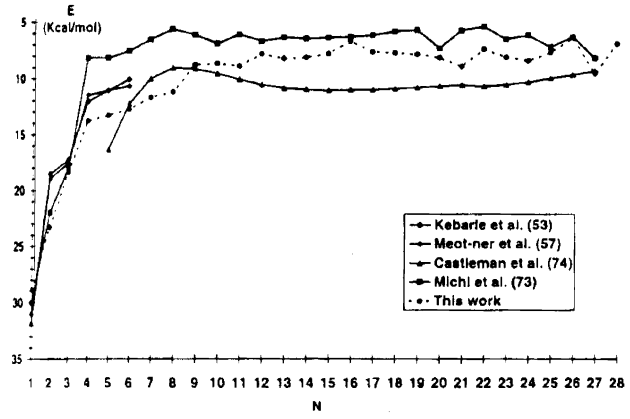

Figure 25. Consecutive bonding energies in the series $H_3O^+(H_2O)_{n-1} + H_2O \rightarrow H_3O^+(H_2O)_n$. The references cited are as follow: Kebarle, refs 196 and 197; Meot-Ner, refs 199 and 157; Michl, ref 147; Castleman, ref 148. Reproduced from ref 198 with permission. Copyright 1995 American Chemical Society.

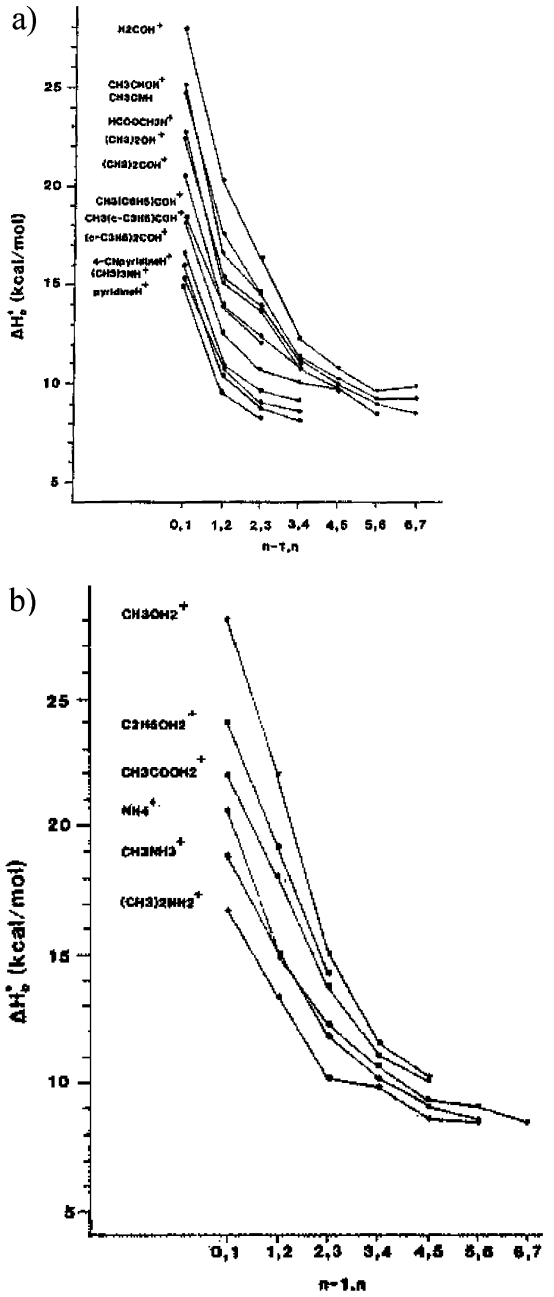

Figure 26. Bonding energies in hydration sequences of (a) monoprotonic and (b) polyprotonic ammonium and oxonium ions. Reproduced from ref 49 with permission. Copyright 1984 American Chemical Society.

sion among the ligand molecules and charge delocalization. This trend has been observed in most solvation sequences. A classic example is the enthalpy sequence in $H_3O^+(H_2O)_n$, which was measured by several authors by equilibrium measurements[157,181,195−197] and by collisional dissociation.[14,147,148] Figure 25 illustrates the long series of IHB clusters measured by dissociation methods.

Figure 26 illustrates the variation in bonding energies, $\Delta H^\circ_{n-1,n}$, in hydration sequences about ammonium and oxonium ions.

Figures 25 and 26 and the data in Tables 4 and 5 illustrate the following thermochemical trends upon adding ligand molecules: The bonding energies, $-\Delta H^\circ_{n-1,n}$, decrease, usually by similar factors of 0.7 in each consecutive clustering step, in many solvation sequences. Shell filling may be followed by a drop of 1−4 kcal/mol in the bonding energy of the next step. The bonding energies and entropies approach the condensation thermochemistry of the bulk solvent ($\Delta H^\circ_{condensation}$ and $\Delta S^\circ_{condensation}$) often already after four to six solvation steps.

The absolute solvation energies decrease with each additional solvent molecule as illustrated in Tables 4−6 and in Figures 25 and 26. This trend continues until $\Delta H^\circ_{n-1,n}$ reaches, in some cases after undershooting, the limiting macroscopic $\Delta H^\circ_{condensation}$, which is often reached surprisingly already after four to six solvation steps. There exist no accurate thermochemical data on larger hydrated clusters, but some theoretical considerations will be discussed below.

The structural changes upon sequential clustering should be different for various core ions and solvent molecules. Nevertheless, the clustering energies for each consecutive step decrease by similar factors in various clustering sequences, so each step can be predicted from the preceding step, starting from the first step, $\Delta H^\circ_{0,1}$. These relations can be used to estimate the partial and bulk hydration energies based on the proton affinity of a base, PA(B), and $\Delta H^\circ_{condensation}(H_2O)$ alone. As we saw above, $\Delta H^\circ_{0,1}$ can be estimated from the ΔPA correlations in eqs 4−7 and Table 2, which can be reformulated in eqs 12 and 13 using $PA(H_2O) = 165$ kcal/mol.

for $OH^+ \cdot OH_2$ bonds:

$$\Delta H^\circ_{0,1} = 80 - 0.30PA(B) \text{ kcal/mol} \quad (12)$$

for $NH^+ \cdot OH_2$ bonds:

$$\Delta H^\circ_{0,1} = 73 - 0.26PA(B) \text{ kcal/mol} \quad (13)$$

The cumulative integrated hydration enthalpies by n H_2O molecules, $\Delta H^\circ_{0,n}$, are remarkably constant multiples of the first step, $\Delta H^\circ_{0,1}$, and their value can be predicted by eqs 14−17 on this basis.

$$\Delta H^\circ_{0,2} = (1.8 \pm 0.1)\Delta H^\circ_{0,1} \quad (14)$$

$$\Delta H^\circ_{0,3} = (2.3 \pm 0.1)\Delta H^\circ_{0,1} \quad (15)$$

$$\Delta H^\circ_{0,4} = (2.8 \pm 0.1)\Delta H^\circ_{0,1}$$
(oxonium and monoprotonic ammonium ions) (16)

$$\Delta H^\circ_{0,4} = (3.1 \pm 0.1)\Delta H^\circ_{0,1}$$
(polyprotonic ammonium ions) (17)

These relations were found to apply in the hydration sequences of 22 onium ions, as well as of the alkali ions, and they apply even in solvation sequences with CH_3OH, NH_3, H_2S, and CH_3CN ligand molecules.[49]

The integrated enthalpy of solvation by four H_2O molecules, $\Delta H^\circ_{0,4}$, can be estimated by eqs 16 and 17 usually within ±1 kcal/mol, which is well within the cumulative experimental error of the four solvation steps. The relation between $\Delta H^\circ_{0,1}$ and $\Delta H^\circ_{0,4}$, combined with the correlation between $\Delta H^\circ_{0,1}$ and ΔPA above, yields accurate estimates, within ±2 kcal/mol, of the four-molecule hydration energy, $\Delta H^\circ_{0,4}$, based

Table 4. Thermochemistry of Stepwise Gas-phase Hydration

Hydration $BH^+(H_2O)_n$

	$-\Delta H^\circ_{n-1,n}$ [a]									$-\Delta S^\circ_{n-1,n}$ [a]						
n [b]	1	2	3	4	5	6	7	8	cond [c]	1	2	3	4	5	6	refs
Alcohols, Ethers, Ketones, Acids																
H_3O^+	32.1	20.4	17.2	12.2	11.6	11.2	11.2	9.8	10.5	26.4	21.3	27.8	24.0	24.5	27.8	*d*
$CH_3OH_2^+$	26.4	20.4	14.4	11.6	9.4	9.2			10.5	26.2	28.1	25.5	22.6	19.6	21.2	*d*
$C_2H_5OH_2^+$	24.0	19.0	13.8	11.9	9.7				10.5	26.0	27.4	25.2	24.4	20.9		5
n-$C_3H_7OH_2^+$	23.9	17.9	11.0	9.5	8.8				10.5	28.0	26.3	22.9	20.7	20.8		153
CH_3CHOH^+	25.0	16.8	17.0	11.3	9.4	9.3			10.5	27.6	25.2	27.9	21.4	18.8	21.7	49
$(CH_3)_2OH^+$	23.3	15.4	13.4	10.2					10.5	27.6	28.2	24.2	19.0			49,152,200
$(CH_3)_2COH^+$	20.5	13.6	12.7	10.3	10.3				10.5	26.0	23.2	21.9	20.2	23.5		49
$(CH_3COOH)H^+$	20.4	17.8	12.9	10.8					10.5	23.0	26.4	23.2	20.4			183
Amines																
NH_4^+	20.2	14.2	13.1	11.5	10.2	9.1	8.4		10.5	23.9	22.0	23.7	25.2	24.7	22.0	*d*
$CH_3NH_3^+$	17.8	14.6	12.4	10.3	8.5				10.5	24.2	25.4	25.2	22.0	20.9		201,49
$C_2H_5NH_2^+$	17.5	14.7	13.2						10.5	25.9	29.7	30.8				201,202
$(CH_3)_2NH_2^+$	15.0	13.5	11.3	10.5	9.4	8.4			10.5	22.9	24.7	24.4	25.2	24.4	21.2	49
$(CH_3)_3NH^+$	14.5	11.4	10.0						10.5	24.2	24.8	24.9				91,49,203
Doubly Charged Diamines																
$H_3N(CH_2)_6NH_3^{2+}$	17.8	17.3								21.0	23.1					95
$H_3N(CH_2)_8NH_3^{2+}$	16.9	16.8								21.5	23.8					95
$H_3N(CH_2)_{10}NH_3^{2+}$	16.8	16.8								22.8	25.2					95
$H_3N(CH_2)_{12}NH_3^{2+}$	15.7	15.7	13.4	13.6						20.1	23.2	21.5	24.5			95
Nitriles, Sulfide																
$HCNH^+$	27.4	21.4	17.2						10.5	29.6	25.3	26.2				199
CH_3CNH^+	22.5	16.2	15.6	11.2	10.4	10.1			10.5	24.5	25.1	24.8	21.8	23.4	25.5	49,199,204
H_3S^+	21.2	20.3							10.5	24.5	21.8					132

[a] Units are as follows: $\Delta H^\circ_{n-1,n}$ (kcal/mol); $\Delta S^\circ_{n-1,n}$ (cal/(mol K)). [b] In the hydration series, $\Delta H^\circ_{n-1,n}$ corresponds to the addition of the nth H_2O molecule to the core ion. [c] Bulk condensation enthalpy of water. [d] Average of acceptable literature values in the NIST tables.[29]

Table 5. Thermochemistry of Neat Clusters

Neat Clusters B_nH^+

	$-\Delta H^\circ_{n-1,n}$ [a]									$-\Delta S^\circ_{n-1,n}$ [a]						
n [b]	1	2	3	4	5	6	7	8	cond [c]	1	2	3	4	5	6	refs
Alcohols, Ethers, Ketones, Acids																
H_3O^+	32.1	20.4	17.2	12.2	11.6	11.2	11.2	9.8	10.5	26.4	21.3	27.8	24.0	24.5	27.8	*d*
$(CH_3OH)_nH^+$	32.5	21.2	15.1	12.4	11.4	10.6	10.5	9.4	8.4	28.8	27.0	26.4	25.0	27.3	28.1	*d*
$(C_2H_5OH)_nH^+$	32.1								10.0	28.5						205,50
$(n$-$C_3H_7OH)_nH^+$	31.0	20.2	14.3	11.8	10.9	11.1			11.2	28.5	27.2	24.6	23.9	25.4	28.8	50,181,178
$((CH_3)_2O)_nH^+$	31.4	10.1								30.8	27.9					103,206
$((CH_3)_2CO)_nH^+$	30.7	12.2	8.5							29.9	23.0	17.0				181
$(CH_3COOH)_nH^+$	28.1	18.5	12.7	12.1					12.8	28.3	24.5	21.1				183
Amines																
$(NH_3)_nH^+$	25.2	16.6	14.9	12.2	7.8	6.2	5.0	4.0	5.6	26.3	24.4	26.0	26.2	21.9		
$(CH_3NH_3)_nH^+$	23.6	16.0	13.4	7.8						25.5	27.2	26.1	22.5	22.5		39,178
$((CH_3)_2NH_2)_nH^+$	22.5	16.4	9.9	7.9	6.3					26.9	27.2	26.1	22.5	22.5		178
$((CH_3)_3N)_nH^+$	22.2	6.5	8.3	8.8	7.4				5.2	28.8						39,207,203,178
Nitriles, Sulfide, Phosphide																
$(HCN)_nH^+$	28.1	13.8	11.8	9.2					6.0	27.5	23.0	25.0	26.0			102,199
$(CH_3CN)_nH^+$	30.0	9.3	7.3	6.5	5.5				7.9	26.4	19.9	18.4	15.0	13.2		199,204
$(H_2S)_nH^+$	15.1	8.2	8.4	6.7	6.1				4.5	20.3	19.1	24.5	24.7	24.0		132,61
$(PH_3)_nH^+$	11.5	9.2	7.3	6.5						25.9	22.3	18.4	15.0			65

[a] Units are as follows: $\Delta H^\circ_{n-1,n}$ (kcal/mol); $\Delta S^\circ_{n-1,n}$ (cal/(mol K)). [b] In the neat cluster series, $\Delta H^\circ_{n-1,n}$ corresponds to the addition of the nth neutral molecule to the protonated core ion. [c] Bulk condensation enthalpy of the neutral ligand. [d] Average of the acceptable literature values in the NIST tables.[29]

on PA(B) alone.

oxonium ions ($ROH_2^+(H_2O)_4$ and $R_2OH^+(H_2O)_4$ clusters):

$$\Delta H^\circ_{0,4} = 223 - 0.84\mathrm{PA(B)}\ \text{kcal/mol} \qquad (18)$$

primary and secondary ammonium ions ($RNH_3^+(H_2O)_4$ and $R_2NH_2^+(H_2O_4)$ clusters):

$$\Delta H^\circ_{0,4} = 207 - 0.71\mathrm{PA(B)}\ \text{kcal/mol} \qquad (19)$$

For pyridinium and substituted pyridinium ions, pyridinium·$H^+(H_2O)_4$, a somewhat different relation,

Table 6. Thermochemistry of Stepwise Hydration and Neat Clusters of Anions

	$-\Delta H^\circ_{n-1,n}$[a]									$-\Delta S^\circ_{n-1,n}$[a]						
n[b]	1	2	3	4	5	6	7	8	cond[c]	1	2	3	4	5	6	refs
Hydration $A^-(H_2O)_n$																
OH^-	26.6	17.6	15.4	12.0	11.5	11.2	10.4	9.8	10.5	22.5	21.3	24.4	21.1	24.1	23.2	*d*
CH_3O^-	24.6	19.2	14.8	11.0					10.5	22.9	25.3	24.4	20.0			180
$HCOO^-$	16.0	13.8							10.5	23.0	24.0					55
CH_3COO^-	16.1	12.8	12.0						10.5	21.4	19.8	20.0				55,79,167
CN^-	13.7	11.7	10.7	9.8					10.5	19.2	18.1	19.8	20.0			162
F^-	27.4	17.9	14.5	13.7	12.8	10.9	10.4	11.2	10.5	20.1	20.5	21.7	26.8	28.4	29.8	159
Cl^-	14.1	12.7	11.8	10.6	9.5	8.6	8.1		10.5	19.8	20.9	22.6	29.4	21.7	21.2	*d*
HS^-	14.2	12.6	11.7						10.5	18.7	20.4	23.5				79,56
Neat Clusters $A^-\cdots nA$																
$CH_3O^-\cdots nCH_3OH$	28.8	21.4	15.0	11.4					8.4	20.8	27.8	26.3	22.4			180
$CH_3COO-\cdots nCH_3COOH$	29.3	19.6	12.5						12.8	29.6	28.6	22.7				55,183
$CN^-\cdots nHCN$	21.2	16.4	12.6	10.9	9.8	8.5			6.0	20.6	21.8	21.2	24.8	20.2	20.4	8,43
$F^-\cdots nHF$	45.8															208
$Cl^-\cdots nHCl$	23.5[d]	14.6	11.7	10.3						23.1[d]	22.4	23.4	26.7			188
$HS^-\cdots nH_2S$	13.2								4.5	19.7						79

[a] Units are as follows: $\Delta H^\circ_{n-1,n}$ (kcal/mol); $\Delta S^\circ_{n-1,n}$ (cal/(mol K)). [b] In the hydration series, $\Delta H^\circ_{n-1,n}$ corresponds to the addition of the nth H_2O molecule as shown. In the neat cluster series, $\Delta H^\circ_{n-1,n}$ corresponds to the addition of the nth neutral molecule to the protonated or deprotonated core ion. [c] Bulk condensation enthalpy of the neutral ligand. [d] Average of the acceptable literature values in the NIST tables.[29]

$\Delta H^\circ_{0,4} = 185 - 0.64\mathrm{PA(B)}$ kcal/mol, applies.

Surprisingly, these relations can be extended to predict the bulk solvation enthalpies of most ions. The 4-fold hydrated clusters, $BH^+(H_2O)_4$, can be transferred into liquid water to form the BH^+_{aq} hydrated ion. The experimental data show that the enthalpies of hydration of the clusters, $\Delta H^\circ_{g\rightarrow aq}(BH^+\cdot 4H_2O)$ are a constant -73 ± 3 kcal/mol for diverse ions. Combined with eqs 18 or 19, the bulk solvation energies, $\Delta H^\circ_{g\rightarrow aq}(BH^+)$, can be predicted on the basis of PA(B) alone. This relation can be expressed by eq 20

$$-\Delta H^\circ_{g\rightarrow aq}(BH^+) = a - 0.84\mathrm{PA(B)}\ \text{kcal/mol} \quad (20)$$

When constant a of 252 kcal/mol for alkyloxonium ions and 262 kcal/mol for alkylammonium ions is used, eq 20 predicts the solvation energies ranging from 63 to 101 kcal/mol for diverse ions with an SD of ± 2 kcal/mol (Table 11, columns 8 and 9 below). Even the deviations from these relations are structurally reasonable as ions with aromatic substituents and pyridine are solvated less efficiently by 4−8 kcal/mol than predicted by the PA, due to reduced hyrophobic solvation. It is surprising that the complex energetics of ion solvation can be reduced to such a simple relation. This results from a canceling variation of solvation terms as described below.

As noted above, after the fourth step $\Delta H^\circ_{n-1,n}$ approaches the limiting bulk-phase value of $\Delta H^\circ_{condensation}(H_2O) = -10.5$ kcal/mol within ± 1 kcal/mol in most hydration sequences (Figures 25 and 26 and Tables 4 and 5). This suggests that the strong ionic interactions are contained mostly in the bonding energies of the first four solvent molecules.

The fact that the effects of solvation are concentrated in the first few solvent molecules is born out also by solvation effects on the structures of the core ions themselves. Ab initio calculations showed that bond lengths and charge distributions in the cluster change less with each additional solvent molecule (Figures 23 and 24). Solvation effects on the structure of the core ion are also largest for the first inner-sphere solvent molecules. For example, the first four H_2O molecules have the largest effect on stretching the C−C bond by 0.026 Å in $CH_3COO^-(H_2O)_6$, and the effects of additional H_2O molecules are small enough to expect that structures of CH_3COO^- in this cluster and in bulk solution are similar.[209]

For anion clusters, Larson and McMahon calculated the consecutive clustering energies of Cl^- with H_2O, HCl, and CH_3CN molecules and of F^- by H_2O and HF up to four ligand molecules, using eq 10 above, by first recalculating the acid dissociation energy of the solvated ions using eq 21.

$$\Delta H^\circ_{acid}((RH)_nA^- - H^+) = \Delta H^\circ_{acid}(A^- - H^+) + \sum \Delta H^\circ_{j-1,j} \quad (j = 1 \text{ to } n-1) \quad (21)$$

The calculated ΔH°_{acid} of the clustered anion can then be inserted into eq 21 to calculate the bonding energy of the next ligand molecule. Larson and McMahon found that this procedure predicted the binding energies of 16 clusters with a standard deviation of ± 1.6 kcal/mol.[8]

As noted above, equilibrium measurements on hydrated clusters are limited to six to eight H_2O molecules, as the bonding energies approach $\Delta H^\circ_{condensation}(H_2O) = -10.5$ kcal/mol and these clusters can be observed only near the temperature where water vapor condenses. However, near this temperature, the distribution of clusters broadens and shifts to larger clusters. It can be shown that in the equilibrium populations of large clusters the thermochemistry of which reached the limiting value of $\Delta G^\circ_{n-1,n} \approx \Delta G^\circ_{condensation}$, the maximum population of the nth cluster is a fraction $n^n/(n+1)^{n+1}$ of the total population. The result is that any cluster containing 10 or more H_2O molecules constitutes less than 3.5% of the total cluster population under any equilibrium condition. Furthermore, it is also observed experimentally and can be shown mathematically that clusters of increasingly larger sizes can be

observed by equilibria over increasingly more narrow temperature ranges. These effects limit the clusters accessible to equilibrium measurements and the accuracies of the measurements.[178]

In summary, empirical relations allow estimation of the partial solvation enthalpies by one to four H_2O molecules, and even the bulk solvation enthalpies based on the proton affinity alone, to within the experimental accuracy of ±2 kcal/mol for diverse ions. These relations can be useful for estimating the thermochemistry of hydration of protonated ions and protonated functional groups of biomolecules.

3.1.4. Shell Filling

a. Thermochemical Effects of Shell Filling. In some clustering series, the bonding energies drop after a shell is filled at step $n = s$, and the next ligand molecule starts an outer shell at $n = s + 1$. Entropy effects are also observed as ΔS°_D increases before shell filling due to the increasing steric interference of ligand molecules and then decreases at the beginning of an outer shell due to the unhindered rotation of the first molecule in a new shell. The shell-filling effect was first noted in the series $NH_4^+(NH_3)_n$ at $s = 4$ solvent molecules.[36,149,210−213]

Without shell filling at the sth ligand molecule, the value of ΔH°_D decreases monotonically, and the difference between each consecutive step becomes smaller. However, the drop in the bonding energy after the shell-filling step s introduces a larger decrease in the bonding energy at this step than in the preceding step ($s - 1$) or following step ($s + 1$), and this leads to eq 22.[157]

$$(\Delta H^\circ_{(s-2,s-1)} - 2\Delta H^\circ_{(s-1,s)} + \Delta H^\circ_{(s,s+1)}) \begin{cases} < 0 & \text{no shell} \\ > 0 & \text{shell filled} \end{cases} \quad (22)$$

A difficulty with thermochemical evidence for shell filling is that the effects are often within the error limits of the measurements, because three clustering steps each with its usual associated uncertainty of ±1.5 kcal/mol must be compared.

Shell effects are illustrated in clustering sequences in Figure 27 where three ligand molecules complete the first shell and in some of the clustering sequences in Figure 26 where three water molecules complete the second shell. A review of solvation sequences by H_2O, CH_3OH, HCN, CH_3CN, NH_3 and alkylamines, H_2S, and $(CH_3)_2SO$ showed that shell-filling effects according to eq 22 are observed in 10 out of 61 known clustering series. Shell-filling effects after the sth solvent molecule were observed in $H_3O^+ \cdot nH_2O$ ($s = 3$), $NH_4^+ \cdot nNH_3$ ($s = 4$), $CH_3OH_2^+ \cdot nH_2O$ ($s = 2$), and $CH_3OH_2^+ \cdot nCH_3OH$ ($s = 2$) and in the hydration of CH_3CHOH^+, $(CH_3)_2OH^+$, and CH_3CNH^+ ($s = 3$, second shell), as well as in $K^+ \cdot CH_3CN$ ($s = 3$), $K^+ \cdot (CH_3)_2SO$ ($s = 2$), $K^+ \cdot n(H_2N(CH_2)_2NH_2)$ ($s = 2$), and $OH^- \cdot nH_2O$ ($s = 3$)[157] and later also in the neat cluster series $CH_3NH_3^+ \cdot nCH_3NH_2$, n-$C_3H_7NH_3^+ \cdot n(n$-$C_3H_7NH_2)$, and $(CH_3)_2NH_2^+ \cdot n(CH_3)_2NH$.[178]

The thermochemical effects are illustrated in Figure 27. Interestingly, the shell-filling effects in each series are comparable, about a drop of 3−5 kcal/mol in ΔH°_D below the extrapolated value from the preceding steps, although shell filling occurs at different steps. An interesting effect is that shell filling occurs after three H_2O molecules both about H_3O^+ and OH^-, the latter suggesting hydrogen bonds of water molecules to each of the three oxygen lone pairs in the hydroxyl anion. Similarities in geometries and shell-filling effects in the clusters of H_3O^+ and OH^- were confirmed by ab initio calculations.[194]

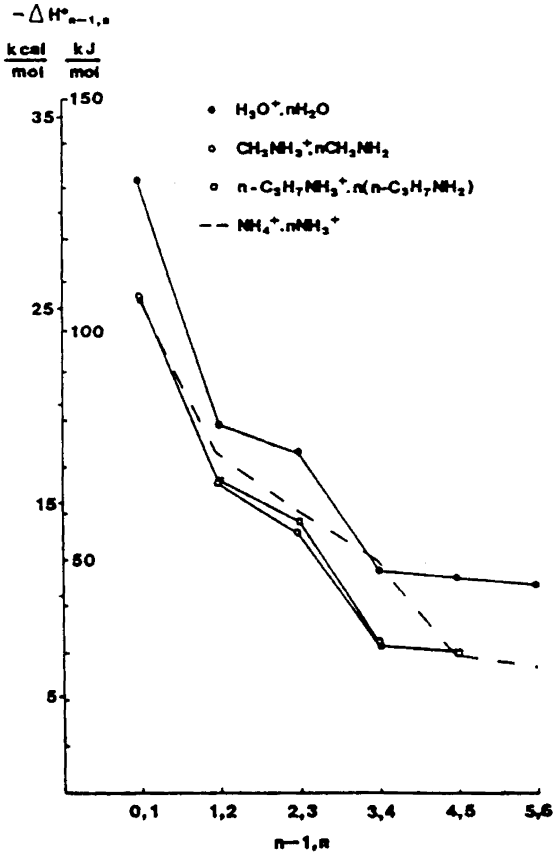

Figure 27. Enthalpy sequences for neat clusters about core ions with three bonding hydrogens with shell filling at the 2,3 step. For comparison, the clustering series for $NH_4^+ \cdot nNH_3$, where shell filling occurs at the 3,4 step, is also shown. Reproduced from ref 178 with permission. Copyright 1992 American Chemical Society.

Shell-filling effects can be observed by other methods such as the metastable fragmentation of cluster ions, which was used to study hydrated adenine and thymine cations. Both exhibited well-defined hydration shell structures with the first hydration shell complete with four water molecules.[214]

Shell effects may not be observed by equilibrium measurements when the bonding energies approach the limiting condensation energies already before shell filling occurs. In these cases, the bonding energy cannot drop further significantly. For example, in Figure 26, three monoprotonic oxonium ions show the filling of the second shell after $n = 3$, but other monoprotonic ions do not show this effect, because for these clusters $-\Delta H^\circ_{2,3}$ is <12 kcal/mol, close to the 10.5 kcal/mol condensation enthalpy of water. The bonding energy cannot become significantly smaller after shell filling.

Another factor that can obscure shell filling is the possible formation of open-shell and closed-shell

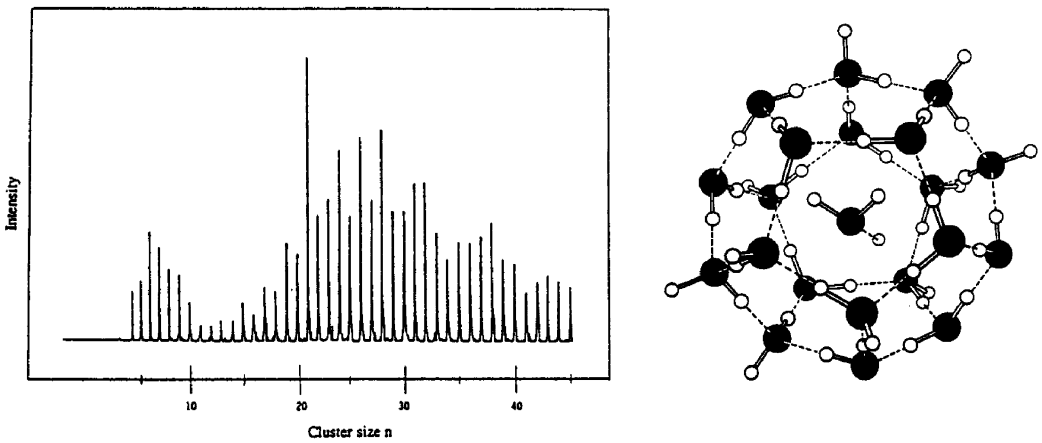

Figure 28. Pentagonal didodecahedral hydrogen-bonded structure of $(H_2O)_{21}H^+$ with a central encaged H_3O^+ ion. Reproduced from ref 219 with permission. Copyright 1996 American Chemical Society.

isomers of comparable energies. This can cause the observed lack of shell effects in $NH_4^+(H_2O)_n$,[199] in $HCN(NH_3)_mH^+$, and in $(HCN)_n(NH_3)H^+$ clusters.[186]

Large shell effects occur in methyl-blocked clusters. For example, in $(CH_3)_2O)_nH^+$, $((CH_3)_2CO)_nH^+$, $(CH_3OCH_2CH_2OCH_3)_nH^+$, and $(CH_3CN)_nH^+$, the first IHB of the dimers is strong, 30−32 kcal/mol, but the second bond must form through weaker CH·X bonds or a long T-shaped hydrogen bond, and ΔH°_D drops to <12 kcal/mol. An intermediate case occurs in $(HCN)_nH^+$, where CH·N bonds are present in the HCN·HCN·H$^+$·NCH·NCH chain, but these do not block bonds strongly since HCN is a relatively efficient hydrogen donor. Shell filling in clusters with blocked ligands was observed in mixed clusters of NH_4^+ solvated by NH_3 and CH_3CN, CH_3CHO, and $(CH_3)_3N$ ligands.[207,215−217]

Thermochemical shell effects in non-hydrogen-bonded clusters were investigated experimentally and theoretically by Hiraoka and co-workers in $(N_2)_n^+$,[145] $(N_2)_nH^+$,[144] $(CO)_n^+$,[146] $(CO)_nH^+$,[144] $(CO_2)_n^+$,[142] and $(CO_2)_nH^+$.[144] This group also investigated bonding and shell effects in the clusters with weak CH···X bonds in $CH_3N_2(N_2)_n^+$ at $n = 3$, 6, and 8,[98] in complexes of $C_2H_5^+$, s-$C_3H_7^+$, and t-$C_4H_9^+$ with CO_2 and N_2O,[99] and in the complexes $F^-(C_2H_4)_4$ and $Cl^-(CH_3CHCH_2)_3$.[113]

b. Shell Filling Effects in Cluster Distributions and Magic Numbers. Shell filling causes "magic numbers" in cluster distributions generated under nonequilibrium conditions by supersonic beam expansion. For example, $(H_2O)_n(Me_3N)_mH^+$ and $(NH_3)_n(Me_3N)_mH^+$ clusters showed maximum intensities when the number of outer blocked ligands was equal to the number of free hydrogens on the protonated cores. The number of Me_3N molecules that filled shells about $(H_2O)_nH^+$ and $(NH_4)_nH^+$ suggested that the IHBs in the cores formed cyclic structures[207,216,217] and that in larger clusters rings can merge into stable cryptands and clathrates such as in $(H_2O)_{21}H^+$ (Figure 28). These structures could be identified by titrating the ligands attached to the core. The related literature was reviewed recently.[218,219] Other examples of the reduced reactivities of closed-shell clusters were observed in the slow reactions of alkyl blocked dimers, $(MeCN)_2H^+$, $(Me_2O)_2H^+$, and $(Me_2CO)_2H^+$, and in mixed clusters, $(EtOH)(MeCN)_2H^+$ and $(HCOOH)(MeCN)_2H^+$.[53,220−224]

How large a thermochemical effect is needed to cause magic numbers in cluster distributions? In mixed clusters formed in supersonic beam expansion, peaks corresponding to shell-filled $(CH_3CN)_2(CH_3OH)_nH^+$ or $(CH_3)_3N_{m+2}(H_2O)_mH^+$ clusters were larger than peaks formed by adding further CH_3CN or $(CH_3)_3N$ ligands in blocked positions even when the difference between the total bonding energies was only 2−3 kcal/mol. The observed clusters are formed by the dissociation of larger clusters in the beam, and the observations suggest that the final dissociation steps occur in cold clusters where small energy differences can have large kinetic effects. Therefore, the distributions of clusters generated by supersonic beams are sensitive probes of even small energy effects of shell filling.[203]

We may ask whether there is a relation between solvent shells in clusters and in solution. Several theoretical papers addressed this question. Tunon and co-workers studied H_3O^+ and OH^- with a hydration shell of three H_2O molecules in the gas phase or in bulk solvent. They found that the central H_3O^+ ion retains 0.796 of the charge and an inner shell of three H_2O solvent molecules, even in the presence of nine solvent molecules. The OH^- ion also retained −0.782, −0.592, and −0.676 charge in the presence of three or six discrete solvent molecules or three H_2O molecules and a continuum solvent, respectively. Bulk solvation changed the most stable conformation from one in which the three H_3O inner shell dipoles point away from the OH^- dipole to one where they are almost parallel to this dipole, reversing a 5.2 kcal/mol energy difference. Further solvation increased the geometrical changes caused by the first solvent shell, but both H_3O^+ and OH^- retained a distinct inner shell of three H_2O molecules upon higher solvation in these models.[194,225] Monte Carlo calculations showed that the inner shell effects about H_3O^+ can be discerned even in the presence of 40−50 H_2O molecules.[198]

3.1.5. The Evolution of Hydrogen-Bond Networks and Isomeric Clusters

Pertinent to shell filling is the fact that outer shells can start before an inner shell is completed (similar

to shell filling in atoms). As clusters build up, IHB networks with noncyclic, cyclic, and three-dimensional clusters can have similar energies and may coexist in equilibrium.

The addition of each solvent molecule increases the number of possible structural isomers. Typically, several structures with similar energies are separated by small barriers and they may interconvert in thermal populations, providing low-energy pathways for proton transfer. Isomeric clusters can affect shell filling, participate in the formation of covalent or noncovalent adducts, and affect thermochemical and spectroscopic measurements.

Early ab initio studies of Newton and Ehrenson on isomeric protonated water clusters found cyclic structures comparable in energy to open isomers.[226,227]

The fact that isomers may coexist in equilibrium in thermal cluster populations was discussed by Meot-Ner and Speller,[157] and Deakyne and co-workers calculated the energies of isomers with filled shells or mixed inner/outer shells in $(H_2O)_nH^+$, $(NH_3)_nH^+$, $(NH_3)_m(H_2O)_nH^+$, $(HCN)_m(H_2O)_nH^+$, and $(MeCN)_m(H_2O)_n$ clusters.[36,228] More recently, cluster distributions and IR spectroscopy of clusters at 170 ± 20 K identified coexisting isomers with five- and six-membered rings and cage structures of $(H_2O)_nH^+$ clusters,[230] isomers and cyclic structures in mixed methanol−water and methanol−water−acetonitrile clusters,[231,232] isomers with or without intramolecular IHBs in $(H_2NCH_2CH_2NH_2)(H_2O)_3H^+$ clusters,[233] isomers with a H_3O^+ core or a protonated dimer core in protonated water/ketone clusters,[104] and water bonded directly to $C_6H_6^{\bullet+}$ or forming rings in ionized benzene/water clusters.[120]

In general, the energy differences between isomeric clusters are often small, and enthalpy and entropy differences often compensate each other since tightly bound low-energy isomers tend to have smaller entropies, which decreases the free energy differences.

The presence of isomeric clusters can affect equilibrium measurements of association reactions. A lower cluster B_nH^+ may be in equilibrium with a mixture of $B_{n+1}H^+$ isomers each with a different $\Delta H^\circ_{n-1,n}$ and $\Delta S^\circ_{n-1,n}$ value. The results can yield apparent van't Hoff plots that do not represent exactly any of the isomers.[157] For example, if $\Delta H^\circ_{n-1,n}$ for one product is −15.0 kcal/mol and $\Delta S^\circ_{n-1,n}$ is −23.0 cal/(mol K), then the presence of isomers with $\Delta H^\circ_{n-1,n}$ of −19.0, −17.0, −13.0, or −11.0 kcal/mol and the same $\Delta S^\circ_{n-1,n}$ will yield composite van't Hoff plots yielding apparent $\Delta H^\circ_{n-1,n}$ values of −19.0, −16.8 to −14.8, and −15.0 kcal/mol, respectively. Such systems may yield broken or curved van't Hoff plots, but this is not detectable if the energies of the isomers are similar. The composite results are close to the more stable isomer, but they are not precise.[157] However, when one isomer is a weakly bonded cluster and the other isomer is a strongly bonded covalent adduct, the effects may be observed as broken van't Hoff plots such as the $C_2H_5^+ + H_2$ adducts[129] or as curved van't Hoff plots as in the association of t-$C_4H_9^+$ with various bases.[123]

Examples where filled and open-shell structures have similar energies within 2 kcal/mol are $NH_4^+(H_2O)_n$ and in $(NH_3)_n(HCN)_mH^+$ clusters containing more than four molecules.[36,228] These results were confirmed by more recent high-level calculations and spectroscopy on the $NH_4^+(H_2O)_n$ clusters ($n = 0-5$), which found an isomer with closed shell and cyclic and noncyclic isomers of similar energies at $n = 4$ and a four-membered ring and a fifth double acceptor H_2O molecule at $n = 5$.[234,235]

Similar effects of many isomeric clusters of comparable energies were shown by molecular mechanics calculations on large protonated water clusters[198] and by spectroscopy and theoretical calculations on water/methanol clusters.[236] Isomeric clusters of comparable energies, in some of which outer shells start before an inner shell is completed, may be common in large clusters.

Isomeric clusters of similar energies occur also in solvated anions. For example, ab initio calculations on $I^-(H_2O)_n$ ($n = 1-6$) found flexible potential surfaces in particular for $n = 5$ and 6 with four nearly isoenergetic conformers for $n = 6$. These conformers have surface and near-surface structures with coordination numbers of 4 H_2O molecules about the ions.[237]

3.1.6. Location of the Ion: Internal versus External Solvation

As the solvent shell grows, solvent molecules may fill a shell about the core ion and keep building up shells about it with the ion inside the solvent cluster (internal solvation). Alternatively, outer solvent molecules can attach to the first inner molecule and build a solvent cluster to which the ion is attached on the outside (external solvation). Isomers of either form and close in energy were found in early calculations on $NH_4^+(H_2O)_n$ clusters,[36] and some of the isomers were observed later by spectroscopy.[234,235] The solvent may even remove the proton, leaving the neutral solute on the outside, such as in $MeCNH^+(H_2O)_n \rightarrow MeCN(H_2O)_nH^+$[228] or in $Me_2OH^+(H_2O)_n \rightarrow Me_2O(H_2O)_nH^+$.[230]

The location of the ion was investigated extensively in the hydration of halide anions. The larger ions, Cl^-, Br^-, and I^-, are surface-solvated by water and methanol, while F^- is inside the hydrated cluster.[88] External solvation of halide ions, but internal solvation of Na^+ was also suggested by liquid-drop theory.[238] The development of solvent structure in clusters about halide ions and implications about the inner solvent shell in solution were reviewed recently.[86]

Halide anions and protonated alkylated cations often remain on the surface in small clusters but assume inner positions as the solvent surrounds the ions upon higher solvation.[237,239] For example, in alkylated oxonium and ammonium ions, the first six to eight H_2O molecules are expected to cluster about the ionized functional group, leaving the hydrophobic alkyl substituents on the outside. Indeed, water clusters appear to solvate alkylated ions such as protonated n-octylamine and 1-adamantylamine in this manner with the amine positioned on the surface of the water cluster. This was indicated by magic

numbers in the solvating water clusters in studies using electrospray−FTICR.

However, the alkyl groups become solvated when the cluster is transferred to bulk solution. Cluster thermochemistry separates the "inner" and "external" (hydrophobic) solvation energies, allowing calculation of the various solvation terms, as discussed below.

3.1.7. Approach to Condensation

As the cluster size increases, the outer shells become increasingly shielded from the ionic charge, which remains concentrated mostly on the core ion. The structure assumes liquid-like characteristics with hydrogen-bonded networks including rings and three-dimensional cages. Also similar to liquids, where hydrogen bonds constantly break and reform, many isomeric clusters of comparable energies can be present in equilibrium. With these features, the bonding energies should approach $\Delta H°_{condensation}$ of the bulk liquid.

In fact, the trends in bonding energies, $\Delta H°_{n-1,n}$, with increasing cluster size have been measured in clustering sequences of many ligands and of a given ligand, H_2O, about many ions. In all cases, the binding energies converge to the respective bulk liquid $\Delta H°_{condensation}$ already after a few, usually four to six, solvent molecules. This applies in ionic clusters of small molecules with liquid condensation energies of 1−2 kcal/mol such as Ar, H_2, CO, and N_2 that were measured up to 10−16 molecules by Hiraoka, in clustering series of hydrogen-bonding species such as $(NH_3)_nH^+$ and $(H_2O)_nH^+$ with condensation enthalpies of 5−10 kcal/mol, clustering series of more complex molecules, some with even larger condensation energies, such as alcohols from CH_3OH to t-C_4H_9OH and also CH_3COOH, HCN, and CH_3CN and $(CH_3)_3N$. In hydration sequences, the bonding energies converge to $\Delta H°_{condensation}(H_2O)$ regardless of the core ions, from the hydration of Na^+, K^+, and H_3O^+ to larger core ions such as protonated alcohols and amines and also anions such as OH^-, CH_3COO^-, and halide anions. In each case, $\Delta H°_{n-1,n}$ converges to 8−10 kcal/mol, close to $\Delta H°_{condensation}(H_2O) = 10.5$ kcal/mol, after four to eight ligand molecules. The convergence of clustering sequences to the bulk limit was summarized.[178]

The approach to bulk $\Delta H°_{condensation}$ already after four to eight steps implies that liquid-like structures form even in these small clusters. The strength of a single neutral OH···O bond is 5 kcal/mol, and the observed limiting value of $-\Delta H°_{n-1,n}$ of about 10 kcal/mol for $n > 4$ in hydration sequences implies that two net new hydrogen bonds form by the addition of each H_2O molecule. This requires liquid-like cyclic and three-dimensional hydrogen bond structures. These conclusions from the thermochemistry were confirmed by the ab initio and spectroscopic results discussed below.

3.2. Mixed Clusters

3.2.1. Unlimited and Blocked IHB Networks

In clusters formed in natural processes such as atmospheric nucleation and in mixed liquids and solution, several different components usually aggregate into multicomponent hydrogen-bonded networks. Two main types of networks can be distinguished. In the first type, both components have bonding hydrogens, can serve both as acceptors and donors, and can therefore form indefinite hydrogen-bond networks. The thermochemistry of such clusters was measured in mixtures of H_2O with NH_3[149] and H_2S[61,64] and in both anionic and cationic clusters in mixtures of H_2O with CH_3OH,[180] CH_3COOH,[183] and H_2SO_4.[240,241]

In the second type of mixture, one component, usually water, can serve both as acceptor and donor and forms a strongly hydrogen-bonded protonated core surrounded by alkyl-blocked components that can serve only as acceptors. The thermochemistry of such clusters was measured in mixtures of H_2O with $(CH_3)_2O$,[103] $(CH_3)_2CO$,[242] $CH_3OCH_2CH_2OCH_3$,[154] HCN,[199,186] and CH_3CN[228] and also in nonaqueous mixtures of $CH_3OH/(CH_3)_2O$,[103] CH_3OH/CH_3CN,[243] and HCN/NH_3.[162] Clusters containing HCN are intermediate between the two types because it can serve as a strong acceptor but also as a donor of CH···X type bonds.

3.2.2. The Location of the Proton

The nature of the IHB network, unlimited or blocked, affects the location of the proton in the clusters.

The position of the proton in nonblocked clusters was investigated both by theory and spectroscopy. For example, ab initio calculations addressed ammonia/water clusters where the proton is usually on an NH_4^+ core ion, consistent with the higher PA(NH_3) vs PA(H_2O). However, Figure 24 above shows a cluster where NH_4^+ is attached to a $(H_2O)_3$ water cluster in an outer position. The proton affinity of H_2O (165 kcal/mol) plus the total binding energy of $(H_2O)_3H^+$ is 207 kcal/mol, just above the proton affinity of NH_3 (204 kcal/mol). Correspondingly, the calculated structure shows that the proton is partially transferred to water. However, such structures with NH_3 in outer positions are high-energy isomers that may not exist in equilibrium mixtures.[36] In $MeOH/H_2O$ clusters the proton tends to be located on $MeOH_2^+$ but H_2O^+-centered isomers can have comparable energies. The structures of protonated NH_3/H_2O clusters[234,235] and $MeOH/H_2O$ clusters[236] will be discussed in the spectroscopy section.

In mixed clusters of nonblocked and blocked components, the proton usually resides on the component with the higher proton affinity. However, a proton can reside on the weaker base due to two effects. The proton can form a H_3O^+ core ion when blocked molecules with higher proton affinity attach to it and exert balancing attractions that keep the proton on the core ion. Second, several water molecules can form a $(H_2O)_nH^+$ core where the strong IHBs stabilize the proton in this center. Figure 29 illustrates these effects in Me_2O/H_2O clusters as suggested first by Grimsrud and Kebarle.[103]

The first combined experimental and ab initio study that showed a proton located on the component with the lower PA was performed by Meot-Ner,

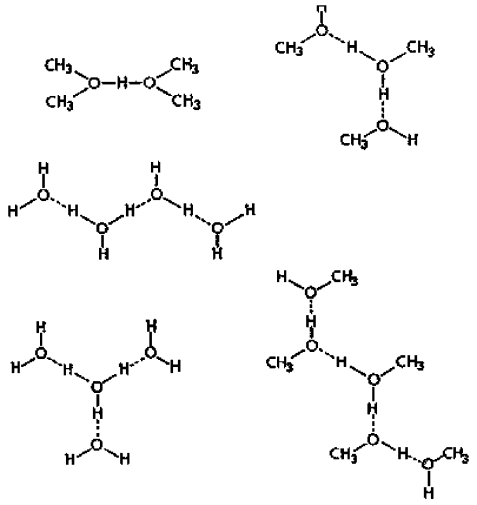

Figure 29. Structures of protonated water/dimethyl ether and methanol/dimethyl ether clusters with a protonated water or methanol core and, when dimethyl ether is present, a blocked dimethyl ether periphery. Reproduced from ref 103 with permission. Copyright 1973 American Chemical Society.

Deakyne, and co-workers on CH_3CN/H_2O clusters.[228] This type of structure is shown in Figure 30 in $MeCN(H_2O)_2H^+$ in which $PA(H_2O)$ plus the binding energy of $(H_2O)_2H^+$ is 198 kcal/mol, greater than PA(MeCN) (186.2 kcal/mol). Correspondingly, the proton is transferred from MeCN to a $(H_2O)_2H^+$ dimer. A similar effect was observed spectroscopically in protonated Me_2O/H_2O clusters where the proton is transferred to a H_3O^+ core ion in $(Me_2O)(H_2O)_3H^+$.[230]

The Castleman group[207,216,217] examined the $(CH_3)_2O/H_2O$, $(CH_3)_2CO/H_2O$, $(CH_3)_3N/H_2O$, $(CH_3)_3N/NH_3$, and pyridine/NH_3 clusters by metastable and collisional induced dissociation (CID). They concluded that H_3O^+ or NH_4^+, respectively, are the core ions when the cluster size is large enough to form a closed hydrogen-bonded shell, even where the proton affinity of core the species (H_2O) is lower by 61.8 kcal/mol than that of the ligand $(CH_3)_3N$ (Figure 31). In this type of structure, the maximum content of the blocked B molecule can be represented as $(H_2O)_nB_{n+2}H^+$ or $(NH_3)_nB_{2n+2}H^+$ with a protonated water or ammonia core of which the outer H atoms are all occupied by methyl-blocked ligands. These formulas apply as long as no cyclic hydrogen-bond networks are formed.

There is some evidence that blocked ligands may not always surround a H_3O^+ or NH_4^+ core ion. In $((CH_3)_2CO)_2(H_2O)H^+$ and $(pyridine)_2(NH_3)H^+$, collisional dissociation yielded only the loss of H_2O and NH_3 molecules, respectively, suggesting that these were bound weakly to the $((CH_3)_2CO)_2H^+$ or $(pyridine)_2H^+$ dimers.[207,216,217] However, the clusters could have rearranged before dissociation. In fact, evidence for protonated cores surrounded by blocked ligands was observed in related systems by SIFT experiments and ab initio calculations. In such studies, Lifschitz and co-workers identified stable clusters where NH_4^+, protonated amines, or $MeOH_2^+$ are surrounded by blocked CH_3CN or CH_3COCH_3 ligands.[53,222−224,244,245]

In $(HCOOH)_n(H_2O)H^+$, structures with a H_3O^+ core ion start to dominate at $n = 4$. For larger clusters, with $n = 5-8$, folded structures with a central H_3O^+ core ion and terminating with cyclic, neutral H-bonded $(HCOOH)_2$ dimers (Figure 32) were calculated as more stable than linear structures terminated by H_2O and HCOOH, but only by a few kilocalories per mole. Experimentally, the coexistence of all of these structures is indicated because H_2O, HCOOH, and $(HCOOH)_2$ loss channels all occur upon CID.[246]

The location of the proton on H_3O^+ surrounded by blocked bases was also confirmed by IR spectroscopy.[104,230,247]

Similar groupings of a central $(H_2O)_nH^+$ unit between more basic polar groups can be formed also when the polar groups are located on a polyfunctional

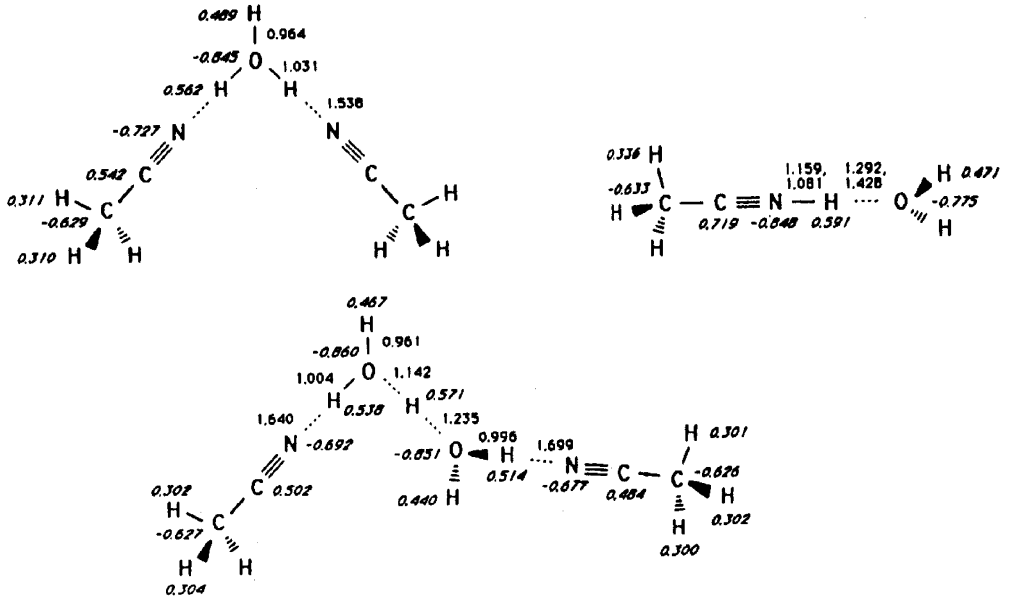

Figure 30. Calculated structures of $(CH_3CN)(H_2O)H^+$, $(CH_3CN)_2(H_2O)H^+$, and $(CH_3CN)_2(H_2O)_2H^+$, where in the latter two clusters the balancing attractions of two CH_3CN molecules keep the proton on a water core, despite the lower proton affinity of water. Reproduced from ref 228 with permission. Copyright 1986 American Physical Society.

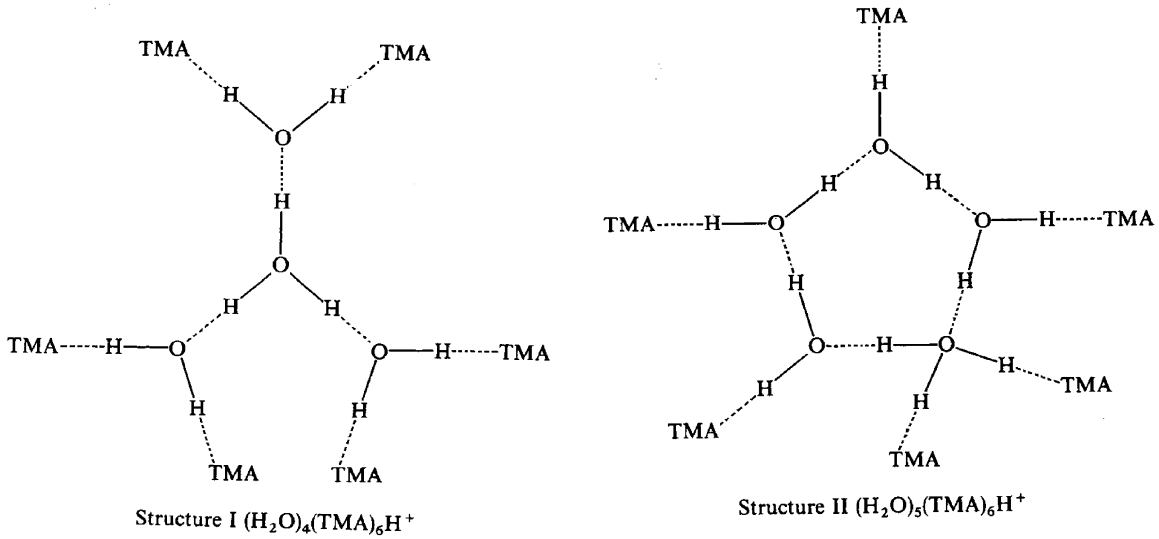

Figure 31. Structures derived from collisional dissociation of mixed protonated clusters of trimethylamine and water. The proton is located on a H_3O^+ core ion. Reproduced from ref 217 with permission. Copyright 1991 American Chemical Society.

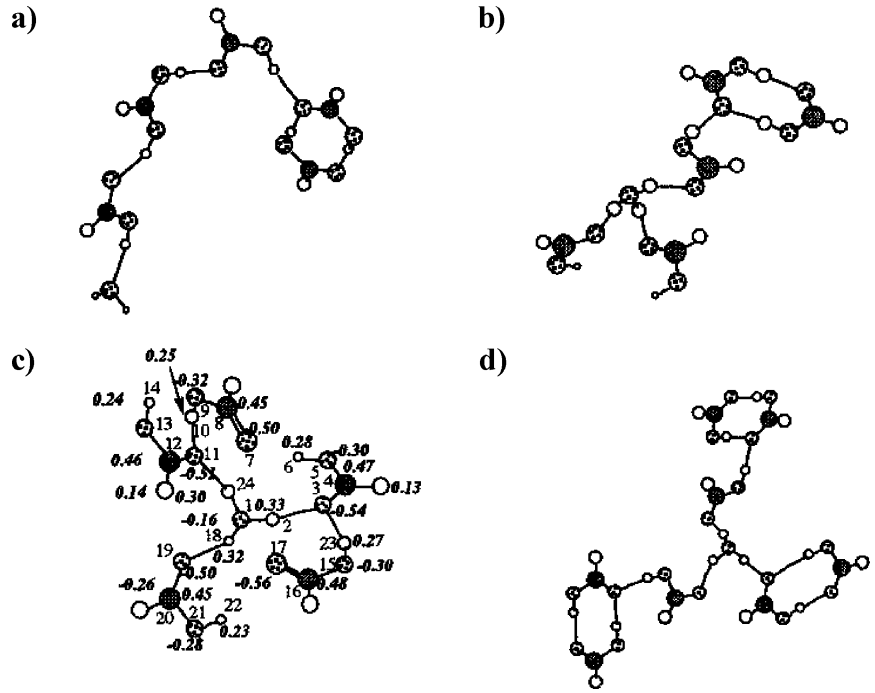

Figure 32. Structures indicated in (a−c) $(HCOOH)_5(H_2O)H^+$ clusters and (d) $(HCOOH)_8(H_2O)H^+$ clusters. The proton is located in a H_3O^+ core ion in structures b, c, and d. Reproduced from ref 246 with permission. Copyright 1997 Elsevier.

molecule. In biology, this allows the proton to move through a water that is surrounded by more basic groups in proteins.

An extreme example of a proton on a H_3O^+ center occurs in the cation-bridged, that is, salt-bridged, cluster $CH_3COO^-\cdot H_3O^+\cdot CH_3COO^-\cdot H_2O$ where the H_2O molecule has a PA lower by 140 kcal/mol than each of the neighboring CH_3COO^- ions.[183] The low energy of the charge-separated intermediate results from the location of the proton between two negative charges that attract the proton in opposite directions. Such charge-separated isomers can constitute low-energy intermediates for proton transfer between carboxylic groups in biological systems.

In summary, the proton can be located in a protonated core stabilized by ionic hydrogen bonds, even when the core is formed by a weak base surrounded by stronger but blocked base molecules. Such structures were confirmed by various experiments and by calculations, and they play significant roles in biology.

3.2.3. Relations between Cluster Composition and Binding Energies

Figures 33 and 34 show the thermochemical data for IHB networks in mixed clusters as illustrated in the CH_3OH/H_2O cationic and anionic clusters.

The numbers under the formulas in Figures 33 and 34 indicate the stabilities of the ionic hydrogen-bond networks in terms of the energy required for dissociation to the highest-energy monomer ion and neutral components. The effects of increasing mole

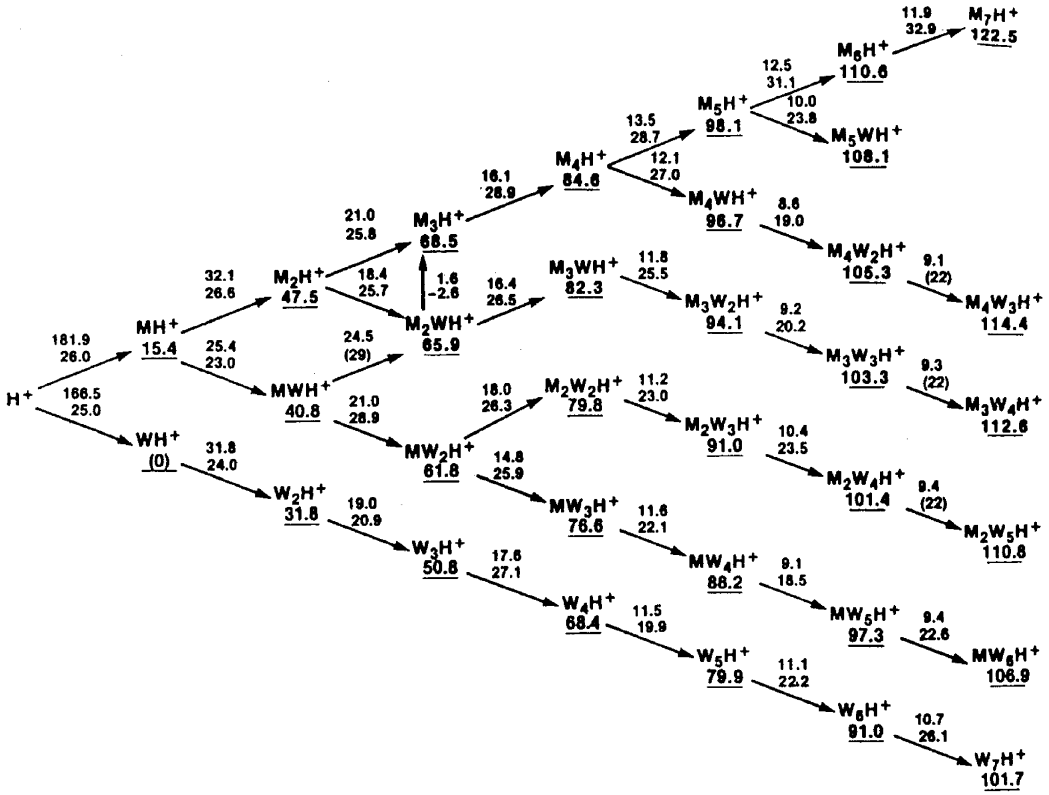

Figure 33. Thermochemistry of protonated hydrogen-bond networks in methanol/water mixed clusters, $(CH_3OH)_m(H_2O)_nH^+$. Numbers above arrows indicate ΔH°_D (top) and ΔS°_D (bottom) for the step indicated. Vertical arrows indicate ligand exchange reactions. Numbers under formulas indicate enthalpies of dissociation to H_3O^+ and neutrals. Reproduced from ref 180 with permission. Copyright 1986 American Chemical Society.

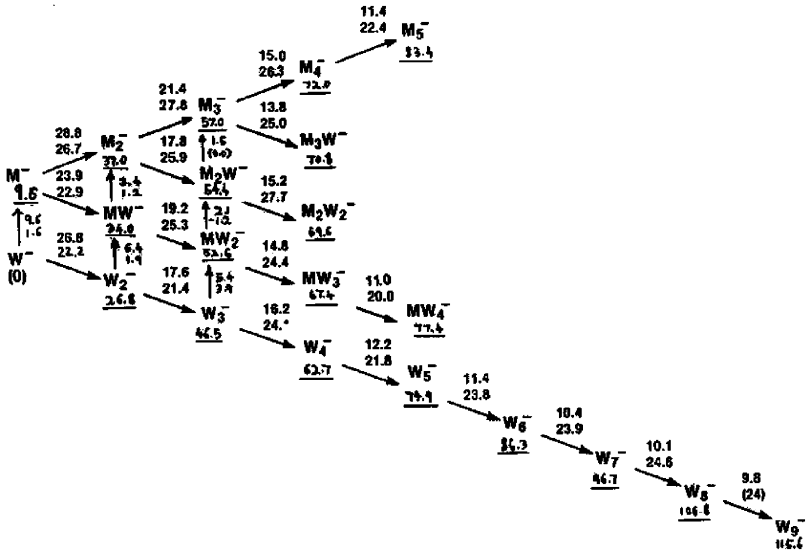

Figure 34. Thermochemistry of anionic hydrogen-bond networks in methanol/water mixed clusters $((CH_3OH)_n(H_2O)_m - H)^-$. Numbers above arrows indicate ΔH°_D (top) and ΔS°_D (bottom) for the step indicated. Vertical arrows indicate ligand exchange reactions. Numbers under formulas indicate enthalpies of dissociation to OH^- and neutrals. Reproduced from ref 180 with permission. Copyright 1986 American Chemical Society.

fraction of the organic component can be observed by proceeding vertically up a given column, comparing clusters of a constant rank, $m + n$. Note that the term "rank" may be more precise than "size" to describe the number of components, because various clusters with equal number of components may have different physical sizes.

The stabilities increase with increasing enrichment of the component with the higher PA or, in anion clusters, of the component with the greater gas-phase acidity. For example, the trend of increasing stability of $(MeOH)_m(H_2O)_nH^+$ four-membered clusters with increasing MeOH content can be noted in Figure 33 and was also confirmed by ab initio calculations and

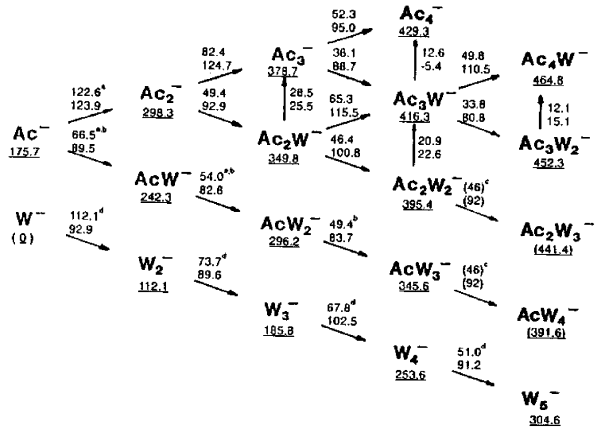

Figure 35. Thermochemistry of anionic hydrogen-bond networks in acetic acid/water mixed clusters. See caption to Figure 33 for meaning of numbers. Reproduced from ref 183 with permission. Copyright 1999 American Chemical Society.

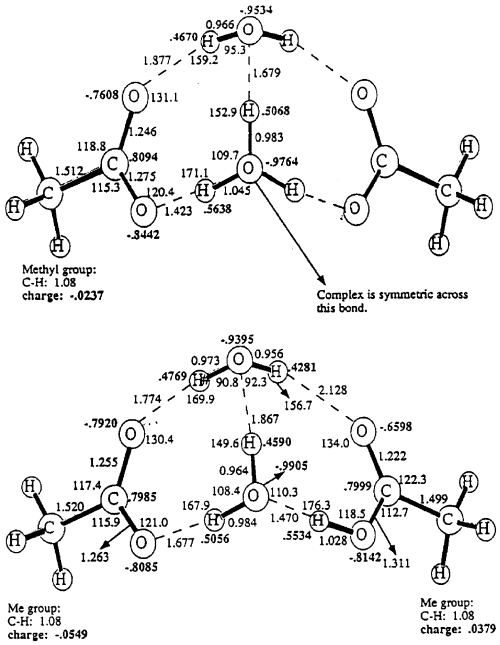

Figure 36. Water-bridged (bottom panel) and salt-bridged (top panel) geometries of some anionic acetic acid/water clusters calculated by the Gaussian 92 method, optimized at the SCF/4-31G level. Reproduced from ref 183 with permission. Copyright 1999 American Chemical Society.

spectroscopy.[236] This is also the trend in protonated and in anionic clusters of acetic acid and water in Figure 35, even when complex geometries such as in Figure 36 arise because of two functional groups in the acetate ion. In these clusters, the strong $OH^+\cdots O$ or $O^-\cdots HO$ bonds that can form unlimited IHB networks and enrichment by the stronger base or acid always increases the stability.

However, when one of the components can form stronger IHBs, enrichment in this component may be stabilizing. This is the case in ammonia/water clusters (Figure 24) where some of the bonds are $OH^+\cdots O$, some $NH^+\cdots O$, and some $NH^+\cdots N$ bonds. Although the proton affinity of NH_3 (204 kcal/mol) is much higher than that of H_2O (165 kcal/mol), the stabilities of the $(H_2O)_nH^+$ clusters increase with increasing size more than those of the $(NH_4)_nH^+$ clusters because of the stronger $OH^+\cdots O$ bonds in the former.

3.3. Effects of Partial Solvation on Acidities, Basicities, and on Ionic Aggregation

3.3.1. Effects of Partial Solvation on Basicities

Gas-phase ion chemistry made an important contribution to acid/base chemistry by measuring intrinsic solvent-free molecular acidities and basicities. Comparison with solution shows that ion solvation is as significant as molecular properties. Solvation effects can compress, and sometimes reverse, the relative acidities and basicities. This was shown in early studies on the acidities of alcohols and the basicities of amines by Brauman and Blair,[248,249] Kebarle,[5] McIver and co-workers,[250] and Bohme and co-workers.[11,251,252]

Since these early measurements, the gas-phase acidities and basicities of thousands of compounds were compiled.[27,30,128,253] These data allow an analysis of structural effects on molecular acidities and basicities, and comparison with solution quantifies the solvation effects.[20]

The solvation effects are illustrated by comparing the relative enthalpies of protonation in the gas phase and in solution (Table 11). Among the oxonium and ammonium ions listed, $\Delta H_{prot,g}$ varies by 45.4 and 30.7 kcal/mol, while $\Delta H°_{prot,aq}$ varies only by 3.3 and 5.5 kcal/mol, respectively. In some cases solvation reverses the relative basicities. The physical effects of solvation on basicities were investigated recently by ab initio calculations on the stepwise hydration of ammonia, methylamine, dimethylamine, and trimethylamine and their protonated ions. The first water molecules add distinctly, while larger numbers of water molecules form hydrogen-bond networks. The thermochemistry leads toward the anomalous basicities of ammonia and alkylamines in solution.[254] Cluster studies show the stepwise buildup of these solvation effects.

When a base B is protonated in water, the proton is transferred from a solvated $H_3O^+_{aq}$ ion to form a solvated BH^+_{aq} ion. The process also releases a solvated H_2O molecule and takes up a solvated B molecule. Equation 23 shows the cluster equivalent of this process.

$$H_3O^+(H_2O)_n + B(H_2O)_n \rightarrow BH^+(H_2O)_n + H_2O(H_2O)_n \quad (23)$$

The effects of stepwise solvation are reflected by the variation of the thermochemistry with n. The energies of the neutral clusters in eq 23 are usually not available, but for n donor acids and bases, the energies of neutral hydrogen bonds are likely to be comparable. Most of solvation effects in reaction 23 may be attributed therefore to ion solvation as in reaction 24, the thermochemistry of which can be

$$H_3O^+(H_2O)_n + B \rightarrow BH^+(H_2O)_n + H_2O \quad (24)$$

calculated from proton affinities and the thermo-

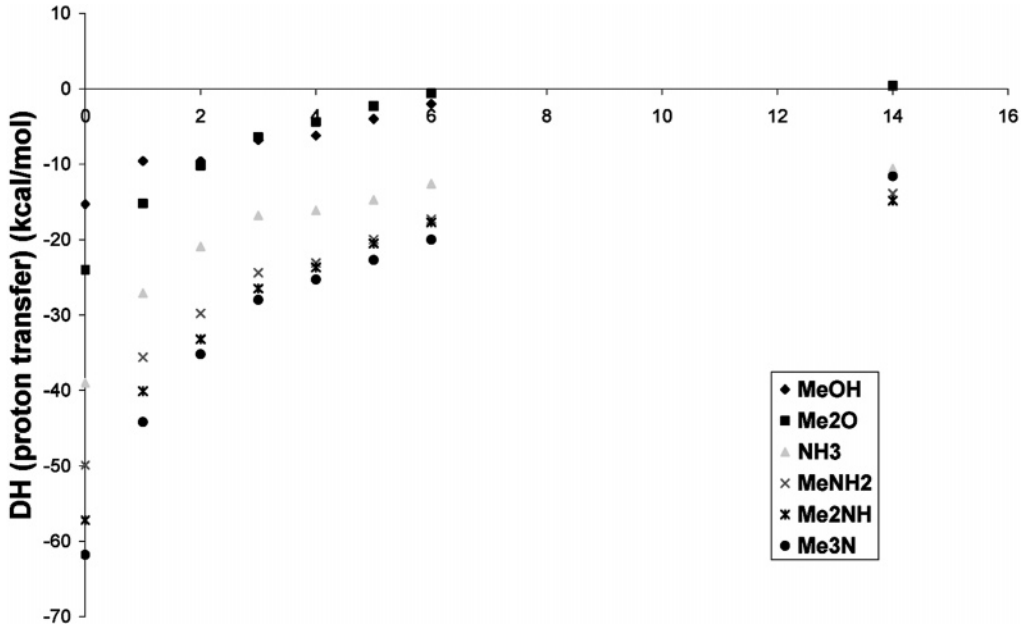

Figure 37. Enthalpies of proton transfer from water to base B as a function of n-fold ion solvation for $H_3O^+(H_2O)_n + B \rightarrow BH^+(H_2O)_n + H_2O$. The exothermicity decreases with increasing n as proton transfer from H_3O^+ to bases B becomes less exothermic with increasing solvation due to the strong hydration of the H_3O^+ ion. In general, proton transfer from weaker bases B to stronger bases B′ (vertically down at each n) becomes less exothermic with increasing n due to the stronger hydration of the BH^+ ions. The relative values approach the relative heats of protonation in solution. The figure shows the compression of relative enthalpies of protonation (approximately, the relative basicities) with stepwise solvation toward the values in bulk water, represented by "$n = 14$". Values were calculated from eq 26 using cluster data from Table 4, enthalpies of ion hydration from Table 10, and proton affinities from Table 11.

chemistry of the $H_3O^+(H_2O)_n$ and $BH^+(H_2O)_n$ clusters. Reaction 25 and the corresponding eq 26 show the

$$BH^+(H_2O)_n + B' \rightarrow B'H^+(H_2O)_n + B \quad (25)$$

$$\Delta H^\circ_{25} = [PA(B) - PA(B')] + [\Delta H^\circ_{0,n}(B'H^+ \cdot nH_2O) - \Delta H^\circ_{0,n}(BH^+ \cdot nH_2O)] \quad (26)$$

effects of n-fold hydration on the relative heats of protonation. Using $B' = H_2O$ in eq 26 yields the enthalpy of proton transfer from water to base B as a function of n-fold solvation.

Analogous relations apply for anion clusters and relative acidities. Note that eq 26 neglects the relative clustering energies of the neutrals, that is, it corresponds to reaction 25. Figure 37 shows the results for several bases. The main observation is that increasing solvation compresses and in some cases reverses the differences between the intrinsic molecular basicities and acidities of molecules. For example, solvation by six H_2O molecules decreases the enthalpies of proton transfer from H_3O^+ to alkylamines from −40 to −60 kcal/mol to −12 to −20 kcal/mol, while further bulk solvation decreases these values by a much smaller factor, to −10 to −16 kcal/mol. Solvation in the clusters decreases the differences between enthalpies of protonation because ions of stronger bases are solvated less efficiently than H_3O^+, according to the $\Delta H^\circ_D/\Delta PA$ correlations. This trend carries over to aqueous solution where solvation causes the irregular basicities of alkylamines and compresses the differences between the basicities of oxygen and nitrogen bases (Figure 37). Similar effects also apply in anions, where solvation compresses the relative acidities of alcohols and carboxylic acids. This was shown by the classical studies of Brauman and Blair on the acidities of alcohols.[248,249] and by recent results on $NH_2^-(NH_3)_n$ ($n = 0-2$) where NH_2^- is a stronger base than H^- in the gas phase but two ammonia solvent molecules reverse this order.[255]

In conclusion, comparisons with gas-phase chemistry show that solvation effects can be as significant as intrinsic molecular parameters in determining relative acidities and basicities. Cluster studies show that most of the solvation effects, often 80% or more, result from the first four to eight solvent molecules.

3.3.2. Effects of Partial Solvation on Ionic Aggregation

Equation 27 represents aggregation with solvent displacement of an n-fold solvated ion and neutral to form an $(n - 1)$ solvated dimer ion.

$$BH^+(H_2O)_n + B(H_2O)_n \rightarrow B_2H^+(H_2O)_{n-1} + H_2O(H_2O)_n \quad (27)$$

Again, focusing on strong ion solvation and disregarding the effects of weaker and unknown bonding energies in the neutral clusters leads to reaction 28 to model the effects of ion solvation on aggregation.

$$BH^+(H_2O)_n + B \rightarrow B_2H^+(H_2O)_{n-1} + H_2O \quad (28)$$

The thermochemistry of reaction 28 is shown by the second step vertically up (from $BH^+(H_2O)_n$ to $B_2H^+(H_2O)_{n-1}$) in clustering energy diagrams such as in Figures 33−35. The reaction enthalpy is shown in Figure 38 for clusters with various degrees of solva-

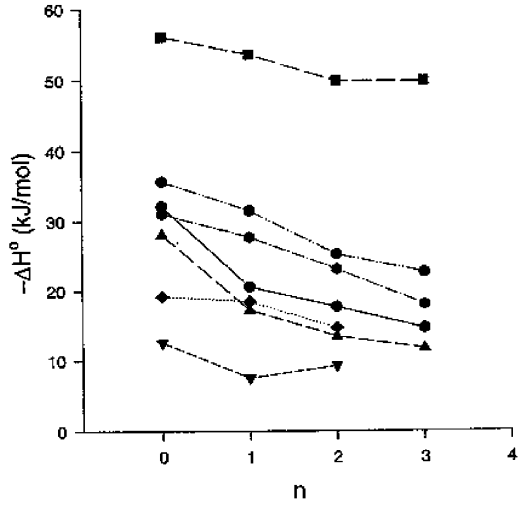

Figure 38. Enthalpies of dimer formation with solvent displacement for the reactions $A^-(H_2O)_n + AH \rightarrow A_2^-(H_2O)_n + H_2O$ in anionic and $BH^+(H_2O)_n + B \rightarrow B_2H^+\cdot(H_2O)_{n-1} + H_2O$ in cationic mixed clusters of water with (from top to bottom lines as they start at $n = 0$) acetic acid (anionic), dimethylamine (cationic), acetic acid (cationic), *n*-propylamine (cationic), methanol (cationic), ammonia (cationic), and methanol (anionic) clusters. The figure shows that dimer formation with water replacement between carboxylate ions and carboxylic acids (top plot) is more exothermic at any degree of hydration than in the other systems. The exothermicity reflects the combination of the formation of a strong $RCOO^-\cdot HOOCR$ bond formed with the displacement of a weak $RCOO^-\cdot HOH$ bond. Preferential aggregation in the carboxylate/carboxylic acid system also applies in higher steps of aggregation, see Figure 39. This effect may contribute IHB networks in the formation of membranes by carboxylic acids. Reproduced from ref 183 with permission. Copyright 1999 American Chemical Society.

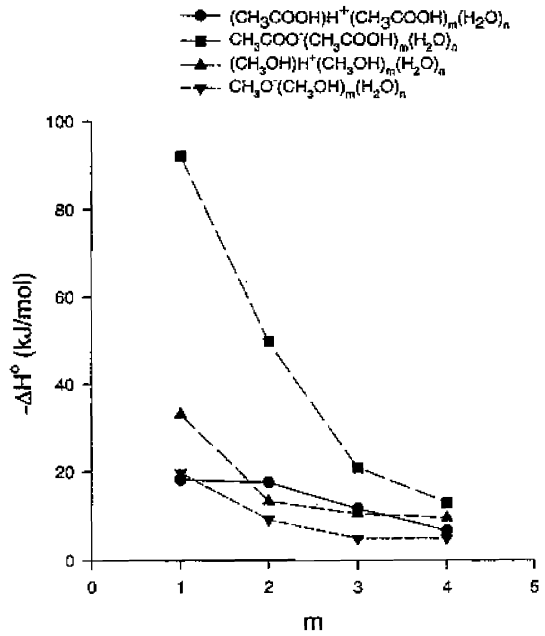

Figure 39. Enthalpies of stepwise aggregation with solvent displacement as modeled by clusters that contain four ligand molecules in anionic and cationic methanol/water and acetic acid/water clusters. The *x*-axis indicates that the *m*th molecule of the nonaqueous component is displaced by the *m*th water molecule. The figure shows that the aggregation of carboxylate ions/carboxylic acids (top plot) is more exothermic than that in the other systems because a strong $RCOO^-\cdot HOOCR$ bond replaces a weaker $RCOO^-\cdot HOH$ bond. The preference for aggregation by carboxylate/carboxylic acids vs other systems is strongest in the first aggregation steps. Reproduced from ref 183 with permission. Copyright 1999 American Chemical Society.

tion. Reaction 28 may be exothermic if the $BH^+\cdot B$ bond is stronger than the $BH^+\cdot H_2O$ bond, but this difference decreases as the number of H_2O molecules in the cluster increases and they solvate the monomer ion more efficiently. Consequently, increasing solvation decreases the exothermicity of aggregation with solvent displacement.

Solvation effects on higher aggregation steps with solvent displacement are represented by the cluster reaction 29, which corresponds to consecutive steps vertically up in clustering diagrams such as in Figures 33−35.

$$B_nH^+(H_2O)_m + B \rightarrow B_{n+1}H^+(H_2O)_{m-1} + H_2O \quad (29)$$

Figure 39 shows the enthalpy of reaction 29 for four-membered mixed clusters. In general, the exothermicities are largest for the first step of aggregation and decrease with adding each further acid or base molecule. The exothermicities of the aggregation steps decrease with increasing mole fraction of the organic component because each consecutive step becomes less significant in stabilizing further the already stabilized charge.

Figure 39 allows us to compare the thermochemistry of ionic aggregation of various acids and bases. As may be expected, aggregation with solvent displacement is favorable when a strong new $BH^+\cdot B$ bond (or $A^-\cdot HA$ bond in anions) displaces a weak $BH^+\cdot H_2O$ bond (or $A^-\cdot H_2O$ bond) to the solvent. This effect favors the ionic aggregation of oxygen bases and oxygen acids that form strong $OH^+\cdot O$ or $O^-\cdot HO$ bonds compared with the aggregation of nitrogen bases that form weaker $NH^+\cdot N$ bonds. These effects also favor the aggregation of strong acids or bases the ions of which form weak bonds with the H_2O molecules that are easier to displace.

Figures 33−35 show that adding the stronger acid or base component binds to the clusters more strongly even in large clusters. This shows that the correlations between hydrogen bond energies and PA differences apply even in large clusters.

In conclusion, structures of mixed clusters were inferred first from thermochemistry and have been verified by ab initio calculations, dissociation methods, reactivity, and spectroscopy. The results show that nonblocked bases can form unlimited ionic hydrogen-bonded networks involving chains and rings, sometimes with distinct shells. The ionic effects are strongest in the inner shells of four to six molecules bonded to the core ions, which retain most of the charge even in large clusters and in solution. In mixed clusters, where unlimited IHB networks are possible, the inner shell contains the component with the higher proton affinity. The stabilities of clusters of a given rank $m + n$ increase with the mole fraction of the component that has the higher PA or acidity. In mixtures of blocked and unblocked components, the proton can remain on the unblocked component

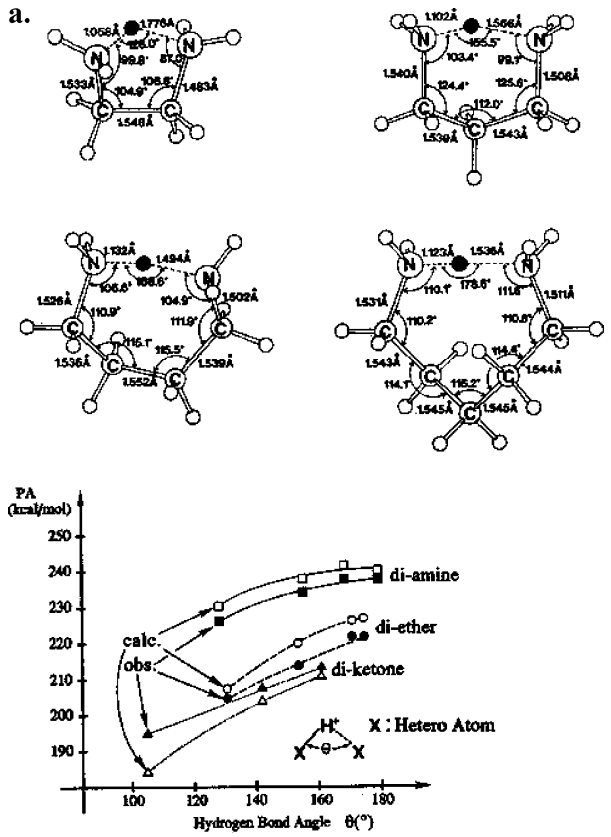

Figure 40. Calculated structures of protonated diamines at the RHF/3-21G level. Note that the bent NH^+-N angles approach linear geometry with increasing ring size. The bottom plot shows the correlation between the internal bond angle and the stabilization of the proton by the internal IHB as reflected in the proton affinities of difunctional compounds. With increasing approach to optimized 180° bond angle, the internal hydrogen bond formed upon protonation becomes stronger and the proton affinities of diamines increase correspondingly. Reproduced from ref 256 with permission. Copyright 1992 American Chemical Society.

even if it has the lower proton affinity when this component forms a core of strong IHBs surrounded by a shell of the blocked components.

4. Complex Molecules: Intramolecular and Multiple Bonds

4.1. Intramolecular Hydrogen Bonds

4.1.1. Stabilities, Ring Size, and Strain Effects

When polyfunctional molecules are protonated, strong internal IHBs (iIHBs) can form with cyclic structures (Figures 40 and 41). The internal bonds stabilize the ions and increase the PAs of the parent molecules. However, internally bonded structures are constrained, and their formation results in negative entropy changes. Nevertheless, the overall free energy effects are usually stabilizing.

Intramolecular IHB formation was first observed by Bowers and co-workers in the increased basicities of diamines.[258] The enthalpy and entropy effects were investigated using temperature studies by Yamdagni and Kebarle and by Meot-Ner and co-workers in proton-transfer equilibria of diamines and triamines,[39,259] protonated polyethers and crown ethers,[260,261] and diketones.[260,262] Studies by the McMahon and Stone groups found similar effects in dialcohols,[262,263] amino alcohols, and methoxy alcohols.[257,259] The cyclic internally bonded structures were confirmed by ab initio calculations on diamines, polyethers, methoxy alcohols,[154,256,257] and other molecules[264−271] and also confirmed by H_2O and MeOH loss through metastable and collisional dissociation.[272] Cyclic iIHB structures and solvent effects thereon were confirmed also by recent IR predissociation spectroscopy studies, especially by the group of Y. T. Lee and co-workers.[233,247,273−276]

Internal hydrogen bonds can also form involving CH donors. Figure 42 shows such structures with $CH\cdots O^-$ bonds in the *n*-decanoate anion that were studied by Norrman and McMahon.

The thermochemistry of internal IHBs (iIHBs) can be evaluated by comparing the PAs of polyfunctional vs monofunctional bases, leading to the results in Table 7. These comparisons make the assigned iIHB strengths dependent on the chosen reference bases.[39,258,259] The internal bond strengths can be also obtained from theory by calculating the energies of the open and cyclized forms of the ion.[272]

The overall stability of an iIHB was characterized by Meot-Ner and co-workers in terms of the temperature required to open the bond, $T_{open} = \Delta H^\circ_{iIHB}/\Delta S^\circ_{iIHB}$, at which half of the equilibrium population is open.[259] Stabilities in these terms are listed in Table 7, which suggests that some stable internal bonds may never open thermally since at the required temperatures, for example, when $T_{open} > 600$ K, ions may pyrolize first. For these ions in Table 7, the internally hydrogen-bonded structure will always dominate.

The thermochemical ring-opening effect was demonstrated experimentally by Norrman and McMahon in ions of some longer-chain acids that form unconventional $CH\cdot O^-$ intermolecular bonds as shown in Figure 42. Proton-transfer equilibria involving *n*-decanoic and 2-ethylhexanoic acids showed curved van't Hoff plots, which suggested an equilibrium population that contained folded and unfolded conformations. For example, 45% of the decanoate population was folded at 435 K, but only 4% was folded at 669 K because the iIHB opened at high temperatures because of entropy effects. The data lead to $\Delta H^\circ_{iIHB} = -7.3$ kcal/mol and $\Delta S^\circ_{iIHB} = -17.2$ kcal/mol for decanoate and −16.8 cal/(mol K) 2-ethylhexanoate. For the shorter chain *n*-butanoate, $\Delta H^\circ_{iIHB} = -0.7$ kcal/mol and $\Delta S^\circ_{iIHB} = -2.5$ cal/(mol K) were calculated. The stabilities of the internal bonds calculated from these data in terms of T_{open} are 424, 435, and 280 K, respectively, consistent with weak $CH\cdots O^-$ internal bonds.[112]

The strain energies reflect constraints on the iIHB geometry imposed by the backbones that connect functional groups.[39,257,259,263] With increasing ring size the strain decreases and the strengths of the internal bonds increase. The bonds become nearly linear and essentially fully optimized when four or more methyl groups separate the functional groups (Figures 40 and 41). This is observed in Table 7 where ΔH°_{strain}

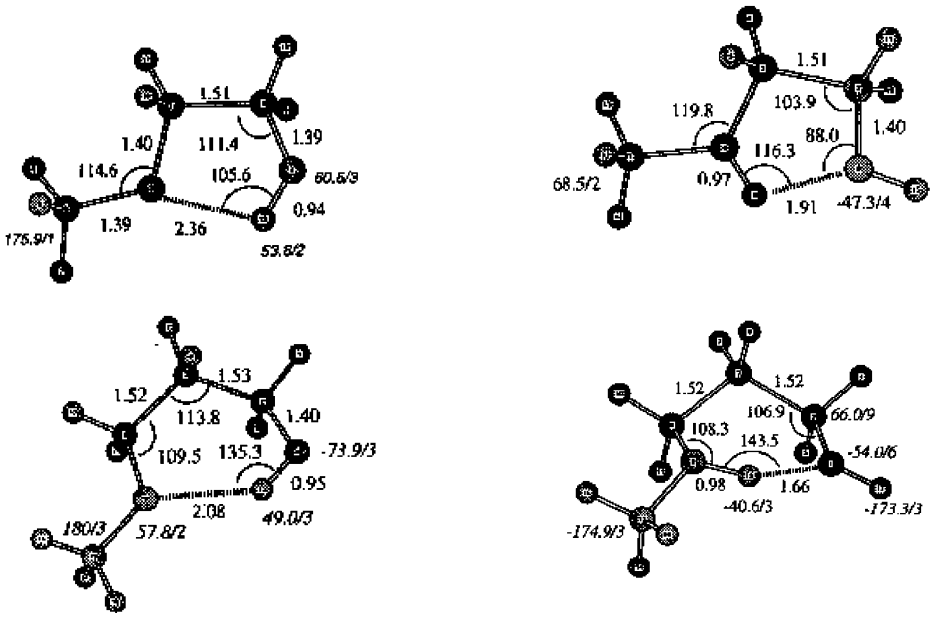

Figure 41. Calculated structures of neutral and protonated methoxy alcohols at the HF/6-31G* level. The internal bonds in the neutrals (left side figures) are displaced by shorter, more optimized and stronger internal bonds in the ions. The internal hydrogen bond becomes more optimized with ring size. Reproduced from ref 257 with permission. Copyright 1998 American Chemical Society.

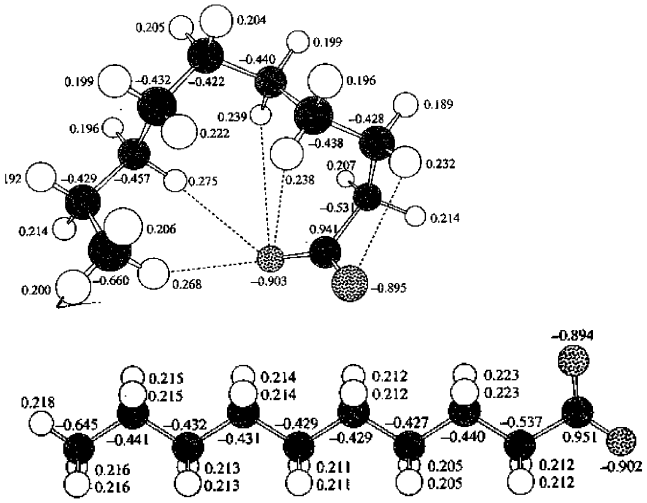

Figure 42. Internally hydrogen-bonded cyclic conformation of *n*-decanoate with five CH···O$^-$ bonds, and the open isomer. Note increased positive charges on the bonding hydrogens and negative charges on the donor CH carbons and acceptor O$^-$ atoms upon hydrogen bond formation. Reproduced from ref 112 with permission. Copyright 1999 American Chemical Society.

decreases and the stabilization, as expressed by T_{open}, increases with increasing ring size. For a given ring size, the stability of intramolecular OH$^+$···O bonds is greater than that of NH$^+$···N bonds, in accordance with the relative intrinsic strengths of these bonds.

Table 7 shows that various bifunctional ions of equal chain length have comparable strain energies. The strain is largest for the smallest rings with two methylene groups between the substituents ($n = 2$), which form five-membered rings containing the carbons, heteroatoms, and binding proton. These rings have comparable strain energies of 15−24 kcal/mol for the listed compounds. The strain energies are substantially smaller, 6−14 kcal/mol, for $n = 3$ structures, which form six-membered rings, and becomes almost negligible within error limits, up to only 2 kcal/mol, for $n = 4$ and 5, which form seven- or eight-membered rings. The consistency among various ions of equal ring size is encouraging, considering that assigning the iIHB strengths for various types of internal bonds (OH$^+$···H, NH$^+$···O, NH$^+$···N) involves comparisons with different reference compounds.

Most internal hydrogen bonds were studied in protonated polyamines, polyethers, and diketones where all the heteroatoms are of the same type. However, Meot-Ner and co-workers also studied protonated amino alcohols where the functional groups are different.[259] Szulejko and McMahon extended subsequently experimental and theoretical studies to methoxy alcohols.[257] Table 7 shows some of these results. Figures 40 and 41 illustrate that the bond lengths and angles in diamines and methoxy alcohols optimize with increasing ring size. For example, the ab initio OH$^+$−O bond length in (MeO-$(CH_2)_n$OH)H$^+$ decreases for $n = 2$, 3, and 4 from 1.91 to 1.66 and 1.53 Å, and the bond angle increases from 116.3° to 143.5° and 165.3°, approaching the optimal 180°.

Additional polar groups in the ion can further stabilize the ion by forming multiple intramolecular hydrogen bonds and by additional electrostatic stabilization of the charge.[261] The protonation of the crown ethers in Table 7 involves large negative entropy changes, although the neutrals are already cyclic, as these structures stiffen upon protonation.[260,261]

In protonated polyfunctional ions, the proton may be located on the site with the highest PA, but it may also be on a group with a lower PA if this leads to stabilization by stronger hydrogen bonds. For example, in the triamine $H_2N(CH_2)_2NH(CH_2)_2NH_2$, the site with the highest PA is the central secondary

Table 7. Enthalpies, Energies, Strain, and Stability of Intramolecular IHBs in Protonated Polyfunctional Ions BH^{+a}

base (B)	PA[b]	$\Delta H°_{iIHB}$[c]	$\Delta H°_{strain}$[d]	$\Delta S°_{iIHB}$[e]	stability (T_{open})[f]	refs[g]
			Diamines			
$[CH_3(CH_2)_2NH_2]$	219.4					
$H_2N(CH_2)_2NH_2$	227.4	8	16	11	727	259,39
$H_2N(CH_2)_3NH_2$	235.8	16	8	17	942	259,39
$H_2N(CH_2)_4NH_2$	240.3	21	3	18	1167	259,39
			Triamines			
$[(CH_3CH_2CH_2)_2NH]$	230.2					
$H_2N(CH_2)_2NH(CH_2)_2NH_2$	237.5[h]	7	17	7	1000	259
$H_2N(CH_2)_3NH(CH_2)_3NH_2$	247.5[h]	17	7	15	1134	259
			Amino Alcohols			
$[(CH_3(CH_2)_2NH_2]$	219.4					
$H_2N(CH_2)_2OH$	222.4	3	14			259
$H_2N(CH_2)_3OH$	230.0	11	6	12	917	259
$H_2N(CH_2)_4OH$	235.3	16	1	17	941	259
			Dialcohols			
$[CH_3(CH_2)_2OH]$	188.0					
$HO(CH_2)_2OH$	195.0	7	24	13	538	263
$HO(CH_2)_3OH$	209.4	22	9	17	1294	263
$HO(CH_2)_4OH$	218.8	31	0	23	1348	263
			Methoxy Alcohols			
$[CH_3O(CH_2)_2CH_3]$	194.8					
$CH_3O(CH_2)_2OH$	198.8[i]	6.8[i]	19.5	2.5[i]	2720	263
$CH_3O(CH_2)_3OH$	213.5[i]	16.3[i]	10.0	14.0[i]	1164	263
$CH_3O(CH_2)_4OH$	219.4[i]	22.4[i]	3.9	15.0[i]	1493	263
$CH_3O(CH_2)_5OH$	219.5[i]	22.0[i]	4.3	18.0[i]	1222	263
			Diethers and Polyethers			
$[CH_3O(CH_2)_2CH_3]$	194.8					
$CH_3O(CH_2)_2OCH_3$	205.1	10[j]	21	4.3	2326	260
$CH_3O(CH_2)_3OCH_3$	214.4	20[j]	11	6.0	3340	260
$CH_3O(CH_2)_4OCH_3$	222.6	28	3	16.8	1667	261
$CH_3O(CH_2)_5OCH_3$	222.6	28	3	17.3	1618	261
$CH_3O(CH_2)_2O(CH_2)_2OCH_3$	219.6	25[j]	6	13.8	1812	260
$CH_3O(CH_2)_2O(CH_2)_2O(CH_2)_2OCH_3$	226.2	31[j]		18.6	1667	260
12-crown-4	221.6	27		8.3	3253	261
15-crown-5	225.6	31		11.1	2793	261
18-crown-6	231.1	36		22.0	1636	261
			Diketones			
$[CH_3COCH_2CH_3]$	197.7					
$CH_3COCOCH_3$	191.7	−6[k]	30	2.6		260
$CH_3COCH_2COCH_3$	208.8	1	30	3.6	278	260
$CH_3COCH_2CH_2COCH_3$	213.2	6	25	7.0	857	260
			Amino Acid Derivatives			
$[CH_3CONHCH_3]$	212.7					
$CH_3CONHCH_2COOCH_3$ (CH_3CO-Gly-OCH_3)	223.7[l]	11[l]	20	12[l]	917	150
$CH_3CONHCH(CH_3)COOCH_3$ (CH_3CO-Ala-OCH_3)	224.7[l]	12[l]	19	15[l]	800	150

[a] Units of $\Delta H°_{iIHB}$ and $\Delta H°_{strain}$ are in kcal/mol, those of $\Delta S°_{iIHB}$ in cal/(mol K), and those of T_{open} in K. Monofunctional reference compounds are shown in brackets. [b] Proton affinities from NIST tables[27] unless noted otherwise. [c] Enthalpies of opening of internal bonds obtained from $\Delta H°_{iIHB} = PA(B) - PA(B_{ref})$ where B_{ref} is the reference compound shown in brackets. [d] Strain energies from the difference between $\Delta H°_{iIHB}$ and $\Delta H°_D$ of protonated dimer ions as reference: for diamines, symmetric $NH^+\cdots N$ dimers, $\Delta H°_D$ = 23 kcal/mol; for amino alcohols, the $CH_3NH_3^+\cdots CH_3OH$ dimer, $\Delta H°_D$ = 17 kcal/mol; for diols and diethers, symmetric $OH^+\cdots O$ dimers, $\Delta H°_D$ = 30 kcal/mol; for methoxy alcohols, the dimer $(CH_3)_2OH^+\cdots CH_3OH$, $\Delta H°_D$ = 26.3 kcal/mol.[261,257] [e] Entropies of ring opening of internal bonds as assigned in the original references. For the diamines, average values are from refs 39 and 259. [f] Temperatures of internal ring opening calculated from $T_{open} = \Delta H°_{iIHB}/\Delta S°_{iIHB}$ (see text). [g] References for the original data. [h] From ref 259. [i] Values assigned in ref 257. [j] For the diethers and glymes, refs 260 and 261 give similar PAs and entropies of protonation. [k] The reduced PA compared with the monofunctional reference ketone reflects the effects of the internal dipole. [l] Data based on ref 150.

amine group, the protonation of which can form a small ring ($n = 2$) with a terminal amine group. The other two primary amine groups have lower PAs, but their protonation could form a larger ring with an optimized bond. Therefore either location may be preferred. The increase in PA vs monofunctional primary or secondary amines would be consistent with either, but the entropy effect is small and suggests protonation on the central amine group, which is stabilized by forming a small hydrogen-bonded ring with one of the other amine groups.[259] Protonation of the central amine group in the larger

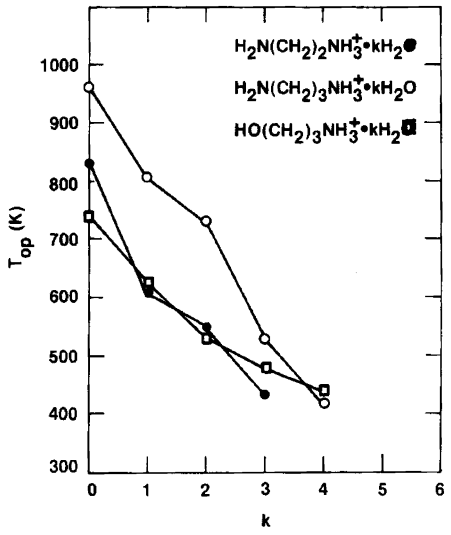

Figure 43. The effects of the stepwise solvation of protonated diamines on the stability of the internal hydrogen bond as expressed by the bond opening temperature, T_{open}, calculated from thermochemical cycle 30. Reproduced from ref 259 with permission. Copyright 1980 American Chemical Society.

$H_2N(CH_2)_3NH(CH_2)_3NH_2$ diamine can form a more optimized ring, resulting in increased proton affinity (Table 7).

The strain energies cannot be evaluated in polyfunctional ions that have more than two polar groups. The increased iIHB energies for these compounds in Table 7 reflect stabilization of the charge by several polar groups[261] and the overall energy effects cannot be factored reliably. However, in the triamines where the additional substituent is less polar, the strain energies are comparable to the diamines with $n = 2$ and 3, respectively. This also suggests that the proton is located on the central amine groups and is stabilized primarily by hydrogen bonding to one other amine group.

Intramolecular iIHBs can also form in distonic radical ion reaction intermediates, such as in the decomposition of $(CH_3OCH_2CH_2OH)^{\bullet+}$.[277,278]

4.1.2. Mutual Effects of Internal and External Solvation

The internal bond can be weakened or displaced by external solvent molecules. The effects of stepwise solvation on the intramolecular bond may be calculated from the thermochemistry of clustering of water molecules on a protonated difunctional ion, compared with an analogous monofunctional ion (reaction 30).

$$\begin{array}{ccc} & \overset{c}{\longrightarrow} & \\ BH^+_{open} + nH_2O & \longrightarrow & BH^+_{open}(H_2O)_n \\ \downarrow a & & \downarrow d \\ & \underset{b}{\longrightarrow} & \\ BH^+_{cyclic} + nH_2O & \longrightarrow & BH^+_{cyclic}(H_2O)_n \end{array} \qquad (30)$$

The thermochemistry of reaction 30a can be found from the comparing the protonation and that of reactions 30b and 30c from comparing the clustering thermochemistry of a bifunctional and an analogous monofunctional base. The cycle yields the thermochemistry of reaction 30d for ring closure of the n-fold solvated bifunctional ion.

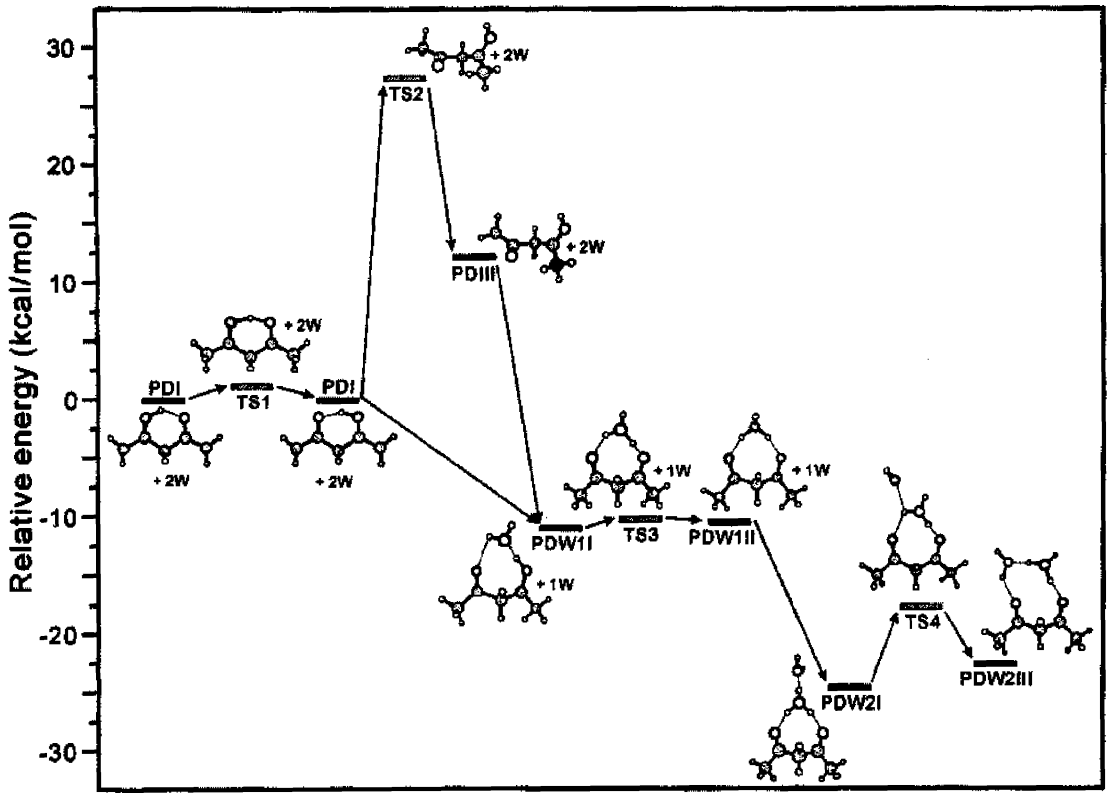

Figure 44. Energy relations between unsolvated and mono- and dihydrated clusters of $(MeCOCH_2COMe)(H_2O)_nH^+$, denoted as PDW, including transition state energies between various conformations. The ab initio structures illustrate that the proton can be located on a H_3O^+ center that bridges between the ketone oxygens and that there are small barriers between conformations, allowing the proton to move between the ketone groups or along the water chain. Reproduced from ref 275 with permission. Copyright 2003 Taylor and Francis (www.tandf.co.uk).

Table 8. Thermochemistry of Complexation of H^+, H_3O^+, and $MeOH_2^+$ by Polydentate Ligands[a]

	H^{+b}		H_3O^{+c}		$MeOH_2^{+d}$
	$\Delta H°_D$, $\Delta S°_D$	$\Delta G°_D(298)$	$\Delta H°_D$, $\Delta S°_D$	$\Delta G°_D(298)$	$\Delta H°_D$, $\Delta S°_D$
		Monodentate			
Me_2O	189.0, *21.1*	182.7	49.8, *30.0*	40.9	35.0, *24.7*
Me_2CO	194.0, *23.8*	186.9	49.5, *26.0*	41.8	
		Bidentate			
$2Me_2O$	220.4, *51.9*	204.9	63.3, *56.3*	46.5	55.0, *54.5*
$2Me_2CO$	224.0, *53.1*	208.2	73.7, *56.9*	56.8	
MeCO-Gly-OMe	223.7, *38.2*	212.3			
MeCO-Ala-OMe	224.7, *41.1*	212.5	72.1, *42.6*	59.4	
G1[e]	208.4, *32.4*	198.7	58.6, *30.0*	49.7	
		Tridentate			
$3Me_2O$	230.5, *79.8*	206.7	80.0, *82.9*	55.3	
$3Me_2CO$	235.5, *75.2*	213.1	92.2, *87.0*	66.3	
G2[e]	222.0, *40.3*	210.0	72.0, *49.8*	57.2	
		Tetradentate			
$4Me_2CO$	245.2, *97.2*	216.2	(100), *(112)*[f]	(67)[f]	
2G1[d]	236.0, *60.7*	217.9	83.2, *63.1*	64.4	
G3	230.0, *44.6*	216.7	83.9, *59.7*	66.1	
12-crown-4	225.0, *34.3*	214.8			58.3, *40.6*
		Hexadentate			
$6Me_2CO$			(116), *(162)*[f]	(68)[f]	
3G1[d]	246.2, *85.8*	220.6	97.9, *(89.3)*	71.3	
2G2[d]	244.9, *77.5*	221.8	99.0, *87.2*	73.0	
18-crown-6[c]	233.8, *48.0*	219.5	88.5, *55.8*	71.9	67.6, *50.0*

[a] Units are as follows: $\Delta H°$ and $\Delta G°$ in kcal/mol; $\Delta S°$ (in italics) in cal/(mol K). [b] The complexation energy of the proton, calculated from PA and GB values from ref 27. Entropies of protonation include the loss of entropy of the free proton (26.0 cal/(mol K)). Thermochemical data for polyethers and crown ethers as listed in ref 154, based on data in refs 260 and 261. [c] Data for H_3O^+ complexes from refs 154 and 242. [d] Data for complexes of $MeOH_2^+$ and of 18-crown-6 from ref 281. The data for complexes of H_3O^+ and $MeOH_2^+$ with polyethers were obtained from the association equlibria of (polyether)H^+ with H_2O or MeOH and thermochemical cycles. [e] G1 = glyme ($MeO(CH_2)_2OMe$), G2 = diglyme ($MeO(CH_2)_2O(CH_2)_2OMe$). [f] Estimated values in parentheses are based on usual cluster trends, considering that after three Me_2CO ligands the further ligands are bonded weakly in the outer sphere.

The effect of partial solvation on the stabilities of the internal bonds in protonated diamines is shown in Figure 43, where four H_2O molecules decrease T_{open} almost to room temperature. The trend explains why intramolecular iIHBs may not form in protonated polyamines in bulk solution where full solvation may decrease T_{open} below the ambient temperature.

Conversely, internal hydrogen bonds weaken the external bonds to the solvent molecules. The internal functional group may be seen as the first ligand molecule, and the bond to the nth solvent molecule becomes equivalent to a bond to the $(n + 1)$th solvent molecule of an analogous monofunctional ion.

Partially solvated ions with internal hydrogen bonds were investigated by IR spectroscopy studies of $H_2NCH_2CH_2NH_3^+(H_2O)_3$[233] and of $(MeCOCH_2COMe)(H_2O)_nH^+$ ($n = 0-3$).[275] Figure 44 illustrates the energy scheme of the unfolding steps that open the iIHB and the evolution of the two-water bridged isomers. This work illustrates the mechanism by which the water molecules help to open the internal bond. Adding water molecules delocalizes the charge, the water interposes between the functional groups, and the distance between the bridged ketone oxygens increases. With addition of zero to three water molecules, the energy difference between the most stable closed form and the open form decreases from 11.9 to 7.1, 3.8, and 3.6 kcal/mol, and the difference in the ketone O−O distance between the closed and open forms decreases in parallel. These changes decrease the barrier for ring opening.

This work also showed that conformational changes that transfer the proton between the ketone groups are possible with relatively low activation energies. Similar water bridges may allow proton transfer with low activation energy through water channels in proteins.[154,242]

4.2. Polydentate Bonding

4.2.1. Thermochemistry and Structures of Polydentate Complexes

Protonated ions can form bonds to several functional groups of a polydentate ligand. Polydentate bonding increases the bond strengths of the complexes (increased $\Delta H°_D$) but also leads to constrained structures with low entropies (increased $\Delta S°_D$). Tables 8 and 9 present the thermochemistry of polydentate complexes and some monodentate complexes for comparison.

The first complexes with thermochemical evidence for polydentate IHB structures were reported by Meot-Ner and co-workers in protonated dimers of nucleic bases,[279] in polydentate complexes of protonated amines with polyethers and crown ethers,[90,154,280] and in the complexes of the glycine and alanine derivatives, $CH_3CONHCH(R)COOCH_3$ (R = H or CH_3).[150] Sharma and Kebarle also measured the thermochemistry of complexes of H_3O^+ and $CH_3OH_2^+$ with polyethers and crown ethers (Tables 8 and 9).[281] Some of these data were confirmed recently by Fourier transform ion cyclotron resonance mass

Table 9. Thermochemistry of Polydentate and, for Comparison, Some Monodentate Complexes[a]

ligands	monoprotonic ions			triprotonic ions		tetraprotonic ion
	pyridineH$^+$	pyridazineH$^+$	Me_3NH^+	$MeNH_3^+$	c-C_6H_{11}–NH_3^+	NH_4^+
			Monodentate			
Me_2CO	(22, *25*)	(23, *25*)	19.5, *29.4*	25.9, *26.0*	(22, *25*)	28.3, *26.4*
Et_2O	22.5, *32.9*	(23, *25*)	(23, *25*)	22.0, *25.0*	22.0, *31.8*	(27, *25*)
			Bidentate			
$2Me_2CO$				(44, *50*)	(37, *50*)	48.6, *51.3*
$MeOCH_2CH_2OMe$ (G1)[b]	25.4, *31.4*		26.7, *34.8*	30.1, *30.1*	29.4, *35.5*	38, *36*
$MeO(CH_2)_3OMe$	26.5, *35.8*		25.5, *33.1*	31.2, *32.0*	28.4, *35.0*	
MeCONHCH(Me)COOMe (MeCO-Ala-OMe)			29.7, *27.6*	40.1, *35.1*	37.8, *40.9*	
			Tridentate			
$3Me_2CO$					(48, *75*)	64.4, *77.3*
G2[b]	31.5, *36.5*	32.4, *36.1*	32.8, *40.0*		39.7, *44.6*	46.6, *35.7*
			Tetradentate			
$4Me_2CO$						77.5, *101.7*
2G1[b]						61.2, *69.5*
G3[b]	34.7, *38.3*		34.6, *40.0*		43.3, *44.8*	
12-crown-4	36.1, *40.0*	37.0, *40.8*	35.8, *41.5*		37.2, *34.8*	
			Pentadentate			
15-crown-5	41.0, *42.6*				42.3, *36.5*	
			Hexadentate			
$6Me_2CO$						(96), *(145)*
3G1[b]						75.6, *96.8*
2G2[b]						77.3, *86.6*
18-crown-6	42, *44*	42, *44*	41, *40*		46, *38*	(70)
			Nucleic Bases			
pyridineH$^+$·pyridine			23.7, *28*			
adenineH$^+$·adenine			30.3, *39*			
cytsineH$^+$·cytosine			38.3, *37*			

[a] Units are as follows: ΔH°_D in kcal/mol; ΔS°_D (in italics) in cal/(mol K). Data from ref 260, except for complexes of NH_4^+ from ref 90 and nucleic bases from ref 279. Data in parentheses were estimated from PA correlations and from clustering trends. [b] G1 = glyme ($MeO(CH_2)_2OMe$), G2 = diglyme ($MeO(CH_2)_2O(CH_2)_2OMe$), G3 = triglyme ($MeO(CH_2)_2O(CH_2)_2O(CH_2)_2OMe$).

spectrometry (FTICR).[282] Polydentate bonding in these complexes was confirmed theoretically.[283] Similar polydentate structures are involved in complexes of metal ions with crown ethers and in molecular recognition.[10] Structures with multiple IHBs were proposed even in simple systems such as the complexes of I^- with H_2O, HCOOH, and MeCOOH.[76]

Polydentate bonding has significant thermochemical effects. The complexes of polyethers in Table 8 have greater bond strengths than those of a single ether or acetone ligand. The bonding energies of the proton and hydronium ion to polydentate ligands increases with the number of functional groups, as observed in comparing mono-, bi-, tri-, tetra-, and hexadentate complexes in Tables 8 and 9. However, the binding energies are affected by geometrical constraints. For example, in the tetradentate complexes of H^+ in Table 8, the total bond strengths are greatest when the complexes are assembled from four free Me_2CO molecules. The bonding energies decrease as the complexes are assembled from two G1 or one G3 or one 12-crown-4 molecule, where the functional groups are increasingly constrained on fewer ligand molecules.

While more ligand molecules or ligand groups increase the bonding energies, they also increase the entropy losses upon forming the complex. For example, the ΔH°_D values of the tetradentate complexes of H^+ in Table 8 vary by 20.2 kcal/mol, and those of ΔS°_D vary compensatingly by 62.9 cal/(mol K). As a result, the free energies of the complexes, $\Delta G^\circ_D(298)$, remain nearly constant. Similar effects are observed in Table 8 for the complexes of H^+ and H_3O^+ with various ligands.

The excess stabilization energy due to multiple bonding denoted by ΔH°_{MB} can be assigned by comparing the dissociation energy of complex of a polydentate ligand with that of a reference monodentate ligand. A suitable reference monodentate ligand for polyethers is Me_2CO the PA of which is comparable to MeOEt, the structural unit of glymes and crown ethers. The *excess* polydentate stabilization energies of the three ions H^+, H_3O^+, and NH_4^+ by a given ligand are similar (Tables 8 and 9), especially in the larger complexes, although the *absolute* bonding energy of H^+ to a given ligand is greater by about 150 kcal/mol than that of H_3O^+ and by 170 kcal/mol than that of NH_4^+. The data in Tables 8 and 9 shows that the excess bonding energies (PA(B) − PA(Me_2-CO)) of the polyethers to H^+, H_3O^+, and NH_4^+ are as follows: G1, 14, 9, 10; G2, 28, 23, 18; 2G1, 42, 34, 33; 3G1, 52, 48, 47; 2G2, 51, 50, 49; 18-crown-6, 40, 39, 42 kcal/mol, respectively. This supports the suggestion of Sharma and Kebarle that the excess polydentate stabilization is due to nonspecific electrostatic interactions.[281] Otherwise, multiple hydrogen bonding to H^+ would involve weaker "bifurcated bonds",[284] while H_3O^+ and NH_4^+ could form several stronger IHBs with the polar groups of these ligands, which would result in significantly different excess stabilization energies of these ions.

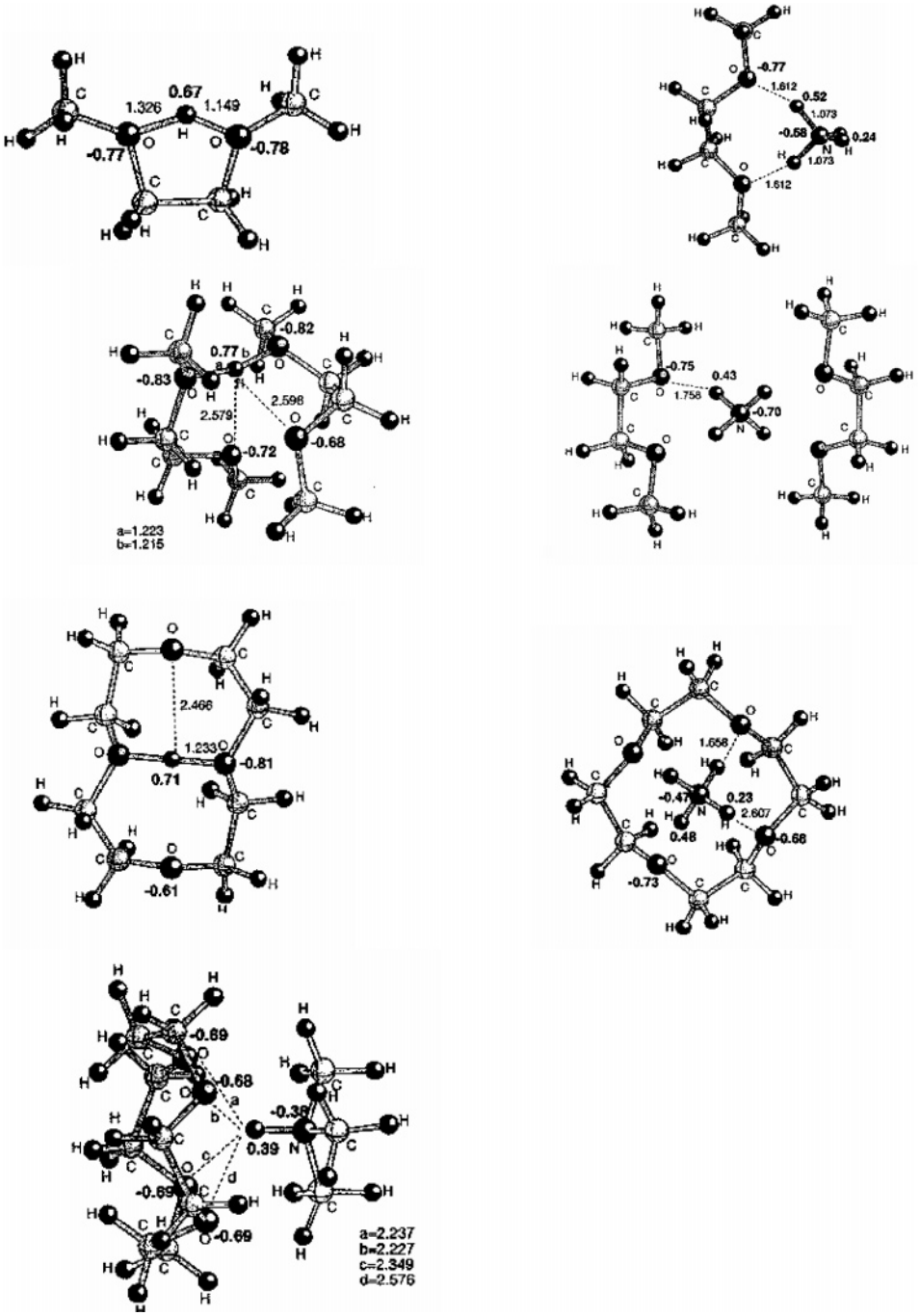

Figure 45. Geometries and atomic charges of complexes of $MeOCH_2CH_2OMe$ (glyme or (G1)), two G1 molecules and 12-crown-4 with H^+ and NH_4^+, and 12-crown-4 with Me_3NH^+ calculated by B3LYP/4-21G(*) density functional theory methods. Reproduced from ref 283 with permission. Copyright 1998 American Chemical Society.

Ion−dipole interactions in polydentate complexes were shown by ab initio calculations. For example, the B3LYP DFT method gave good agreement with the experimental binding energies of the complexes of $CH_3OCH_2CH_2OCH_3$ (glyme (G1)), glyme dimer (2G1), and 12-crown-4 (12c4) with the H^+, $MeOH_2^+$, NH_4^+, $MeNH_2^+$, Me_2NH^+, and Me_3NH^+ ions. The B3LYP/4-21G(*) geometries of several complexes are shown in Figure 45. The complexes with H^+, that is, the protonated species, are stabilized by internal hydrogen bonds, forming a five-membered ring in $G1H^+$. In the protonated dimer $(G1)_2H^+$, the proton is bound by two short 1.2 Å bonds to an oxygen of each glyme molecule and is stabilized additionally by two long 2.6 Å ion−dipole bonds with the other two oxygens. Similarly, in $(12\text{-crown-4})H^+$ the proton is stabilized by short hydrogen bonds with two opposite oxygens and is stabilized further by two long 2.4 Å ion−dipole bonds with the other two oxygens.[283]

In the complexes of $MeOH_2^+$, NH_4^+, $MeNH_3^+$, and $Me_2NH_2^+$ with $CH_3OCH_2CH_2OCH_3$, the ions form two short 1.6−1.7 Å IHBs with two ether oxygens, while Me_3NH^+ forms one short 1.6 Å IHB and one long 2.9 Å ion−dipole bond. In complexes with two glyme molecules, $MeOH_2^+$ forms two short IHBs and two long ion−dipole bonds, while NH_4^+ forms four hydrogen bonds that involve all the available oxygens. In the complex of 12-crown-4 with $MeOH_2^+$, similar

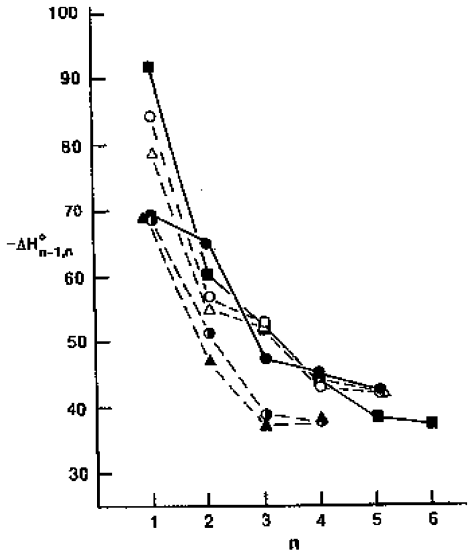

Figure 46. Effects of internal hydrogen bonds on the hydration of ions, as reflected in the enthalpies of stepwise hydration of protonated ketones, ethers, and diethers (kJ/mol): (○) $(CH_3)_2COH^+$; (△) $(n\text{-}C_3H_7)_2OH^+$; (◐) $CH_3N(CH_3)_2\text{-}COH^+$; (▲) $(c\text{-}C_3H_5)_2COH^+$; (●) $(CH_3OCH_2CH_2OCH_3)H^+$ all solvated by H_2O molecules; (■) solvation of $(CH_3OCH_2CH_2\text{-}OCH_3)H^+$ by CH_3OH molecules. The hydration of the protonated diether is anomalous as the first step disrupts the internal bond in the $(CH_3OCH_2CH_2OCH_3)H^+$ ion, while the increased bond strength in the second step suggests forming two hydrogen bonds in a solvent-bridged structure. The third water molecule bonds to the water bridge in an outer position, resulting in a large drop of bonding energy. See Figure 47 for structures. Reproduced from ref 154 with permission. Copyright 1994 American Chemical Society.

to the complex with the proton, there are two 1.5 Å IHBs with two opposite oxygens of the crown ether, while with NH_4^+ there are two unequal bonds of 1.6 and 2.6 Å. The monoprotonic Me_3NH^+ ion gives a different structure without any short IHBs but with four longer bonds of 2.2−2.6 Å of the proton to each oxygen that together stabilize the structure.[283] Figure 45 shows some of these structures.

In these complexes, the proton is located on the small core molecule even when the PAs of the surrounding ether groups are much higher. This is supported by the ab initio structures of complexes of H_3O^+ and NH_4^+ with $CH_3OCH_2CH_2OCH_3$, a ligand that is similar to the structural units of the crown ethers, where the proton also remains on the H_3O^+ core ion.[90,154,283] As in mixed unblocked/blocked clusters, the central proton is balanced by opposing attractions of the surrounding polar groups.

4.2.2. Solvent Bridges in Polydentate Complexes

In protonated complexes of polydentate molecules, water can form bridges between the functional groups. The thermochemical effects in Figure 46 show an anomalous enthalpy sequence for the hydration of $(CH_3OCH_2CH_2OCH_3)H^+$ compared with the hydration of a monofunctional ether. The exothermicity of adding the first H_2O molecule to the protonated diether is decreased because forming the bond requires disrupting the internal hydrogen bond. The second H_2O molecule creates a $(H_2O)_2H^+$ bridge

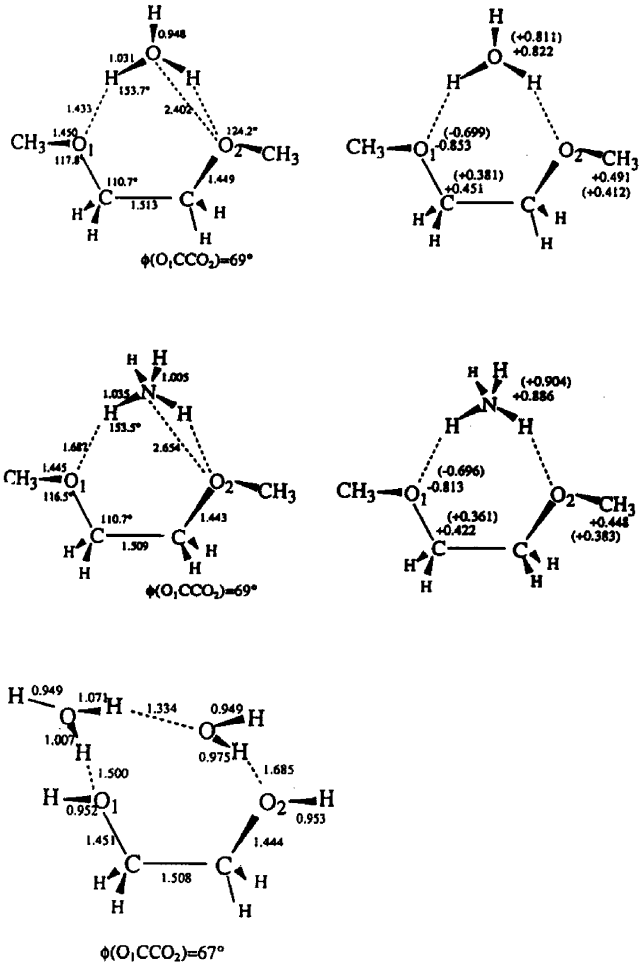

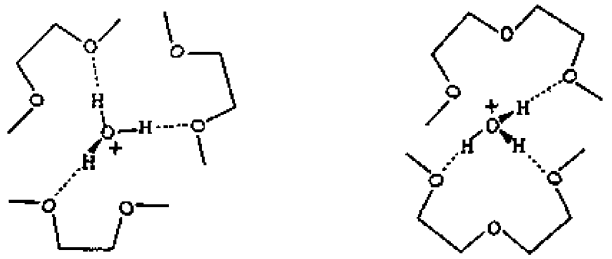

Figure 47. The top figures show the calculated geometries and atomic and group charges in the polydentate complexes of $MeOCH_2CH_2OMe$ with H_3O^+, of $MeOCH_2CH_2OMe$ with NH_4^+, and of $HOCH_2CH_2OH$ with $(H_3O^+\cdot OH_2)$, all using the 4-31G basis set and Gaussian 88, 90, and 92 methods. The bottom figures show proposed polydentate complexes of three bidentate glyme and two tridentate diglyme molecules with H_3O^+ based on thermochemistry. Reproduced from refs 90 and 154 with permission. Copyright 1994 and 1996 American Chemical Society.

between the ether groups. The bonding energy of the third H_2O molecule drops since it starts an outer shell.

The calculated geometries in Figure 47 are consistent with the thermochemical indications. Similar to mixed blocked clusters, the proton is located on the central core ion although the proton affinity of water is smaller than that of the ether groups. In (MeO-

$(CH_2)_2OMe)(H_2O)_2H^+$ the two water molecules constitute a protonated water bridge between the functional groups of the polydentate ligand.

Solvent-bridged structures can form also in clusters of protonated diketones and H_2O molecules, although rigid small diketones, such as that in $MeCOCH_2$-$COMe)H^+(H_2O)_2$, may not be able to accommodate the water bridge.[275] When bridged structures form, they can provide low-energy pathways for proton transfer between functional groups, by switching hydrogen bonds through the water chain.

5. Spectroscopy of Hydrogen-Bonded Clusters

Indirect structural information on IHBs from thermochemistry, reactivity, and ab initio calculations is now being confirmed by direct spectroscopic observations.

Many studies on cationic clusters use vibrational predissociation spectroscopy. An IR photon excites a vibrational mode associated with the hydrogen bond and dissociates the bond, resulting in the loss a ligand molecule, which can be detected by mass spectrometry. Alternatively, the photons may detach a probe molecule such as Ar or H_2 that is bonded weakly to the cluster.

The infrared spectra of $(H_2O)_nH^+$ clusters were obtained first by Schwartz in 1977[285] with vibrational assignments from ab initio calculations by Newton[226,227] and followed by many higher level calculations.[286] Spectra of the H_3O^+ core ions helped to assign spectra of larger clusters.[287−291]

The IR studies of clusters[236,292] were advanced in particular by Y. T. Lee and co-workers. This group produces low temperature, 170 ± 20 K, clusters by corona discharge followed by supersonic expansion and storage in an ion trap. The clusters are irradiated with IR photons from pulsed lasers, and the fragments are detected. The power-normalized vibrational predissociation spectra of the clusters are compared with spectra calculated by ab initio theory. The absorption bands of X−H bonds are shifted when they form hydrogen bonds, and this shift allows identification of the hydrogen bonding sites. The IR vibrational predissociation spectroscopy of clusters has been applied with success since 1985.[293−296] Another method, photoelectron spectroscopy, has been applied to probe the structures of anionic clusters.[219,255,297] This section will illustrate some of the results relevant to the thermochemical studies.

5.1. Shell Filling, Isomers, and the Location of the Proton

5.1.1. Spectroscopy of Clusters with Unlimited IHB Networks

Early studies by Y. T. Lee and associates addressed ionic hydrogen bonds in $(H_2)_nH^+$ clusters.[293,295] The first study on strong IHBs in the hydronium ion clusters, $H_3O^+(H_2O)_n(H_2)_m$, showed that the H_2 molecules were weakly bonded to outer water OH bonds with dissociation energies of 3−4 kcal/mol.[292] More recently, the structures of $(H_2O)_nH^+$ clusters were investigated by the spectroscopy of hydrogen-bonded and free O−H stretches. Structures centered on H_3O^+ and on a symmetric $(H_2O)_2H^+$ were observed. Several $(H_2O)_7H^+$ isomers including a five-membered ring, six-membered rings, and three-dimensional cage structures were identified with the five-membered ring favored by a combination of enthalpy and entropy effects.[229]

Similarly, in methanol clusters, $(MeOH)_nH^+$, with $n = 4$, a linear isomer was found, while for $n = 5$, linear and cyclic isomers were identified with the proton localized on one or delocalized between two methanol units.[230]

In methanol−water mixed clusters, $(MeOH)$-$(H_2O)_nH^+$, at $n = 2$ methanol and the water dimer can equally share the proton. At $n = 3$ and 4, distinct methanol-centered $MeOH_2^+(H_2O)_3$ and water-centered $H_3O^+(MeOH)(H_2O)_2$ isomers were identified. In larger clusters, the structures become similar to protonated water clusters, including, at $n = 5$, the formation of a five-membered ring.[231,232]

For example, a typical recent study addressed four-membered clusters of water and methanol, $(MeOH)_n$-$(H_2O)_{n-4}H^+$. Figure 48 illustrates the results for $(H_2O)_4H^+$ and $(MeOH)_3(H_2O)H^+$. The spectra support structures with a $MeOH_2^+$ core ion, a chain of MeOH molecules, and H_2O molecules attached at the end. This is reasonable energetically because MeOH has a higher PA than H_2O. However, ab initio calculations for each mixed cluster gave several isomers with similar energies within a range of 2 kcal/mol, and these isomers may be in equilibrium in a thermal population. The ab initio studies also confirmed the thermochemical results that the cluster stabilities increase with increasing MeOH mole fraction.[236]

Recent high-level calculations and spectroscopy of the $NH_4^+(H_2O)_n$ clusters ($n = 0−5$) found that at $n = 4$ the closed-shell isomer has the lowest energy, but cyclic and noncyclic isomers were both observed by IR spectroscopy in a supersonic jet at about 170 K.[234] The calculated lowest energy isomer at $n = 5$ contained a four-membered ring and the fifth H_2O molecule acted as a double proton acceptor. This calculated structure was confirmed spectroscopically.[235]

The cluster $CH_3NH_3^+(CH_3NH_3)_3$ with a closed solvent shell was also identified spectroscopically.[298]

5.1.2. Spectroscopy of Mixed Clusters of Nonblocked and Blocked Components

A recent study addressed mixed $(Me_2O)(H_2O)_nH^+$ clusters. The spectroscopic and ab initio results, illustrated in Figure 49, indicated that the proton is located on the ether when it is solvated by one H_2O molecule. With two H_2O molecules, the proton is shared by the ether and the water dimer, and with three or more H_2O molecules, the proton is transferred completely to water. However, at $n = 2$ and 3, the calculations showed several isomers with comparable energies within 2 kcal/mol, where the position of the proton was affected by hydrogen cooperativity and zero-point energy effects.[230]

The location of the proton on H_3O^+ surrounded by blocked bases was confirmed further by IR spectroscopy in clusters of H_3O^+ with two molecules of

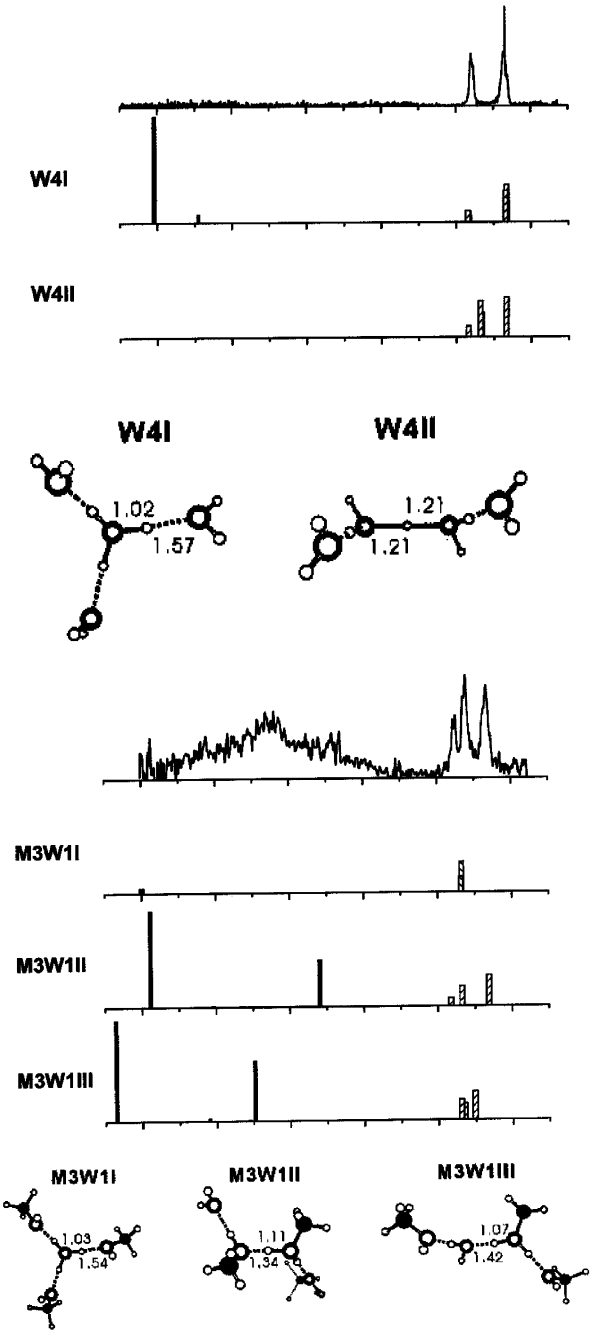

Figure 48. The top panel shows experimental and theoretical IR vibrational predissociation spectra and structures of $(H_2O)_4H^+$. The spectra support the Eigen structure W4I with a central H_3O^+ core ion. The bottom panel shows the $(MeOH)_3(H_2O)H^+$ spectra and structures. The spectra support the structure M3W1II with a linear MeOH chain centered about a $MeOH_2^+$ core ion with H_2O attached to a MeOH molecule at the end of the chain. Reproduced from ref 236 with permission. Copyright 2004 American Chemical Society.

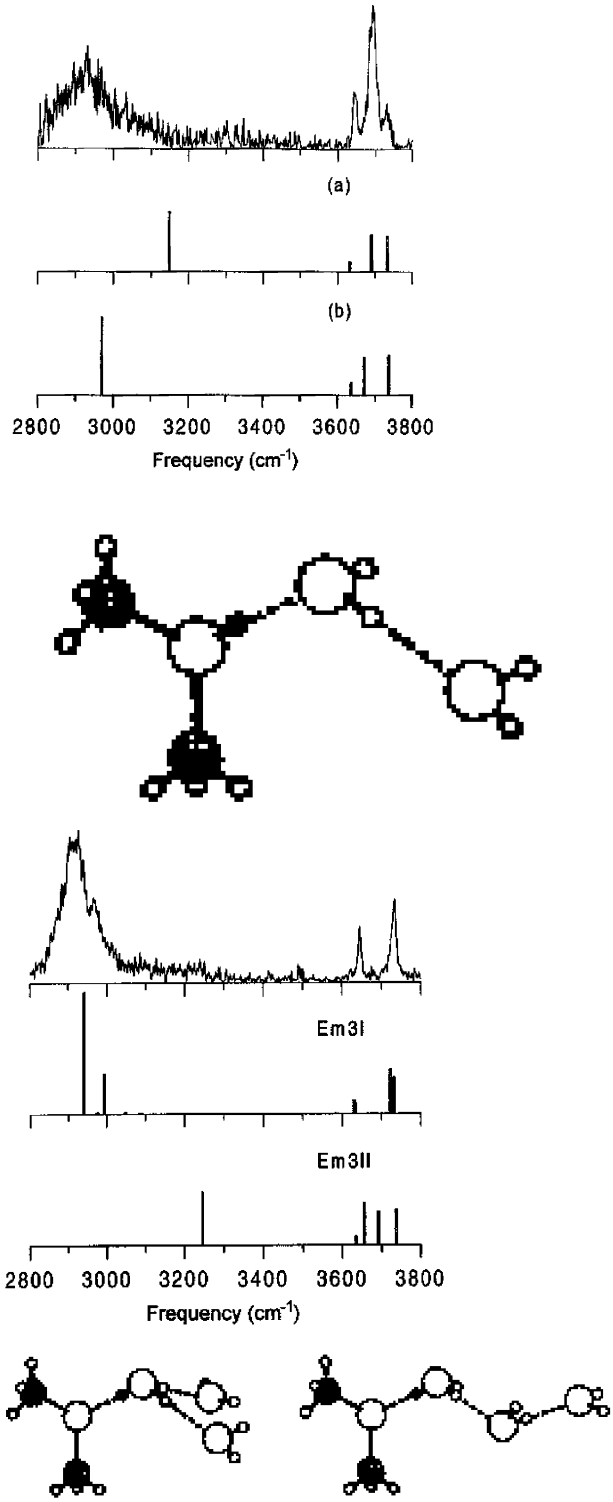

Figure 49. The top panel shows experimental and theoretical IR vibrational predissociation spectra and structures of $(Me_2O)(H_2O)_2H^+$ showing the proton on Me_2O. The bottom panel shows spectra and structures of Me_2O-$(H_2O)_3H^+$ showing the proton on a $(H_3O)^+$ core ion, consistent with the symmetric structure Em3I (top theoretical spectrum, left structure) rather than the linear Em3II structure (bottom theoretical spectrum, right structure). Reproduced from ref 230 with permission. Copyright 1999 American Chemical Society.

dimethyl ether, methyl ethyl ether, acetone, acetaldehyde,[104] and formamide.[247]

Mixtures of isomers were present in clusters formed by supersonic expansion and studied by IR spectroscopy in mixed clusters of water with dimethyl ether, methyl ethyl ether, acetone, and acetaldehyde. The proton can be located on a H_3O^+ core surrounded by the blocked ligands, or the blocked components can form a hydrogen-bonded dimer, and water is attached by CH···O bonds to the methyl groups. These isomers displayed different OH stretching spectra.[104]

The location of the proton was also investigated spectroscopically in protonated formamide and in its the neat clusters. The spectra confirmed protonation on the oxygen atom of the amide group.[273] In the hydrated clusters, $H_2NCH_2COH^+(H_2O)_n$ ($n = 3$) isomers protonated on the formamide oxygen and isomers with water-protonated H_3O^+ centers were identified from NH and OH stretching spectra; similar to blocked clusters, at $n = 4$ the proton shifted to water producing a H_3O^+ ion core.[247]

5.1.3. Spectroscopy of Carbon-Based Hydrogen Bonds

Complexes of CH donors were investigated by vibrational predissociation spectroscopy and DFT ab initio calculations on $(Me_2O)_2H^+ \cdot H_2O$ ions produced by supersonic expansion. Two types of isomers, one with water bonded by a $CH^{\delta+}\cdots O$ bond to the methyl groups of the $(Me_2O)_2H^+$ dimer and a H_3O^+-centered isomer, were identified by different hydrogen-bonded and non-hydrogen-bonded OH stretches of the water molecule. Similar observations were made in analogous clusters of Et_2O, Me_2CO, and MeCHO. The H_3O^+-ion-centered isomers are likely to be the most stable ones because they were identified in collisional dissociation experiments as discussed below.[104]

Spectroscopic studies by Dopfer and co-workers on complexes of cyclic $C_3H_3^+$ and linear H_2CCCH^+ with N_2 showed evidence for planar $C_3H_3^+$ ions and linear $CH\cdots NN$ bonds.[105] In another study, the IR dissociation spectra of clusters of protonated benzene $C_6H_7^+$ with Ar, N_2, CH_4, and H_2O ligands indicated weak bonds, 9.5 kcal/mol with N_2 and 11.5 kcal/mol with CH_4, where the ligands perturbed only slightly the aliphatic and aromatic CH vibrations of the ion.[106]

5.1.4. Spectroscopy of Carbon-Based Bonds in Ionized Aromatics

Unconventional IHBs can involve aromatic molecules that can serve as π acceptors or CH donors. The group of Fujii, Mikami, and co-workers studied several such systems by the IR spectroscopy of clusters, and recently summarized this work.[118]

Results on the benzene−water system were described above in the section on radical ions. Several isomers were observed in the benzene cation solvated by several water and methanol ligands. With one ligand molecule, the IR spectrum showed only an isomer in which the oxygen of the first ligand molecule forms two IHBs with adjacent protons of $C_6H_6^{\bullet+}$ in the aromatic plane. In contrast, the spectra of clusters with two to four H_2O and two CH_3OH ligands provided evidence for isomers where each ligand molecule forms separate H-bonds to the central cation or where at least one ligand forms a hydrogen bond to a second ligand.[118−120]

The benzene−water system with one to six H_2O molecules was observed also in the OH and CH stretching vibrational region and by ab initio DFT calculations. This work also found that in the $n = 1$ cluster cation the water oxygen is in the benzene plane and forms two identical IHBs with two adjacent benzene hydrogens. The IR spectra of the $n = 2$ cluster showed two isomers, one with two H_2O molecules bonded to benzene and one in which they bonded to each other, which also applied in the $n = 3$ cluster. Higher clusters showed spectra that were very similar to that of protonated water clusters $(H_2O)_nH^+$, indicating that the proton was transferred from benzene to water to form $C_6H_5^{\bullet}\cdot(H_2O)_nH^+$ clusters.[141]

Isomeric structures were observed also in the complex of $C_6H_6^{\bullet+}$ with CH_3COOH by vibrational and electronic spectra and ab initio calculations. A band was assigned to the O−H stretching vibration of the cis-isomer of acetic acid in the hydrogen-bonded complex (horizontal cis-isomer), and another band to the vertical trans-isomer where the acetic acid interacts with the π electron system of the benzene cation. The spectra also showed intermolecular charge transfer between a carbon atom of benzene and the carbonyl oxygen atom of acetic acid.[121]

Complexes of phenol were also investigated by spectroscopy. Bonds of $OH\cdots\pi$ type were found in $(phenol/benzene)^{\bullet+}$, $(phenol/C_2H_2)^{\bullet+}$, and $(phenol/C_2H_4)^{\bullet+}$ complexes. The hydrogen bonds in the neutral complexes were enhanced significantly by ionization. The nature of the π bond, whether an olefin or aromatic ligand, did not affect strongly the spectral shifts.

The phenol−water system was investigated also by two-photon ionization and fluorescence spectroscopy by Kleinermanns and co-workers. They found that with one and two water molecules no proton transfer occurs in $C_6H_5OH^{\bullet+}(H_2O)_n$ clusters, but with $n = 4$, linear and solvated isomers were observed. The latter, where the phenol ion is solvated, shows proton transfer to form $C_6H_5O^{\bullet+}(H_2O)_nH^+$ clusters. With $n = 8$, two filled shells and the beginning of a new shell were observed.[299] With n up to 20, the water forms bi-, tri-, and tetracoordinated hydrogen-bonded structures similar to water and ice surfaces.[300]

In complexes of phenol with one to four NH_3 ligand molecules, the high proton affinity of the ligand causes proton transfer to occur already to the first NH_3 ligand molecule or to several NH_3 molecules to form $C_6H_5O^{\bullet}(NH_3)_nH^+$ clusters.[301,302]

5.1.5. Spectroscopic Consequences of Intramolecular and External Solvation

The group of Y. T. Lee investigated the relation between intramolecular and external solvation in the diketone hydrates $(MeCOCH_2COMe)(H_2O)_nH^+$ ($n = 0-3$). The calculations showed that the unsolvated ion contains an internal ionic hydrogen bond (iIHB), which is replaced by a H_3O^+ bridge in the monosolvated ion. Further replacement of the iIHB occurs with two H_2O molecules. After three or more water molecules, the proton is transferred to water, and the water bridges between the ketone groups can open. The IR spectra in Figure 44 showed evidence both for open and water-bridged isomers.[275]

A new type of unconventional intramolecular IHBs was observed in the cis conformation of the ortho isomers of the $CH_3C_6H_4OH^{\bullet+}$ and $C_2H_5C_6H_4OH^{\bullet+}$ radical cations. Here the alkyl groups act as hydrogen acceptors, rather than in their usual roles as donors.[122]

Intermolecular bonds in complexes of diamines were investigated in $(H_2NCH_2CH_2NH_2)(H_2O)_3H^+$; the IR spectra indicated a bicyclic structure assisted by an internal IHB. This isomer coexists with monocyclic open isomers at 150 K, and the relative abundances of the isomers were consistent with a combination of enthalpy and entropy effects.[233]

An internal IHB was observed spectroscopically in the ethanolamine component of the (phenol−ethanolamine)$^{\bullet+}$ complex.[303] These spectroscopic studies confirmed the earlier conclusions from thermochemistry about the relations between external solvation and intramolecular IHBs.[259]

5.1.6 IHB Networks about Anions

The formation of ionic hydrogen bonds causes a red shift of the stretching modes of the hydrogen-bonding proton, both in anions and in cations.[219,255,297] For example, the frequencies of the OH stretching mode in the vibrational spectrum of the complex $OH^-\cdot H_2O$ were found to be red-shifted.[304] The ion−molecule stretching vibrational frequencies in the binary complexes $X^-\cdot H_2O$ (X = Cl, Br, I) were investigated via argon predissociation spectroscopy.[305] Larger clusters were observed through the 3200−3800 cm^{-1} vibrational IR predissociation spectra of the Br^- and I^- clustered by up to six H_2O molecules. The spectra of these anionic clusters become increasingly similar after three or more water molecules, which displayed a very wide unresolved band reminiscent of the bulk water spectrum. A blue shift with increasing solvation suggested the strengthening of the interwater hydrogen-bonding network at the expense of the hydrogen bonds to the halide.[306]

In solvation by water, F^- undergoes internal solvation, remaining on the inside of the solvent clusters, but Cl^-, Br^-, and I^- undergo external or surface hydration, being on the surface of the cluster. This also applies in the solvation of Cl^- and I^- by methanol.[88] External solvation of halide ions was also shown by liquid-drop and statistical theories.[238]

A recent review covered hydration shells about halide ions, discussing how clusters can elucidate the behavior of the inner water molecules in contact with the anion. For example, vibrational predissociation spectroscopy showed the morphology of the small water networks attached to anions. Charge transfer in the binary interaction and its effects on the structures of the larger hydrogen-bond networks were discussed.[86]

Solvation of F^- anion by MeOH was investigated by vibrational predissociation spectroscopy. The strong hydrogen-bond between the anion and the hydroxyl group shifted some O−H stretching frequencies into the C−H stretch region. Ab initio calculations combined with experiment showed that the fluoride anion is on the surface of the methanol solvent cluster, which starts to form methanol−methanol hydrogen bonds after four or more methanol molecules.

Spectroscopy was applied by Bieske and co-workers to clusters that involve unconventional $CH\cdots X^-$ bonds such as the $Cl^-\cdots CH_4$ dimer[307] and halide anions clustered by acetylene with a coordination number of four. The spectra of these anions was reviewed recently.[308]

Photoelectron spectroscopy has been applied to many anionic clusters, especially by K. H. Bowen and co-workers. For example, solvent effects on acidities/basicities were studied in $NH_2^-(NH_3)_n$ ($n = 1$ and 2). The spectra implied that the clusters consist of intact amide ions solvated by ammonia, the geometry of which is distorted from that of a free ammonia molecule due to the hydrogen bond. The gas-phase basicities showed that while NH_2^- is a stronger base than H^- in the gas phase, the addition of only two ammonia solvent molecules reverses these relative basicities.[255]

Similar studies were applied to the methylated species $Me_2N^-(Me_2NH)$.[309] Photoelectron spectra to IHB systems include measurements of the binding energies of NO^- to H_2O, NH_3, and H_2S.[310]

An interesting case of IHB formation was found in anions formed by electron attachments to uracil−glycine and uracil−phenylalanine complexes. The most stable structure of (uracil−glycine)$^{\bullet-}$ was a distonic anion dimer $(H_2C(NH_2)COO^-)$(uracilH$^{\bullet}$), formed by barrier-free proton transfer in the anionic complex.[311]

In summary, spectroscopic studies can be based on shifts in vibrational frequencies caused by the formation of hydrogen bonds. The spectra show distinct cluster structures that sometimes coexist in equilibrium. Spectra show "internally solvated" structures where the solvent molecules are bonded directly to the core ion, which is inside the solvent cluster. In special cases, the core ion is H_3O^+ surrounded by stronger base blocked ligands. Alternatively, the solvent molecules can be attached to each other, the ion is attached to one of the solvent molecules, and it is on the outside of the solvent cluster. In this case, the ion is "externally solvated", and the solvent cluster has neutral-like structure and spectra.

When the ion is "internally solvated", the surrounding solvent molecules can loosen or open the internal bond or form a protonated solvent bridge between functional groups. When two to four H_2O molecules are present, the proton often shifts to form a strongly hydrogen-bonded $(H_2O)_nH^+$ cluster that is hydrogen-bonded to a deprotonated ligand or radical. In the clusters, the solvent tends to form cyclic or three-dimensional structures. Spectroscopic observations confirm these structural features that were inferred previously from thermochemistry and predicted by ab initio studies.[228,259]

6. Kinetics of Hydrogen Bond Formation and Dissociation

6.1. Formation and Dissociation of Hydrogen Bonds

6.1.1. Formation of Hydrogen-Bonded Clusters

The formation of IHBs occurs mostly by association reactions (eq 31). An excited complex $(B_1H^+\cdot B_2)^*$

$$B_1H^+ + B_2 \underset{k_b}{\overset{k_c}{\rightleftharpoons}} (B_1H^+\cdot B_2)^* \xrightarrow{k_s} B_1H^+\cdot B_2 \quad (31)$$

forms with collision rate k_c (between B_1H^+ and B_2) and becomes stabilized also near the collision rate k_s (between $(B_1H^+ \cdot B_2)^*$ and a third-body molecule) to form the adduct or dissociates with unimolecular rate coefficient k_b back to reactants. The overall forward rate coefficient, $k_f = k_c(k_s/(k_b + k_s))$ depends on the relation between the rate of stabilization, k_s, and the rate of back-dissociation, k_b. In particular, the rate of back-dissociation, k_b, which competes with product formation, decreases with increasing IHB bond strength, with increasing number of degrees of freedom of the complex, and with decreasing temperature. These factors therefore increase the rate of formation of the complex.

The temperature dependence of the rate coefficient k_f of the overall association reactions 31 may be expressed in the form $k_f = AT^{-n}$.[312] Usually temperature coefficients of T^{-2} to T^{-4} are observed in small ions and molecules. In a sequence of clustering reactions, the rate coefficients k_f tend to increase at higher steps where the number of degrees of freedom in the complex is larger, and as a result, equilibrium may be achieved faster in higher steps than in lower steps. For example, Kebarle and co-workers observed such effects in a detailed study of the $(H_2O)_nH^+$ system.[197]

6.1.2. Reaction Driven by Hydrogen-Bond Formation: Associative Proton Transfer Reactions

Forming a hydrogen bond of 20−30 kcal/mol can contribute a significant driving force for ionic reactions. The hydrogen bond can form, for example, when molecules of a polar solvent extract a proton from a radical ion in reaction 32.

$$RH^{\bullet +} + nB \rightarrow B_nH^+ + R^{\bullet} \qquad (32)$$

The first examples were reported in 1970 by Sieck and Searles[313] who observed the extraction of a proton from radical ions of butane, pentane, and hexane isomers in termolecular reactions with two H_2O molecules to form the $(H_2O)H^+$ dimer. More recently, Meot-Ner, El-Shall, and co-workers observed reaction 32 between $RH^{\bullet +} = C_6H_6^{\bullet +}$ and C_6H_5-$CH_3^{\bullet +}$ formed by resonant-two-photon ionization and B = MeOH, EtOH, MeCOOEt, or MeCN, to form the respective protonated dimers.[314] These reactions are rendered exothermic by the formation of the hydrogen bond in B_2H^+, and therefore, this bond formation must occur in the reaction intermediate, which is a three-body complex of $RH^{+\bullet}$ + 2B molecules, concerted with proton transfer to make the reactions energetically feasible.

Associative transfer reactions with the formation of a hydrogen bond were observed also following the resonance two-photon ionization of clusters of toluene with H_2O, MeOH, Me_2O, and NH_3 molecules.[315,316]

Associative proton-transfer reactions can require more than two neutral molecules to extract the proton. For example, when $C_6H_6^{\bullet +}$ reacts with nH_2O molecules, the enthalpy change of reaction 32 is 46, 14, −7, and −25 kcal/mol for $n = 1-4$. The overall reaction is exothermic for $n = 3$, but it proceeds with the stepwise buildup and stabilization of the $C_6H_6^{\bullet +}$-$(H_2O)_n$ cluster followed by reaction 33 of which the enthalpy change is 46, 23, 10, 0, and −3 kcal/mol for $n = 1-5$.

$$C_6H_6^{\bullet +}(H_2O)_{n-1} + H_2O \rightarrow [C_6H_6^{\bullet +}(H_2O)_n]^* \rightarrow [C_6H_5^{\bullet}(H_2O)_nH^+]^* \rightarrow C_6H_5^{\bullet} + (H_2O)_nH^+ \qquad (33)$$

At $n = 4$, the reaction becomes thermoneutral and energetically feasible. The reaction is a five-body process, and the enthalpy assembling the reactive complex from $C_6H_6^{\bullet +}$ + $4H_2O$ molecules into the $C_6H_6^{\bullet +}(H_2O)_4$ complex is −35 kcal/mol. Correspondingly, this reaction shows an unprecentedly large negative activation energy of −34 ± 1 kcal/mol, expressed alternatively as $k = AT^{-67\pm4}$. In general, high-order associative transfer reactions that require the assembling of multibody complexes are expected to have unusually large negative temperature coefficients.[117]

Such reactions can be therefore significant in astrochemical environments at low temperatures, where they may proceed at collision rate. For example, ionized aromatics in interstellar clouds and solar nebulae can serve as nuclei for the attachment of water and other polar molecules. The solvated aromatics, or the product protonated clusters can form centers for nucleation to form interstellar grain particles.

Several other kinetic effects of IHBs were observed. Associative reactions can be driven by the formation of ionic hydrogen bonds to eliminate a radical, reaction 34.

$$CH_3CH_2OH^{\bullet +} + H_2O \rightarrow CH_2OH^+(H_2O) + CH_3^{\bullet} \qquad (34)$$

Analogous reactions occur between $C_2H_5OH^{\bullet +}$ and CH_2O or CH_3OH and between $(C_2H_5)_2O^{\bullet +}$ and H_2O, C_2H_5OH, $(CH_3)_2O$, $(CH_3)_2CO$, $(C_2H_5)_2O$, or CH_3-CN.[108,317] Hydrogen-bonded dimers are reaction intermediates in the association of $CH_3OCH_2^+$ with alcohols.[318] Ionic hydrogen bonds can also affect the kinetics by solvating the ions. For example, the reactivity of the hydroxyl anion was observed to be affected by solvation by H_2O molecules.[319]

6.1.3. Reactions Driven by Hydrogen-Bond Formation or Dissociation: Internal Hydrogen Bonds and Entropy-Driven Reactions

The exothermic formation of an internal hydrogen bond can provide the driving force for proton transfer (PT) reactions to polyfunctional molecules. Conversely, the positive entropy change upon dissociating the internal bond can also drive or accelerate the deprotonation of polyfunctional ions.

Most exothermic PT reactions proceed near the collision rate. This includes PT reactions to polyfunctional molecules that are made exothermic by the formation of internal hydrogen bonds in the product ion. Without formation of the internal bond, proton transfer to a single functional group of the molecule may be endothermic and slow.

In the reverse direction, the dissociation of an internal hydrogen bond releases a constrained cyclic structure, which leads to a positive entropy change. In some of these reactions, $\Delta H°$ is positive but $\Delta G°$ is negative. Reactions were observed that are endothermic by up to 8 kcal/mol and would normally be unobservably slow, but they are fast and proceed near the collision rate with near unit efficiency because $\Delta G°$ is negative.

These reactions are "intrinsically fast" because they are not slowed by barriers and the kinetics are controlled only by the thermochemistry. The reaction efficiency in either direction is determined only by the overall thermochemistry according to the simple relation $r = K/(1 + K)$ where K is the equilibrium constant in that direction. In these reactions, the formation or dissociation of iIHBs affects the kinetics directly through their effects on the thermochemistry.[206] Because of the direct relation of rates to thermochemistry, this type of reaction can be used for bracketing the gas-phase basicities of molecules: a fast reaction with a reference base indicates that the molecule has lower basicity than the reference base and vice versa.[320]

In reactions where the formation or opening of an IHB drives a proton-transfer reaction, it affects the energy and density of states of the transition state, and therefore, it must be concerted with the proton-transfer process.

The first examples of such "entropy-driven reactions" including IHB formation were observed in reactions of diamines.[259] The kinetics were generalized and analyzed for other reactions with significant entropy changes.[206] Similar effects were observed also in biomolecules, such as proton transfer from (lysine)-H^+ the increased PA of which can be attributed to an internal IHB.[9] Internal hydrogen bonds and their entropy effects are common in polyfunctional biomolecules, and their kinetic effects are also expected to be common in the reactions of biomolecules.

6.2. Hydrogen-Bonded Complexes as Reaction Intermediates

Hydrogen-bonded complexes may be intermediates in the dissociation of protonated or radical ions. These intermediates may involve lone-pair bases or unconventional carbon-based IHBs.

An example of an $OH^+\cdots O$ hydrogen-bonded complex, $(H_2O\cdots H\cdots O{=}C{-}OH)^{\bullet+}$, was identified by metastable and collision-induced dissociation and theory in the dissociation of ionized dihydroxyfumaric acid $(HOOCC(OH){=}C(OH)COOH)^{\bullet+}$ leading to $(H_2O\cdots H\cdots OCO)^{\bullet+}$ and H_3O^+ products.[140] The $\Delta H°_D$ vs PA correlations gave 24.4 kcal/mol for the bond strength of this complex, but it remains to be shown whether these relations apply in complexes of radical ions.

Complexes with carbon-based IHBs were identified in numerous reaction intermediates. For example, such complexes occur in the reactions of CH_3^+ and $CH_4^{\bullet+}$ ions. An early example of $CH^+\cdots O$ bonded complexes was identified by Futrell and co-workers in the hydride transfer reaction $CH_3^+ + CH_3OH \rightarrow CH_2OH^+ + CH_4$,[107] and more recently, ICR studies and ab initio calculations showed such complexes in the reactions of CH_4^+ with H_2O, CH_3OH, and $(CH_3)_2O$.[108]

In other reactions, theory showed $CH_3CNR^+\cdot OH_2$ and $CH_3CN\cdot ROH_2^+$ with $CH\cdots O$ and $CH\cdots N$ bonds as intermediates in the dissociation and rearrangement of $CH_3CNH^+\cdots ROH$ complexes.[321] The complex $H_2O\cdots H_2CCO^{\bullet+}$ with a calculated bonding energy of 14 kcal/mol occurs in the decomposition of $(HOCH_2)CO^{\bullet+}$.[135−137] The c-$C_3H_6^{\bullet+}\cdot H_2O$ complex in the dissociation of n-$C_3H_7OH^{\bullet+}$ may be a T-shaped bidentate complex with a bonding energy of 10.4 kcal/mol.[138,139]

Complexes with hydrogen bonds between protonated functional groups and olefinic or aromatic π bonds were also observed. For example, theory showed a complex involving a hydrogen bond between NH_4^+ and the π bond in $H_2C{=}CH_2$.[94] An analogous complex, $(H_2O)H^+(C_2H_4)$, with an energy about 12 kcal/mol above $C_2H_5OH_2^+$ was also demonstrated.[109,110] A complex of $HCNH^+\cdot C_2H_4$, with a CH^+ or NH^+ donor group bonded to the olefin π bond was observed in the isomerization $CH_3CH_2CNH^+ \leftrightarrow CH_3CH_2NCH^+$.[111]

Complexes with a hydrogen bond between an OH^+ group and a double bond were also indicated in the loss of methanol from protonated methoxyhexenes.[322] Hydrogen exchange between an OH group and a double bond in this intermediate can facilitate hydrogen transfer between the leaving methanol and the remaining hydrocarbon ion.

7. Ionic Hydrogen Bonds in Biomolecules

Ionic hydrogen bonds are ubiquitous in biology. IHBs contribute to the solvation of ionized groups by water and by polar groups in desolvated protein interiors. These interactions contribute to protein folding and aggregation, enzyme energetics,[323] molecular recognition, neurotransmitters, and receptors and in membranes and photosystems.[324,325]

The energetics of individual IHBs cannot be isolated in complex biosystems, but they can be inferred from similar interactions in clusters. Studies on actual gas-phase bio-ions became possible recently with the advent of electrospray[326] coupled with HPMS[155] or mobility cells,[327] collisional dissociation,[14] blackbody infrared radiative dissociation ZETRID/BIRD,[15,18] or Fourier transform ion cyclotron resonance (FTICR).[9,10,18,328]

These studies confirmed that effects observed in model molecules, such as intramolecular and polydentate IHBs, are indeed significant in biomolecules. New IHB interactions such as the solvation of multiply protonated ions, zwitterions,[329,330] and salt bridges[331] were also observed. The following sections and Table 10 review some representative results, proceeding from simple to complex biomolecules in each section.

7.1. Peptides and Proteins

7.1.1. Intramolecular Solvation, Conformation, and Basicities

Studies of peptides and proteins show trends that were observed first in model molecules. For example,

Table 10. Thermochemistry of Ionized Biomolecules[a]

ion	ligand	PA or ΔH°_D	ΔS°_{prot} or ΔS°_D	GB or ΔG°_D	method[b]	comments	refs
			Proton Affinity or Gas Basicity				
glycine		212[c]		204[c]	PHPMS, ICR		372,373, 334,335, 27
$(Gly)_3$		231[c]		219[c]	CID		333,334, 335,27
$(Gly)_4$		233[c]		222[c]	CID		333,334, 335,27
$(Gly)_6$				227[c]			334,335, 27
$(Gly)_8$				237[c]		increasing PA, GB with n due to internal solvation	334,335, 27
alanine		216		207			27
β-Ala				211			338
Ala-Gly				211			338
β-Ala-Gly				218			338
MeCO-Gly-OMe		217	−12	206		ΔS°_{prot} indicates internal IHB	150
MeCO-Ala-OMe		224	−15	212		ΔS°_{prot} indicates internal IHB	150
valine		218		210			27
leucine		219		211			27
lysine		238		227		increased PA, GB due to internal solvation	27
gramicidin S				>243			16
(gramicidin S)H^+				215		decreased GB vs uncharged protein due to Coulomb repusion	16
				Hydration			
$GlyH^+$	H_2O			9.7	ES/HPMS		155
	$2H_2O$			7.2	ES/HPMS		155
	$3H_2O$			5.4	ES/HPMS		155
$(Gly)_2H^+$	H_2O			8.8	ES/HPMS		155
	$2H_2O$			6.2	ES/HPMS		155
$(Gly)_3H^+$	H_2O			6.7	ES/HPMS		155
	$2H_2O$			5.8	ES/HPMS		155
$(Gly)_4H^+$	H_2O			5.8	ES/HPMS	weaker bonding to H_2O in larger peptides due to internal solvation	155
$ValH^+$	H_2O	19.3	36.3	8.4	PHPMS	large ΔS° indicates bridging between $-NH_3^+$ and $-COOH$ by ligand	374
$ProH^+$	H_2O	18.9	36.8	7.7	PHPMS	large ΔS° indicates bridging by ligand	374
CH_3COOCH_2-$CH_2N(CH_3)_3^+$ [d]	H_2O	8.0	22.0	1.5	PHPMS	weak interaction in $CH^{\delta+}\cdots OH_2$ bond	124
$CH_3CONCH(CH_3)$-$COOCH_3^-$ [e]	H_2O	15.2	20.9	9.0	PHPMS		187
	$2H_2O$	13.0	19.8	7.1	PHPMS		187
$((Gly)_2 - H)^-$	H_2O	11.0	14.5		mobility	solvation of $-COO^-$ group	349
	$2H_2O$	9.5	15.2		mobility	solvation of $-COO^-$ group	349
	$3H_2O$	8.2	14.4		mobility	solvation of $-COO^-$ group	349
	$4H_2O$	7.4	13.7		mobility	solvation of $-COO^-$ group	349
$((Ala)_2 - H)^-$	H_2O	11.7	17.1		mobility	solvation of $-COO^-$ group	349
	$2H_2O$	9.6	16.0		mobility	solvation of $-COO^-$ group	349
	$3H_2O$	8.6	15.6		mobility	solvation of $-COO^-$ group	349
	$4H_2O$	7.1	13.0		mobility	solvation of $-COO^-$ group	349
$(Ala)_3H^+$	H_2O	12.3	23.3	5.4	mobility	solvation of $-NH_3^+$ group	350
	$2H_2O$	11.3	22.6	4.6		solvation of $-NH_3^+$ group	350
	$(3-5)H_2O$	8.7−7.6				solvation of $-NH_3^+$ group	350
$(Ala)_5H^+$	H_2O	10.5	21.3	4.2		internal solvation weakens bond to water	350
	$(2-4)H_2O$	8.5−9.0					350
(Ala-Ala-Arg-Ala-Ala)H^+	H_2O	10.2	23		mobility		350
	$2H_2O$	8.4	18		mobility		350
$(BPTI + 6H^+)^{6+}$	H_2O	21.3	62	2.8	mobility	large ΔS indicates locking of protein by inserted H_2O	13
	$2H_2O$	16	42	3.5	mobility		13
	$3H_2O$	14	34	4.0	mobility		13
(cytochrome $c + 5H^+)^{5+}$	$(1-5)H_2O$			3.5	mobility	$\Delta G_{n-1,n}$ approximately constant for $n = 1-5$	359
(cytochrome $c + 7H^+)^{7+}$	H_2O			4.4	mobility		359
	$(2-7)H_2O$			4.3−3.8	mobility	$\Delta G_{n-1,n}$ decreases slightly for $n = 1-7$	359

Table 10. (Continued)

ion	ligand	PA or ΔH°_D	ΔS°_{prot} or ΔS°_D	GB or ΔG°_D	method[b]	comments	refs
			Bio-ions + Organic Ligands				
$ValH^+$	NH_3	20.9	28.8	8.4	PHPMS	ΔS° indicates no bridging of $-NH_3^+$ and $-COOH$ by ligand	374
$ValH^+$	CH_3NO_2	19.8	27.8	12.4	PHPMS		374
$CH_3COOCH_2CH_2N(CH_3)_3^+$ [d]	Me_2CO	13.2	21.7	6.7	PHPMS		124
	3-$CH_3C_6H_4OH$	12.8	(24)	5.6	PHPMS		124
	$C_6H_5CH_3$	8.1	15.5	3.5	PHPMS		124
$CH_3CONCH(CH_3)COOCH_3^-$ [e]	MeOH	18.0	(25)	10.6	PHPMS		187
			Biomolecule Dimers				
$ValH^+$	Val	20.7			PHPMS		374
$ProH^+$	Pro	20.0			PHPMS		374
$GlyH^+$	Gly	26.5			BIRD	$-NH_3^+\cdots NH_2$ and $-NH_3^+\cdots CO$ multiple bonds	18
$AlaH^+$	Ala	25.8			BIRD		18
$GlyH^+$	Ala	26.5			BIRD		18
$LysH^+$	Lys	26.5			BIRD		18
$((Gly)_2 - H)^-$	$(Gly)_2$	34.9			mobility	ΔH°_D from E_a (dissociation)	349
$((Ala)_2 - H)^-$	$(Ala)_2$	32.2			mobility	ΔH°_D from E_a (dissociation)	349
leucine enkephalin H^+ (YGGFL)H^+	leucine enkephalin	46.5 (36.6); 36.9			ES thermal dissoc, using log A = 21.7 (or 17.2); BIRD	multiple IHBs indicated	364
adenineH^+	adenine	30.3	39	18.7		large ΔH°_D and ΔS°_D indicates two IHBs in the dimers	279
thymineH^+	thymine	30.1	37	19.1		large ΔH°_D and ΔS°_D indicates two IHBs in the dimers	279
cytosineH^+	cytosine	38.3	37	27.3		large ΔH°_D and ΔS°_D indicates three IHBs in the dimers	279

[a] Units are as follows: PA, GB, ΔH°_D, and ΔG°_D in kcal/mol; ΔS°_{prot} and ΔS°_D in cal/(mol K). [b] Methods are as follows: PHPMS, pulsed high-pressure mass spectrometry; ICR, ion cyclotron resonance; CID, collisional induced dissociation threshold measurements; ES/HPMS, electrospray high-pressure mass spectrometry; mobility, variable temperature ion mobility equilibrium measurements; BIRD, black body IR dissociation. [c] Data from several sources, evaluated values cited from ref 27. [d] Acetylcholine. [e] (MeCO-Ala-OCH_3 − H)$^-$.

internal IHBs can form in functionalized amino acids such as in protonated lysine.[332] Internal IHBs also contribute to the gas-phase basicities of peptides that increase with peptide size that allows better internal solvation. The basicities decrease with increasing charge due to Coulomb repulsion between the protonated functions.[333−335] The PAs and GBs of amino acids, peptides, and proteins were reviewed.[336] As to conformations, long chains, low charge states, and low temperatures favor compact geometries.

Before the new methods of volatilization, IHB interactions in proteins were modeled by the sufficiently volatile amino acid derivatives $CH_3CONHCH_2COOCH_3$ (CH_3CO-Gly-OCH_3) and $CH_3CONHCH(CH_3)COOCH_3$ (CH_3CO-Ala-OCH_3). The two carbonyl groups in these molecules are positioned similarly to adjacent amide groups in peptides. Protonation forms an intramolecular IHB, and the thermochemistry suggests an internal bond of 11−12 kcal/mol between these groups,[150] less than the 30 kcal/mol of unconstrained $OH^+\cdots O$ bonds, due to constrained geometries. The seven-membered ring includes the proton, two −C=O bonds, and five single bonds with flexible bond angles. The strain of 18−19 kcal/mol is similar to five-membered IHB rings $(XCH_2CH_2X)H^+$ in ions that also contain five single bonds including the hydrogen bond (Table 7).

The proton affinities of further N-acetylated amino acid methyl esters of glycine, leucine, phenylalanine, proline, glutamic acid, and arginine have been calculated and characterized at B3LYP/6-31++G(d,p) level, and proton affinities of 15 similarly derivatized amino acids have been measured experimentally. The proton is attached to the carbonyl group in most cases. The proton affinities of all N-acetyl amino acid methyl esters are higher than those of the corresponding underivatized amino acids, reflecting stabilization of the ions by intramolecular hydrogen

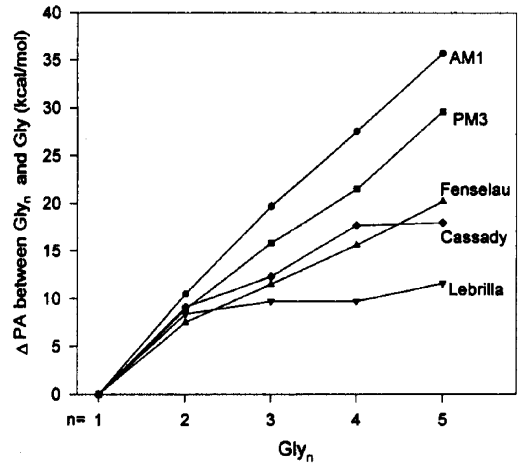

Figure 50. Proton affinities of polyglycines as a function of chain length. Reproduced from ref 340 with permission. Copyright 1995 American Chemical Society.

bonding.[337] These results confirmed and extended earlier studies on glycine and alanine derivatives.[150]

Longer chains between functional groups allow more optimized intramolecular IHBs. For example, Lebrilla and co-workers found that the gas-phase basicities of β-alanine and β-alanine−glycine are higher by 7 kcal/mol than analogous derivatives of α-alanine, because the longer chain in the β isomers allows more stable iIHBs. The gas-phase basicity (GB) of *N*-acetylglycine amide is higher by 5 kcal/mol than that of *N*-acetylglycine itself because a stronger iIHB forms between the two amide groups of similar PAs in the amide, in accordance with ΔH°_D vs ΔPA correlations. The increased GB of *N*-acetylglycine amide is similar to that of triglycine, and the iIHB simulates interactions between adjacent amide groups in peptides.[338]

The gas-phase basicities of polyglycines increase with size. The proton is localized on the terminal amine group, and the proton affinity increases with increasingly efficient internal solvation.[333−335,339] Semiempirical AM1 and PM3 calculations reproduced the trend observed in Figure 50 and showed that the increasing PA from Gly_1 to Gly_5 is caused by internally solvated conformations, while in extended conformations the PA would remain constant. For example, internal solvation of the charged site in Gly_5H^+ accounted for 83% of the increase of its PA relative to glycine.[340]

Internally solvated structures were identified experimentally by ion mobility in (Ala-Ala-Arg-Ala-Ala)H^+ and its N-acetylated and $-COOCH_3$ derivatives. They also had similar biding energies to H_2O molecules, which also supported a common structure. However, a salt-bridged structure also becomes energetically accessible as a transition state for H/D exchange in the monohydrated ion.[341]

Counterman and Clemmer and co-workers studied the effects of peptide size and multiple protonation on the conformation of polyprolines $[Pro_n + zH]^{z+}$ ($n = 3-56$; $z = 1-6$) using ion mobility and molecular modeling calculations. Protonation at the N-termini allowed hydrogen bonds to backbone carbonyl groups of the second and third proline residues. Singly charged ions favored more compact globular and hairpin-like conformers. The shorter and low protonation state peptides with $n = 5-11$ and $z = 1$ and $n = 10-22$ and $z = 2$ and highly charged $z = 3-6$ ions favored relatively extended conformations, but as the polymer size increased, the higher charge state ions become more compact.[342]

These authors also studied quadruply protonated polyalanines ($[Ala_n + 4H]^{4+}$, $n = 29-49$). The results indicated that $[Ala_n + 4H]^{4+}$ favors stretched helices, stabilized by $i \rightarrow i + 3$ and $i \rightarrow i + 4$ hydrogen-bonding, where the latter increases with polymer length, constituting about 65% of the interactions in $n = 36$ and 85% in $n = 48$ peptides.[343] In the triply charged polyalanines ($n = 27-39$, $z = 3$) at room temperature, extended helical structures and compact hinged helix-coils were observed, but these conformations unfolded at higher temperatures, and the peptides adopted extended helical structures. The activation energies for the transition increased by about 1 kcal/mol per residue from $n = 27$ to 39, because the increased size allowed more efficient hydrogen bonds that must be released in the transition.[344,345]

Folded conformations were observed also in dinucleotides, and the degree of hydrogen bonding in a given conformation appeared to be the primary determinant of the energy.[346]

Many biomolecules are multiply protonated in solution and biological environments, and electrospray can also generate multiply charged states in the gas phase. The multiply charged ions assume extended conformations because of Coulomb repulsion,[16,17,331,347] and the ionized state decreases the gas-phase basicity for adding further protons. For example, the GB of gramicidin S is >243 kcal/mol, while the GB of (gramicidin S)H^+ is only 215 kcal/mol. This difference suggested a Coulomb energy of >28 kcal/mol and a dielectric polarizability <1.2 in this ion.[16]

7.1.2. Interactions between Internal and External Solvation

In early studies, we observed that in protonated diamines the iIHBs can be weakened by external solvation and, conversely, bonding to solvent molecules is weakened by internal bonds.[259] Similarly, the internal bond in the protonated dipeptide analogue $(CH_3CO\text{-}Ala\text{-}OCH_3)H^+$ reduces the binding energy of this ion to the first H_2O solvent molecule to 13 kcal/mol, instead of the 16 kcal/mol expected from ΔPA correlations. This results because internal solvation provides the first solvent group and H_2O becomes in effect the second solvent molecule of the protonated group.[150]

Our early study of the hydration of valineH^+ by a H_2O molecule showed a bonding energy of 19.3 kcal/mol,[348] and a similar bonding energy of 17 kcal/mol can be estimated for glycineH^+ from recent work by Kebarle and co-workers.[155] These values are similar to those expected for protonated amines and suggest that internal solvation of the amine function in these protonated amino acids is not significant. Similarly, the binding energy of the deprotonated (glycine − H)$^-$ and (alanine − H)$^-$ anions of 12 kcal/mol[349] is

expected for a free carboxylate anion. However, the solvation energy of the internally solvated deprotonated dipeptides, $(Gly{\cdot}Gly - H)^-$ and $(Ala{\cdot}Ala - H)^-$, by one water molecule is smaller by 3 kcal/mol,[349] suggesting that internal solvation in the dipeptide anions (iIHBs) weakens the bond to the H_2O molecule. The first four H_2O molecules solvate primarily the anionic carboxylate function with one bridging IHB to the terminal amine group.[349]

Similarly, Kebarle and co-workers studied the hydration of protonated amino acids and small peptides. They found that the dissociation free energy, ΔG°_D, of $Gly_nH^+\cdots H_2O$ decreased from 9.8 to 8.8, 6.7, and 5.7 kcal/mol for $n = 1-4$ with increasing peptide size because of increasingly efficient internal solvation in the larger peptides,[155] similar to the trend found earlier in protonated diamines $(H_2N(CH_2)_n\text{-}NH_2)H^+$.[259] Similarly, internal IHBs in $LysH^+$ and $(Gly{\cdot}Lys)H^+$ decreased the free energy of hydration by H_2O molecules.[155]

Bowers and co-workers measured the H_2O binding energies of small protonated peptides as 7−15 kcal/mol. Small two to three residue peptides bonded water more strongly than larger peptides that are solvated more strongly internally. Also, water molecules bind more strongly to peptides in higher charge states because of the higher charge densities of the binding protons and possibly because of their more extended, less internally solvated conformations.[350]

Another effect of external solvation is that it can favor the formation of salt bridges. For example, the pentapeptide $(Ala\text{-}Ala\text{-}Arg\text{-}Ala\text{-}Ala)H^+$ and its Ac- and -OMe derivatives are internally solvated, but adding a H_2O molecule facilitates a salt-bridge structure that can serve as a transition state for H/D exchange in a relay mechanism.[341]

The formation of zwitterions is a question of long-standing interest. The solvation of the ionic groups of the zwitterions, which involves IHB interactions with the solvent, are critical for forming the zwitterion. The question of how much solvation is needed to form zwitterions has been addressed by Williams and co-workers, who found that in cationated valine this requires only three to six H_2O molecules.[351] For protonated arginine dimer and protonated bradikynin, ab initio calculations suggested that an internal ion−zwitterion (or salt-bridge) structure is the most stable conformation.[352] Zwitterions may be stabilized also by internal solvation. They were found not to be the most stable forms of polyglycine,[353] but mobility studies suggested compact zwitterionic forms, stabilized by internal solvation, in the protonated $(serine)_8H^+$ octapeptide.[354]

Jarrold and co-workers measured the binding energies of a H_2O molecule to protonated dipeptides, and their calculations found that both the unsolvated and solvated peptides have multiple conformations. The water molecule causes conformational changes by creating a bridge or by the loss of internal cation$\cdots\pi$ interactions.[355]

These workers also studied the effects of conformation, charge, and composition on binding a water molecule to alanine-based peptides. More association was found in globular peptides than in helical ones, and this difference was used to establish that the globular to helix transition occurs at eight residues.[356]

The ability to establish a network of hydrogen bonds to several different hydrogen-bonding partners emerged as a critical factor for the ability to bind water molecules. Another important factor is the shielding of the ionic site that binds the water molecule. For example, peptides containing a protonated histidine, the charge of which is delocalized and not shielded well, binds water more strongly than peptides that contain a protonated lysine, of which the localized charge is shielded more effectively.[357]

7.1.3. Thermochemical and Structural Effects of Hydration

In conformationally extended multiply protonated ions, the separated ionized groups interact individually with solvent molecules. The Kebarle group generated the diprotonated diamine ions $H_3N(CH_2)_p\text{-}NH_3^{2+}$ in a high-pressure mass spectrometer source and measured the binding energies to water molecules. The results are illustrated in Table 4 above. The clusters $(NH_3^+(CH_2)_pNH_3^+)(H_2O)_n$ for $p = 5-12$ and $n = 1-6$ showed hydration enthalpies larger by 2 kcal/mol than analogous protonated monoamines. For example, for $NH_3^+(CH_2)_6NH_3^+(H_2O)$, $\Delta H^\circ_{0,1} = 17.3$ kcal/mol compared with 15.2 kcal/mol for the monoamine. The solvation enthalpies decrease slowly with increasing chain length p to 15.7 kcal/mol for $p = 12$. Extrapolating the curve of $\Delta H^\circ_{0,1}$ vs p suggests that for $p = 1-4$, the bond energy may be 20−30 kcal/mol, much larger than that for singly charged ammonium ions. These trends can be understood in terms of the Coulomb interaction between the protonated groups. In contrast to monoprotonated ions where $\Delta H^\circ_{n-1,n}$ decreases monotonically with n, in the diamines the binding of the first and second, third and fourth, and fifth and sixth H_2O molecules are comparable, showing that the water molecules attach alternatingly to the protonated end-groups and each has little effect on the charge densities on the other end group.[95]

In $(gramicidin\ S + 2H)^{2+}(H_2O)_n$, electrospray produces clusters with up to 50 H_2O molecules. In this molecule, two protonated ornithine residues can hydrogen bond to carbonyl oxygens of the peptide backbone as shown in Figure 51. The internal hydrogen bonds are displaced by external solvation when about 24 or more water molecules solvate each protonated group, and the ion assumes a structure similar to that in solution.[328] At electrospray capillary temperatures of 435−455 K where some solvent from the clusters evaporates, magic numbers are observed at $n = 8$, 11, and 14, which indicate particular stability. Solvation by less than six H_2O molecules was insufficient to displace the internal bonds, and these clusters had low abundances, while a magic number at 11 H_2O molecules indicated a water bridge. A magic number at $n = 40$ H_2O molecules suggested that two water clathrates of 20 molecules attach to the protonated ornithine groups, opening up the folded unsolvated structure.[358] The magic numbers are due to the solvation of charged ornithine residues by three to four H_2O molecules and the

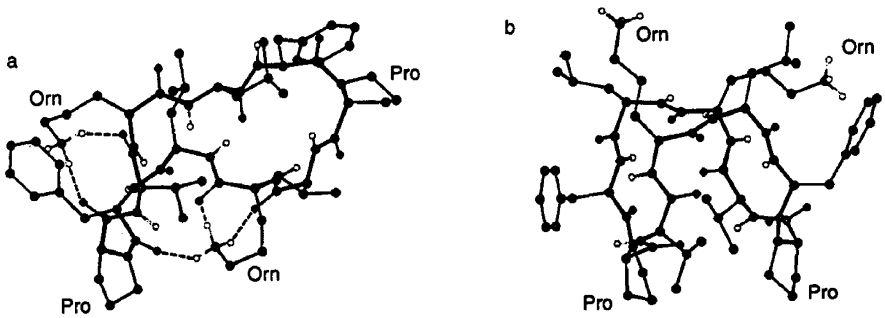

Figure 51. Representative low-energy structures of gramicidin S $(M + 2H)^{2+}$ ions in (a) a vacuum and (b) water obtained by molecular modeling using a dielectric constant of 1.0 and 78, respectively. Intramolecular hydrogen bonding is indicated by dashed lines in the gas-phase ion. Reproduced from ref 328 with permission. Copyright 1997 Elsevier.

formation of additional $-NH^+OH_2\cdots OH_2\cdots OC-$ salt bridges. At higher capillary temperatures, the unsolvated ions dominate as each protonated ornithine side chain becomes internally solvated by three peptide CO groups.[328] Internal solvation is even more efficient in the singly protonated ion, where the absence of Coulombic repulsion allows optimal folding and five amide CO groups solvate the protonated ornithine amine group, causing an increase in the gas-phase basicity to >243 kcal/mol, compared with 222.5 kcal/mol for an isolated ornithine residue.[16]

Jarrold and co-workers examined protein hydration using ion mobilities in a drift cell. Attachment thermochemistry of the first solvent molecule to the 58 residue bovine pancreatic trypsin inhibitor $(BPTI + 6H)^{6+}$, $\Delta H^\circ_{0,1} = -21.3$ kcal/mol and $\Delta S^\circ_{0,1} = -62$ cal/(mol K), indicates four IHBs of the first H_2O molecule to cysteine and tyrosine residues, which can order the formation of a pocket, resulting in a large conformational constraint. The five further H_2O molecules have $\Delta H^\circ_{n-1,n}$ of -13 to -16 kcal/mol and entropy changes, $\Delta S^\circ_{n-1,n}$, of -38 to -42 cal/(mol K), close to the values for the initial hydration of solid protein films. Some of these may be the three structural H_2O molecules that are known to form a cluster hydrogen-bonded to five amino acid residues.[13]

Further, binding free energies in solvated (cytochrome $c + nH)^{n+}(H_2O)_m$ with a broad distribution of charge states showed that the $\Delta G^\circ_{n-1,n}(271\ K)$ values for solvation by one to five H_2O molecules are -4.5 to -3.6 kcal/mol for the +5 state and -3.6 to -3.4 kcal/mol for the +7 state, showing stronger solvation for the lower charge state.[359] The results show that at 253 K and $P(H_2O) = 0.73$ Torr with an increase in charge state from 4 or 5 to 7−13, the conformation opens from folded to linear and the number of solvent molecules decreases from about 50 to about 30. These data show that the lower charge state folded conformation is better solvated, probably because of cooperative effects, such as multiple IHBs to water molecules in pockets and water bridges between charged groups. The +7 charged state requires 29 water molecules for partial folding. Apomyoglobin gave similar results.[360]

Internal solvation of the charged group was also indicated by molecular dynamics simulation of the nine-residue protonated bradykinin.[361] The first results on the internal and external solvation of protonated peptides and proteins was reviewed recently.[362]

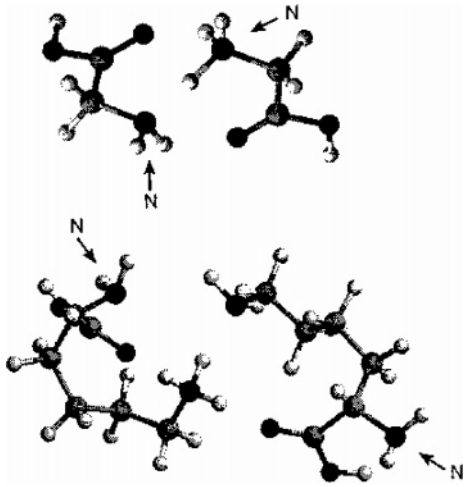

Figure 52. Protonated dimers of glycine and lysine. Reproduced from ref 18 with permission. Copyright 1997 American Chemical Society.

These studies illustrate that the gas-phase hydration of biological ions can identify and quantify the role of water biological structure.

7.1.4. Intermolecular Association and Polydentate Bonding

Biomolecules associate in many natural processes and IHBs, including multiple hydrogen bonding, contribute significantly. We observed early examples in the complexes of polyprotonic ions such as $MeNH_3^+$ bonding to the dipeptide-like MeCO-Ala-OMe molecule. Table 9 shows that, compared with a monoprotonic Me_3NH^+ ion, which can form only one IHB, the binding energy of the polydentate complex with $MeNH_3^+$ increases from 29.7 to 40.1 kcal/mol and the complexation entropy changes from -27.6 to -35.1 kcal/mol.[150]

Complexes of MeCO-Ala-OMe were also measured by BIRD thermal photodissociation.[363] This method was applied also to the binding energies of protonated amino acid dimers, giving binding energies of 26 kcal/mol that varied little among the amino acids. The bonding energies are consistent with the $NH^+\cdots O$ bonds between the $-NH_3^+$ group of the ionic component and the −COOH group of the neutral component, based on the correlations in Table 2 and the PAs of these groups. Figure 52 shows the structures of these dimers.[18]

In dimers of dipeptides, a dissociation energy of 24.3 kcal/mol was calculated for (Ala·Ala − H)$^-$··· (Ala·Ala) dissociating to the components in their minimum energy conformations but about 35 kcal/mol if the components separate and retain the same geometries as in the dimer. The latter agreed with the experimental activation energy for dissociation, suggesting a dimer-like transition state.[349]

The complexing energy of the deprotonated (Gly·Gly − H)$^-$ and (Ala·Ala − H)$^-$ by the neutral dipeptides was found to be comparable to solvation by four H_2O molecules.

The binding energy of the dimer of the pentapeptide leucine enkephalin, $(YGGFL)_2H^+$, was equated to the 46.5 kcal/mol activation energy for its thermal dissociation (k_{507} = 24.5 s^{-1}) in the electrospray capillary.[364] This large binding energy and an unusually large log A = 21.7 (log s^{-1}), due to a high-entropy transition state, suggest a constrained multiply bonded dimer, but the complex desolvation/dissociation processes in electrospray makes these values only approximate. The same rate coefficient, using a more conventional log A = 17.2 obtained from a blackbody IR dissociation (BIRD), gives an activation energy, ΔH°_D (E_a), of 36.6 kcal/mol, in very good agreement with the ΔH°_D (E_a) of 36.9 kcal/mol from the BIRD study of this dimer.[365] These binding energies are stronger than a single IHB, especially if it is weakened by internal solvation in the protonated monomer. The results therefore indicate multiple IHB interactions.

The dissociation energies of alanine and glycine peptides were also studied using thermally activated dissociation kinetics. Activation energies and entropies were determined for dissociation of the diprotonated Ac-$(GA)_7$K···Ac-A$(GA)_7$K + 2H$^+$ (Ac = acetyl, G = glycine, A = alanine, and K = lysine) dimer with the dominant conformation of a V-shaped helical dimer and for the dissociation of the (2Ac-$(GA)_7$K)···Ac-A$(GA)_7$K) + 3H$^+$ and (Ac-$(GA)_7$K···2Ac-A$(GA)_7$K) + 3H$^+$ pinwheel-shaped helical trimers. The activation energies were 22 kcal/mol for the dissociation of the dimer and 17 and 18 kcal/mol for the trimers. The mobility method yielded high-pressure limiting activation energies that may be equated with the intermolecular bonding energies. In addition, the mobility also yields information on the conformations of the dissociating complexes. Therefore, ion mobility may be the method of choice for measuring bonding energies based on dissociation of adducts.[366]

Ion mobility was applied also to the association of protonated polyalanine peptides. Mixtures of helix-forming monomers were found to form V-shaped helical dimers and pinwheel-shaped helical trimers tethered together by lysine residues and stabilized by cooperative interaction of the combined charge with the helix dipoles. Mixtures of globular monomers were found to form mainly globular multimers.[367] The first results on unsolvated and partially solvated proteins and peptides were reviewed recently.[362]

Polydentate bonding was proposed in reaction intermediates. Beauchamp and co-workers studied H/D exchange between polyglycine and D_2O and proposed two polydentate IHB structures, NH_3^+···OD_2···OC− → −H_2N···HDO···H$^+$OC−, as a relay mechanism for the H/D exchange reaction. They also studied exchange reactions with ND_3 and found a mechanism suggestive of a −H_2N···NH_4^+···OC− complex. These authors also examined zwitterionic salt bridges in oligopeptides and presented evidence for a salt bridge in the IHB complex between betaine and ND_3 in the reaction $(CH_3)_3N^+CH_2COOH$···ND_3 → $(CH_3)_3N^+CH_2COO^-$···HND_3^+.[340]

7.2. Nucleic Bases and Nucleotides

Nucleic bases are strong intrinsic acids and bases and can therefore form strong hydrogen bonds. Gas-phase studies allow insights into hydrogen bonding between neutral base pairs in DNA itself.

The neutral hydrogen bonds in DNA are strengthened by the acidities of the hydrogen donor groups of the nucleic bases. These donor capabilities are enhanced by the presence of multiple nitrogen atoms in the rings of these heterocyclic bases. In fact, their intrinsic acidities are as strong as possible without being ioinized in the DNA interiors.[368] Knowing the intrinsic gas-phase acidities allows extension of the correlation between acidities and hydrogen bond strengths to the neutral hydrogen bonds.[68,69] Applying this to hydrogen bonds between DNA base pairs suggests that about 1 kcal/mol, or 20%, of these hydrogen bond strengths may be contributed by their enhanced acidities. Without this factor, the hydrogen bonds that bind DNA base pairs in the helix may not be stable under biological conditions. This may therefore explain why molecules with multiple nitrogen atoms in heterocyclic rings were selected to encode genetic information.[368]

The nucleic bases are also strong bases in the gas phase, but their protonation energies are attenuated by 32 kcal/mol by solvation compared with ammonia, for example. In the gas phase, their protonated ions can form strongly hydrogen-bonded dimers, and the increased ΔH°_D and ΔS°_D of the dimers vs $(pyridine)_2H^+$ indicates that two hydrogen bonds bind $(adenine)_2H^+$ and $(thymine)_2H^+$ and three bonds bind $(cytosine)_2H^+$, in planar bonding arrangements similar to the neutral base pairs.[279]

The advent of electrospray allows the study of nucleotides in the gas phase. The conformations of 16 anionic deprotonated dinucleotides were investigated by Bowers and co-workers using ion mobilities. Combined with molecular mechanics/dynamics, the results showed conformations where the nucleic bases in the dinucleotides are stacked, hydrogen-bonded, or separated with barriers heights of 0.8−12.9 kcal/mol among the conformers.[369] In thymine−guanine deprotonated dinucleotides, the degree of hydrogen bonding in a given conformation appeared to be the primary determinant of the energy.[346]

The bonding in deprotonated nucleotide dimers were also investigated by BIRD thermal dissociation. The results showed that the dissociation energy in the guanosine−cytosine dimer anion is much higher than other combinations, suggesting that Watson/Crick base pairing is maintained in the gas phase.

Further, the dissociation energies of doubly deprotonated oligonucleotide heptamers were also studied, and the activation energies were found to depend on the identity of the leaving nucleic base.[370,371]

In summary, a rapidly advancing literature deals with biological ions in the gas phase. The interactions are similar to those observed earlier in model organics: internal and external solvation in which IHBs play significant roles; the presence of isomeric structures with comparable energies; association of ions and molecules through multiple IHBs; the formation of solvent bridges. The advent of electrospray allows measurement of the thermochemistry of these interactions in the gas phase. These studies give insights into fundamental bioenergetics, such as the interrelations between internal and external solvation and their effects on conformation. Cluster models can be used to estimate the energy contributions of IHBs in biological systems, as described in the next sections.

7.3. Cluster Models of Bioenergetics

Many biological processes are controlled by ionic intermediates. The intermediates may be stabilized by hydrogen bonds to polar groups in proteins more than they are stabilized by water. This decreases the activation energies of reactions through these intermediates.[323]

Cluster models can help to quantify these interactions. Both clusters and protein interiors are unsolvated or partially hydrated environments. In both environments, peptide amide NH groups are strong acids and CO groups are strong bases, which allows them to form strong IHBs. Cluster models allow evaluation of these contributions, keeping in mind that the geometrical constraints of biopolymers and the surrounding dielectric solvent are absent in the model clusters and the large biomolecules are replaced by more simple molecules.

7.3.1. Enzymatic Hydration of CO_2

In a reaction catalyzed by carbonic anhydrase, OH^- reacts with CO_2 to produce HCO_3^- with a rate constant of 7.5×10^7 M^{-1} s^{-1} (or 1.2×10^{-13} cm^3 s^{-1}), faster by about 4 orders of magnitude than the reaction in aqueous solution, where $k = 8.5 \times 10^3$ M^{-1} s^{-1}. The catalytic mechanism was proposed to strip the OH^- from its solvation sphere, assuming that the desolvated ion is more reactive.[375] To test this proposal, Yang and Castleman[376] examined the reactions of the IHB bonded clusters $OH^-(H_2O)_n$ with CO_2. They observed mostly dissociative reactions (eq 35).

$$OH^-(H_2O)_n + CO_2 \rightarrow HCO_3^-(H_2O)_{n-m} + mH_2O \quad (35)$$

For combinations of $n = 0-5$ and $m = 0-3$, the reactions are exothermic by 34−88 kcal/mol, the exothermicity somewhat decreasing with increasing size n and with increasing dissociation m. Rate coefficients, measured at 130 K where large clusters are stable, were found to decrease with increasing cluster size and became slow, below 0.80×10^{-10} cm^3 s^{-1}, that is, collision efficiencies below 0.1, for $n > 10$, as shown in Figure 53. However, at low solvation, the reaction becomes faster and approaches unit collision efficiency. This supports the proposed role of the enzyme to provide an environment where the OH^- ion is only partially solvated.

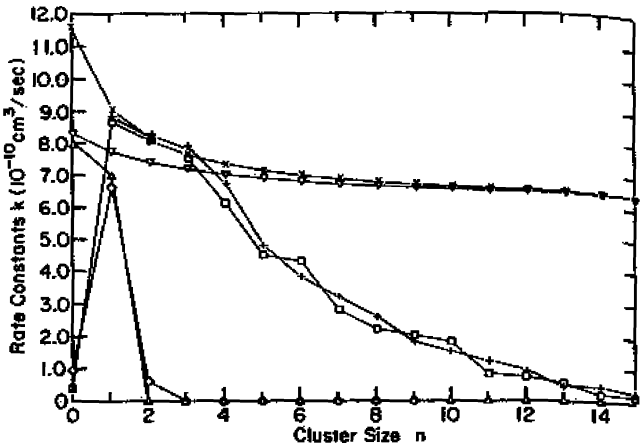

Figure 53. Rate constants of the reaction $OH^-(H_2O)_n + CO_2 \rightarrow HCO_3^-(H_2O)_{n-m} + m(H_2O)$ as a function of solvation. Reproduced from ref 376 with permission. Copyright 1991 American Chemical Society.

7.3.2. Enzyme Energetics: IHBs and Backbone Amide Groups

Proteolytic enzymes such as trypsin dissociate the peptide bonds of substrates. The active site is illustrated in Figure 54. Four IHB interactions are present in the resting state in Figure 54a. Two of these are $COO^-\cdots$HNimidazole and $COO^-\cdots$HOR bonds that can be modeled by the bonding of CH_3COO^- to imidazole and CH_3OH, respectively. The bonds between $RCOO^-$ and protein amide NH groups are modeled by the bonding of CH_3COO^- to the amide NH function in the dipeptide analogue $CH_3CONHCH(CH_3)COOCH_3$ (i.e., CH_3CO-Ala-OCH_3), with a bonding energy of 30.2 kcal/mol for the first and 21.2 kcal/mol for the second molecule. Considering the mutual effects of the ligands, the total IHB interaction in the resting state is estimated as 65 kcal/mol.[187]

The essential step is proton transfer from a serine OH group to imidazole that creates an anionic "tetrahedral intermediate". This intermediate can hydrogen bond to NH groups of neighboring protein amide links (right-hand side of Figure 54b). The hydrogen bonds in the resting state and transition state are modeled by the cluster interactions shown in Figure 54c. Interactions in the $CH_3COO^-\cdot CH_3CO$-Ala-OCH_3 complex suggest that these additional hydrogen bonds of the tetrahedral intermediate to the peptide backbone amide groups can contribute a driving force of 32 kcal/mol to the formation of the transition state. Additional driving force is provided by the formation of the salt bridge between the (imidazole)H^+ cation and a carboxylate group. The strong IHBs between the amide NH groups and carboxylate ions result from the large intrinsic acidities of the protein amide groups.[368]

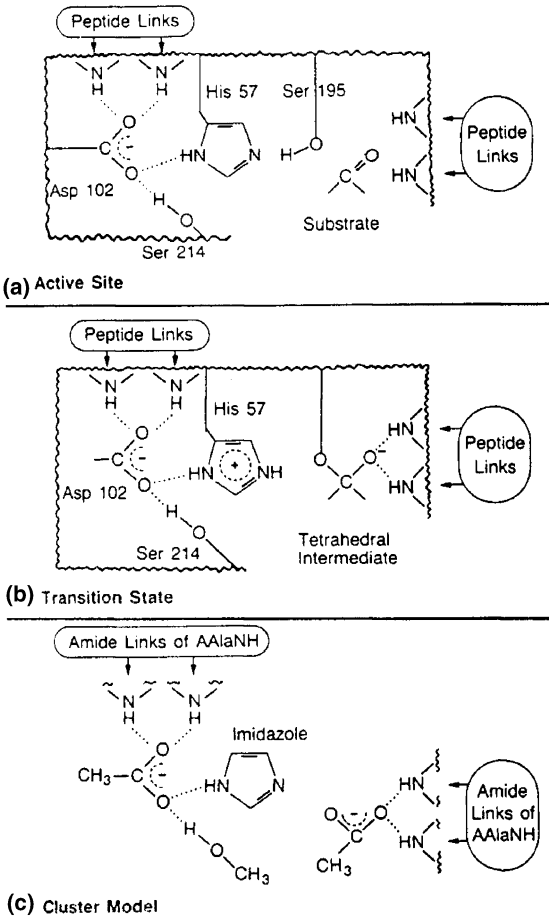

Figure 54. Panel a depicts the resting state of the active site of trypsin with four IHB bonds. Panel b depicts the reactive intermediate with a salt bridge and new IHBs to the peptide backbone. Panel c shows a cluster model of the active site. The ionic hydrogen bonds to the peptide backbone are represented in the model by bonds to amide groups in the dipeptide analogue $CH_3CO-Ala-OCH_3$, that is, ($CH_3CONHCH(CH_3)COOCH_3$). Reproduced from ref 187 with permission. Copyright 1988 American Chemical Society.

7.3.3. The Formation of Biological Membranes

Figures 38 and 39 showed that the formation of $RCOO^-\cdots HOOCR$ bonds between ionized and neutral carboxylic acids is more exothermic than the formation of other types of IHBs.[183] The exothermicity reflects the formation of a strong $RCOO^-\cdots HOOCR$ bond while displacing a weak $RCOO^-\cdots H_2O$ bond. Membrane formation in solutions of carboxylic acids would be favored when such IHB networks can form, when both ionized and neutral carboxylic groups are present at pH values near the pK_a of the acids.[183] This was indeed observed in the formation of membrane-bound vesicles from C_8 and higher carboxylic acids. The addition of alcohols also facilitated membrane formation, presumably because the ROH groups can also hydrogen bond strongly to the $RCOO^-$ functional groups. The cluster data can therefore explain why carboxylate functions are efficient for forming membranes in solution.[377]

7.3.4. Proton Transport in Membranes

The membrane channel in gramicidin is spanned by a water chain that conducts protons by a fast "hopping" mechanism through shifting $OH^+\cdots O$ bonds.

This mechanism raises some interesting questions. How can the proton, well solvated in water, enter the less efficient, two-dimensional water chain? How can it move across the chain without being trapped by the surrounding protein amide groups that are strong bases?

In the protein channel, the proton is stabilized by strong ionic hydrogen bonds between the protonated water chain and the surrounding peptide amide CO groups. Proton entry from aqueous solution is simulated by transfer from neat water clusters to mixed acetone−water clusters as in reaction 36.

$$(H_2O)_6H^+ + 3Me_2CO \rightarrow (Me_2CO)_3(H_2O)_3H^+ + 3H_2O \quad (36)$$

Cluster thermochemistry shows that this reaction is exothermic by 19 kcal/mol due to the stabilizing effects of the strongly basic polar CO groups. The amide CO groups in the membrane may facilitate similarly the entry of protons from bulk water.

The mixed clusters of water and blocked ligands discussed above, such as the thermochemistry of acetone/water clusters, suggest that a central H_3O^+ unit is surrounded by more basic Me_2CO molecules. The central proton is stabilized by opposing attractions of the surrounding dipoles.

Similarly, the protonated water chain can bridge between the amide CO groups of the protein, and the proton can remain in the water chain due to the opposing attractions of the surrounding protein amide dipoles. In protonated diketone/water clusters, the second H_2O molecule showed anomalously strong bonding, and ab initio calculations showed that this is due to a $H_3O^+\cdots H_2O$ bridge between the polar groups. Similarly, the proton remains in the water chain in the membrane due to the balance of opposing dipoles of more basic protein amide groups. The proton can be transferred between the polar groups with an energy barrier of only a few kilocalories per mole by shifting bonds in the $H_3O^+\cdots H_2O$ bridge.[242]

We observed in clusters protonated water cores surrounded by blocked ligands. These clusters illustrate the mechanism by which a water chain in a protein channel can facilitate the entry of a proton from solution, allow the proton to remain in the water chain, and provide a low-energy bridged pathway for proton transport.

7.3.5. Acetylcholine Neuroreceptors

Acetylcholine (ACh^+) is a neurotransmitter cation that contains a quatenary amine group and an ester group that can form an intramolecular hydrogen bond (Figure 55). To reach the receptor site, the ACh^+ molecule must enter from aqueous solution to a 20 Å deep groove lined with aromatic residues and transit this groove. The quaternary amine group of ACh^+ can interact by $CH^{\delta+}\cdots\pi$ hydrogen bonds with aromatic residues that line the groove. These bonds must stabilize acetylcholine sufficiently to allow entry from water where it is fully solvated, but they must interact weakly enough to avoid trapping it. Comparison between solvation by H_2O or the aromatic

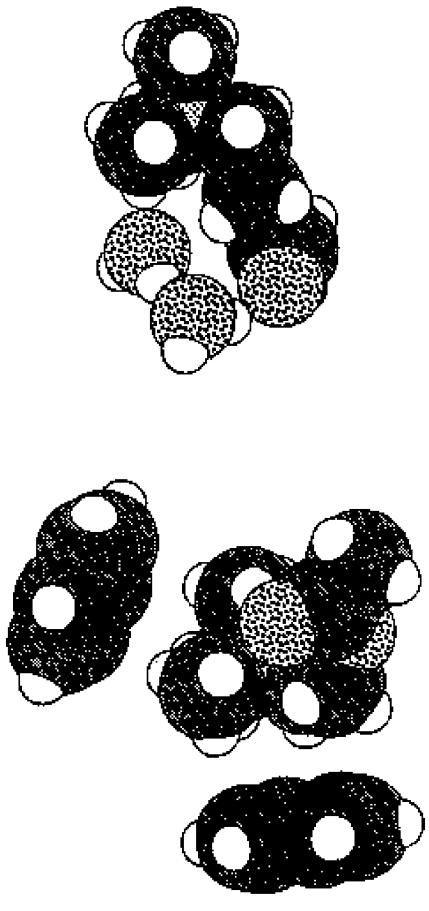

Figure 55. Panel a shows the open isomer of acetylcholine bridged by two water molecules. Panel b shows the internally hydrogen-bonded structure of acetylcholine interacting with two benzene molecules. The clusters simulate the conformational change of acetylcholine upon entry from water into a groove lined by aromatic residues in transit to the neuroreceptor. Reproduced from ref 124 with permission. Copyright 1999 American Chemical Society.

groups is made possible by the energetics of the $ACh^+(H_2O)$, $ACh^+(C_6H_6)$, and $ACh^+(C_6H_5CH_3)$ complexes. All have weak bonding energies of 9.0, 8.6, and 9.5 kcal/mol, respectively. This suggests that the aromatic residues provide stabilizing interactions similar to that of water. This allows acetylcholine to enter the groove in the receptor lined by aromatic groups, and this allows the reactions to proceed.[124]

Ab initio calculations supported the existence of an internal bond in ACh^+. This internal bond may be weakened by hydration when the ion is in water. With two H_2O molecules, the formation of a solvent bridge favors the open conformation shown in Figure 55a in solution. Upon desolvation, acetylcholine can form an internally hydrogen-bonded conformation shown in Figure 55b that is stabilized by about 4.5 kcal/mol compared with an open conformation. This internal solvation and nonconventional $CH^{\delta+}\cdots\pi$ bonds with the aromatic residues in the channel can compensate for the loss of aqueous solvation when the ion enters the channel. The aromatic groups can also lower the energy barrier to the formation of the all-trans ACh^+ conformation required at the receptor site.[124]

In summary, cluster models provide the energetics of specific ion−neutral interactions in enzymes, membranes, and neuroreceptors, which cannot be measured in the complex biological systems themselves. These models show that polar protein groups can form strong IHBs with ions, which facilitate reactions that proceed through ionic intermediates.

8. Ionic Hydrogen Bonds in the Condensed Phase

Parallel with the gas-phase IHB studies, IHBs in solution have been also investigated, especially by the group of G. Zundel, using IR continuum absorption to identify IHB networks. These studies show that many IHB effects in the gas phase have analogies in solution. The work was reviewed recently.[378] This section will summarize solution results that parallel the gas-phase behavior.

8.1. Dimers, Intramolecular Bonds, and IHB Chains

8.1.1. Homodimers and Heterodimers

The first studies dealt with homoconjugated hydrogen bonds (i.e., symmetric dimers or homodimers) in membranes of polystyrene sulfonic acid. Upon hydration, these solutions showed an IR continuum absorption between 1800 and 3400 cm^{-1} due to the release of a proton and the formation of the $H_5O_2^+$ ion.[379]

Observations with other concentrated acids showed that this absorption band develops when two or more H_2O molecules are available per free proton, confirming the $H_5O_2^+$ assignment.[380] The continuum absorption was assigned to fast proton fluctuation between the two H_2O components. Calculations identified a double minimum proton potential in the IHB, where a small potential can admix the ground and first excited states and allow rapid proton motion between the minima (about 10^{13} Hz), leading to a polarizability larger by 2 orders of magnitude than normal electron polarizabilities.[381] This assignment was confirmed by field and salt effects and temperature and deuteration effects.[382,383] The absorption continuum requires interaction with the polar solvent. If the IHB is polarized by local fields, the proton polarizability decreases considerably.

Symmetric $OH^+\cdots O$ bonds were found in solution of alcohols, $NH^+\cdots N$ bonds in imidazole, and $OH\cdots O^-$ bonds in $H_3O_2^-$ in concentrated aqueous KOH and in CH_3OK/CH_3OH. Similar to the gas phase, the IR studies showed intramolecular IHBs in ionized polyfunctional molecules, such as in protonated diamines and deprotonated diols.

In the gas phase, the IHB bond strength in alkylpyridine homodimers was 24 ± 1 kcal/mol independent of alkyl substitution and of the basicities of the monomers. Similarly, in solution, the barriers, force constants, proton polarizabilities, and barriers of proton vibration and the bonding strengths were found to be independent of the pK_a for protonated pyridine homodimers.

Heteroconjugated bonds of the type OH···N → O^-···H^+N were also observed in solution, for example, in interactions of carboxylic acid and phenol donors with nitrogen base acceptors.[384,385] In analogy with the gas-phase relations between PA differences and bond strengths, these condensed-phase systems can be viewed as heterodimers in which the extent of proton transfer and the bond strength depend on the proton affinity difference of the O^- and N proton acceptors (or the pK_a difference of the OH and NH^+ donors). In fact, it was shown that the gas-phase $\Delta H°_D/\Delta$PA correlations can be extended continuously to these pairs, even though the gas-phase ΔPA values of the O^- and N acceptors extend over 100 kcal/mol. In solution, the free energy required to form the ionized forms is much smaller ($\Delta G°$ proton transfer = 1.0 to 3.2 kcal/mol) because of the solvation of the ionized forms. Polar solvents, especially water, shift the proton transfer equilibria in the hydrogen bonds strongly to the charge-separated forms and, in the extreme, can dissociate the hydrogen bonds,[386] similar to the weakening of IHBs in the gas phase by solvent molecules.

8.1.2. Intramolecular and Polydentate Bonds

In parallel to the gas phase, intramolecular IHBs were demonstrated by IR absorption continuum in OH···O^- bonds in diols,[387] NH···N^- bonds in diamines,[388] OH^+···O bonds in protonated dinitroso compounds,[389] and NH^+···N bonds in protonated dipyperidinyl alkanes.[390]

The IR spectra showed a polarizable proton that can move among several minima in protonated crown ethers,[391] consistent with polydentate complexing of the proton. However, the proton became fixed when it was complexed by an amine group.[378]

These observations are consistent with the polydentate complexing of the proton and the hydronium ion by crown ethers and polyethers in the gas phase. The IR evidence leaves open the possibility that in solution also a H_3O^+ ion or a protonated structure with several H_2O molecules and a proton, rather than the proton itself, is complexed by the ethers. This can add further polarizability to the proton.

Polarizable bonds where the ion can move between several minima are also observed in systems where metal ions such as Li^+, Na^+, or K^+ replace H^+ in the bond.[392−396]

8.1.3. Hydrogen-Bond Chains

Theoretical studies of proton shifts in multiple-minima IHB systems in $HCOO^-$···H_2O···H_2O··· HCOOH chains found increasing proton polarizability with increasing hydrogen bond chain length.[397−399] These systems are similar to the CH_3COO^-···H_2O··· H_2O···CH_3COOH clusters that were investigated in the gas phase experimentally and theoretically.[183]

Hydrogen bond chains can form also intramolecularly between several substituents on the same molecule. For example, evidence for large proton polarizabilities was found also in aromatic systems with mixed carboxylate and phenolic substituents.[378]

Large proton polarizabilities were observed in polylysine or poly(glutamic acid) + NaH_2PO_4 systems, due to hydrogen bonds of NH_3^+···$H_2PO_2^{2-}$··· $H_2PO_2^-$···NH_2 bridged systems. Another IHB chain system was demonstrated by IR continuum in deprotonated poly(hydroxy pentacene) derivatives and in substituted Mannich bases. In these systems, the protons may move in a three-well system or be localized in any of the minima, according to the relative pK_a values.[378]

The condensed-phase studies show large proton polarizabilities, indicating that the proton can move through hydrogen bond chains in water between end groups, even when the end groups have higher proton affinities than water. This is similar to gas-phase results that showed that the proton can remain on central solvent molecules even when they are between molecules with higher proton affinities.

8.2. Biological Systems

An important class of ionic hydrogen bonds was observed in amino acid polymers that model proteins. Evidence for homoconjugated NH^+···N bonds between amino acid side chains was shown in polyhistidine films,[400,401] for OH···O^- bonds in poly(glutamic acid), and for SH···S^- bonds in polycysteine films.[402,403] The IR absorbance continuum in poly(glutamic acid) is at a pH where half of the carboxylic groups are ionized. This is similar to the formation of vesicles in aliphatic carboxylic acid solutions, which also appear at pH values where mixtures of ionized and neutral groups are present.[404] Homoconjugated bonds were also observed in $(Asp\text{-}Asp)^-$, $(Cys\text{-}Cys)^-$, $(Glu\text{-}Glu)^-$, $(Tyr\text{-}Tyr)^-$, $(His\text{-}His)^+$, and $(Lys\text{-}Lys)^+$.

Also significant are heteroconjugated bonds with large proton polarizability that can conduct protons, which were observed between side-chain groups in Asp-His, Cys-Lys, Glu-His, Tyr-Arg, and Tyr-Lys hydrogen bonds.[405,406] In mixtures with hydrogen acceptors or donors, water can shift the proton-transfer equilibrium toward the ionized forms, and at high hydration, the solvent can dissociate these bonds.[405,406] These effects demonstrate the significance of partially hydrated regions in protein interior regions where ionic hydrogen bonds are needed, such as in membrane proton wires and at enzyme active sites. For example, bridged systems involving carboxylate ions, tyrosine residues, and a Schiff base are active in the proton pump of bacteriorhodopsin.[378,407,408]

The IR continuum also indicated a mobile polarizable proton in ATP synthetase, where the proton pathway starts with a carboxylic group of alanine and involves phenolic tyrosine, carboxylic glutamate, histidine, carboxylic lysine, and amine arginine groups and probably bridging structural water molecules along a 60 Å long path.[402,403,406,409]

Serine proteases, modeled in the gas phase, were also examined for IHB effects in solution. Both studies considered the transition state with a protonated His57 imidazole and with a network of IHB interactions involving the Asp102 COO^- and the tetrahedral oxyanion groups, according to the model of Warshel and Russell, who pointed out the energetic significance of the IHBs.[323] The gas-phase model suggested that the IHBs of the Asp102 shown in

Figure 54 contribute up to 65 kcal/mol to help proton transfer to the histidine and the IHBs of the tetrahedral oxyanion intermediate contribute up to 32 kcal/mol to help proton transfer from Ser195 to histidine by stabilizing the resulting oxyanion intermediate. In the solution study, difference spectra between trypsin and anhydrotrypsin supported the protonated imidazole intermediate and the existence of polarizable IHBs around it, resulting in an IR absorption continuum.[410]

In addition, IR spectroscopic studies also demonstrated an IHB network of two carboxylates and a H_2O molecule as providing the catalytic action in pepsin-like aspartate proteases.[411]

An IR continuum showed that the proton wire in the gramicidin channel involves a pathway of hydrogen bonds with high proton polarizability,[412] in agreement with the gas-phase ketone/water cluster models of this system.[242]

Ionic hydrogen bonds allow the proton to move with little barrier between several minima in a large volume, resulting in very large proton polarizabilities, which are largest along, or nearly along, the direction of the bond. Because of the large polarizability, the bonds are affected strongly by electric fields caused by the surrounding solvent, by other polarizable IHBs, and by ions in the solution.

As a result, the hydrogen bonds are controlled easily by neighboring charged groups. This allows biological systems to control the movement of charges by controlling IHB chains that conduct and pump the charges.

8.3. Ionic Hydrogen Bonds in Solids

Ionic hydrogen bonds affect crystal structure.[3] As in solution, the energy contributions of IHBs in solids cannot be isolated, but gas-phase data can give indications about their energy contributions. At least, the gas-phase bond strengths provide upper limits, because geometry and continuum effects decrease the strengths of ionic hydrogen bonds in solids. This section will note a few examples that show analogy in solids with gas-phase interactions in homodimers, heterodimers, anionic IHBs, carbon-based IHBs, and intramolecular bonds.

Homoconjugated $NH^+\cdots N$ bonds were investigated in aminopyridine and in quinuclidinium−quinuclidine crystals[413] and $OH\cdots O^-$ bonds in carboxylate−carboxylic acid crystals,[414] which showed intense continuum absorption with light polarized along the hydrogen bond. Heteroconjugated $OH\cdots N \leftrightarrow O^-\cdots H^+N$ bonds were shown by IR absorbance in phenol + amine crystals.[415]

Extensive networks of anionic IHBs were observed in crystals of deprotonated phthalic acid, C_6H_4-1,2-$(COOH)_2$, upon self-assembly of the anions into honeycomb superstructures held together by neutral $O-H\cdots O$ and charged $O-H\cdots O^-$ hydrogen bonds. The crystals also accommodate organometallic cations via charge-assisted $C-H^{\delta+}\cdots O^{\delta-}$ hydrogen bonds. The formation of IHBs helps the assembly of hydrogen-bonded networks, and IHBs to water molecules stabilize the crystal structures.[416]

Intramolecular hydrogen bonds in Schiff bases in the solid state were shown by crystallography and by ab initio calculations. Both neutral and ionic internal bonds were observed. In this case, geometry effects made the ionic $NH\cdots O^-$ bonds weaker than the neutral hydrogen bonds.[417]

These are just a few examples of charge-assisted ionic hydrogen bonds that were observed in solids. Recent reviews cover the roles of ionic hydrogen bonds in the solid state,[418] including $CH\cdots O$ bonds[419] and hydrogen bonds involving organometallics[420] and metal ions.[421] The roles of IHBs in crystal engineering were also reviewed recently.[3,422,423]

9. Relations between Clusters and Bulk Solvation

9.1. Relations between Small Clusters and Bulk Solvation

9.1.1. An Overview of the Thermochemical Results

Cluster studies yield insights into ion solvation. In particular, clusters reveal the energetics of strong interactions in inner solvent shells. Further clustering can continue until a macroscopic solvent builds up about the ion, and in principle, cluster energetics can lead to truly single-ion solvation energies. Accurate data are not available on large clusters, but various models bridge between small clusters and bulk solvation.[5,20,33,35,51,153,163,164,219,239,424−433]

An important finding, first noted by Kebarle, is that the *relative* solvation energies by the first four to six water molecules reproduce the *relative* bulk hydration energies of ions. Also, after these few solvent molecules the binding energies, $\Delta H^\circ_{n-1,n}$, approach the macroscopic condensation energy of water, −10.5 kcal/mol. These relations have been observed in many diverse systems, starting with monatomic alkali metal and halide ions, and were commented upon by Kebarle, Taft, Castleman, Klots, Hiraoka and their co-workers.[5,20,51,153,164,163,174,424−426,428] Similar findings were extended by Meot-Ner to diverse onium ions, including large ions with bulky substituents, and the data were used to analyze physical factors in ion solvation.[33,35,49]

A thermochemical analysis of these observations yields some unexpected results. It shows the following: (1) Solvation factors that should be physically independent vary nevertheless in an almost exactly compensating manner for ions of diverse structures. (2) The cumulative excess binding energies of large clusters (obtained from eq 40 below) from $n = 5$ to ∞ are a constant -70 ± 3 kcal/mol for diverse ions or (3) alternatively, cluster-based, truly single-ion solvation energies are less negative by 70 ± 3 kcal/mol than conventional solvation energies obtained from solutions of ion pairs. (4) Cluster data include strong IHB interactions, which allows decomposing the ion solvation energies into simple contributions by each protic and alkyl hydrogen.

The analysis will be summarized here.

Table 11. Relative Enthalpies of Protonation Bases B, Solvation and Clustering Energies of Bases B and Ions BH^+, and Relative Solvation Enthalpies of the Clusters $BH^+ \cdot 4H_2O$[a]

	$-\Delta H°_{prot,g}$ (B)[b] (PA(B))	$\delta\Delta H°_{prot,g}$ (B)[b]	$\delta\Delta H°_{prot,aq}$ (B)[c]	$\delta\Delta H°_{g\to aq}$ (B)[c]	$\delta\Delta H°_{g\to aq}$ (BH^+)[d]	$\delta\Delta H°_{0,4}$ ($BH^+ \cdot n(H_2O)$)[e]	$-\Delta H°_{g>aq}$ (BH^+)[f]	$-\Delta H°_{g>aq}$ (BH^+)[g] calcd	$-\Delta H°_{0,4}$ ($BH^+ \cdot n H_2O$)[e]	$-\Delta H°_{g\to aq}$ ($BH^+ \cdot 4H_2O$)[h]
					Protonated Alcohols, Ethers, and Ketones					
H_3O^+	165.0	39.0	12.6	−2.0	−28.4	−21.2	117.0	113.4	83.7	75.3
$MeOH_2^+$	180.3	23.7	13.1	−2.1	−12.7	−10.3	101.3	100.5	72.8	70.5
$EtOH_2^+$	185.6	18.4	12.1	−4.1	−10.4	−7.4	99.0	96.1	69.9	71.1
Me_2OH^+	189.0	15.0	11.9	−0.9	−4.0	0.6	92.6	93.2	61.8	72.8
Et_2OH^+	198.0	6.0	11.8	−2.6	3.2	6.7	85.4	85.7	55.8[i]	71.6
Me_2COH^+	194.0	10.0	11.8	−1.6	0.2	5.4	88.4	89.0	57.1	73.3
$C_6H_5CHOH^+$	199.3	4.7	14.4	−3.1	6.6	6.7	82.0	84.6	55.8[i]	68.2
$Me(c\text{-}C_6H_{11})COH^+$	201.1	2.9	14.2	−4.4	6.9	8.5	81.7	83.1	54.0[i]	69.7
$Me(C_6H_5)COH^+$	205.8	−1.8	17.3	−4.6	14.5	9.1	74.1	79.1	53.4	62.9
$Me(c\text{-}Pr)COH^+$	204.3	−0.3	11.1	−3.5	7.9	12.3	80.7	80.4	50.2	72.4
$(c\text{-}Pr)_2COH^+$	210.4	−6.4	12.0	−6.2	12.2	16.8	76.4	75.3	45.7	72.7
					Amide					
$Me(NMe_2)COH^+$	217.0	−13.0	14.9	−7.6	20.3	15.2	68.3	69.7	47.3	63.0
					Protonated Amines					
NH_4^+	204.0	(0)	(0)	(0)	(0)	(0)	88.6	90.6	62.5	68.1
$MeNH_3^+$	214.9	−10.9	−0.7	−2.6	7.6	8.5	81.0	81.2	54.0	69.0
$EtNH_3^+$	218.0	−14.0	−1.2	−4.5	8.3	5.9	80.3	78.5	51.9	70.4
$t\text{-}C_4H_9NH_3^+$	223.3	−19.3	−1.9	−5.6	11.8	13.3	76.8	74.0	49.2[i]	69.6
$c\text{-}C_6H_{11}NH_3^+$	223.3	−19.3	−1.9	−6.4	11.0	13.1	77.6	74.0	49.4[i]	70.2
$Me_2NH_2^+$	222.2	−18.2	0.5	−4.7	14.0	13.1	74.6	74.9	49.4	67.2
$Et_2NH_2^+$	227.6	−23.6	−0.3	−6.8	16.5	16.7	72.1	71.0	45.8[i]	68.3
Me_3NH^+	226.8	−22.8	3.7	−4.7	21.8	18.2	66.8	71.5	44.3	64.5
Et_3NH^+	234.7	−30.7	2.2	−8.2	24.7	25.4	63.4	64.2	37.3[i]	68.6
pyridineH$^+$	222.2	−18.0	7.7	−3.4	22.3	21.4	66.3	74.9	41.1	67.2
$C_6H_5NH_3^+$	210.9	−6.9	5.1	−4.4	7.6	5.3	81.0	84.6	57.2[i]	65.8
					Alkali Metal Ions					
Na^+							106.4[j]		76	72.4
K^+							88.0[j]		60	70.0
Rb^+							82.0[j]		53	71.0
Cs^+							76.0[j]		48	70.0

[a] All values in kcal/mol. Differential values for process X represent $\delta\Delta H°(X) = \Delta H°_x(B) - \Delta H°_x(NH_3)$. Negative values for B or BH^+ represent more exothermic processes than for NH_3 or NH_4^+, respectively. Absolute reference values were obtained as follows: $\Delta H°_{g\to aq}(NH_3) = -8.0$ kcal/mol;[444] $\Delta H°_{prot,g}(NH_3) = -204$ kcal/mol;[27] $\Delta H°_{prot,g}(NH_3) = -12.6$ kcal/mol; $\Delta H°_{g\to aq}(NH_4)^+ = -88.6$ kcal/mol, based on $\Delta H°_{g\to aq}(H^+) = -272$ kcal/mol,[425] which using $\Delta H°_{g\to aq}(H_2O) = -10.5$ kcal/mol and $PA(H_2O) = 165$ kcal/mol yields $\Delta H°_{g\to aq}(H_3O^+) = -117.0$ kcal/mol; $\Delta H°_{0,4}(NH_4^+) = -62.5$ kcal/mol[34] yields $\Delta H°_{g\to aq}(NH_4^+ \cdot 4H_2O) = -68.1$ kcal/mol. A recent value of $\Delta H°_{g\to aq}BH^+) = -274.8$ kcal/mol[430−433] will make the numbers in column 8 for $-\Delta H°_{g\to aq}(BH^+)$ and in column 11 for $-\Delta H°_{g\to aq}(BH^+ \cdot 4H_2O)$ larger by 2.8 kcal/mol. [b] From data of ref 27. [c] Reference 20. [d] From data of columns 2−4 and eq 37. [e] Based on experimental cluster energetics $\Delta H°_{1,4}(BH^+ \cdot nH_2O)$ unless noted otherwise.[33] The cumulative experimental error of the four hydration steps is estimated as ±3 kcal/mol. [f] Calculated from the relative solvation energies in column 6, using $\Delta H°_{g\to aq}(NH_4^+) = -88.6$ kcal/mol as absolute reference value. [g] Calculated from the correlations $-\Delta H°_{g\to aq}(BH^+) = 252-0.84(PA(B))$ for alkyloxonium and $262-0.84(PA(B))$ for alkylammonium ions. [h] Solvation energies of the $BH^+ \cdot 4H_2O$ clusters, calculated from eq 38, using conventional $\Delta H°_{g\to aq}(BH^+)$ values from column 8 and cluster binding energies $\Delta H°_{0,4}(BH^+ \cdot nH_2O)$ from column 10. These values are also equal to the sum of the excess cluster ion binding energies $\Delta H°_{5,N(exc)}$ from $n = 5$ to ∞ and to the difference between the conventional and cluster-based solvation energies. [i] Calculated cluster binding energies from PA correlations in eqs 18 and 19. [j] Based on Wagman et al. *J. Phys. Chem. Ref. Data* **1982**, *11* (Suppl 2), and on $\Delta H°_{g\to aq}(H^+) = -272$ kcal/mol.[425]

9.1.2. Relative Ion Solvation Energies in Small Clusters and in Solution

The relative ion solvation energies are calculated from a thermochemical cycle that leads to eq 37.

$$\begin{array}{ccc} B_1H^+_g + B_{2\,g} & \text{->} & B_2H^+_g + B_{1\,g} \\ \downarrow & & \downarrow \\ B_1H^+_{aq} + B_{2\,aq} & \text{->} & B_2H^+_{aq} + B_{1\,aq} \end{array}$$

$$\delta\Delta H°_{g\text{->}aq}(BH^+) = \Delta H°_{g\text{->}aq}(B_2H^+) - \Delta H°_{g\text{->}aq}(B_1H^+) = \delta\Delta H°_{g\text{->}aq}(B) + \delta\Delta H°_{prot(aq)} - \delta\Delta H°_{prot(g)} \quad (37)$$

Here the $\Delta H°_{prot}$ values are protonation enthalpies, and the differential values $\delta\Delta H°$ represent the differences between the respective values for two ions or neutrals. The aqueous values refer to infinitely dilute solutions, and the gas-phase species are in equilibrium with these solutions. Importantly, the terms on the RHS of eq 37 do not include ion solvation energies. Therefore, the *relative* ion solvation energies can be derived from well-established enthalpies of solvation of neutral bases and their relative enthalpies of protonation in the gas phase and solution. These values are independent of *absolute* ion solvation energies derived by indirect methods.[434,435]

The relative bulk solvation enthalpies from eq 37 can be compared with the relative partial solvation enthalpies in small clusters. The results show that the relative 4-fold solvation energies reproduce the relative bulk solvation energies (within the experimental uncertainty of ±3 kcal/mol) for diverse onium ions and even alkali metal ions (Table 11, columns 6

Table 12. Solvation Factors in the Hydration of Ions[a]

			$-\Delta H°$ solvation factors					$-\Delta H°$ factors per hydrogen	
	ionic radii[b] (Å)	$-\Delta H°_{g>aq}$ (BH^+)[c]	dielectric[d]	cavity[e]	total continuum[f]	hydrophobic[g]	IHB[h]	hydrophobic/ $n(CH)$[i]	IHB/ $n(XH^+)$[j]
Protonated Alcohols, Ethers, and Ketones									
H_3O^+	1.74	117.0	72.8	−6.5	66.3	(4.9)[k]	45.8		15.2
$MeOH_2^+$	2.08	101.3	62.6	−9.2	53.4	9.9	38.0	3.3	19.0
$EtOH_2^+$	2.35	99.0	56.5	−11.8	44.7	14.3	40.0	2.9	20.0
Me_2OH^+	2.36	92.6	56.2	−11.9	44.3	21.6	26.8	3.6	26.8
Et_2OH^+	2.77	85.4	49.2	−16.4	32.8	27.1	25.6	2.7	25.6
Me_2COH^+	2.48	88.4	53.8	−13.2	40.6	24.0	23.9	4.0	23.9
$C_6H_5CHOH^+$	2.92	82.0	46.8	−18.3	28.5	26.4	27.2	4.4	27.2
$Me(c\text{-}C_6H_{11})COH^+$	3.20	81.7	43.4	−21.8	21.6	33.0	27.2	2.4	27.2
$Me(C_6H_5)COH^+$	3.07	74.1	45.0	−20.1	24.9	23.6	25.7	2.9	25.7
$Me(c\text{-}Pr)COH^+$	2.75	80.7	49.4	−16.2	33.2	27.6	20.0	3.4	20.0
$(c\text{-}Pr)_2COH^+$	2.97	76.4	46.3	−18.8	27.5	31.4	17.6	3.1	17.6
Amide									
$Me(NMe_2)\text{-}COH^+$	2.81	68.3	48.4	−16.9	31.5	19.2	17.7	2.1	17.7
Protonated Amines									
NH_4^+	1.81	88.6	70.4	−7.0	63.4	0.0	25.2		6.3
$MeNH_3^+$	2.16	81.0	60.6	−10.0	50.6	4.9	25.6	1.6	8.5
$EtNH_3^+$	2.41	80.3	55.2	−12.4	42.8	10.0	27.6	2.0	9.2
$t\text{-}C_4H_9NH_3^+$	2.81	76.8	48.6	−16.8	31.8	15.7	29.4	1.7	9.8
$c\text{-}C_6H_{11}NH_3^+$	3.02	77.6	45.7	−19.4	26.3	20.1	31.3	1.8	10.4
$Me_2NH_2^+$	2.42	74.6	55.0	−12.6	42.4	12.0	20.2	2.0	10.1
$Et_2NH_2^+$	2.82	72.1	48.3	−17.1	31.2	19.8	21.1	2.0	10.6
Me_3NH^+	2.64	66.8	51.2	−14.8	36.4	17.9	12.6	2.0	12.6
Et_3NH^+	3.12	63.4	44.4	−20.8	23.6	30.6	9.8	2.0	9.8
$pyridineH^+$	2.72	66.3	49.9	−15.8	34.1	22.0	10.3	4.4	10.3
$C_6H_5NH_3^+$	2.87	81.0	47.7	−17.6	30.1	12.9	38.1	2.6	12.7
Alkali Metal Ions									
K^+	1.33	88.0[l]	91.0	−3.8	87.2		0.8[m]		
Rb^+	1.47	82.0[l]	83.9	−4.6	79.3		2.7[m]		
Cs^+	1.67	76.0[l]	75.4	−5.9	69.5		6.5[m]		

[a] All values in kcal/mol. Data derived from cluster-based analysis of solvation factors, see ref 35 and text. [b] Ionic radii from ref 35 based on ionic volumes from ref 445. [c] Conventional single-ion solvation energies from Table 11. [d] Dielectric charging of the solvent cavity, calculated in ref 35 using a double-shell model of ref 445. [e] Surface tension energy of the cavity created to accommodate a spherical ion.[35] [f] Sum of dielectric and cavity terms in columns 4 and 5, respectively. [g] Hydrophobic solvation of the alkyl substituents obtained from eq 43 using the solvation energy of the clusters, $\Delta H°_{g\rightarrow aq}(BH^+\cdot 4H_2O)$, in Table 11 and the parameters for $\Delta H°_{dielectric}$, $\Delta H°_{cavity}$ for the $BH^+\cdot 4H_2O$ clusters used in refs 33 and 35. The values of $\Delta H°_{hydrophobic}$ are somewhat different from those in refs 33 and 35 because the new PA values of ref 27 and $\Delta H°_{residual\ hydrogen\ bonds}$ were used in the present calculations. Using the reference value $\Delta H°_{g\rightarrow aq}(H^+) = -274.8$ kcal/mol,[430−433] the values of $-\Delta H°_{g\rightarrow aq}(BH^+)$ in column 3 and the values of $-\Delta H°_{g\rightarrow aq}$(hydrophobic) in column 7 will increase by 2.8 kcal/mol. [h] Enthalpy of ionic hydrogen bonding. [i] Hydrophobic solvation energy per alkyl hydrogen. [j] Ionic hydrogen bond energy per protic hydrogen. [k] The calculated "$-\Delta H°_{hydrophobic}$" for H_3O^+ reflects, rather, significant IHB interactions past the first shell for this ion. [l] See footnote *j* in Table 11. [m] An analysis similar to that for the onium ions applied to metal ions gives small values for this term, consistent with the fact that $\Delta H°_{hydrophobic}$ is absent in the solvation of metal ions. References 430, 431,432, and 433.

and 7). Using the solvation enthalpies of larger clusters gives similar results, since the relative cluster binding enthalpies do not change much after $n = 4$.

For example, the *relative* clustering energies, $\delta\Delta H°_{0,4}(BH^+\cdot nH_2O)$, reproduce the *relative* bulk ion solvation energies, $\delta\Delta H°_{g\rightarrow aq}(BH^+)$, of ions as diverse as K^+, Rb^+, Cs^+, NH_4^+, $MeOH_2^+$, $C_6H_5CHOH^+$, $MeNH_3^+$, $c\text{-}C_6H_{11}NH_3^+$, Me_3NH^+, and Et_3NH^+ (Table 11). The absolute bulk hydration energies of these ions vary over 35 kcal/mol, yet the variation over this large range is reproduced by the binding energies of only four H_2O molecules.

These results have unexpected structural implications. In the clusters, the first water molecules solvate only the protonated functional groups. The alkyl substituents of varying sizes and structures are not solvated by four and even by up to 20 H_2O molecules.[358] The enthalpies of the cavity, dielectric, and hydrophobic terms in bulk solvation vary by up to 30 kcal/mol among the ions in Table 12. These factors are absent in the clusters, but the *relative* cluster binding energies nevertheless reproduce the *relative* bulk solvation enthalpies. This means that the factors that are added only in bulk solution vary in an almost exactly canceling manner for the diverse ions in Table 12. This is remarkable because these solvation terms result from independent physical forces.

Absolute solvation energies can be calculated from the relative values, using the single-ion solvation energy of a reference ion. The reference values used below are $\Delta H°_{g\rightarrow aq}(H^+) = -272$ kcal/mol or the value for the reference ion, $\Delta\Delta H°_{g\rightarrow aq}(NH_4^+) = -88.6$ kcal/mol (See footnotes to Table 11 for data sources). The single-ion solvation energies based on these values, which are obtained conventionally from ion pairs, are denoted as $\Delta H°_{g\rightarrow aq}(BH^+)_{conventional}$ below.

9.1.3. Thermochemical Relations between Clusters and Bulk Solvation

Solvation in clusters and in solution can be related through a thermochemical cycle.

$$\begin{array}{ccc} BH^+_g + nH_2O_g & \text{->} & (BH^+\cdot nH_2O)_g \\ \downarrow \quad \downarrow & & \downarrow \\ BH^+_{aq} + nH_2O_{aq} & = & (BH^+\cdot nH_2O)_{aq} \end{array}$$

$$\Delta H^\circ_{g\text{->}aq}(BH^+) = \Delta H^\circ_{0,n} - n\Delta H^\circ_{cond}(H_2O) + \Delta H^\circ_{g\text{->}aq}(BH^+\cdot nH_2O) \quad (38)$$

Here $\Delta H^\circ_{0,n}$ is the sum of the first n cluster binding energies and $\Delta H^\circ_{g\rightarrow aq}(BH^+\cdot nH_2O)$ is the energy of transferring the $BH^+\cdot nH_2O$ cluster to solution. Equation 38 can be used in two alternative ways. If the ion solvation energy $\Delta H^\circ_{g\rightarrow aq}(BH^+)$ is known (for example, assigned the conventional value $\Delta H^\circ_{g\rightarrow aq}(BH^+)_{conventional}$), then eq 38 yields the cumulative binding energies of clusters ($\Delta H^\circ_{0,n}$). Alternatively, if the cluster binding energies $\Delta H^\circ_{0,n}$ are known up to a large enough N (see below), then $\Delta H^\circ_{g\rightarrow aq}(BH^+)$ in eq 38 yields the cluster-based single-ion solvation energy $\Delta H^\circ_{g\rightarrow aq}(BH^+)_{cluster\text{-}based}$.

For either application, stepwise solvation can be continued until step N where the binding energies $\Delta H^\circ_{n-1,n}$ become equal to the bulk condensation energy $\Delta H^\circ_{condensation}(H_2O)$. After this step, eq 38 simplifies to eq 39 as follows. After step N an infinite number of solvent molecules can be added without further energy change since in each further step, $[\Delta H^\circ_{n-1,n} - \delta H^\circ_{cond}(H_2O)]$ cancels. This infinite further stepwise solvation is equivalent to transferring the $BH^+\cdot NH_2O$ cluster, which is in effect an infinitely dilute single-ion solution, to bulk solution. The last term in eq 38, that is, $\Delta H^\circ_{g\rightarrow aq}(BH^+\cdot NH_2O)$, then vanishes, and eq 38 simplifies to eq 39.

$$\Delta H^\circ_{g\rightarrow aq}(BH^+) = \Delta H^\circ_{0,N} - N\Delta H^\circ_{cond}(H_2O) \quad (39)$$

Note that each term $(\Delta H^\circ_{n-1,n} - \Delta H^\circ_{cond}(H_2O))$ represents the excess cluster ion binding energy $\Delta H^\circ_{n-1,n(excess)}$ of the nth solvent molecule versus the macroscopic condensation energy of water. The cluster-based solvation energy $\Delta H^\circ_{g\rightarrow aq}(BH^+))_{cluster\text{-}based}$ calculated from eq 39 is then simply the sum of the excess cluster ion binding energies through step N.

Equation 39 has two alternative applications, depending on assumptions about large clusters. We shall now consider these applications.

9.2. Binding Energies of Large Clusters

For this application, it is convenient to decompose the clustering sequence to small clusters up to size s and to large clusters from $s + 1$ to N. Equation 39 can then be rearranged to eq 40 to calculate the cumulative excess binding energies of large clusters.

$$[\Delta H^\circ_{s+1,N} - (N - s)\Delta H^\circ_{cond}(H_2O)] = \Delta H^\circ_{g\rightarrow aq}(BH^+) - [\Delta H^\circ_{0,s} - s\Delta H^\circ_{cond}(H_2O)] \quad (40)$$

Here $\Delta H^\circ_{s+1,N}$ represents the sum of the cluster binding energies from the $(s + 1)$th to the Nth water molecule. For small clusters, we may use, for example, $s = 4$ since data are usually available to this size and since the experimental binding energies after $n = 4$ approach $\Delta H^\circ_{cond}(H_2O) = -10.5$ kcal/mol (Table 4). For $\Delta H^\circ_{g\rightarrow aq}(BH^+)$, we may use here the conventional single-ion solvation energies. In conjunction with the binding energies of the $n = 1-4$ clusters (Table 11, columns 8 and 10), eq 40 yields the cumulative excess cluster ion binding energies from $n = 5$ to infinity. The results (Table 11, column 11) show that the cumulative excess cluster ion binding energies are -70 ± 3 kcal/mol for diverse ions.

In fact, various theories, for example, the liquid drop model, predict that the binding energies $\Delta H^\circ_{n-1,n}(BH^+\cdot nH_2O)$ should exceed the bulk condensation energy, up to large cluster sizes.[238] The resulting cumulative excess energy of -70 kcal/mol may build up in many steps, for example, as an excess binding energy of 0.1 kcal/mol in hundreds of steps.

9.3. Cluster-Based Ion Solvation Energies

The preceding section, using the conventional solvation energies $\Delta H^\circ_{g\rightarrow aq}(BH^+)_{conventional}$ in eqs 39 and 40, yielded significant cumulative excess binding energies for large clusters. However, the present data suggests that these excess cluster ion binding energies may be negligible. In fact, the experimental binding energies approach the macroscopic $\Delta H^\circ_{condensation}(H_2O)$ already for $n = 4$ in most hydration sequences (Table 4) and remain constant near this value up to $n = 26$ where the data are available (Figure 25). It is reasonable that once the limiting macroscopic binding energy is reached, it will remain constant until macroscopic solvation. This is also supported structurally in Figure 24, as the charge on the hydrogens of the first four H_2O molecules become neutral-like and liquid-like water structures start to form in clusters after $n = 5$.

Accordingly, neutral-like macroscopic binding energies may apply after $n = 4-6$. With this assumption we can use $N = 4$ in eq 39 to calculate the cluster-based single-ion solvation energies $\Delta H^\circ_{g\rightarrow aq}(BH^+)_{cluster\text{-}based}$ using the experimental cluster data.

As eq 39 shows, for $N = 4$, the calculated $-\Delta H^\circ_{g\rightarrow aq}(BH^+)_{cluster\text{-}based}$ is equal to the binding energies $-\Delta H^\circ_{0,4}$ plus 42 kcal/mol. These cluster-based values are smaller than the conventional values by 70 ± 3 kcal/mol, that is, $\Delta H^\circ_{g\rightarrow aq}(BH^+)_{conventional} - \Delta H^\circ_{g\rightarrow aq}(BH^+)_{cluster\text{-}based} = \Delta H^\circ_{g\rightarrow aq}(BH^+\cdot 4H_2O)$ is a constant -70 ± 3 kcal/mol for diverse ions (Table 11, last column). The difference between the conventional and cluster-based solvation energies is illustrated also in Figure 56.

Note that the clusters are truly single-ion solutions, while the classical single ion solvation energies are derived from solutions of ion pairs. The comparison would then imply that counterion interactions contribute -70 ± 3 kcal/mol to the solvation energies of ions, even in the dilute solutions from which the conventional values were derived by various methods.[425,430-433]

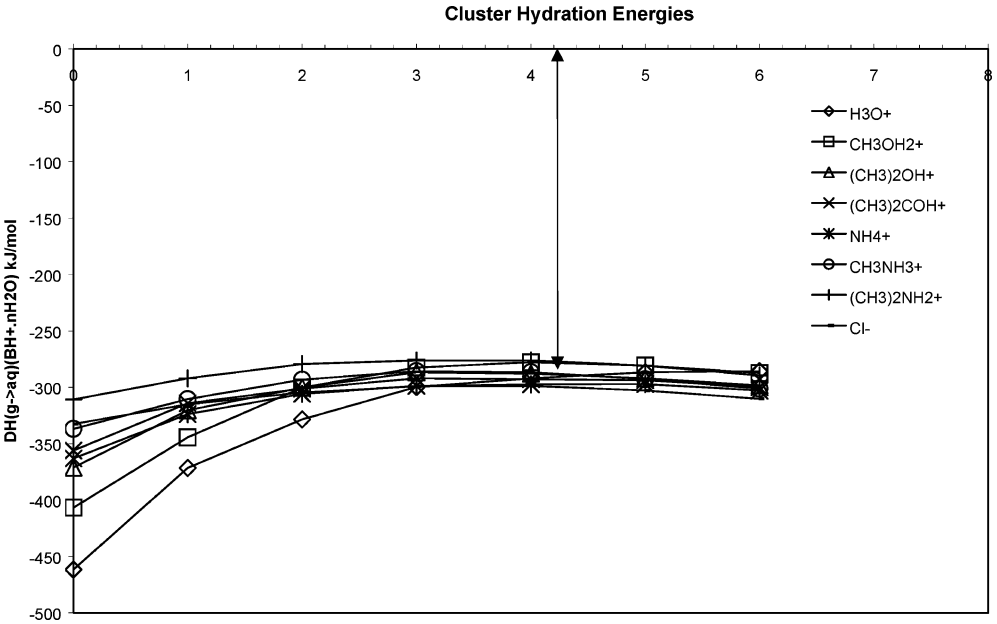

Figure 56. The difference between conventional and cluster-based ion solvation energies as a function of cluster size n. In eq 38, if $\Delta H^\circ_{g\rightarrow aq}(BH^+)$ on the LHS is assigned the conventional value, and if $\Delta H^\circ_{g\rightarrow aq}(BH^+)_{cluster\text{-}based}$ is assigned as $(\Delta H^\circ_{0,n} - n\Delta H^\circ_{condensation}(H_2O))$, then the cluster solvation energy $\Delta H^\circ_{g\rightarrow aq}(BH^+\cdot nH_2O)$ is equal to the difference $[\Delta H^\circ_{g\rightarrow aq}(BH^+)_{conventional} - \Delta H^\circ_{g\rightarrow aq}(BH^+)_{cluster\text{-}based}]$. If the cluster-based solvation energies approached the conventional values with increasing n, then $\Delta H^\circ_{g\rightarrow aq}(BH^+\cdot nH_2O)$ should approach zero with increasing n. However, the plots approach -70 ± 3 kcal/mol (-292 ± 12 kJ/mol), reflecting the difference between conventional and cluster-based ion solvation energies.

Finally, cycle 38 was used by the present author and others.[33,35,194,225] Other authors used an alternative cycle that starts with BH^+ and nH_2O molecules.[5,239,429] The water molecules are clustered stepwise to the ion, or clustered to each other to give $(H_2O)_n$ and BH^+ is then transferred to the water cluster. Both paths give a $BH^+(H_2O)_n$ cluster that approaches a single-ion bulk solution with increasing n. The cycle gives eq 41.

$$\Delta H^\circ_{g\rightarrow aq}(BH^+)_{cluster\text{-}based} = \Delta H^\circ_{0,n}(BH^+\cdot nH_2O) - \Delta H^\circ_{0,n-1}(H_2O\cdot nH_2O) \quad (41)$$

Here the summation is carried to a size n where the ionic and neutral cluster binding energies become equal. If $n = 4$ is used as above, then this model gives cluster-based ion solvation energies larger by about 20 kcal/mol than eq 39 (depending on the binding energies assigned to neutral water clusters). These values are still smaller by about 45 kcal/mol than the conventional single-ion solvation energies.

In summary, the cluster data quantifies the cumulative excess cluster ion binding energies for large clusters ($n = 5$ to infinity) as 70 kcal/mol for diverse ions; or alternatively, the cluster data yield single-ion solvation energies that are smaller by 70 kcal/mol than the conventional values. The correct interpretation can be decided experimentally by accurate binding energies of large clusters. Either way, the results can be significant for ionic nucleation and for electrolyte theory.

9.3.1. Predicting Hydration Energies from Proton Affinities

We observed that the 4-fold hydration energies, $\Delta H^\circ_{0,4}(BH^+\cdot nH_2O)$, reproduce the relative bulk solvation energies, that is, the difference between the clustering and bulk solvation energies are constant, for diverse ions. We also observed above that $\Delta H^\circ_{0,4}$ can be predicted from the first solvation energy, $\Delta H^\circ_{0,1}$, which in turn can be predicted from the proton affinities, PA(B) − PA(H_2O). When these relations are combined, the bulk hydration energies of diverse ions can be predicted from PA(B) by the simple relation $-\Delta H^\circ_{g\rightarrow aq}(BH^+) = a - 0.84(PA(B))$ kcal/mol, with $a = 252$ kcal/mol for alkyloxonium ions and 262 kcal/mol for alkylammonium ions[35] (eq 20 above).

The unexpected canceling variation of solvation terms leads to the relation between the clustering energies, $\Delta H^\circ_{0,4}(BH^+\cdot nH_2O)$, and the bulk solvation energies. It is this effect therefore that also leads to the simple relations between gas-phase proton affinities and bulk hydration enthalpies. This relation is surprising since ion hydration involves complex forces. A relation between proton affinities and solvation energies was noted also by Hiraoka.[429]

Comparing columns 8 and 9 in Table 11 shows that the experimental solvation energies are reproduced by these simple relations for a wide range of ions with a standard deviation of ±2 kcal/mol, well within the experimental accuracy of the PA and solvation energy data.

Deviations from these relations are reasonable structurally. These deviations occur for ions that contain aromatic groups, $C_6H_5CHOH^+$, $Me(C_6H_5)$-COH^+, and pyridineH^+. The hydration energies of the phenyl-substituted ions are smaller by 2−3 kcal/mol and that of pyridineH^+ by 8.6 kcal/mol than predicted from the PAs. These solvation energies may be decreased compared with aliphatic compounds because of the inefficient hydrophobic solvation of the aromatic groups, which have few CH donors.

9.4. Cluster-Based Analysis of Solvation Factors

9.4.1. A Cluster-Based Procedure to Calculate Solvation Factors

Table 11, column 9 shows that the conventional *absolute* hydration energies vary by over 27 kcal/mol among the alkyloxonium and by 17 kcal/mol among the alkylammonium ions listed.

Assuming the conventional single-ion solvation energies, the cluster data can be used to decompose ion hydration energies to physical factors. Usually, it is hard to quantify the strong IHB interactions in the inner solvent shell. However, this can be overcome by a cluster-based analysis, since the strong inner-shell IHBs are included mostly in the first four H_2O molecules. The analysis yields physically reasonable solvation terms for the contributions of the protic and alkyl hydrogens of the ions (Table 12). In this manner, the cluster-based analysis decomposes the complex factors of ion solvation into a few physically reasonable terms.[33,35]

The procedure can be summarized as follows.

1. The solvation energies, $\Delta H^\circ_{g\rightarrow aq}(BH^+\cdot 4H_2O)$, of the clusters, obtained from eq 38, include the strong IHB interactions in the inner shell. The dielectric and solvent cavity terms for solvating the clusters are calculated from continuum models. The remaining solvation energy yields $\Delta H^\circ_{hydrophobic}$, the solvation energies of the alkyl groups.

2. The solvation energies, $\Delta H^\circ_{g\rightarrow aq}(BH^+)$, of the ions are then used to calculate the solvation factors of the bare nonclustered ions themselves. The dielectric and solvent cavity terms are calculated by continuum models. The hydrophobic terms are assigned from step 1. The remaining solvation energy yields ΔH°_{IHB}, the ionic hydrogen bond energies between the protic hydrogens of the protonated functional group and water molecules in the inner solvent shell.

The procedure and results are described in more detail in the next section. The solvation of ions involves the energy terms in eq 42,

$$\Delta H^\circ_{g\rightarrow aq}(BH^+) = \Delta H^\circ_{cavity} + \Delta H^\circ_{dielectric} + \Delta H^\circ_{IHB} + \Delta H^\circ_{hydrophobic} \quad (42)$$

the energy required to form a cavity to accommodate the ion (ΔH°_{cavity}), the dielectric charging of the solvent about the ion ($\Delta H^\circ_{dielectric}$), hydrogen bonds of the ions to the inner-shell water molecules (ΔH°_{IHB}), in the solvation of the clusters, also the neutral-like residual hydrogen bonds of the inner-shell water molecules to the rest of the solvent (ΔH°_{RHB}), and hydrophobic solvation of the alkyl groups ($\Delta H^\circ_{hydrophobic}$).

9.4.2. Solvation Factors of the ($BH^+\cdot 4H_2O$) Clusters

Equation 43 is used:

$$\Delta H^\circ_{g\rightarrow aq}(BH^+\cdot 4H_2O) = \Delta H^\circ_{cavity}(BH^+\cdot 4H_2O) + \Delta H^\circ_{dielectric}(BH^+\cdot 4H_2O) + \Delta H^\circ_{hydrophobic} + \Delta H^\circ_{RHB} \quad (43)$$

The energies for creating and charging a cavity to accommodate the cluster $BH^+\cdot 4H_2O$ are calculated from continuum models. The term ΔH°_{RHB} is the energy of the $n + 4$ (for an ion BH^+ with n protic hydrogens) residual neutral-like hydrogen bonds of the four inner-shell solvent molecules to the surrounding water molecules. These bonds should be neutral-like since the cluster bonding energies become equal to the bulk condensation energy of neutral water after clustering by four H_2O molecules. The present analysis used $\Delta H^\circ_{RHB} = \Delta H^\circ_{condensation}(H_2O)/2 = -5.25$ kcal/mol. With use of the cluster solvation energies from eq 38 and these calculated terms, the remaining energy is assigned to $\Delta H^\circ_{hydrophobic}$, the solvation of the alkyl groups.

9.4.3. Solvation Factors of the BH^+ Ions

Equation 42 is used. The energies for creating and charging a cavity to accommodate the ion BH^+ are calculated from continuum models. It is assumed that $\Delta H^\circ_{hydrophobic}(BH^+)$ is equal to $\Delta H^\circ_{hydrophobic}(BH^+\cdot 4H_2O)$ found in the preceding section, since the hydrophobic solvation is not affected significantly by the hydration of the protonated functional group in the clusters. The remaining solvation energy is assigned to ΔH°_{IHB}, the contribution of strong ionic hydrogen bonds to the solvation energy.

The results of the analysis are presented in Table 12. The analysis yields solvation factors that vary reasonably with ion structure.

Continuum Terms. The total calculated continuum terms (cavity + dielectric charging, Table 12, column 6) change strongly with ion size, from −66.3 kcal/mol for H_3O^+ to −21.6 kcal/mol for $Me(C_6H_{11})COH^+$ and from −63.4 kcal/mol for NH_4^+ to −23.6 kcal/mol for Et_3NH^+. Both the cavity and dielectric terms become less favorable for large ions, as the energy to create a cavity surface becomes more positive and the dielectric charging becomes less negative with increasing ionic size. These terms are the main factors that decrease the solvation energies of large ions.

Hydrophobic Solvation. The analysis yields hydrophobic solvation terms that vary reasonably with the number of alkyl hydrogens (Table 12, column 7). It is a small factor for the $MeOH_2^+$ and $MeNH_3^+$ ions that have small alkyl substituents (−9.9 and −4.8 kcal/mol, respectively), and it is similar for these ions that both have three alkyl hydrogens. It becomes a major term for ions such as $Me(C_6H_{11})COH^+$ (−33.0 kcal/mol) and Et_3NH^+ (−30.6 kcal/mol). For the ions in Table 12, the contribution of each alkyl hydrogen is -3.5 ± 1 kcal/mol per hydrogen for most oxonium ions and -1.8 ± 0.2 kcal/mol per alkyl hydrogen for most ammonium ions (Table 12, column 9). The hydrophobic solvation per CH hydrogen decreases somewhat in the larger ions as the charge is more dispersed and each CH hydrogens carries less positive charge. Aromatic CH hydrogens appear to be solvated more strongly, as the charge is more concentrated on each hydrogen on the hydrogen-deficient substituents. However, there are fewer CH donors on aromatic substituents, and this decreases somewhat the total hydrophobic solvation energies of ions with aromatic substituents.

$$\begin{aligned}
\Delta H^\circ_{\text{hydrophobic}} = \quad & (-3.5 \pm 1)n_{\text{CH}}\ \text{kcal/mol} && \text{alkyloxonium ions} \\
& (-2.5 \pm 0.3)n_{\text{CH}}\ \text{kcal/mol} && \text{alkylammonium ions} \\
\Delta H^\circ_{\text{IHB}} = \quad & (-25 \pm 2)n_{\text{OH}^+}\ \text{kcal/mol} && \text{monoprotonic oxonium ions} \\
& (-19 \pm 1)n_{\text{OH}^+}\ \text{kcal/mol} && \text{polyprotonic oxonium ions} \\
& (-10 \pm 2)n_{\text{NH}^+}\ \text{kcal/mol} && \text{alkylammonium ions}
\end{aligned} \tag{44}$$

Ionic Hydrogen Bonds. The calculated IHB terms vary consistently with the number of protic hydrogens (Table 12, column 8), contributing −45.8 kcal/mol for H_3O^+ with three protic hydrogens, −39 ± 1 kcal/mol for oxonium ions with two, and −25 ± 2 kcal/mol for most oxonium ions with one protic hydrogen. Similarly, the IHB terms decrease regularly with the number of protic hydrogens in the ammonium ions, where it is a major term for NH_4^+ (−25.2 kcal/mol) but only a minor term for monoprotonic ions such as Et_3NH^+ (−9.8 kcal/mol). In general, the IHB term is larger for oxonium ions than for comparable alkylammonium ions as expected on the basis of ΔPA correlations. When the analysis is applied to non-hydrogen-bonding alkali metal ions, it indeed yields negligible terms for the IHB terms (Table 12, column 8).

The results show that each alkyl or protic hydrogen makes an approximately constant contribution to ion solvation (Table 12, column 10). The intermolecular forces in ion solvation are therefore decomposed to simple contributions per alkyl or protic hydrogen. The hydrogen bonding energies are described by eq 44, where n_{CH} is the number of alkyl hydrogens and n_{OH^+} and n_{NH^+} are the numbers of protic hydrogens of alkyloxonium and alkylammonium ions. The weaker IHB bonds of the ammonium vs oxonium ions to the inner H_2O molecules are consistent with the ΔPA correlations discussed above.

Table 12 shows that in the hydration of ions with several protons, such as H_3O^+, most polyprotonic oxonium ions, and NH_4^+ and RNH_3^+ ions, IHB is the dominant intermolecular force, while in larger ions with less protic and more CH hydrogens, the hydrophobic terms are larger. These results are reasonable structurally.

The fact that the output of the analysis is reasonable structurally is encouraging, since no structural information was input. The analysis is based purely on the experimental binding energies of clusters and ion solvation energies and the continuum models for the cavity and dielectric terms based on ion radius alone. Nevertheless, the results correlate well with structure, and even deviations such as those observed for aromatics are structurally plausible.

Finally, note that energy factors such as the solvation factors calculated here, covalent versus electrostatic components of bond energies, or inductive and resonance effects are purely theoretical. The isolated energy terms do not exist physically and are not subject to experimental measurement. Nevertheless, the analysis is useful for understanding ion solvation, because it decomposes the complex intermolecular forces into a few simple, physically reasonable terms. The results can help in estimating the solvation energies of further onium ions.

10. Conclusions and Outlook

Ionic hydrogen bonds are important in many natural and industrial processes. Mass spectrometric cluster studies have provided a quantitative understanding of these forces.

Correlations between Bond Strengths and the Relative Acidities and Basicities of the Components. The first basic findings were correlations between IHB bond energies and the relative basicities or acidities of the components. These correlations reflect the efficiency of sharing the bonding proton. The relations apply to dimers with various components and extend to larger clusters and even to bulk solvation. The correlations provide means to estimate IHB energies in more complex systems, such as in biomolecules.

Unconventional, Internal, and Polydentate Bonds. Special cases occur with carbon-based IHB donors and receptors. Also, polyatomic molecules exhibit internal and polydentate IHB complexes with energetics that correlate with structure in terms geometry, bond strain, and multiple IHB formation. Thermochemical information was obtained also about the interactions between internal and external solvation and solvent bridges.

Hydrogen-Bond Networks. In larger clusters, unlimited hydrogen-bond networks may form, or limited networks surrounded by alkyl-blocked components. In the blocked cluster, the proton can be located in a strongly hydrogen-bonding core, even when it is surrounded by blocked components that are stronger bases. This has important consequences in biological membrane transport.

Effects on Acidities and Basicities. Gas-phase studies revealed the intrinsic molecular acidities and basicities of molecules. Comparison with solution showed that solvent effects can greatly compress or reverse the relative acidities and basicities. Cluster studies show the stepwise development of the solvent effects and demonstrate that up to 80% of the effects can be due to the inner-shell solvent molecules.

Biomolecules and the Condensed Phase. The principal trends observed in model organic ions—ΔPA correlations, internal and polydentate bonds, solvent bridges—have been found more recently to be ubiquitous and crucial in biomolecules. Also, the contributions of IHBs to enzyme energetics, membrane transport, and molecular recognition can be assessed quantitatively from cluster models.

More recently, spectroscopic and ion mobility studies have confirmed many structural conclusions from thermochemistry. Similar IHB effects are observed also in solution and in crystals.

Partial and Bulk Solvation. The comparison of ion solvation in small clusters and in bulk solution yields unexpected results. Partial solvation of the

protonated functional groups by as few as four to six water molecules reproduces the relative bulk solvation energies. This result indicates an exactly canceling variation of cavity, dielectric, and hydrophobic solvation factors among diverse ions, although these factors should be physically independent. This effect allows prediction of bulk ion solvation energies based only on gas-phase proton affinities.

Large Clusters and Single Ion Solvation Energies. The data on small clusters, combined with conventional bulk solvation energies, yield quantitative information on the cumulative binding energies of large clusters that bridge between clusters and solution. Alternatively, the cluster data can be used to calculate cluster-based single-ion solvation energies. However, the cluster-based values are much smaller than the conventional values. These results on large clusters and ion solvation energies can be fundamental to the energetics of nucleation and electrolyte solutions. The correct interpretation of the present thermochemical data will require accurate measurements of the binding energies of large clusters.

Cluster-Based Analysis of Solvation Factors. The strong contributions of ionic hydrogen bonds of ions to the inner solvent shells are included in the energies of small clusters. The experiment-based solvation energies of the clusters allows an analysis that quantifies these IHB contributions, as well as the continuum and hydrophobic solvation energies. The analysis yields structurally reasonable terms, assigning the hydrogen-bonding contributions by each alkyl and protic hydrogen.

Outlook. Ionic hydrogen bonds are significant in many aspects of chemistry. The basic properties of these bonds have been established in the last four decades, and their study has developed into a mature quantitative science. Extensions of the thermochemical studies to biomolecules and large clusters and structural studies by spectroscopy and ion mobility are active fields that pose challenges for the next decades.

11. Acknowledgment

The author thanks NASA, Grant NNG04GH45G, for partial funding of this work. I also thank Mrs. H. D. Mautner for help with organizing the manuscript, figures, and references.

12. References

(1) Moore, T. S.; Windmill, T. F. *J. Chem. Soc.* **1912**, *1011*, 1635.
(2) Pauling, L. *The Chemical Bond: A Brief Introduction to Modern Structural Chemistry*; Cornell University Press: Ithaca, New York, 1967.
(3) Aakeroy, C. B.; Beatty, A. M. *Aust. J. Chem.* **2001**, *54*, 409.
(4) Field, F. H. *J. Am. Chem. Soc* **1969**, *91*, 2827.
(5) Kebarle, P. *Annu. Rev. Phys. Chem*. **1977**, *28*, 445.
(6) Caldwell, G.; Rozeboom, M. D.; Kiplinger, J. P.; Bartmess, J. E. *J. Am. Chem. Soc.* **1984**, *106*, 4660.
(7) Larson, J. W.; McMahon, T. B. *J. Am. Chem. Soc.* **1984**, *106*, 517.
(8) Larson, J. W.; McMahon, T. B. *J. Am. Chem. Soc.* **1987**, *109*, 6230.
(9) Gorman, G. S.; Amster, J. I. *J. Am. Chem. Soc.* **1993**, *115*, 5729.
(10) Dearden, D. V.; Liang, Y.; Nicoli, J. B.; Kellersberg, A. J. *Mass Spectrom.* **2001**, *36*, 989.
(11) Mackay, G. I.; Bohme, D. K. *J. Am. Chem. Soc.* **1978**, *100*, 327.
(12) Bowers, M. T.; Kemper, P. R.; vonHelden, G.; vanKoppen, P. A. M. *Science* **1993**, *260*, 1446.
(13) Woenckhaus, J.; Hudgins, R. R.; Jarrold, M. F. *J. Am. Chem. Soc.* **1997**, *119*, 9586.
(14) Dalleska, N. F.; Honma, K.; Armentrout, P. B. *J. Am. Chem. Soc.* **1993**, *115*, 12125.
(15) Dunbar, R. C.; McMahon, T. B.; Tholmann, D.; Tonner, D. S.; Salahub, D. R.; Wei, D. *J. Am. Chem. Soc.* **1995**, *117*, 12819.
(16) Gross, D. S.; Williams, E. R. *J. Am. Chem. Soc.* **1995**, *117*, 883.
(17) Gross, D. S.; Schnier, P. D.; Rodriguezcruz, S. E.; Fagerquist, C. K.; Williams, E. R. *Proc. Natl. Acad. Sci. U.S.A.* **1996**, *93*, 3143.
(18) Price, W. D.; Schnier, P. D.; Williams, E. R. *J. Phys. Chem. B* **1997**, *101*, 664.
(19) Yamdagni, R.; Kebarle, P. *J. Am. Chem. Soc.* **1976**, *98*, 1320.
(20) Taft, R. W. *Prog. Phys. Org. Chem.* **1983**, *14*, 248.
(21) Meot-Ner (Mautner), M.; Sieck, L. W. *J. Am. Chem. Soc.* **1991**, *113*, 4448.
(22) Szulejko, J. E.; McMahon, T. B. *J. Am. Chem. Soc.* **1993**, *115*, 7839.
(23) Smith, B. J.; Radom, L. *J. Am. Chem. Soc.* **1993**, *115*, 4885.
(24) East, A. L. L.; Smith, B. J.; Radom, L. *J. Am. Chem. Soc.* **1997**, *119*, 9014.
(25) Hunter, E. P. L.; Lias, S. G. *J. Phys. Chem. Ref. Data* **1998**, *27*, 413.
(26) Meot-Ner (Mautner), M. *Int. J. Mass Spectrom.* **2003**, *227*, 525.
(27) Hunter, E. P.; Lias, S. G. Proton Affinity Evaluation. In *NIST Chemistry WebBook*; Linstrom, P. J., Mallard, W. G., Eds.; NIST Standard Reference Database Number 69; National Institute of Standards and Technology: Gaithersburg, MD, March 2003 (http://webbook.nist.gov).
(28) Keesee, R. G.; Castleman, A. W. *J. Phys. Chem. Ref. Data* **1986**, *15*, 1011.
(29) Meot-Ner (Mautner), M.; Lias, S. G. Binding Energies Between Ions and Molecules, and The Thermochemistry of Cluster Ions. In *NIST Chemistry WebBook*; Linstrom, P. J., Mallard, W. G., Eds.; NIST Standard Reference Database Number 69; National Institute of Standards and Technology: Gaithersburg, MD, March 2003 (http://webbook.nist.gov).
(30) Bartmess, J. E. Negative Ion Energetics Data. In *NIST Chemistry WebBook*; Linstrom, P. J., Mallard, W. G., Eds.; NIST Standard Reference Database Number 69; National Institute of Standards and Technology: Gaithersburg, MD, March 2003 (http://webbook.nist.gov).
(31) Deakyne, C. A. In *Molecular Interactions*; Scheiner, S., Ed.; John Wiley: New York, 1997; p 217.
(32) Scheiner, S. In *Molecular Interactions*; Scheiner, S., Ed.; John Wiley: New York, 1997.
(33) Meot-Ner (Mautner), M. In *Molecular Structure and Energetics*; Liebman, J. F., Greenberg, H., Eds.; VCH Publishers: New York, 1987; Vol. 4, p 71.
(34) Meot-Ner (Mautner), M.; Lias, S. G. Binding Energies between Ions and Molecules and the Thermochemistry of Cluster Ions. In *NIST Chemistry Webbook*; Linstrom, P. J., Mallard, W. G., Eds.; NIST Standard Reference Database Number 69; National Institute of Standards and Technology: Gaithersburg, MD, July 2001 (http://webbook.nist.gov).
(35) Meot-Ner (Mautner), M. *J. Phys. Chem.* **1987**, *91*, 417.
(36) Deakyne, C. A. *J. Phys. Chem.* **1986**, *90*, 6625.
(37) Desmeules, P. J.; Allen, L. C. *J. Chem. Phys.* **1980**, *72*, 4731.
(38) Yamdagni, R.; Kebarle, P. *J. Am. Chem. Soc.* **1971**, *93*, 7139.
(39) Yamdagni, R.; Kebarle, P. *J. Am. Chem. Soc.* **1973**, *95*, 3504.
(40) Davidson, W. R.; Sunner, J.; Kebarle, P. *J. Am. Chem. Soc.* **1979**, *101*, 1675.
(41) French, M. A.; Ikuta, S.; Kebarle, P. *Can. J. Chem*. **1982**, *60*, 1907.
(42) Meot-Ner (Mautner), M.; Sieck, L. W.; Koretke, K. K.; Deakyne, C. A. *J. Am. Chem. Soc.* **1997**, *119*, 10430.
(43) Meot-Ner (Mautner), M.; Cybulski, S. M.; Scheiner, S.; Liebman, J. F. *J. Phys. Chem.* **1988**, *92*, 2738.
(44) Bieske, E. J.; Nizkorodov, S. A.; Bennett, F. R.; Maier, J. P. *Int. J. Mass Spectrom. Ion. Processes* **1995**, *149*, 167.
(45) Bieske, E. J.; Nizkorodov, S. A.; Bennett, F. R.; Maier, J. P. *J. Chem. Phys.* **1995**, *104*, 5152.
(46) Hobza, P.; Zahradnik, R. *Chem. Phys. Lett.* **1993**, *208*, 497.
(47) Scheiner, S. *Acc. Chem. Res.* **1985**, *18*, 174.
(48) Meot-Ner (Mautner), M. *J. Am. Chem. Soc.* **1984**, *106*, 1257.
(49) Meot-Ner (Mautner), M. *J. Am. Chem. Soc.* **1984**, *106*, 1265.
(50) Larson, J. W.; McMahon, T. B. *J. Am. Chem. Soc.* **1982**, *104*, 6255.
(51) Bromilow, J.; Abboud, J. L. M.; Lebrilla, C. B.; Taft, R. W.; Scorrano, G.; Lucchini, V. *J. Am. Chem. Soc.* **1981**, *103*, 5448.
(52) Arshadi, M.; Kebarle, P. *J. Phys. Chem.* **1970**, *74*, 1483.
(53) Feng, W. Y.; Ling, Y.; Lifschitz, C. *J. Phys. Chem.* **1996**, *100*, 35.
(54) Meot-Ner (Mautner), M.; Sieck, L. W. *J. Phys. Chem.* **1985**, *89*, 5222.
(55) Meot-Ner (Mautner), M.; Sieck, L. W. *J. Am. Chem. Soc.* **1986**, *108*, 7525.

(56) Sieck, L. W.; Meot-Ner (Mautner), M. *J. Phys. Chem.* **1989**, *93*, 1586.
(57) Larson, J. W.; McMahon, T. B. *J. Am. Chem. Soc.* **1983**, *105*, 2945.
(58) Meot-Ner (Mautner), M. *J. Am. Chem. Soc.* **1988**, *110*, 3858.
(59) Meot-Ner (Mautner), M.; Field, F. H. *J. Chem. Phys.* **1977**, *66*, 4527.
(60) Hiraoka, K.; Saluja, P. P. S.; Kebarle, P. *Can. J. Chem.* **1976**, *57*, 2159.
(61) Meot-Ner (Mautner), M.; Field, F. H. *J. Am. Chem. Soc.* **1977**, *99*, 998.
(62) (a) Hiraoka, K.; Takimoto, H.; Yamabe, S. *J. Phys. Chem.* **1986**, *90*, 5910. (b) Meot-Ner (Mautner), M.; Sieck, L. W. *J. Am. Chem. Soc.* **1983**, *105*, 2956. (c) Norrman, K.; McMahon, T. B. *Int. J. Mass Spectrom.* **1999**, *183*, 381.
(63) Witt, M.; Grutzmacher, H. F. *Int. J. Mass Spectrom.* **1997**, *165*, 49.
(64) Hiraoka, K.; Kebarle, P. *Can. J. Chem.* **1977**, *55*, 24.
(65) Long, J. W.; Franklin, J. L. *J. Am. Chem. Soc.* **1974**, *96*, 2320.
(66) Meot-Ner (Mautner), M. *J. Am. Chem. Soc.* **1989**, *111*, 2830.
(67) Allison, C. E.; Cramer, J. A.; Hop, C. E. C.; Szulejko, J. E.; McMahon, T. B. *J. Am. Chem. Soc.* **1991**, *113*, 4469.
(68) Zeegers-Huyskens, Th. *J. Mol. Struct. (THEOCHEM)* **1986**, *135*, 93.
(69) Zeegers-Huyskens, Th. *J. Mol. Struct. (THEOCHEM)* **1988**, *177*, 125.
(70) Zeegers-Huyskens, Th.; Huyskens, P. L. In *Intermolecular forces. An Introduction to Modern Methods and Results*; Huyskens, P. L., Luck, W. A. P., Zeegers-Huyskens, Th., Eds.; Springer-Verlag: Berlin, Heidelberg, 1991; p 24.
(71) Zeegers-Huyskens, Th. *J. Mol. Liq.* **1995**, *67*, 33.
(72) Chandra, A. K.; Nguyen, M. T.; Uchimaru, T.; Zeegers-Huyskens, T. *J. Phys. Chem. A* **1999**, *103*, 8853.
(73) Chandra, A. K.; Hguyen, M. T.; Zeegers-Huyskens, T. *J. Chem. Phys.* **2000**, *255*, 149.
(74) Payzant, J. D.; Yamdagni, R.; Kebarle, P. *Can. J. Chem.* **1971**, *49*, 3308.
(75) Caldwell, G.; Kebarle, P. *Can. J. Chem.* **1985**, *63*, 1399.
(76) Caldwell, G.; Kebarle, P. *J. Am. Chem. Soc*. **1984**, *106*, 967.
(77) Evans, D. H.; Keesee, R. G.; Castleman, A. W. *J. Chem. Phys.* **1987**, *86*, 2927.
(78) Larson, J. W.; Szulejko, J. E.; McMahon, T. B. *J. Am. Chem. Soc.* **1988**, *110*, 7604.
(79) Meot-Ner (Mautner), M. *J. Am. Chem. Soc.* **1988**, *110*, 3854.
(80) Gao, J.; Garner, D. S.; Jorgensen, W. L. *J. Am. Chem. Soc.* **1986**, *108*, 4784.
(81) Cuming, J. B.; French, M. A.; Kebarle, P. *J. Am. Chem. Soc.* **1977**, *99*, 6999.
(82) Elmsley, J. E.; Hoyte, O. P. A.; Overill, R. E. *J. Chem. Soc., Perkin Trans. 2* **1977**, 2079.
(83) Sieck, L. W. *J. Phys. Chem.* **1985**, *89*, 5552.
(84) Pudzianowski, A. T. *J. Chem. Phys.* **1995**, *102*, 8029.
(85) Pudzianowski, A. D. *J. Phys. Chem.* **1996**, *100*, 4781.
(86) Robertson, W. H.; Johnson, M. A. *Annu. Rev. Phys. Chem.* **2003**, *54*, 173.
(87) Robertson, W. H.; Weddle, G. H.; Johnson, M. A. *J. Phys. Chem. A* **2003**, *107*, 9312.
(88) Corbett, C. A.; Martinez, T. J.; Lisy, J. M. *J. Phys. Chem. A* **2002**, *106*, 10015.
(89) Liebman, J. F.; Romm, M. J.; Meot-Ner (Mautner), M.; Cybulski, S. M.; Scheiner, S. *J. Phys. Chem.* **1991**, *95*, 1112.
(90) Meot-Ner (Mautner), M.; Sieck, L. W.; Liebman, J. F.; Scheiner, S. *J. Phys. Chem*. **1996**, *100*, 6445.
(91) (a) Meot-Ner (Mautner), M.; Sieck, L. W. *J. Am. Chem. Soc.* **1983**, *105*, 2956. (b) Mo, O.; Yanez, M.; Elguero, J. *J. Org. Chem.* **1987**, *52*, 1713.
(92) Glasstone, S. *Trans. Faraday Soc.* **1937**, *33*, 200.
(93) Meot-Ner (Mautner), M.; Deakyne, C. A. *J. Am. Chem. Soc.* **1985**, *107*, 468.
(94) Deakyne, C. A.; Meot-Ner (Mautner), M. *J. Am. Chem. Soc.* **1985**, *107*, 474.
(95) Blades, A. T.; Klassen, J. S.; Kebarle, P. *J. Am. Chem. Soc.* **1996**, *118*, 12437.
(96) Uggerud, E. *J. Am. Chem. Soc.* **1994**, *116*, 6873.
(97) Klassen, J. S.; Blades, A. T.; Kebarle, P. *J. Am. Chem. Soc.* **1994**, *116*, 12075.
(98) Hiraoka, K.; Takao, K.; Nakagawa, F.; Iino, T.; Ishida, M.; Fujita, K.; Hiizumi, K.; Yamabe, S. *Int. J. Mass Spectrom.* **2003**, *227*, 391.
(99) Hiraoka, K.; Shoda, T.; Kudaka, I.; Fujimaki, S.; Mizuse, S.; Yamabe, S.; Wasada, H.; Wasada-Tsutsui, Y. *J. Phys. Chem. A* **2003**, *107*, 775.
(100) Meot-Ner (Mautner), M.; Ross, M. M.; Campana, J. E. *J. Am. Chem. Soc.* **1985**, *107*, 4839.
(101) Hiraoka, K.; Takimoto, H.; Yamabe, S. *J. Am. Chem. Soc.* **1987**, *109*, 7346.
(102) Meot-Ner (Mautner), M. *J. Am. Chem. Soc.* **1978**, *100*, 4694.
(103) Grimsrud, E. P.; Kebarle, P. *J. Am. Chem. Soc.* **1973**, *95*, 7939.
(104) Hahndorf, I.; Jiang, J. C.; Chang, H. C.; Wu, C. C.; Chang, H. C. *J. Phys. Chem. A* **1999**, *103*, 8753.
(105) Dopfer, O.; Roth, D.; Maier, J. P. *J. Am. Chem. Soc*. **2002**, *124*, 494.
(106) Solca, N.; Dopfer, O. *Chem.—Eur. J*. **2003**, *9*, 3154.
(107) Smith, R. D.; Futrell, J. H. *Chem. Phys. Lett.* **1976**, *41*, 64.
(108) Audier, H. E.; Koyanagi, G. K.; McMahon, T. B.; Tholman, D. *J. Phys. Chem.* **1996**, *100*, 8220.
(109) Bouchoux, G.; Hoppiliard, Y. J. *J. Am. Chem. Soc.* **1990**, *112*, 9110.
(110) Swanton, D. J.; Marsden, D. C. D.; Radom, L. *Org. Mass Spectrom.* **1991**, *26*, 227.
(111) Bouchoux, G.; Nguyen, M. T.; Longevaille, P. *J. Am. Chem. Soc.* **1992**, *114*, 10000.
(112) Norrman, K.; McMahon, T. B. *J. Phys. Chem. A* **1999**, *103*, 7008.
(113) Hiraoka, K.; Katsuragawa, J.; Sugiyama, T.; Kojima, T.; Yamabe, S. *J. Am. Soc. Mass Spectrom.* **2001**, *12*, 144.
(114) Wincel, H. *Int. J. Mass Spectrom.* **2003**, *226*, 341.
(115) Ma, J. C.; Dougherty, D. A. *Chem. Rev.* **1997**, *97*, 1303.
(116) Lee, J. Y.; Lee, S. J.; Choi, H. S.; Cho, S. J.; Kim, K. S.; Ha, T. K. *Chem. Phys. Lett.* **1995**, *232*, 67.
(117) Ibrahim, Y.; Alsharaeh, E.; Dais, K.; Meot-Ner (Mautner), M.; El-Shall, M. S. *J. Am. Chem. Soc.* **2004**, *126*, 12766 and unpublished results.
(118) Fujii, A.; Patwari, G. N.; Ebata, T.; Mikami, N. *Int. J. Mass Spectrom.* **2002**, *220*, 289.
(119) Fujii, A.; Ebata, T.; Mikami, N. *J. Phys. Chem. A* **2002**, *106*, 8554.
(120) Solca, N.; Dopfer O. *J. Phys. Chem. A* **2003**, *107*, 4046.
(121) Kosugi, K.; Inokuchi, Y.; Nishi, N. J. *Chem. Phys*. **2001**, *114*, 4805.
(122) Fujimaki, E.; Fujii, A.; Ebata, T.; Mikami, N. *J. Chem. Phys.* **2000**, *112*, 137.
(123) Norrman, K.; McMahon, T. B. *J. Am. Chem. Soc.* **1996**, *118*, 2449.
(124) Deakyne, C. A.; Meot-Ner (Mautner), M. *J. Am. Chem. Soc.* **1999**, *121*, 1546.
(125) Chabinyc, M. L.; Brauman, J. I. *J. Phys. Chem. A* **1999**, *103*, 9163.
(126) Chabinyc, M. L.; Brauman, J. I. *J. Am. Chem. Soc.* **2000**, *122*, 8739.
(127) Afeefy, H. Y.; Liebman, J. F.; Stein, S. E. Neutral Thermochemical Data. In *NIST Chemistry WebBook*; Linstrom, P. J., Mallard, W. G., Eds.; NIST Standard Reference Database Number 69; National Institute of Standards and Technology: Gaithersburg MD, March 2003 (http://webbook.nist.gov).
(128) Lias, S. G.; Bartmess, J. E.; Liebman, J. F.; Holmes, J. L.; Levin, R. D.; Mallard, W. G. Ion Energetics Data. In *NIST Chemistry WebBook*;; Linstrom, P. J., Mallard, W. G., Eds.; NIST Standard Reference Database Number 69; National Institute of Standards and Technology: Gaithersburg MD, March 2003 (http://webbook.nist.gov).
(129) Hiraoka, K.; Kebarle, P. *J. Am. Chem. Soc.* **1976**, *98*, 6119.
(130) Sirois, M.; George, M.; Holmes, J. L. *Org. Mass Spectrom.* **1994**, *29*, 11.
(131) Zagorevskii, D. V.; Palii, S. P.; Holmes, J. L. *J. Am. Soc. Mass Spectrom.* **1994**, *5*, 814.
(132) Hiraoka, K.; Kebarle, P. *J. Am. Chem. Soc.* **1977**, *99*, 360.
(133) Walters, E. A.; Grover, J. R.; White, M. G.; Hui, E. T. *J. Phys. Chem.* **1985**, *89*, 3814.
(134) McAdoo, D. J.; Morton, T. H. *Acc. Chem. Res.* **1993**, *26*, 295.
(135) Terlouw, J. K.; deKoster, C. G.; Heerma, W.; Holmes, J. L.; Burgers, P. C. *Org. Mass Spectrom.* **1983**, *18*, 222.
(136) Postma, R.; Ruttink, P. J. A.; van Duijneveldt, F. B.; Terlouw, J. K.; Holmes, J. L. *Can. J. Chem.* **1985**, *64*, 2798.
(137) Postma, R.; Ruttink, P. J. A.; Terlouw, J. K.; Holmes, J. L. *J. Chem. Soc., Chem. Commun.* **1986**, 683.
(138) Holmes, J. L.; Mommers, A. A.; Szulejko, J. E.; Terlouw, J. K. *J. Chem. Soc., Chem. Commun.* **1984**, 165.
(139) Shao, J. D.; Baer, T.; Morrow, J. C.; Fraser-Monteiro, M. L. *J. Chem. Phys.* **1987**, *87*, 5242.
(140) Hrusak, J.; McGibbon, G. A.; Schwartz, H.; Terlouw, J. K. *Int. J. Mass Spectrom. Ion Processes* **1997**, *160*, 117.
(141) Miyazaki, M.; Fujii, A.; Ebata, T.; Mikami, N. *Phys. Chem. Chem. Phys.* **2003**, *5*, 1137−1148.
(142) Hiraoka, K.; Nakajima, G.; Shoda, S. *Chem. Phys. Lett.* **1988**, *146*, 535−538.
(143) Hiraoka, K.; Nakajima, G. *J. Chem. Phys.* **1988**, *88*, 7709.
(144) Hiraoka, K.; Mori, T. *Chem. Phys.* **1989**, *137*, 345.
(145) Hiraoka, K.; Yamabe, S. *Chem. Phys. Lett.* **1989**, *154*, 139.
(146) Hiraoka, K.; Mori, T.; Yamabe, S. *J. Chem. Phys.* **1991**, *94*, 2697.
(147) Magnera, T. F.; David, D. E.; Michl, J. *Chem. Phys. Lett.* **1991**, *182*, 363.
(148) Shi, Z.; Ford, J. V.; Wei, S.; Castleman, A. W. *J. Chem. Phys.* **1993**, *99*, 8009.
(149) Payzant, J. D.; Cunningham, A. J.; Kebarle, P. *Can. J. Chem.* **1973**, *51*, 3242.
(150) Meot-Ner (Mautner), M. *J. Am. Chem. Soc.* **1984**, *106*, 278.
(151) Banic, C. M.; Iribarne, J. V. *J. Chem. Phys.* **1985**, *83*, 6432.

(152) Hiraoka, K.; Grimsrud, E. P.; Kebarle, P. *J. Am. Chem. Soc.* **1974**, *96*, 3359.
(153) Hiraoka, K.; Takimoto, H.; Morise, K. *J. Am. Chem. Soc.* **1986**, *108*, 5863.
(154) Meot-Ner (Mautner), M.; Sieck, L. W.; Scheiner, S.; Duan, X. F. *J. Am. Chem. Soc*. **1994**, *116*, 7848.
(155) Klassen, J. S.; Blades, A. T.; Kebarle, P. *J. Phys. Chem.* **1995**, *99*, 15509.
(156) Fehsenfeld, F. C.; Ferguson, E. E. *J. Chem. Phys.* **1974**, *61*, 3181.
(157) Meot-Ner (Mautner), M.; Speller, C. V. *J. Phys. Chem.* **1986**, *90*, 6616.
(158) Kebarle, P.; Arshadi, M. *J. Chem. Phys*. **1968**, *49*, 817.
(159) Arshadi, M.; Yamdagni, R.; Kebarle, P. *J. Phys. Chem.* **1970**, *74*, 1475.
(160) Hiraoka, K.; Mizuse, S.; Yamabe, S. *J. Phys. Chem*. **1988**, *92*, 2943.
(161) Keesee, R. G.; Lee, N.; Castleman, A. W. *J. Am. Chem. Soc*, **1979**, *101*, 2599.
(162) Meot-Ner (Mautner), M.; Speller, C. V. *J. Phys. Chem.* **1989**, *93*, 6580.
(163) Lee, N.; Keesee, R. G.; Castleman, A. W. *J. Colloid Interface Sci.* **1980**, *75*, 555.
(164) Hiraoka, K.; Mizuse, S. *Chem. Phys.* **1987**, *118*, 457.
(165) Keesee, R. G.; Castleman, A. W., Jr. *Chem. Phys. Lett.* **1980**, *74*, 139.
(166) Markovich, G.; Pollack, S.; Giniger, R.; Cheshnovsky, O. *J. Chem. Phys.* **1994**, *101*, 9344.
(167) Blades, A. T.; Klassen, J. S.; Kebarle, P. *J. Am. Chem. Soc.* **1995**, *117*, 10563.
(168) Keesee, R. G.; Castleman, A. W. *J. Am. Chem. Soc.* **1989**, *111*, 9015.
(169) Blades, A. T.; Ho, Y.; Kebarle, P. *J. Phys. Chem.* **1996**, *100*, 2443.
(170) Blades, A. T.; Jayaweera, P.; Ikonomou, M. *J. Chem. Phys.* **1990**, *92*, 5900.
(171) Dzidic, I.; Kebarle, P. *J. Phys. Chem*. **1970**, *74*, 1466.
(172) Tang, I. N.; Castleman, A. W. *J. Chem. Phys.* **1972**, *57*, 3638.
(173) Searles, S. K.; Kebarle, P. *Can. J. Chem.* **1969**, *47*, 2619.
(174) Holland, P. M.; Castleman, A. W. *J. Chem. Phys.* **1982**, *76*, 4195.
(175) Tang, I. N.; Castleman, A. W. *J. Chem. Phys.* **1974**, *60*, 3981.
(176) Kochanski, E.; Constantin, E. *J. Chem. Phys.* **1987**, *87*, 1661.
(177) Tang, I. N.; Lian, M. S.; Castleman, A. W. *J. Chem. Phys.* **1976**, *65*, 4022.
(178) Meot-Ner (Mautner), M. *J. Am. Chem. Soc.* **1992**, *114*, 3312.
(179) Guo, B. C.; Conklin, B. J.; Castleman, A. W. *J. Am. Chem. Soc.* **1989**, *111*, 6506.
(180) Meot-Ner (Mautner), M. *J. Am. Chem. Soc.* **1986**, *108*, 6189.
(181) *Int. J. Mass Spectrom. Ion Phys.* **1986**, *68*, 99.
(182) *Int. J. Mass Spectrom. Ion Phys.* **1978**, *26*, 103.
(183) Meot-Ner (Mautner), M.; Elmore, D. E.; Scheiner, S. *J. Am. Chem. Soc.* **1999**, *121*, 7625.
(184) Curtius, J.; Froyd, K. D.; Lovejoy, E. R. *J. Phys. Chem. A* **2001**, *105*, 10867.
(185) Lovejoy, E. R.; Curtius, J. *J. Phys. Chem. A* **2001**, *105*, 10874.
(186) Deakyne, C. A.; Knuth, D.; Speller, C. V.; Meot-Ner (Mautner), M.; Sieck, L. W. *J. Mol. Struct. (THEOCHEM)* **1994**, *307*, 217.
(187) Meot-Ner (Mautner), M. *J. Am. Chem. Soc.* **1988**, *110*, 3075.
(188) Yamdagni, R.; Kebarle, P. *Can. J. Chem.* **1974**, *63*, 1399.
(189) Mayer, P. M. *J. Phys. Chem. A* **1999**, *103*, 5905.
(190) Davidson, W. R.; Kebarle, P. *J. Am. Chem. Soc*. **1976**, *98*, 6125.
(191) Yamdagni, R.; Kebarle, P. *J. Am. Chem. Soc.* **1972**, *94*, 2940.
(192) Hiraoka, R.; Mizuse, S.; Yamabe, S. *J. Phys. Chem*. **1988**, *92*, 3943.
(193) Schindler, T.; Berg, C.; Niedner-Shatteburg, G.; Bondybey, V. *J. Phys. Chem.* **1995**, *99*, 12434.
(194) Tunon, I.; Rinaldi, D.; Ruiz-Lopez, M. F.; Rivail, J. L. *J. Phys. Chem.* **1995**, *99*, 3789.
(195) Kebarle, P.; Searles, S. K.; Zolla, A.; Arshadi, M. *J. Am. Chem. Soc.* **1967**, *89*, 6393.
(196) Cunningham, A. J.; Payzant, A. D.; Kebarle, P. *J. Am. Chem. Soc.* **1972**, *94*, 7627.
(197) Lau, Y. K.; Ikuta, S.; Kebarle, P. *J. Am. Chem. Soc.* **1982**, *104*, 1462.
(198) Kelterbaum, R.; Kochanski, E. *J. Phys. Chem.* **1995**, *99*, 12494.
(199) Speller, C. V.; Meot-Ner (Mautner), M. *J. Phys. Chem.* **1985**, *89*, 5217.
(200) Tholman, D. T.; Tonner, D. C.; McMahon, T. B. *J. Phys. Chem.* **1994**, *98*, 2002.
(201) Lau, Y. K.; Kebarle, P. *Can. J. Chem.* **1981**, *59*, 151.
(202) Lau, Y. K. Ph.D. Thesis, University of Alberta, Edmonton, Alberta, Canada, 1982.
(203) (a) El-Shall, M. S.; Olafsdottir, S.; Meot-Ner (Mautner), M.; Sieck, L. W. *Chem. Phys. Lett.* **1991**, *193*, 1991. (b) El-Shall, M. S.; Daly, G.; Gao, J.; Meot-Ner (Mautner), M.; Sieck, L. W. *J. Phys. Chem.* **1992**, *96*, 507.
(204) Honma, K.; Sunderlin, L. S.; Armentrout, P. B. *J. Chem. Phys.* **1993**, *99*, 1623.
(205) Bomse, D. S.; Beauchamp, J. L. *J. Am. Chem. Soc.* **1981**, *103*, 3292.
(206) Meot-Ner (Mautner), M. *J. Phys. Chem.* **1991**, *95*, 6580.
(207) Wei, S.; Tzeng, W. B.; Castleman, A. W. *J. Phys. Chem.* **1991**, *95*, 585.
(208) Wenthold, P. G.; Squires, R. R. *J. Phys. Chem.* **1995**, *99*, 2002.
(209) Masamura, M. *J. Mol. Struct. (THEOCHEM)* **1999**, *466*, 85.
(210) Hirao, K.; Fujikawa, T.; Konishi, H.; Yamabe, S. *Chem. Phys. Lett.* **1984**, *104*, 184.
(211) Lifshitz, C.; Luage, F. *J. Phys. Chem.* **1989**, *93*, 5633.
(212) Wei, S.; Tzeng, W. B.; Castleman, A. W. *J. Chem. Phys.* **1990**, *92*, 332.
(213) Price, J. M.; Crofton, M. W.; Lee, Y. T. *J. Phys. Chem.* **1991**, *95*, 2182.
(214) Kim, N. J.; Kim, Y. S.; Jeong, G.; Ahn, T. K.; Kim, S. K. *Int. J. Mass Spectrom*. **2002**, *219*, 11.
(215) Tzeng, W. B.; Wei, S.; Castleman, A. W. *J. Phys. Chem.* **1991**, *95*, 5757.
(216) Wei, S.; Tzeng, W. B.; Castleman, A. W. *Z. Phys. D* **1991**, *20*, 47.
(217) Wei, S.; Tzeng, W. B.; Keesee, R. G.; Castleman, A. W. *J. Am. Chem. Soc.* **1991**, *113*, 1960.
(218) Castleman, A. W.; Wei, S. *Annu. Rev. Phys. Chem.* **1994**, *45*, 685.
(219) Castleman, A. W.; Bowen, K. H. *J. Phys. Chem.* **1996**, *100*, 12911.
(220) Feng, W. Y.; Iraqi, M.; Lifshitz, C. *J. Phys. Chem.* **1993**, *97*, 3510.
(221) Feng, W. Y.; Lifshitz, C. *J. Phys. Chem.* **1994**, *98*, 3658.
(222) Feng, W. Y.; Lifshitz, C. *J. Am. Chem. Soc.* **1995**, *117*, 11548.
(223) Feng, W. Y.; Lifshitz, C. *J. Mass Spectrom.* **1995**, *30*, 1179.
(224) Feng, W. Y.; Lifshitz, C. *Int. J. Mass Spectrom. Ion Processes* **1995**, *149*/*150*, 13.
(225) Tunon, I.; Silla, E.; Bertran, J. *J. Phys. Chem.* **1993**, *97*, 5547.
(226) Newton, M. D.; Ehrenson, S. *J. Am. Chem. Soc.* **1971**, *93*, 4971.
(227) Newton, M. D. *J. Chem. Phys.* **1977**, *67*, 5535.
(228) Deakyne, C. A.; Meot-Ner (Mautner), M.; Campbell, C. L.; Hughes, M. G.; Murphy, S. P. *J. Chem. Phys.* **1986**, *84*, 4958.
(229) Jiang, J. C.; Wang, Y. S.; Chang, H. C.; Lin, S. H.; Lee, Y. T.; Nieder-Schatteburg, G.; Chang, H. C. *J. Am. Chem. Soc.* **2000**, *122*, 1398.
(230) Chang, H. C.; Jiang, J. C.; Hahndorf, I.; Lin, S. H.; Lee, Y. T.; Chang. H. C. *J. Am. Chem. Soc.* **1999**, *121*, 4443.
(231) Jiang, J. C.; Boo, D. W.; Lin, S. H.; Lee, Y. T.; Chang, H. C. *J. Chem. Phys.* **2000**, *112*, 176.
(232) (a) Jiang, J. C.; Chaudhuri, C.; Lee, Y. T.; Chang, H. C. *J. Phys. Chem. A* **2002**, *106*, 10937. (b) Daly, G. M.; Gao, J.; El-Shall, M. S. *Chem. Phys. Lett.* **206**, *500*, 1993.
(233) Kim, K. Y.; Chang, H. C.; Lee, Y. T.; Cho, U. I.; Boo, D. W. *J. Phys. Chem. A* **2003**, *107*, 5007.
(234) Wang, Y. S.; Chang, H. C.; Jiang, J. C.; Lin, S. H.; Lee, Y. T.; Chang, H. C. *J. Am. Chem. Soc.* **1998**, *120*, 8777.
(235) Jiang, J. C.; Chang, H. C.; Lee, Y. T.; Lin, S. H. *J. Phys. Chem. A* **1999**, *103*, 3123.
(236) Wu, C. C.; Chaudhuri, C.; Jiang, J. C.; Lee, Y. T.; Chang, H. C. *J. Phys. Chem.*, in press.
(237) Lee, H. M.; Kim, K. S. *J. Chem. Phys.* **2001**, *114*, 4461.
(238) Peslherbe, G. H.; Ladanyi, B. M.; Hynes, J. T. *J. Phys. Chem. A* **1999**, *103*, 2561.
(239) Coe, J. V. *J. Phys. Chem. A* **1997**, *101*, 2055.
(240) Froyd, K. D.; Lovejoy, E. R. *J. Phys. Chem. A* **2003**, *107*, 9800.
(241) Froyd, K. D.; Lovejoy, E. R. *J. Phys. Chem. A* **2003**, *107*, 9812.
(242) Meot-Ner (Mautner), M.; Scheiner, S.; Yu. W. O. *J. Am. Chem. Soc.* **1998**, *120*, 6980.
(243) El-Shall, M. S.; Olafsdottir, S. R.; Meot-Ner (Mautner), M.; Sieck, L. W. *Chem. Phys. Lett.* **1991**, *185*, 193.
(244) Feng, W. Y.; Goldenberg, M.; Lifshitz, C. *J. Am. Soc. Mass Spectrom.* **1994**, *5*, 695.
(245) Martin, J. M. L.; Aviyente, V.; Lifshitz, C. *J. Phys. Chem.* **1997**, *101*, 2597.
(246) Aviyente, V.; Zhang, R.; Varnali, T.; Lifshitz, C. *Int. J. Mass Spectrom Ion Processes* **1997**, *161*, 123.
(247) Chaudhuri, C.; Jiang, J. C.; Wu, C. C.; Wang, X.; Chang, H. C. *J. Phys. Chem. A* **2001**, *105*, 8906.
(248) Brauman, J. I.; Blair, L. K. *J. Am. Chem. Soc.* **1968**, *90*, 6591.
(249) Brauman, J. I.; Blair, L. K. *J. Am. Chem. Soc.* **1970**, *92*, 5986.
(250) McIver, R. T.; Scott, J. A.; Riveros, J. M. *J. Am. Chem. Soc.* **1973**, *95*, 2706.
(251) Bohme, D. K.; Ralshit, A. B.; Mackay, G. I. *J. Am. Chem. Soc.* **1982**, *104*, 1100.
(252) Mackay, G. I.; Rashit, A. B.; Bohme, D. K. *Can. J. Chem*. **1982**, *82*, 2594.
(253) Lias, S. L.; Liebman, J. F.; Levin, R. D. *J. Phys. Chem. Ref. Data* **1984**, *13*, 695.
(254) Caskey, D. C.; Damrauer, R.; McGoff, D. *J. Org. Chem.* **2002**, *67*, 5098.
(255) Snodgrass, J. T.; Coe, J. V.; McHugh, K. M.; Arnold, S. T.; Bowen, K. H. *J. Phys. Chem.* **1995**, *99*, 9675.
(256) Yamabe, S.; Hirao, K.; Wasada, H. *J. Phys. Chem*. **1992**, *96*, 10261.
(257) Szulejko, J. E.; McMahon, T. B.; Troude, V.; Bouchoux, G.; Audier, H. E. *J. Phys. Chem*. **1998**, *102*, 1879.
(258) Aue, D. H.; Webb, H. M.; Bowers, M. T. *J. Am. Chem. Soc.* **1973**, *95*, 2699.

(259) Meot-Ner (Mautner), M.; Hamlet, P.; Hunter, E. P.; Field, F. H. *J. Am. Chem. Soc*. **1980**, *102*, 6393.
(260) Meot-Ner (Mautner), M. *J. Am. Chem. Soc.* **1983**, *105*, 4906.
(261) Sharma, R. B.; Blades, A. T.; Kebarle, P. *J. Am. Chem. Soc.* **1984**, *106*, 510.
(262) Bouchoux, G.; Hoppiliard, Y.; Houriet, R. *New J. Chem.* **1987**, *11*, 225.
(263) Chen, Q. F.; Stone, J. A. *J. Phys. Chem.* **1995**, *99*, 1442.
(264) Hu, C. H.; Shen, M.; Schaefer, H. F. *J. Am. Chem. Soc.* **1993**, *115*, 2923.
(265) Engkvist, O.; Astrand, P. O.; Karlstrom, G. *J. Phys. Chem.* **1996**, *100*, 6950.
(266) Aleman, C.; Navarro, E.; Puiggali, J. *J. Phys. Chem.* **1996**, *100*, 16131.
(267) Aleman, C.; Puiggali, J. *J. Org. Chem.* **1997**, *62*, 307.
(268) Price, D. J.; Roberts, J. D.; Jorgensen, W. L. *J. Am. Chem. Soc.* **1998**, *120*, 9672.
(269) Rodriguez, C. F.; Cunie, A.; Shoeib, T.; Chu, I. K.; Hopkinson, A. C.; Siu, K. W. M. *J. Phys. Chem. A* **2000**, *104*, 5023.
(270) Rodriguez, C. F.; Cunie, A.; Shoeib, T.; Chu, I. K.; Hopkinson, A. C.; Siu, K. W. M. *J. Am. Chem. Soc.* **2001**, *123*, 3006.
(271) Boo, D. W. *Bull. Korean Chem. Soc.* **2001**, *22*, 693.
(272) Furlani, T. R.; Garvey, J. F. *Mol. Phys*. **1997**, *92*, 449.
(273) Wu, C. C.; Jiang, J. C.; Hahndorf, I.; Chaudhuri, C.; Lee, Y. T.; Chang, H. C. *J. Phys. Chem. A* **2000**, *104*, 9556.
(274) Snoek, L. C.; Kroemer, R. T.; Hockridge, M. R. J. *Chem. Phys. Phys. Chem.* **2001**, *3*, 1819.
(275) Wu, C. C.; Chaudhuri, C.; Jiang, J. C.; Lee, Y. T.; Chang, H. C. *Mol. Phys.* **2003**, *101*, 1285.
(276) Chang, H. C.; Jiang, J. C.; Chang, H. C.; Wang, L. R.; Lee, Y. T. *Isr. J. Chem.* **1999**, *39*, 231.
(277) Morton, T. H. *Tetrahedron* **1982**, *38*, 3195.
(278) Audier, H. E.; Milliet, A.; Leblanc, D.; Morton, T. H. *J. Am. Chem. Soc.* **1992**, *114*, 2020.
(279) Meot-Ner (Mautner), M. *J. Am. Chem. Soc.* **1979**, *101*, 2396.
(280) Meot-Ner (Mautner), M. *J. Am. Chem. Soc.* **1983**, *105*, 4912.
(281) Sharma, R. B.; Kebarle, P. *J. Am. Chem. Soc*. **1984**, *106*, 3913.
(282) Ryzhov, V.; Dunbar, R. C. *J. Am. Soc. Mass Spectrom.* **1999**, *10*, 862.
(283) Adoteldo, D.; Aviyente, V.; Martin, J. M. L.; Lifshitz, C. *J. Phys. Chem. A* **1998**, *102*, 6357.
(284) Kim, S. G.; Kim, K. H.; Kim, Y. K.; Shin, S. K.; Ahn, K. H. *J. Am. Chem. Soc.* **2003**, *125* (45), 13819.
(285) Schwartz, H. A. *J. Chem. Phys.* **1977**, *67*, 5525.
(286) Yamabe, S.; Minato, T.; Hirao, K. J. *J. Chem. Phys.* **1984**, *80*, 1576.
(287) Begeman, M. H.; Gudeman, C. S.; Pfaff, J.; Saykally, R. J. *Phys. Chem. Lett.* **1983**, *51*, 554.
(288) Begemann, M. H.; Saykally, R. J. *J. Chem. Phys.* **1985**, *82*, 3570.
(289) Liu, D. J.; Oka, T. *Phys. Rev. Lett.* **1985**, *54*, 1787.
(290) Liu, D. J.; Oka, T.; Sears, T. J. *Chem. Phys.* **1986**, *108*, 335.
(291) Davies, P. B.; Johnson, S. A.; Hamilton, P. A.; Sears, T. J. *Chem. Phys.* **1986**, *108*, 335.
(292) Okumuar, M.; Yeh, L. I.; Myers, J. D.; Lee, Y. T. *J. Phys. Chem.* **1990**, *94*, 3416.
(293) Okumura, M.; Yeh, L. I.; Lee, Y. T. *J. Chem. Phys.* **1985**, *83*, 3705.
(294) Okumura, M.; Yeh, L. I.; Myers, J. D.; Lee, Y. T. *J. Chem. Phys.* **1986**, *85*, 2328.
(295) Okumura, M.; Yeh, L. I.; Lee, Y. T. *J. Chem. Phys.* **1988**, *88*, 79.
(296) Liu, W. L.; Lisy, J. M. *J. Chem. Phys.* **1988**, *89*, 606.
(297) Desfrancois, C.; Baillon, B.; Schermann, J. P.; Arnold, S. T.; Hendricks, J. H.; Bowen, K. H. *Phys. Rev. Lett.* **1994**, *72*, 48.
(298) Michi, T.; Ohashi, K.; Inokuchi, Y.; Nishi, N.; Sekiya, H. *Chem. Phys. Lett*. **2003**, *371*, 111.
(299) Kleinermanns, K.; Janzen, C.; Spangenberg, D.; Gerhards, M. *J. Phys. Chem. A* **1999**, *103*, 5232.
(300) Roth, W.; Schmitt, M.; Sprangenberg, D.; Janzen, C.; Kleinermanns, K. *Chem. Phys.* **1998**, *239*, 1.
(301) Jacoby, C.; Hering, P.; Schmitt, M.; Roth, W.; Kleinermanns, K. *Chem. Phys.* **1998**, *239*, 23.
(302) Schmitt, M.; Jacoby, C.; Gerhards, M.; Unterberg, C.; Roth, W.; Kleinermanns, K. *J. Chem. Phys.* **2000**, *113*, 2995.
(303) Macleod, N. A.; Simons, J. P. *Phys. Chem. Chem. Phys.* **2004**, *6*, 2821.
(304) Price, E. A.; Robertson, W. H.; Diken, E. G.; Weddle, G. H.; Johnson, M. A. *Chem. Phys. Lett.* **2002**, *366*, 412.
(305) Ayotte, P.; Weddle, G. H.; Kim, J.; Johnson, M. A. *J. Am. Chem. Soc.* **1998**, *120*, 12361.
(306) Ayotte, P.; Bailey, C. G.; Weddle, G. H.; Johnson, M. A. *J. Phys. Chem. A* **1998**, *102*, 3067.
(307) Wild, D. A.; Loh, Z. M.; Wolynec, P. P.; Weiser, P. S.; Bieske, E. J. *Chem. Phys. Lett.* **2000**, *332*, 531.
(308) Wild, D. A.; Bieske, E. J. *Int. Rev. Phys. Chem.* **2003**, *22*, 129.
(309) Radisic, D.; Xu, S. J.; Bowen, K. H. *Chem. Phys. Lett.* **2002**, *354*, 9.
(310) Hendricks, J. H.; de Clercq, H. L.; Freidhoff, C. B.; Arnold, S. T.; Eaton, J. G.; Fancher, C.; Lyapustina, S. A.; Snodgrass, J. T.; Bowen, K. H. *J. Chem. Phys.* **2002**, *116*, 7926.
(311) Gutowski, M.; Dabkowska, I.; Rak, J.; Xu, S.; Nilles, J. M.; Radisic, D.; Bowen, K. H. *Eur. Phys. J. D* **2002**, *20*, 431.
(312) Meot-Ner (Mautner), M.; Field, F. H. *J. Chem. Phys.* **1974**, *61*, 3742.
(313) Sieck, L. W.; Searles, S. K. *J. Chem. Phys.* **1970**, *53*, 2601.
(314) Daly, G. M.; Meot-Ner (Mautner), M.; Pithawalla, Y. B.; El-Shall, M. S. *J. Chem. Phys.* **1996**, *104*, 7965.
(315) Bernstein, E. R. *J. Phys. Chem.* **1992**, *96*, 10105.
(316) Brutchky, B. *Chem. Rev.* **1992**, *92*, 1567.
(317) Audier, H. E.; Fossey, J.; Mourgues, P.; McMahon, T. B.; Hammerum, S. S. *J. Phys. Chem.* **1996**, *100*, 18380−18386.
(318) Audier, H. E.; McMahon, T. B. *J. Mass Spectrom.* **1997**, *32*, 201−208.
(319) Raksit, A. B.; Bohme, D. K. *Can. J. Chem.* **1983**, *61*, 1683.
(320) Meot-Ner (Mautner), M. *J. Am. Chem. Soc.* **1982**, *104*, 5.
(321) Ochran, R. A.; Mayer, P. M. *Eur. J. Mass Spectrom.* **2001**, *7*, 267.
(322) Shaffer, S. A.; Sadilek, M.; Turecek, F.; Hop. C. E. C. A. *Int. J. Mass Spectrom. Ion Processes* **1997**, *160*, 137.
(323) Warshel, A.; Russell, S. T. *J. Am. Chem. Soc.* **1986**, *108*, 6596.
(324) Deligiannakis, Y.; Hanly, J.; Rutherford, A. W. *J. Am. Chem. Soc.* **1999**, *121*, 7653.
(325) Wang, J.; El-Sayed, M. A. *J. Phys. Chem. A* **2000**, *104*, 4333.
(326) Fenn, J. B.; Mann, M.; Meng, C. K.; Wong, S. F.; Whitehouse, C. M. *Science* **1989**, *246*, 64.
(327) Cox, K. A.; Julian, R. K.; Cooks, R. G.; Kaiser, R. E. *J. Am. Soc. Mass Spectrom.* **1994**, *5*, 127.
(328) Rodriguez-Cruz, S. E.; Klassen, J. S.; Williams, E. R. *J. Am. Soc. Mass Spectrom.* **1997**, *8*, 565.
(329) Price, W. D.; Jockusch, R. A.; Williams, E. R. *J. Am. Chem. Soc.* **1997**, *119*, 11988.
(330) Price, W. D.; Jockusch, R. A.; Williams, E. R. *J. Am. Chem. Soc.* **1998**, *120*, 3474.
(331) Schnier, P. D.; Price, W. D.; Williams, E. R. *J. Am. Soc. Mass Spectrom.* **1996**, *9*, 972.
(332) Gorman, G. S.; Speir, J. P.; Turner, C. A.; Amster, I. J. *J. Am. Chem. Soc.* **1992**, *114*, 3986.
(333) Wu, Z.; Fenselau, C. *J. Am. Soc. Mass Spectrom.* **1992**, *3*, 863.
(334) Cheng, X.; Wu, Z.; Fenselau, C. *J. Am. Chem. Soc.* **1993**, *115*, 4844.
(335) Wu, Z.; Lebrilla, C. *J. Am. Chem. Soc.* **1993**, *115*, 3270.
(336) Green, M. K.; Lebrilla, C. B. *Mass Spectrom. Rev.* **1997**, *16*, 53.
(337) Addario, V.; Guo, Y. Z.; Chu, I. K.; Ling, Y.; Ruggerio, G.; Rodriquez, C. F.; Hopkinson, A. C.; Siu, K. W. M. *Int. J. Mass Spectrom.* **2002**, *219*, 101.
(338) Wu, J.; Gard, E.; Bregar, J.; Green, M. K.; Lebrilla, C. B. *J. Am. Chem. Soc.* **1995**, *117*, 9900.
(339) Zhang, K.; Zimmerman, D. M.; Chung-Phillips, A.; Cassady, C. J. *J. Am. Chem. Soc.* **1993**, *115*, 10812.
(340) Campbell, S.; Rodgers, M. T.; Marzluff, E. M.; Beauchamp, J. L. *J. Am. Chem. Soc.* **1995**, *117*, 12840.
(341) Wyttenbach, T.; Paizs, B.; Barran, P.; Breci, L.; Liu, D. F.; Suhai, S.; Wysocki, V. H.; Bowers, M. T. *J. Am. Chem. Soc.* **2003**, *125*, 13768.
(342) Counterman, A. E.; Clemmer, D. E. *J. Phys. Chem. B* **2004**, *108*, 4885.
(343) Counterman, A. E.; Clemmer, D. E. *J. Phys. Chem. B* **2002**, *106*, 12045.
(344) Counterman, A. E.; Clemmer, D. E. *J. Am. Chem. Soc.* **2001**, *123*, 1490.
(345) Counterman, A. E.; Clemmer, D. E. *J. Phys. Chem. B* **2003**, *107*, 2111.
(346) Gidden, J.; Bushnell, J. E.; Bowers, M. T. *J. Am. Chem. Soc.* **2001**, *123*, 5610.
(347) Gross, D. S.; Rodriguez-Cruz, S. E.; Bock, S.; Williams, E. R. *J. Phys. Chem.* **1995**, *99*, 4034.
(348) Meot-Ner (Mautner), M.; Field, F. H. *J. Am. Chem. Soc.* **1973**, *96*, 3168.
(349) Liu, D. F.; Wyttenbach, T.; Carpenter, C. J.; Bowers, M. T. *J. Am. Chem. Soc.* **2004**, *126*, 3261.
(350) Liu, D. F.; Wyttenbach, T.; Barran, P. E.; Bowers, M. T. *J. Am. Chem. Soc.* **2003**, *125*, 8458.
(351) Jockusch, R. A.; Lemoff, A. S.; Wlliams, E. R. *J. Phys. Chem. A* **2001**, *105*, 48.
(352) Strittmatter, E. F.; Williams, E. R. *J. Phys. Chem. A* **2000**, *104*, 6069.
(353) Strittmatter, E. F.; Williams, E. R. *Int. J. Mass Spectrom.* **1999**, *187*, 935.
(354) Counterman, D. E.; Clemmer, D. E. *J. Phys. Chem. B* **2001**, *105*, 8092.
(355) Kohtani, M.; Breaux, G. A.; Jarrold, M. F. *J. Am. Chem. Soc.* **2004**, *126*, 1206.
(356) Kohtani, M.; Jarrold, M. F. *J. Am. Chem. Soc.* **2004**, *126*, 8454.
(357) Kohtani, M.; Jarrold, M. F. *J. Am. Chem. Soc.* **2002**, *124*, 11148.
(358) Lee, S. W.; Freivogel, P.; Schindler, T.; Beauchamp, J. L. *J. Am. Chem. Soc.* **1998**, *120*, 11758.
(359) Woenckhaus, J.; Mao, Y.; Jarrold, M. F. *J. Phys. Chem. B* **1997**, *101*, 847.

(360) Fye, J. L.; Woenckhaus, J.; Jarrold, M. F. *J. Am. Chem Soc.* **1998**, *120*, 1327.
(361) Wyttenbach, T.; von Helden, G.; Bowers, M. T. *J. Am. Chem. Soc.* **1996**, *118*, 8355.
(362) Jarrold, M. F. *Annu. Rev. Phys. Chem.* **2000**, *51*, 179.
(363) Jockusch, R. A.; Williams, E. R. *J. Phys. Chem. A* **1998**, *102*, 4543.
(364) Meot-Ner (Mautner), M.; Dongre, A. R.; Somogyi, A.; Wysocki, V. H. *Rapid Commun. Mass Spectrom.* **1995**, *9*, 829.
(365) Schnier, P. D.; Price, W. D.; Stritmatter, E. F.; Williams, E. R. *J. Am. Soc. Mass Spectrom.* **1997**, *8*, 771.
(366) Kaleta, D. T.; Jarrold, M. F. *J. Phys. Chem. B* **2003**, *107*, 14529.
(367) Kaleta, D. T.; Jarrold, M. F. *J. Phys. Chem. A* **2002**, *106*, 9655.
(368) Meot-Ner (Mautner), M. *J. Am. Chem. Soc.* **1988**, *110*, 3071.
(369) Gidden, J.; Bowers, M. T. *J. Phys. Chem. B* **2003**, *107*, 12829.
(370) Schnier, P. D.; Klassen, J. S.; Strittmatter, E. E.; Williams, E. R. *J. Am. Chem. Soc.* **1998**, *120*, 9605.
(371) Strittmatter, E. E.; Schnier, P. D.; Klassen, J. S.; Williams, E. R. *J. Am. Soc. Mass Spectrom.* **1999**, *10*, 1095.
(372) Meot-Ner (Mautner), M.; Hunter, E. P.; Field, F. H. *J. Am. Chem. Soc*. **1979**, *101*, 686.
(373) Locke, M. J.; McIver, R. T. *J. Am. Chem. Soc.* **1983**, *105*, 4226.
(374) Meot-Ner (Mautner), M.; Field, F. H. *J. Am. Chem. Soc.* **1974**, *96*, 3168.
(375) Jonsson, B.; Karlstrom, G.; Wennerstrom, H. *J. Am. Chem. Soc.* **1978**, *100*, 1658.
(376) Yang, X.; Castleman, A. W. *J. Am. Chem. Soc.* **1991**, *113*, 6766.
(377) Apel, C. L.; Deamer, D. W.; Mautner, M. N. *Biochim. Biophys. Acta Biomembranes* **2002**, *1559*, 1.
(378) Zundel, G. In *Advances in Chemical Physics*. Prigogine, I., Rice, S., Eds.; John Wiley and Sons: New York, 2000; Vol. 3, pp 1−217.
(379) Zundel, G.; Noller, H.; Schwab, G. M. *Z. Elektochem. Ber. Bunsen-Ges. Phys. Chem.* **1962**, *66*, 129.
(380) Schioberg, D.; Zundel, G. *Z. Phys. Chem.* **1963**, *67*, 771.
(381) Rabold, A.; Bauer, R.; Zundel, G. *J. Phys. Chem.* **1995**, *99*, 1889.
(382) Zundel, G.; Schwab, G. M. *J. Phys. Chem.* **1963**, *67*, 771.
(383) Danninger, W.; Zundel, G. *J. Chem. Phys.* **1987**, *74*, 2769.
(384) Huyskens, P.; Zeegers-Huyskens, Th. *J. Chem. Phys.* **1964**, *61*, 1964.
(385) Huyskens, P.; Fernandez, G. *Ind. Chem. Belg.* **1973**, *38*, 1237.
(386) Lindemann, R. *J. Chem. Soc., Faraday Trans. 2* **1977**, *73*, 788.
(387) Brzezinski, B.; Zundel, G. *Chem. Phys. Lett.* **1982**, *87*, 400.
(388) Brzezinski, B.; Zundel, G. *J. Chem. Soc., Faraday Trans. 2* **1983**, *79*, 1249.
(389) Brzezinski, B.; Zundel, G. *Can. J. Chem.* **1981**, *59*, 786.
(390) Brzezinski, B.; Zundel, G. *J. Chem. Soc., Faraday Trans. 2* **1980**, *76*, 1061.
(391) Brzezinski, B.; Rabold, A.; Zundel, G. *J. Phys. Chem.* **1995**, *99*, 8519.
(392) Brezinski, B.; Zundel, G. *J. Chem. Phys.* **1984**, *81*, 1600.
(393) Brzezinski, B.; Zundel, G.; Kramer, R. *J. Phys. Chem.* **1988**, *92*, 7012.
(394) Brzezinski, B.; Zundel, G.; Kramer, R. *Chem. Phys. Lett.* **1988**, *146*, 138.
(395) Brezinski, B.; Kramer, R.; Zundel, G. *Chem. Phys. Lett*. **1989**, *157*, 512.
(396) Brzezinski, B.; Olejnik, J.; Zundel, G.; Kramer, R. *Chem. Phys. Lett.* **1989**, *156*, 213.
(397) Eckert, M.; Zundel, G. *J. Phys. Chem.* **1988**, *92*, 7016.
(398) Eckert, M.; Zundel, G. *THEOCHEM* **1988**, *50*, 141.
(399) Eckert, M.; Zundel, G. *J. Phys. Chem.* **1989**, *93*, 5327.
(400) Zundel, G.; Muhlinghaus, J. *Z. Naturforsch.* **1971**, *26B*, 546.
(401) Rastogi, P. P.; Kristof, W.; Zundel, G. *Biochem. Biophys. Res. Commun.* **1980**, *95*, 902.
(402) Kristof, W.; Zundel, G. *Biophys. Struct. Mech.* **1980**, *6*, 209.
(403) Kristof, W.; Zundel, G. *Biopolymers* **1980**, *19*, 1753.
(404) Hargreaves, W. R.; Deamer, D. W. *Biochemistry* **1978**, *17*, 3759.
(405) Lindemann, R.; Zundel, G. *Biopolymers* **1977**, *16*, 2407.
(406) Lindemann, R.; Zundel, G. *Biopolymers* **1978**, *17*, 1285.
(407) Olejnik, J.; Brzezinski, B.; Zundel, G. *J. Mol. Struct.* **1992**, *271*, 157.
(408) Zundel, G. *J. Mol. Struct.* **1994**, *322*, 33.
(409) Gogol, E. P.; Lucken, U.; Capaldi, R. A. *FEBS Lett.* **1987**, *219*, 274.
(410) Wellner, N.; Zundel, G. *J. Mol. Struct.* **1994**, *317*, 249.
(411) Iliadis, G.; Brezinski, B.; Zundel, G. *Biospectroscopy*, in press.
(412) Bartl, F.; Brzezinski, B.; Rozalski, B.; Zundel, G. *J. Phys. Chem. B* **1998**, *102*, 5234.
(413) Baran, J.; Malarski, Z.; Sobczyk, L.; Grech, E. *Spectrochim. Acta* **1988**, *44A*, 933.
(414) Videnova-Adrabinska, V.; Baran, J.; Ratajczak, H.; Orville-Thomas, W. J. *Can. J. Chem.* **1985**, *63*, 3597.
(415) Sobczyk, L. *Phys. Chem. Chem. Phys.* **1998**, *102*, 371.
(416) Braga, D.; Angeloni, A.; Maini, L.; Gotz, A. W.; Grepioni, F. *New J. Chem.* **1999**, *1*, 17.
(417) Dominiak, P. M.; Grech, E.; Barr, G.; Teat, S.; Mallinson, P.; Wozniak, K. *Chem.—Eur. J*. **2003**, *9*, 963.
(418) Steiner, T. *Angew. Chem.* **2002**, *41*, 48.
(419) Steiner, T. *Crystallogr. Rev.* **2003**, *9*, 177.
(420) Epstein, L. M.; Shubina, E. S. *Coord. Chem. Rev*. **2002**, *231*, 165.
(421) Brammer, L. *Dalton Trans.* **2003**, *16*, 3145.
(422) Braga, D.; Grepioni, F.; Desiraju, G. R. *Chem. Rev.* **1998**, *98*, 1375.
(423) Desiraju, G. R. *Acc. Chem. Res.* **2002**, *35*, 565.
(424) Taft, R. W.; Wolf, J. F.; Beauchamp, J. L.; Scorrano, G.; Arnett, E. M. *J. Am. Chem. Soc.* **1978**, *100*, 1240.
(425) Klots, C. E. *J. Phys. Chem.* **1981**, *85*, 3585.
(426) Castleman, A. W.; Holland, P. M.; Keesee, R. G. *Radiat. Phys. Chem.* **1982**, *20*, 57.
(427) Holland, P. M.; Castleman, A. W., Jr. *J. Phys. Chem.* **1982**, *86*, 4181.
(428) Hiraoka, K. *Bull. Chem. Soc. Jpn.* **1987**, *60*, 2555.
(429) Hiraoka, K. *Can. J. Chem*. **1987**, *65*, 1258.
(430) Coe, J. V. *Chem. Phys. Lett.* **1994**, *229*, 161.
(431) Tissandier, M. D.; Cowen, K. A.; Feng, W. Y.; Gundlach, E.; Cohen, M. H.; Earhart, A. D.; Coe, J. V.; Tuttle, T. R. *J. Phys. Chem. A* **1998**, *102*, 7787.
(432) Coe, J. V. *Int. Rev. Phys. Chem.* **2001**, *20*, 33.
(433) Tuttle, T. R.; Malaxos, S.; Coe, J. V. *J. Phys. Chem A* **2002**, *106*, 925.
(434) Rosseinsky, D. R. *Chem. Rev.* **1965**, *65*, 467.
(435) Rosano, H. L.; Christodolou, A. P.; Feinstein, M. E. *J. Colloid Interface Sci.* **1969**, *29*, 335.
(436) Bockris, J. O.; Reddy, A. K. N. *Modern Electrochemistry*; Plenum Press: New York, 1970; Vol. 1, p 61.
(437) Born, M. *Z. Phys.* **1920**, *1*, 45.
(438) Bernal, J. D.; Fowler, R. H. *J. Chem. Phys.* **1933**, *1*, 515.
(439) Abraham, M. H.; Liszi, J. *J. Chem. Soc., Faraday Trans.* **1978**, *74*, 1604.
(440) Jorgensen, W. L.; Gao, J. *J. Phys. Chem.* **1986**, *90*, 2174.
(441) Singh, U. J.; Brown, F. K.; Bash, P. A.; Kollman, P. A. *J. Am. Chem. Soc.* **1987**, *109*, 1607.
(442) Rao, B. J.; Singh, U. C. *J. Am. Chem. Soc.* **1989**, *111*, 3125.
(443) Boudon, S.; Wip, G. *J. Comput. Chem.* **1991**, *12*, 42.
(444) Wagman, D. D.; Evans, W. H.; Parker, V. B.; Schumm, R. H.; Halow, I.; Bailey, S. M.; Churney, K. L.; Nuttall, R. L. *J. Phys. Chem. Ref. Data* **1982**, *11*, Suppl. 2.
(445) Ford, G. P.; Scribner, J. D. *J. Org. Chem.* **1983**, *48*, 2226.

CR9411785